



# **Investigations into the Application of Engineered Bamboo for Future Hybrid Beams**

by

**NIAZ GHARAVI**

BSc, MSc

Thesis submitted in partial fulfilment of the requirements  
of Edinburgh Napier University, for the award of  
*Doctor of Philosophy*

School of Engineering and the Built Environment  
Edinburgh Napier University

August 2019

*To my Wife & Son.*

# **AUTHOR'S DECLARATION**

I declare that the work in this dissertation was carried out in accordance with the requirements of the Edinburgh Napier University's Regulations and Code of Practice for Research Degree Programmes and that it has not been submitted for any other academic award. Except where indicated by specific reference in the text, the work is the candidate's own work. Work done was not part of any collaboration with, or with the assistance of, others. Any views expressed in the dissertation are those of the author.

NIAZ GHARAVI  
SEPTEMBER 2019

# ACKNOWLEDGEMENTS

Firstly, I would like to express my immense appreciation to my Director of Studies, Dr Hexin (Johnson) Zhang, for his encouragement, support and extensive knowledge. His guidance helped me in all the time of research and writing of this thesis. I could not have imagined having a better advisor and mentor for my PhD study. I also wish to thank Dr Kenneth Leitch for his guidance and assistance as my second supervisor.

I would like to thank Peter KK Lee Studentship which enabled me to undertake this research by providing the financial sponsorship. Also, to the technicians at Edinburgh Napier University, especially, Roshan Dhonju, Willie Laing and Stefan Lehneke for all of their technical support during the experiments.

To my friends at E21 kingdom, thanks for listening, offering me advice and making this journey a much joyful ride. Special thanks to Faqhrul, Aisling, Melanie, Juan, Lara, Emine, Suzanne and Mengxiao. I also sincerely appreciate Ruth, Clare and Amaka for proofreading my thesis.

Last but not the least, my deepest appreciation and love goes to my lovely wife, Maisa, for her endless love, patience and support through thick and thin of this journey. Sincere thanks to my far apart family, my parents, brothers and sisters who always believed in me and supported me.

# PUBLICATIONS

## JOURNAL PAPERS:

- Gharavi, N., Zhang, H., Xie, Y., & He, T. (2018). "*End effect on determining shear modulus of timber beams in torsion tests.*" *Construction and Building Materials*, 164, 442-450. DOI: 10.1016/j.conbuildmat.2017.12.191
- Gharavi, N., Maccallum, M., Maciver, A., Mohamed, A., & Zhang, H. (2018). "*Shear Field Size Effect on Determining the Shear Modulus of Glulam beam.*" *Research & Development in Material Science*, 5(3), 1-3.  
DOI: 10.31031/RDMS.2018.03.000575

## CONFERENCE PAPERS:

- Gharavi, N., Zhang, H., & Xie, Y. (2017). "*Evaluation of the End Effect Impact on the Torsion Test for Determining the Shear Modulus of a Timber Beam through a Photogrammetry Approach.*", IN: *International Journal of Mechanical and Mechatronics Engineering*, 11, 676-680. DOI: 10.5281/zenodo.1129778
- Gharavi, N., & Zhang, H. (2018). "*Study on the Impact of Size and Position of the Shear Field in Determining the Shear Modulus of Glulam Beam Using Photogrammetry Approach.*" (Version 10008636). IN: *International Journal of Architectural, Civil and Construction Sciences*, 11.0(3). 10.5281/zenodo.1315953

# ABSTRACT

Over the late decade, sustainability has become mainstream in the built environment due to the widespread awareness of global warming. This has led to the creation and optimisation of engineered wood and bamboo products. Engineered bamboo products possess superior environmental and mechanical characteristics which situate them as appealing candidates in aiding other natural building materials in the path toward sustainability. Whilst many of the studies in this field have only focused on characterising engineered bamboo products, this study aimed to develop engineered bamboo-based composite beams. A prototyping study was conducted to gain a detailed understanding of the proposed hybrid/engineered materials, with a focus on enhancing the strength and retaining the environmental and mechanical characteristics of both materials.

A series of destructive experiments were conducted to evaluate the mechanical properties of the constituent materials and a simplified stress-strain relationship was proposed. A tailor-made and multi-point measurement system based on photogrammetry was developed to acquire three-dimensional information. Using this information, the suitability of the timber-based testing standards for laminated bamboo were examined and the limitations were identified.

Three different composite prototypes were fabricated and tested in three stages in the laboratory environment at Edinburgh Napier University. These composites are: I-beam laminated bamboo and timber hybrid beam (IBHB), laminated bamboo I-beam (BIB) and laminated bamboo double I-beam (BDIB). Throughout the different stages of this study, engineered bamboo-based composite beams have shown

promising potential to be used in the construction industry. Because of their rapid renewability, great strength and higher ductility, these composites are efficient in terms of material use and comprise more than three times higher strength to weight ratio compared to the control samples. Mathematical models to predict the deflection and bending moment were developed based on the linear and non-linear behaviour of laminated bamboo.

The I-bone laminated bamboo provided higher load-bearing capacity while the side timbers contributed toward shear resistance and cross-sectional stability. IBHB exhibited higher flexural strength when compared to the conventional engineered wood materials. The bending modulus of IBHB was also doubled when compared to the control samples. The laminated bamboo I-beam and double I-beam also demonstrated great flexural properties, however, with signs of vulnerability to the horizontal shear failure. Laminated bamboo double I-beam exhibited similar mechanical properties to those of IBHB.

The findings of this study add to the rapidly expanding field of engineered bamboo applications within the future built environment. It has done so by providing an innovative approach to developing new engineered bamboo composites for construction and provides a strong foundation for future research.

# TABLE OF CONTENTS

<b>ACKNOWLEDGEMENTS</b>	<b>iii</b>
<b>PUBLICATIONS</b>	<b>iv</b>
<b>ABSTRACT</b>	<b>v</b>
<b>TABLE OF CONTENTS</b>	<b>vii</b>
<b>LIST OF TABLES</b>	<b>xiv</b>
<b>LIST OF FIGURES</b>	<b>xvi</b>
<b>LIST OF ABBREVIATIONS</b>	<b>xx</b>
<b>LIST OF SYMBOLS</b>	<b>xxii</b>
<b>1 INTRODUCTION</b>	<b>1</b>
1.1 Background and Motivation . . . . .	1
1.1.1 Wood as a sustainable material . . . . .	2
1.1.2 Drawbacks with wood and engineered wood . . . . .	3
1.2 Bamboo as an alternative material . . . . .	4
1.2.1 Engineered bamboo . . . . .	4
1.2.2 The drawbacks with engineered bamboo products . . . . .	5
1.3 The Concept behind this Study . . . . .	5
1.4 Aim and Objectives . . . . .	7
1.5 Thesis Outlines . . . . .	8
<b>2 LITERATURE REVIEW</b>	<b>10</b>

## TABLE OF CONTENTS

2.1	Introduction . . . . .	10
2.2	Bamboo . . . . .	11
2.2.1	Anatomy and Fine Structure . . . . .	12
2.2.2	Bamboo's mechanical properties . . . . .	15
2.2.3	Bamboo's limitations as a construction material . . . . .	15
2.3	Engineered Bamboo . . . . .	16
2.3.1	Bamboo scrimber . . . . .	16
2.3.2	Laminated Bamboo Lumber . . . . .	17
2.3.3	Mechanical characteristics of laminated bamboo lumber . . . . .	18
2.3.4	Environmental impacts of laminated bamboo lumber . . . . .	19
2.4	Engineered Timber and Bamboo Composites . . . . .	20
2.4.1	Wood engineered composites . . . . .	20
2.4.2	Engineered bamboo composites . . . . .	20
2.4.3	Glue laminated bamboo beams . . . . .	21
2.4.4	Bamboo and engineered bamboo as a reinforcement . . . . .	21
2.4.5	Engineered bamboo and timber hybrid beams . . . . .	22
2.4.6	Engineered bamboo and timber I-beams . . . . .	24
2.5	Laminated Bamboo Composite Beams . . . . .	26
2.5.1	The concept of I-bone laminated bamboo hybrid beam . . . . .	26
2.5.2	Cross-sections of the composite beams . . . . .	26
2.5.3	Potential advantages and limitations . . . . .	27
2.5.4	Prospective applications . . . . .	28
2.6	Summary . . . . .	28
<b>3</b>	<b>MATERIAL PROPERTIES AND TESTING METHODS</b>	<b>30</b>
3.1	Introduction . . . . .	30
3.2	Materials . . . . .	31
3.3	Implemented Stereo Vision System . . . . .	32
3.3.1	Limitations with the conventional methods . . . . .	32
3.3.2	What is photogrammetry? . . . . .	33
3.3.3	The principle behind the photogrammetry . . . . .	33
3.3.4	Calibration process . . . . .	35

## TABLE OF CONTENTS

3.3.5	Photogrammetry setup . . . . .	36
3.3.6	Target points . . . . .	36
3.3.7	3-D information acquisition through image processing . . .	38
3.4	Static Bending Test . . . . .	40
3.4.1	Specimen preparation . . . . .	40
3.4.2	Testing procedure . . . . .	41
3.4.3	Results of the static bending test . . . . .	41
3.4.3.1	Characteristic values . . . . .	43
3.4.3.2	Bending modulus . . . . .	44
3.4.4	Impact of the strip orientation on the flexural properties . .	44
3.4.5	Three-point to four-point . . . . .	45
3.5	Tensile Behaviour Parallel to Fibres . . . . .	46
3.5.1	Tensile test specimen preparation . . . . .	46
3.5.2	Results of the Small Clear Specimen tensile test . . . . .	47
3.5.3	Impact of the conditioning environment in the tensile properties	50
3.5.4	Impact of the knots in the tensile properties . . . . .	51
3.5.5	Failure mechanism . . . . .	51
3.6	Compression Test Parallel to Fibres . . . . .	52
3.6.1	Results of the compression test . . . . .	53
3.6.2	Failure mechanism . . . . .	54
3.7	The Constitutive Model . . . . .	55
3.7.1	Proposed stress and strain relationship . . . . .	56
3.8	Testing Methods for Determining the Shear Modulus . . . . .	57
3.8.1	Torsion test . . . . .	58
3.8.1.1	The identified discrepancy in BS EN 408 and ASTM D198 . . . . .	60
3.8.1.2	Saint-Venant's end effect in torsion test . . . . .	60
3.8.1.3	The decay length prediction . . . . .	61
3.8.1.4	The torsion test detailed in the BS EN 408 . . . . .	62
3.8.1.5	Specimens . . . . .	62
3.8.1.6	Experimental procedure . . . . .	62

## TABLE OF CONTENTS

3.8.1.7	Rotation measurement system . . . . .	64
3.8.1.8	Photogrammetry and inclinometers comparison . .	65
3.8.1.9	Analysing process . . . . .	66
3.8.1.10	Results and the proposed decay length . . . . .	67
3.8.1.11	Shear modulus of laminated bamboo lumber . . .	72
3.8.2	The Shear Field Test Method . . . . .	72
3.8.2.1	Constructing square . . . . .	72
3.8.2.2	The concept of the shear field method . . . . .	73
3.8.2.3	Experimental procedure . . . . .	74
3.8.2.4	Analysis of variance on the shear modulus variation	76
3.9	Summary . . . . .	78
<b>4</b>	<b>I-BONE LAMINATED BAMBOO HYBRID BEAM</b>	<b>81</b>
4.1	Introduction . . . . .	81
4.2	Beams and Fabrication Process . . . . .	82
4.2.1	Beams . . . . .	82
4.2.2	Materials . . . . .	82
4.2.3	Fabrication process . . . . .	83
4.2.4	Manufacturing Challenges . . . . .	85
4.2.5	Manufacturing Recommendations . . . . .	86
4.3	Experimental Evaluations . . . . .	88
4.3.1	Beam preparation for testing . . . . .	88
4.3.2	Four-Point bending test . . . . .	88
4.3.3	Measurement apparatus . . . . .	88
4.4	Thermal and Moisture Expansions . . . . .	89
4.4.1	How bamboo behaves due to moisture and thermal changes?	90
4.4.2	The moisture and temperature change in the IBHB . . . . .	91
4.5	Failure Mechanism . . . . .	92
4.5.1	Glulam beam failure . . . . .	92
4.5.2	Laminated bamboo sandwich beam failure . . . . .	92
4.5.3	I-bone laminated bamboo hybrid beam failure . . . . .	93
4.6	Results of the Experimental Evaluations . . . . .	95

## TABLE OF CONTENTS

4.6.1	Flexural properties . . . . .	95
4.6.2	Ductility . . . . .	98
4.6.3	Flexural rigidity . . . . .	100
4.7	Shear Properties of IBHB . . . . .	101
4.7.1	Shear stress calculations . . . . .	101
4.7.2	Determining shear modulus using the Shear Field test method	102
4.7.2.1	Shear distortion measurements . . . . .	102
4.7.2.2	Photogrammetry procedure . . . . .	103
4.7.2.3	Shear modulus determination . . . . .	104
4.8	Analytical Approach for Modelling HIB . . . . .	106
4.8.1	Mid-Span deflection . . . . .	106
4.8.2	Prediction of the flexural bearing capacity . . . . .	107
4.8.2.1	Linear analysis . . . . .	109
4.8.2.2	Non-linear analysis . . . . .	110
4.9	Comparison with other Experimental Studies . . . . .	114
4.10	Summary . . . . .	117
<b>5</b>	<b>LAMINATED BAMBOO I-BEAM AND DOUBLE I-BEAM</b>	<b>119</b>
5.1	Introduction . . . . .	119
5.2	Fabrication Process . . . . .	120
5.2.1	Material . . . . .	120
5.2.2	Dimensions of the I-beams . . . . .	121
5.2.3	Manufacturing challenges . . . . .	121
5.2.4	Final products . . . . .	123
5.3	Experimental Procedures for BIB and BDIB . . . . .	124
5.3.1	Measurements . . . . .	124
5.3.1.1	Specimen's density . . . . .	124
5.3.1.2	Moisture content . . . . .	125
5.3.2	The four-Point bending test . . . . .	125
5.4	Failure Observations . . . . .	126
5.4.1	Laminated bamboo I-beam . . . . .	127
5.4.2	Laminated bamboo double I-beam . . . . .	127

## TABLE OF CONTENTS

5.5	I-Beams in Flexure . . . . .	128
5.5.1	Load deflection analysis . . . . .	129
5.5.2	Flexural properties . . . . .	129
5.5.3	Ductility . . . . .	131
5.5.4	Flexural rigidity . . . . .	131
5.5.5	Importance of side timbers in IBHB . . . . .	134
5.5.6	âĀĀ . . . . .	134
5.6	Shear Stress Calculations . . . . .	134
5.7	Deflection Prediction of the Beams . . . . .	136
5.7.1	Flexural deflection . . . . .	136
5.7.2	Shear deflection . . . . .	136
5.8	Ultimate Bending Moment Capacity Prediction . . . . .	137
5.8.1	Moment capacity of BIB . . . . .	139
5.8.2	Bending moment capacity of BDIB . . . . .	141
5.8.2.1	Linear analysis . . . . .	141
5.8.2.2	Non-linear analysis . . . . .	143
5.9	Discussion and Summary . . . . .	146
<b>6</b>	<b>BUTT-JOINTED LBL IN A HYBRID BEAM</b>	<b>149</b>
6.1	Introduction . . . . .	149
6.2	Butt-Joint in the Four-Point Bending Test . . . . .	150
6.2.1	Specimens . . . . .	150
6.2.2	Experimental procedure . . . . .	150
6.2.3	Results of the four-point bending test . . . . .	152
6.2.4	Deformation behaviour of the tested beams . . . . .	152
6.2.5	Failure analysis . . . . .	152
6.3	Three-Point Bending Test Without Butt-Joints . . . . .	155
6.3.1	Results of the three-point bending test . . . . .	156
6.3.2	Failure Mechanism of the VLHB in three-point bending . . . . .	157
6.4	Analytical Study . . . . .	159
6.4.1	Prediction of the damaged length . . . . .	159
6.4.2	Deflection at the butt joint . . . . .	161

**TABLE OF CONTENTS**

---

6.5 Summary . . . . .	163
<b>7 CONCLUSIONS &amp; RECOMMENDATIONS</b>	<b>165</b>
7.1 Summary of the Studies . . . . .	165
7.2 Academic Impact of this Research . . . . .	168
7.3 Recommendations for Further Study . . . . .	169
<b>REFERENCES</b>	<b>170</b>
<b>APPENDIX A SMALL CLEAR SPECIMEN TESTING DATASET</b>	<b>184</b>

# LIST OF TABLES

TABLES	Page
3.1 Static three-Point bending test results . . . . .	43
3.2 Specimen descriptions for the tensile test . . . . .	49
3.3 Results of small specimen tensile test . . . . .	50
3.4 Small clear specimen compression test results . . . . .	53
3.5 Torsion test specimens' details . . . . .	63
3.6 Measured shear modulus* for small squares (Fig. 3.36a) . . . . .	77
3.7 Measured shear modulus* for medium squares (Fig. 3.36b) . . . . .	77
3.8 Measured shear modulus* for large squares (Fig. 3.36c) . . . . .	77
3.9 Measured shear modulus* based on the square size (Fig. 3.36d) . . . . .	78
4.1 Nominal dimensions of the manufactured beams . . . . .	84
4.2 The four-point bending test outcomes . . . . .	96
4.3 Flexural properties based on the four-point bending test . . . . .	98
4.4 Ductility and stiffness of the tested beams . . . . .	99
4.5 Shear properties of the tested beams . . . . .	104
4.6 Constituent material properties . . . . .	107
4.7 Comparison between experimental and theoretical flexural bearing capacities. . . . .	110
4.8 Non-linear flexural capacity results. . . . .	113
4.9 Comparison of the mean flexural properties for IBHB and other wood-based products . . . . .	116
5.1 The four-Point bending test measurements data . . . . .	126

5.2 The four-Point bending test results of the I-beams . . . . .	131
5.3 Ductility and stiffness of the beams . . . . .	132
5.4 BIB bending moment prediction . . . . .	141
5.5 BDIB bending moment prediction based on the linear stress-strain relationship . . . . .	143
5.6 BDIB nonlinear stress-strain relationship prediction . . . . .	145
5.7 BDIB bending moment prediction for non-linear analysis . . . . .	146
6.1 Four-point bending test readings . . . . .	152
6.2 Four-point bending test results . . . . .	153
6.3 Comparison of 4-Point bending test (with butt-joint) and 3-Point bending test (without butt-joint). . . . .	157
6.4 Calculated damaged length of the hybrid beams . . . . .	161
A.1 Static bending test results for laminated bamboo specimen oriented in the B direction . . . . .	185
A.2 Static bending test results for laminated bamboo specimen oriented in the L direction . . . . .	186
A.3 Static bending test results for C16 timber samples . . . . .	187
A.4 Tensile test results for C16 timber samples. . . . .	188
A.5 Specimen <b>TA</b> tensile test results. . . . .	189
A.6 Specimen <b>TB</b> tensile test results. . . . .	190
A.7 Specimen <b>TC</b> tensile test results. . . . .	191
A.8 Failure modes of the tensile specimen . . . . .	192

# LIST OF FIGURES

FIGURES	Page
1.1 At 18 storeys high, Mjøstårnet is the tallest timber building in the world (www.dezeen.com) . . . . .	3
1.2 Laminated bamboo composite beams cross-sections . . . . .	7
2.2 Bamboo's node structure and fibres orientations (Liese and Köhl, 2015) . . . . .	13
2.1 Anatomy and a section of a bamboo culm (Botanicals) . . . . .	13
2.3 Cell structure of a bamboo (a) Bamboo culm cross section (b) Bamboo culm cross section(c) Vascular bundle of bamboo(V=Vessel, F=Fibre sheath, Ph=Phloem, P=Parenchyma) (Liese, 1987) . . . . .	14
2.4 Bamboo scrimber . . . . .	17
2.5 General production procedures of laminated bamboo board (Rittironk and Elnieri, 2008) . . . . .	17
2.6 Laminated bamboo lumber cross-section . . . . .	18
2.7 Laminated bamboo composite beams cross-sections . . . . .	27
3.1 Binocular stereo vision principle . . . . .	33
3.2 Calibration plates . . . . .	36
3.3 Stereo vision setup in the Shear Field test . . . . .	37
3.4 Photogrammetry target points . . . . .	37
3.5 Extracting the target point based on the dotted target points . . . . .	38
3.6 Extracting the target point based on the crossed target points . . . . .	38
3.7 The photogrammetry's process stages in a torsion test . . . . .	39

3.8	The static three-Point bending test . . . . .	40
3.9	Laminated bamboo's strip orientations . . . . .	41
3.10	Example of load-deflection for static bending test . . . . .	42
3.11	Failure modes for static bending test . . . . .	42
3.12	The bending strength distribution and variation . . . . .	44
3.13	The bending modulus distribution graphs . . . . .	45
3.14	Small Clear Specimen tensile test . . . . .	47
3.15	Tensile stress-strain relationship . . . . .	48
3.16	Tensile strength and modulus comparison and variation . . . . .	50
3.17	: Tensile test failure mechanisms . . . . .	52
3.18	Compression test setup parallel to fibres . . . . .	53
3.19	Stress-strain graph for a compression test . . . . .	54
3.20	Compression test failure modes . . . . .	55
3.21	The stress-strain relationship for the laminated bamboo lumber . . . . .	56
3.22	Proposed stress-strain relationship for the laminated bamboo lumber . . . . .	57
3.23	Failure modes associated with shear stress . . . . .	59
3.24	Shear stress distribution in a torsion specimen . . . . .	60
3.25	Torsion test and the photogrammetry setup . . . . .	63
3.26	Circular gauge and torsion clamping system . . . . .	64
3.27	Inclinometers and developed data-logger . . . . .	65
3.28	Photogrammetry setup for the torsion test . . . . .	65
3.29	Rotation measurements comparison between the photogrammetry and the inclinometers . . . . .	66
3.30	Laminated bamboo lumber's calculated shear modulus . . . . .	68
3.31	Measured shear modulus for timber specimens . . . . .	69
3.32	End effect decay length coefficients of tested aspect ratios . . . . .	71
3.33	The constructing square and the stress distribution . . . . .	73
3.34	The concept of shear deformation in the shear field test method . . . . .	73
3.35	Photogrammetry setup for the shear field test method . . . . .	75
3.36	Four cases of the constructing square's sizes and positions . . . . .	76
4.1	Manufactured beams for this stage of the experiments . . . . .	82

4.2	Schematic cross-sections of the beams . . . . .	83
4.3	Manufacturing procedures . . . . .	84
4.4	Vertical clamping system . . . . .	85
4.5	IBHB foreseeable defect and required groove cut . . . . .	87
4.6	Final products . . . . .	88
4.7	Four-point bending test configurations . . . . .	89
4.8	Four-Point bending test setup . . . . .	89
4.9	IBHB's principal directions with respect to grain direction . . . . .	91
4.10	Glulam Beams' failure . . . . .	92
4.11	Bamboo sandwich beam failure . . . . .	93
4.12	IBHB failed under flexural load . . . . .	94
4.13	I-bone laminated bamboo hybrid beam failure (Glue: MF) . . . . .	94
4.14	I-bone laminated bamboo hybrid beam failure (Glue: PRF) . . . . .	95
4.15	IBHB beams' load-deflection graph . . . . .	96
4.16	Load-deflection comparison between the tested beams . . . . .	97
4.17	Triangulation principle to calculate the curvature . . . . .	99
4.18	Moment-curvature relationship . . . . .	100
4.19	Flexural rigidity variation against the applied bending moment of IBHBs	101
4.20	Stereo vision setup in the four-point bending test . . . . .	103
4.21	Image processing procedure to determine the 3D coordinates of target points . . . . .	105
4.22	Experimental and theoretical mid-span deflections of IBHBs (elastic range)	108
4.23	Proposed laminated bamboo stress-strain relationship . . . . .	108
4.24	Transformed section and corresponding linear stress distribution . . .	110
4.25	Transformed section and corresponding non-linear stress distribution .	111
5.1	Laminated bamboo I-beam and double I-beam . . . . .	120
5.2	BIB and BDIB's nominal dimensions . . . . .	121
5.3	Laminated bamboo I-beams fabrication limitations and challenges . . .	123
5.4	Laminated bamboo I-beams final products . . . . .	124
5.5	The four-point bending test configuration . . . . .	125
5.6	BIB failure observations . . . . .	127

---

5.7	BDIB1 failure observations . . . . .	128
5.8	BDIB2 failure observations . . . . .	128
5.9	The load-deflection graph of the laminated bamboo I-beams . . . . .	130
5.10	Comparison of the load-deflection of the tested beams with IBHB . . . . .	130
5.11	Flexural rigidity of the tested beams . . . . .	133
5.12	Shear stress distribution for BIB and BDIB . . . . .	135
5.13	Experimental and theoretical load-deflection comparison . . . . .	138
5.14	BIB stress distribution . . . . .	139
5.15	BDIB linear stress distribution . . . . .	142
5.16	BDIB nonlinear stress distribution . . . . .	144
6.1	Butt-joint in the laminated bamboo lumber and the composite beam . . . . .	150
6.2	VLHB and GL nominal dimensions . . . . .	151
6.3	Four-point bending test setup . . . . .	151
6.4	Load-deflection of the tested beams in four-point bending test . . . . .	153
6.5	VLHB load-deflection graph . . . . .	154
6.6	VHB3 failure observations . . . . .	154
6.7	Glulam beam failure observations . . . . .	155
6.8	Three-point bending test for BTHB . . . . .	156
6.9	Three-point bending test load-deflection graph . . . . .	158
6.10	Three-point bending failure observations . . . . .	158
6.11	Developed shear and flexural stresses in the damaged length . . . . .	159
6.12	Effective moment of inertia along the hybrid beam . . . . .	161
6.13	Simplified beam for deflection analysis . . . . .	161
6.14	Experimental and calculated beam deflection . . . . .	162

# LIST OF ABBREVIATIONS

- BDIB** Engineered Bamboo Double I-Beam. xi, xii, xv, xviii, xix, 6, 7, 8, 26, 27, 28, 119, 120, 121, 124, 125, 126, 127, 128, 129, 131, 132, 133, 135, 137, 138, 141, 142, 143, 144, 145, 146, 147, 148, 167, 168
- BIB** Engineered Bamboo I-Beam. xi, xii, xv, xviii, xix, 6, 7, 8, 26, 27, 119, 120, 121, 124, 125, 126, 127, 128, 129, 131, 132, 133, 134, 135, 137, 139, 140, 141, 146, 147, 148, 167, 168
- BSB** Laminated Bamboo Sandwich Beam. 82, 83, 84, 88, 92, 93, 95, 97, 98, 99, 104, 114, 116
- GB** Glue Laminated Beam. 82, 83, 84, 92, 93, 95, 98, 99, 104
- IBHB** I-Bone Laminated Bamboo Hybrid Beam. x, xi, xii, xiv, xviii, xix, 6, 7, 9, 26, 27, 28, 29, 81, 82, 83, 84, 86, 87, 88, 91, 93, 94, 95, 96, 97, 98, 99, 100, 101, 104, 106, 109, 110, 112, 113, 114, 115, 116, 117, 118, 120, 124, 125, 126, 129, 130, 131, 132, 133, 134, 146, 147, 167, 168
- LBL** Laminated Bamboo Lumber. 8, 9, 30, 31, 40, 43, 44, 45, 63, 67, 91, 98, 107, 112, 116, 149, 158, 159, 160
- MC** Moisture Content. 125, 126
- MF** Melamine Formaldehyde. xviii, 82, 83, 85, 94, 95, 96, 98, 99, 100, 104, 109, 121, 126, 131, 146, 167
- MOE** Modulus of Elasticity. 22, 97, 98, 116, 129, 131, 147, 152, 153, 156, 157
- MOR** Modulus of Rupture. 97, 98, 114, 116, 129, 131, 134, 147, 152, 153, 156, 157

## **LIST OF ABBREVIATIONS**

---

**OSB** Oriented Strand Board. 22, 23

**PRF** Phenol Resorcinol Formaldehyde. xviii, 82, 83, 85, 93, 94, 95, 96, 98, 99, 100, 104, 117, 160, 167

**SG** Specific Gravity. 98, 114, 116, 124, 131

**SLS** Serviceability Limit State. 106

**ULS** Ultimate Limit State. 106

**VLHB** Vertically Laminated Hybrid Beam. xii, xix, 149, 150, 151, 152, 153, 154, 156, 157, 159, 161, 162, 163

## LIST OF SYMBOLS

$\delta$	Deflection
$\Delta'$	Deflection at the proportionality limit
$\delta_x$	Deflection
$\delta_{serv}$	Allowable deflection
$\epsilon$	Strain
$\epsilon_t$	Tensile strain at the yield point
$\epsilon_{c0}$	Strain at the compressive plastic limit
$\epsilon_{cy}$	Strain at the compressive yield point
$\epsilon_{ep}$	Strain at the compressive elastic-plastic range
$\kappa$	Beam Curvature
$\phi$	beam's rotations
$\sigma$	Normal stress
$\sigma_t$	Tensile stress at the yield point
$\sigma_{c0}$	Stress at the compressive plastic limit
$\sigma_{cy}$	Stress at the compressive yield point
$\sigma_{dev}$	Developed normal stress at the butt-section
$\sigma_{ep}$	Stress at the compressive elastic-plastic range
$\tau$	Shear Stress

## LIST OF ABBREVIATIONS

---

$\tau_{dev}$	Developed shear stress at the butt-section
$A$	Cross-sectional Area
$a$	Distance between loading point to the nearest support
$A_{eff}$	Effective cross-sectional area
$b$	Cross-sectional Thickness
$b_w$	Web's breadth
$E$	Young's Modulus
$E_c$	Compressive modulus
$E_t$	Tensile modulus
$E_{L3P}$	Laminated bamboo's Young's modulus in three-point bending
$E_{LA}$	Young's modulus converted to four-point bending
$F$	Applied Load
$f$	Camera lens focal length
$F'$	Applied load at the proportionality limit
$f_b$	Laminated bamboo's flexural strength
$f_c$	Compressive strength
$f_t$	Tensile strength
$f_{m,k}$	Laminated bamboo's characteristic flexural strength
$G$	Shear modulus
$G_{SF}$	Shear modulus in Shear field test
$G_{tor}$	Shear modulus in torsion test
$h$	Cross-sectional Height
$I$	Second Moment of Area

## LIST OF ABBREVIATIONS

---

$I_e$	Effective second moment of area because of butt-joint
$k_{ep}$	Slope of the elastic-plastic in the constitutive model
$k_{tor}$	Torque stiffness (Torque/rotation)
$l$	Loading span
$l_1$	Distance between the rotation measuring sections at both ends
$l_{dmg}$	Damaged length due to butt-joint
$M$	Bending Moment
$M_u$	Ultimate bending moment
$P$	Applied load
$Q$	First Moment of Area
$T$	Applied torque
$t$	Laminae thickness
$V$	Shear Load
$w$	Displacement

# INTRODUCTION

## 1.1 Background and Motivation

Rapid urbanisation and infrastructure development have caused an increase in pollution and greenhouse gas emission. These have alarmed both governments and private organisations to reduce their environmental impact and promote sustainability in their policies and developments. Whilst the energy industry is seeking more environmentally friendly renewable resources, the building industry is also looking to identify renewable and sustainable resources and the new generation of technology to tackle global warming and the customer satisfaction.

According to the UN Environmental and International Energy Agency, the construction industry is reported as one of the least sustainable industries in the world, as it accounts for 36% of global energy consumption and 39% of total greenhouse gas emissions ([UN Environment and International Energy Agency, 2017](#)). EU countries and many international organisations are reforming their policies to reduce emissions in the built environment ([European Commission, 2012](#)). The UK government is also aiming to halve emissions in the built environment by 2030 ([Committee on Climate Change, 2018](#)).

The construction industry plays a critical role in achieving this goal by taking actions toward using sustainable and eco-friendly building materials. Concrete and steel are, still, the most dominant building materials in many countries, and manufacturing them requires a huge amount of energy and mining of raw resources like sand and aggregate. Because of

these factors, interest has risen towards using more sustainable materials such as wood and engineered wood products in this industry.

### **1.1.1 Wood as a sustainable material**

Wood is a renewable, lightweight and sustainable resource which has been used throughout human history. However, the development of concrete and steel during the industrial revolution reduced the use of wood in the construction industry (Popescu, 2017). During the last decade, due to widespread awareness of global warming and carbon dioxide emissions, sustainability has become mainstream in the built environment. This has led to the creation and optimisation of engineered wood products such as Glue Laminated Timber (Glulam) and Cross Laminated Timber (CLT).

Unlike producing concrete and steel, producing and using wood and its derivative products have substantially lower impact in terms of CO<sub>2</sub> emission. Also, they can be recovered at the end of their service to retain their value. Engineered timber products have led to the construction of tall timber buildings around the world such as Mjøstårnet, Norway (2019), 25 King, Brisbane, Australia (2018), The Stadthaus, London (2009), Bridport House, London (2011) and Tamedia Office Buildings, Zurich, Switzerland (2013), and many more are in the planning stage.

By encouraging the research and investment in developing high value-added timber and engineered wood products, promoting these environmentally friendly products in building and other industries brings a profitable business model to the forestry industry, and encourages them to plant more trees, and plan and develop the forest resources strategically.

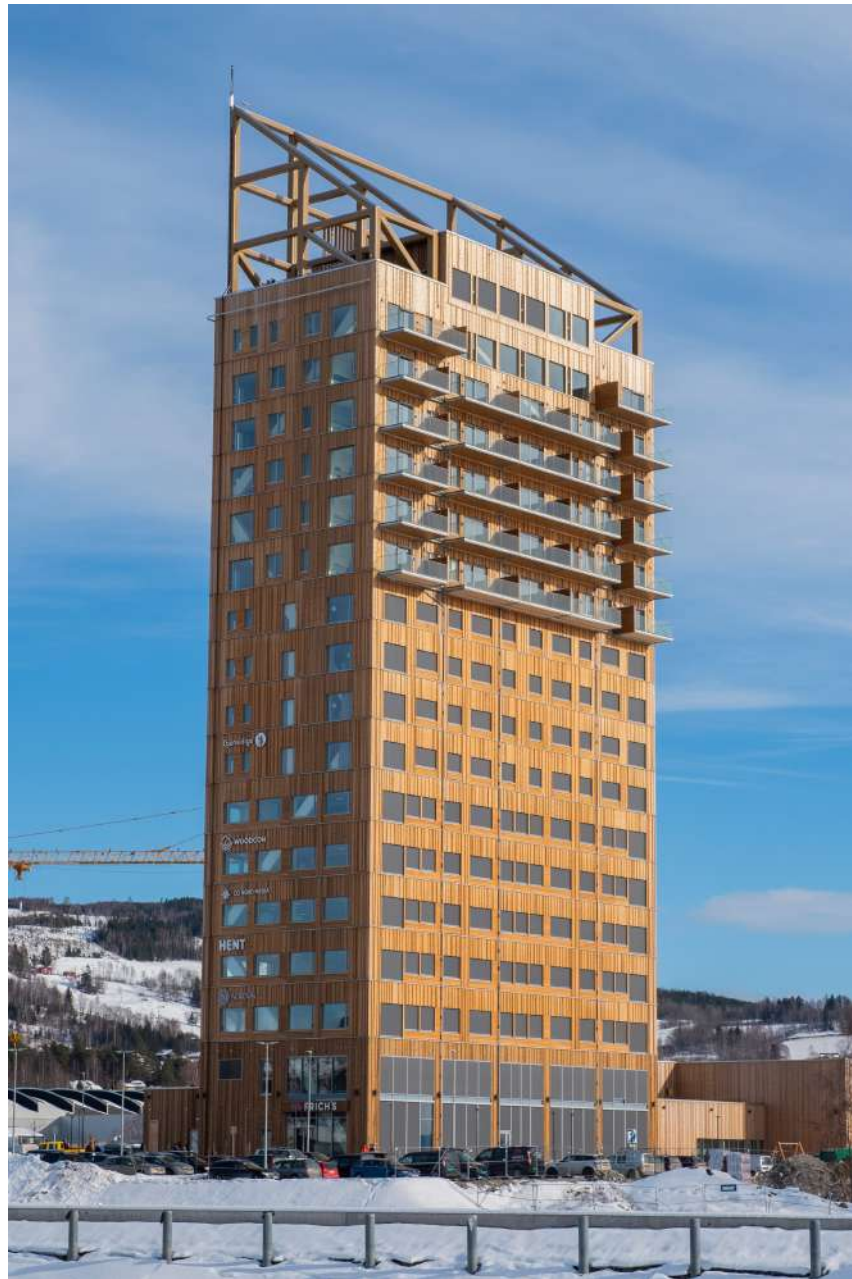


**Figure 1.1:** At 18 storeys high, Mjøstårnet is the tallest timber building in the world ([www.dezeen.com](http://www.dezeen.com))

### 1.1.2 Drawbacks with wood and engineered wood

The share of the wood and engineered wood products in the construction industry is only marginal due to their relatively low flexural stiffness to size ratio, natural defects and exhibiting brittle behaviour under tension. This is despite their long association with human life and particularly as a construction material. It is likely that the interest in using synthetic materials will remain high unless these weaknesses are addressed.

In addition, wood has a long growth cycle, and cultivation is required to preserve the wood resources. Thus, particular attention has been drawn towards finding alternative materials that possess similar environmental benefits but mitigate the limitations of wood.

### **1.2 Bamboo as an alternative material**

Bamboo includes some of the fastest-growing plants on the planet with a reported growth rate of up to 100 cm a day (Liese, 1987). Unlike trees, bamboo's rhizome and root systems can extend up to 150 km/ha. Its ecosystem is highly proactive which means that the new bamboo culm will replace the harvested ones rapidly, usually within a year of harvesting (Yiping et al., 2010; Liese, 1985).

These characteristics of bamboo, together with its ability to capture carbon after harvesting and high biomass production (Liese, 1987), make it a highly renewable and appealing alternative material to combine with wood products in the battle against global warming. Therefore, the primary motivation of this study is to promote the use of engineered bamboo as reinforcement to the low-grade and underutilised timber species in the construction industry.

Bamboo is known as the fastest growing and regarded as one of the strongest and most versatile plant on the planet (Liese, 1985). Whilst in wood, growing rate and strength are usually reciprocal of each other, bamboo is an exception. These two characteristics of bamboo, i.e. fast growth and high strength, are main reasons that interests have risen toward using bamboo for the modern construction.

Bamboo's natural cylindrical form is highly optimised in terms of material use and efficient in terms of load bearing. However, this advantage of bamboo, i.e. natural shape, makes it difficult to form connection during the construction. Engineered bamboo has mitigated this issue by reforming its' natural shape.

#### **1.2.1 Engineered bamboo**

Engineered bamboo is the product of reforming bamboo culm based on the prospected application into a board or lumber. There are several types of engineered bamboo such as bamboo scrimber, ply bamboo and laminated bamboo lumber. Whilst bamboo is primarily

used as scaffolding and supporting poles, engineered bamboo opens a whole new range of applications as an architectural and structural material. Despite great mechanical and environmental advantages, engineered bamboo products possess drawbacks which make engineers reluctant of using it in their designs.

### **1.2.2 The drawbacks with engineered bamboo products**

The bamboo industry currently uses traditional methods of harvesting and processing which make the process inefficient with little to no added-value (Wang et al., 2017). Lack of a reliable production and design guideline prevents investments in plantation and development of bamboo forests.

In addition, there are engineered bamboo products that are butt-jointed at a section to form a longer and wider board. These joints are often concealed with joint-free and smooth surface layers, makes it difficult to differentiate. These butt-jointed materials cannot be used as a structural element, but based on the intended application, e.g. surface or architectural, may be used in the composite material.

Engineered bamboo products are denser than structural timber and Glulam, thus using them as a structural element introduces additional weight to the structure. They are also highly prone to splitting. These drawbacks in engineered bamboo products can be mitigated by combining them with wood which is lighter and performs better in transverse directions.

Bamboo and engineered bamboo products is a nascent field of research, and more collaborative work is required to align the research and development. This study is not only another step toward promoting this material in the construction industry, but also to open new ways of fabricating the engineered materials in the more innovative approach.

## **1.3 The Concept behind this Study**

A recent development in combining engineered bamboo and timber indicated a great potential of producing high-performance and competitive composites material by combining engineered bamboo and timber (Kaboli and Clouston, 2019; Ashaari et al., 2016; Sinha and Clauson, 2012; Lee et al., 1997).

These studies have contributed to the usability of engineered bamboo in softwood Glulam production by using it in the tensile and compressive regions, i.e. top and bottom layers, and timber in the middle. Although this lay-up has significantly improved the flexural properties of the composite material, but also, increased the shear failure in the wood layers. Therefore, to use engineered bamboo to its full potential, reinforcement is needed in the high shear stress area of the cross-section, i.e. mid-depth.

This study focused on developing three prototypes of composite beam using laminated bamboo. These prototypes are illustrated in Figure 1.2 and can be described as follows:

1. An **I-Bone Laminated Bamboo Hybrid Beam** which is created by introducing an I-shaped laminated bamboo in the high shear stress region. By doing so, theoretically engineered bamboo will carry most of the flexural and shear loading while low-grade timbers on the sides can contribute to the horizontal shear resistance and complement to the cross-sectional rigidity and stability.
2. **Engineered Bamboo I-Beam** and **Engineered Bamboo Double I-Beam** which are fully made of laminate bamboo. The multi-web composite beam can be highly efficient by providing greater mechanical performance using less material.

Combining the laminated bamboo and low-grade timber species not only produces a high-performance, cost-effective and efficient building material but also beneficial in terms of contributing to the economy of the underutilised wood resources.

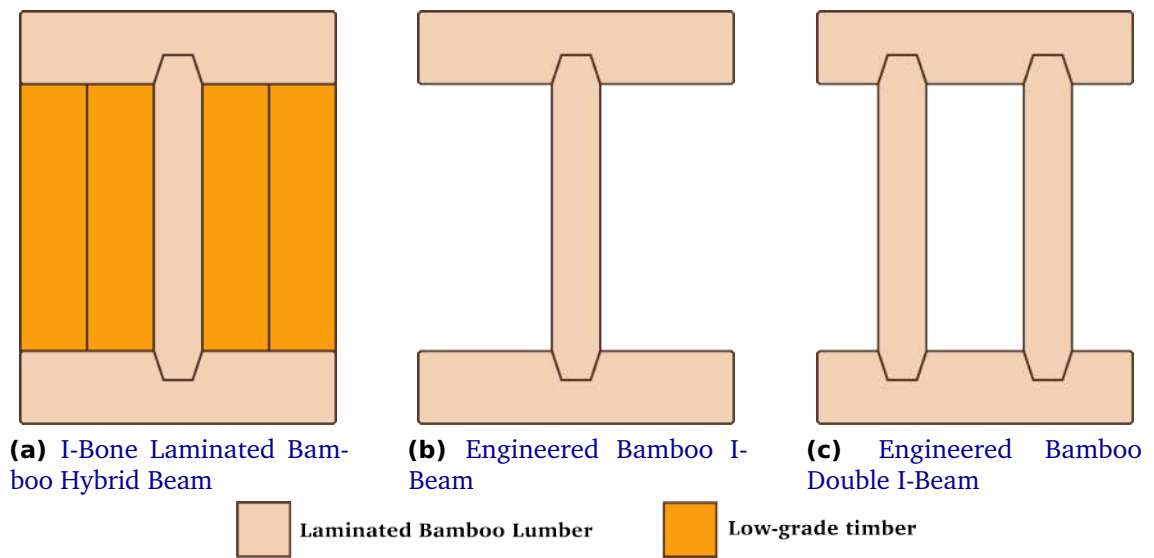


**Figure 1.2:** Laminated bamboo composite beams cross-sections

## 1.4 Aim and Objectives

The primary aim of this study is to develop an I-bone laminated bamboo and low-grade timber hybrid beam and laminated bamboo I-beam and double I-beam. The focus was on experimental evaluations and mathematical modelling.

The aim of this study can be achieved upon successful completion of the following objectives:

1. To investigate the mechanical and physical properties of the constituent materials through a series of experiments.
  - Investigating the tensile and compressive behaviour of the material.
  - Investigate the flexural behaviour of the laminated bamboo lumber
  - Physical properties of the constituent materials for compatibility.
  - Evaluating the suitable testing methods to determine the shear modulus of the laminated bamboo.
2. To develop an [I-Bone Laminated Bamboo Hybrid Beam](#).
  - Manufacturing and developing a guideline for assembly of the hybrid beam.
  - Investigating the flexural properties of the hybrid beam and failure pattern.

- Develop mathematical models to approximate the ultimate values.
3. To develop [Engineered Bamboo I-Beam](#) and [Engineered Bamboo Double I-Beam](#).
    - Manufacturing laminated bamboo I-beam and double I-beam
    - Investigating mechanical properties through experimental and mathematical studies.
  4. To investigate the impact of the butt-jointed laminated bamboo in a vertically laminated composite beam.

Each of these objectives will be addressed in a separate chapter.

### 1.5 Thesis Outlines

#### Chapter 2: Literature Review

This chapter presents a critical review of the background and properties of bamboo and engineered bamboo and their advantages and disadvantages as a construction material. Engineered bamboo timber composite materials are introduced and the gap within this area was identified. Finally, insights into the concept of I-beam laminated bamboo hybrid beam and I-beams are covered and their potential characteristics and prospective applications are outlined.

#### Chapter 3: Material Properties, Testing Methods and Constituent Model

This chapter comprises an introduction of the methodology used, i.e. photogrammetry, for various measurements during the Small Clear Specimen testing and structural size tests. The procedure and results of Small Clear Specimen tests are presented in this chapter and a tri-linear stress-strain model based on the results of these experiments were proposed.

Different methods of evaluating the shear properties of the laminated bamboo are described and the shear modulus of the [Laminated Bamboo Lumber \(LBL\)](#) was determined using the torsion test. The torsional behaviour, in particular, Saint-Venant's end effect of structural timber and laminated bamboo is also investigated through the torsion test. The identified discrepancy elucidated and the recommendation to the current testing standard, i.e. BS EN 408, for the torsion test is included in this chapter.

### **Chapter 4: I-Bone Laminated Bamboo-Timber Hybrid Beam**

Production and prototyping of the [I-Bone Laminated Bamboo Hybrid Beam](#) is presented in this chapter. The experimental results, failure observations, advantages and challenges of the production process are also presented. Mathematical models to approximate the ultimate values, based on the linear and non-linear behaviour of laminated bamboo, are developed and proposed. A comparison between the mechanical properties of this hybrid beam with other reported composite beams was drawn and presented.

### **Chapter 5: Laminated Bamboo I-beam and Double I-beam**

The production and fabrication process of laminated bamboo I-beam and double I-beam were described and the production challenges were outlined. The results of the experimental investigations together with the failure observations is presented in this chapter. A comparison between the [I-Bone Laminated Bamboo Hybrid Beam](#) and these composite beams were made and the impact of the side timbers was identified. Mathematical models developed to estimate the ultimate bending moment and deflection of the beams.

### **Chapter 6: Butt-Jointed [LBL](#) in a Vertically Laminated Hybrid Beam**

The impact of the butt-jointed laminated bamboo lumber in the vertically laminated composite beam was evaluated through a series of experimental and analytical investigations.

### **Chapter 7: Conclusions and Recommendations**

A summary of the conducted studies along with the major contributions of this research is presented in this chapter. Recommendations for further studies are also outlined.

### **Appendix A: Small Clear Specimen Testing Dataset**

# LITERATURE REVIEW

## 2.1 Introduction

In Chapter 1 the advantages and disadvantages of using timber products in the construction industry were outlined. An introduction to bamboo as a highly renewable and sustainable material was also outlined. Bamboo possesses great characteristics that make it an appealing candidate to substitute timber products in many regions. In its natural form, bamboo evolved in such a way that is efficient, strong and flexible raw material.

In the late decades, due to widespread awareness of global warming, the search for a sustainable and renewable material has risen in the construction industry. This, subsequently, has led to the development of several engineered wood products. Engineered bamboo products are among those which were developed to promote sustainable construction. Fast growth rate, high strength to weight ratio and wide availability are some of the engineered bamboo's advantages.

Bamboo's natural hollow tubular shape and longitudinal fibre orientation make it highly effective in terms of load-bearing when compared to other solid rectangular cross-sections. Despite these strengths, bamboo is not a desirable building material for the modern construction mainly because of its longitudinal variability and tubular cross-sections which makes connections an arduous task.

Bamboo forests cover about 22 million hectares of the world's surface but the bamboo industry has not been efficient in utilising this strong and fast-growing natural resource

(Wang et al., 2017). Therefore, research is focused more on developing and optimising engineered bamboo products using both traditional bamboo processing techniques and modern engineered timber production methods. In this chapter, bamboo and engineered bamboo products will be introduced. Their mechanical and physical properties will be described. Finally, state of art towards combining engineered bamboo and timber in peruse of producing high-performance structural composite elements will be presented.

### 2.2 Bamboo

Bamboo is a giant grass belonging to a family that is known as *Poaceae* and subfamily of *Bambusoideae*. It is regarded as one of the most versatile and the fastest growing plant on Earth. However, its growth rate varies depending on the species, location, climate and soil condition (Liese and Köhl, 2015).

Throughout human civilisation, bamboo has a long and deep relationship with human life, from providing food to being burned as an energy source. There are nearly 1500 identified species of bamboo categorised into 119 genera and classified into three main tribes: *Arundinarieae* (also known as temperate woody bamboos), *Bambuseae* (tropical woody bamboos) and *Olyreae* (hervaceous bamboos) (Clark et al., 2015). Among these three tribes, woody bamboos possess unique characteristics that make them promising wood substitutes. For example, they have an extremely fast growth rate and are stronger in the periphery, which makes them effective in resisting bending stress, and they can create great structures due to the nodes which create diaphragms to mitigate buckling (Trujillo et al., 2013).

Bamboos are naturally found in a range of different habitats, from humid tropical forests to temperate regions. With the exception of Europe, there are natural bamboo forests in every continent. Due to variety in species and habitats, different bamboos exhibit different characteristics (Benton, 2015). The growth rate may vary from 20cm to 100cm a day, wall thickness varies from solid cross-section to as thin a couple of centimetres, the position and distance between nodes, and culm straightness which may be nearly straight or zigzag (Liese, 1987). These differences alter the properties of bamboo, most notably the straightness which is very important when it comes to engineered bamboo production.

Bamboo's growth pattern has similarities with both grass and tree. It grows like grass

with respect to cylindrical aerial stems (culms), lance-shaped leaves and flowering but is distinguishable by culm longevity. It is similar to a tree in branching and lignification. The growth pattern is similar to the palm tree exhibiting only primary growth with almost no secondary growth (Clark et al., 2015). This means they emerge from the shoot-root system, i.e. rhizome, with distinctive circumference and grow only vertically without significant change in diameter throughout their lifetime.

Their vertical growth is mainly through the elongation of internodes until reaching their full length of 10-30 m within 2-4 months. The primary diameter of the culm is determined by the age, health and size of the bud, where it develops from the rhizome. The diameter and thickness of the culm and stem increase only marginally during and stops upon completion of elongation (Banik, 2015b).

This primary growth follows by lignification where bamboo culm gains strength during the rest of its life. For the construction applications, the ideal harvesting seasons are autumn and winter at the age of 3-5 years. Bamboos older than 5 years are stronger and harder but the outer layer of the culm will become impermeable for treatments (Banik, 2015a).

### 2.2.1 Anatomy and Fine Structure

Properties of the bamboo culm are mainly determined by its anatomy and fine structure (Liese, 1985). Bamboo culm is divided into nodes and internodes (Figure 2.1a). Internodes are fundamentally hollow tubes (Figure 2.1b) which their cells oriented axially along the culm height.

Whereas, the nodes are solid joints that their cells vastly oriented transversely (Figure 2.2). In most bamboos, the axial cells, i.e. vascular bundles, pass through the transverse cells of the nodes into the next internode. This allows the nodes act as the diaphragm and contribute toward resisting the lateral forces from the wind.

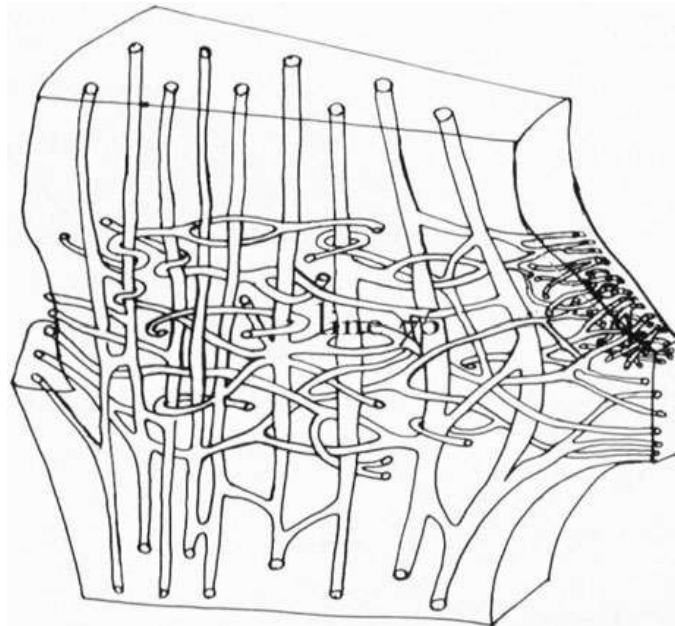
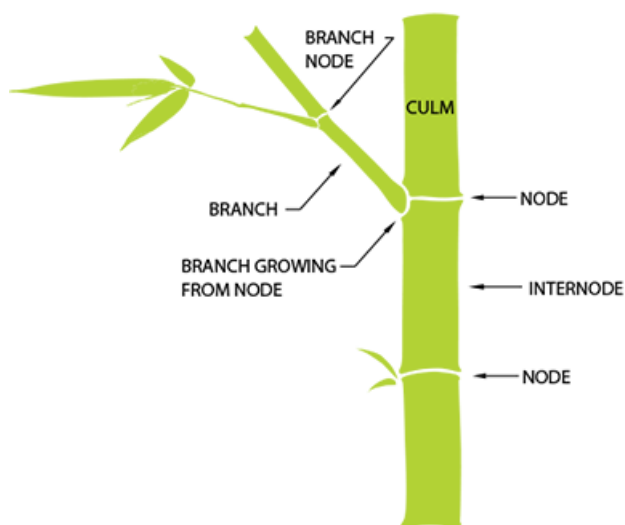


**Figure 2.2:** Bamboo’s node structure and fibres orientations (Liese and Köhl, 2015)



**(a)** Anatomy of a bamboo culm



**(b)** Section of a bamboo culm

**Figure 2.1:** Anatomy and a section of a bamboo culm (Botanicals)

With respect to the fine structure, the constructive members of a bamboo wall can be divided into three parts. *Epidermis*, which is the shiny and hard outer most layer, *parenchyma*, which is a soft matrix material that contributes about 50% of volume and *vascular bundle*, which is a dark and hard material accounts for the other 50% of a bamboo culm’s volume. The percentage of these contents may vary based on the species, but their distribution

pattern is similar within a culm both horizontally and vertically (Liese, 1987).

The epidermis contains wax and silica which weaken the adhesive bonding of bamboo, therefore, it is removed for the engineered bamboo production. The vascular bundle, on the other hand, is the primary load-bearing structure of bamboo which consists of Metaxylem Vessels (V), Fibres (F) and Phloem (Ph) (Figure 2.3) (Liese and Köhl, 2015).

The shape and form of a vascular bundle vary in different bamboos but comprises the same components. The vascular bundle is embedded in a matrix of parenchyma cells. The formation of the vascular bundle is clearly visible in the cross-section of a bamboo (Figure 2.3b). The Metaxylem vessels (V) is responsible for transferring water along the culm. Fibres, which can be in the form of sheaths or individual strands, contribute about 40% of the volume and 60-70% of the weight of the culm. Fibres determine the strength and specific gravity of the bamboo culm (Liese, 1987).

Phloem is responsible for transportation of foods and assimilates to the different parts of bamboo culm and storing them in the parenchyma through large and small tubes which connected each other with pores (Liese, 1987). Vascular bundles are much denser and smaller in size in the outer layer of the wall and become sparse and bigger toward the inner layer. Consequently, fibres, as the muscles of bamboo culm, also follow a similar distribution pattern. In the height of the culm, fibres are distinctly more in the upper part of the culm resulting in the superior slenderness (Liese and Köhl, 2015; Amada et al., 1997).

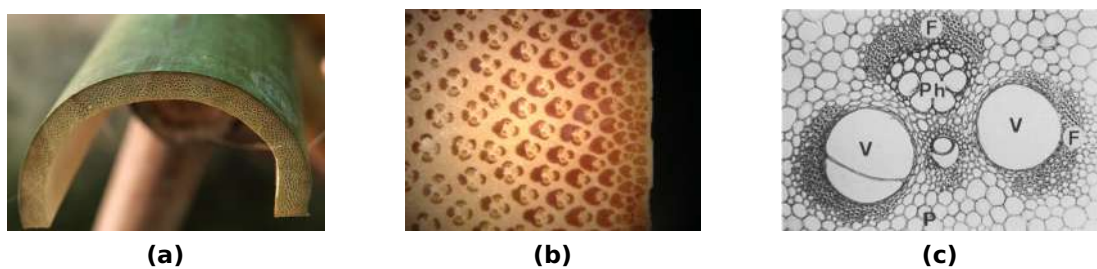


**Figure 2.3:** Cell structure of a bamboo (a) Bamboo culm cross section (b) Bamboo culm cross section (c) Vascular bundle of bamboo (V=Vessel, F=Fibre sheath, Ph=Phloem, P=Parenchyma) (Liese, 1987)

### 2.2.2 Bamboo's mechanical properties

Bamboo and wood share similar attributes, for example, both are orthotropic materials with similar physical and thermal behaviours. Bamboo presents its advantages over other building materials in its eco-friendliness as it is a highly renewable material. Bamboo's mechanical properties rival the structural timber, and in some species possesses the strength that is comparable to the high-grade hardwood, e.g. D40. (Kaminski et al., 2016). The strength of bamboo increases parabolically from the inner layers to the outer layer of the wall. This is due to fibre distribution across the radial direction. Bamboo fibres are reported to exhibit the tensile strength as high as 610MPa, while the parenchyma matrix has the tensile strength of about 50 N/mm<sup>2</sup> (Amada et al., 1997).

To quantify the mechanical performance, studies have reported that *Phyllostachys pubescens* Mazel (referred to as Moso bamboo) exhibits tensile modulus ranging from 5-25 kN/mm<sup>2</sup> and the tensile strength of 100-400 N/mm<sup>2</sup> (Amada et al., 1997; Lakkad and Patel, 1981). In contrast, bamboo is weak in perpendicular-to-fibres direction; this is due to lack of fibres in the transverse direction. The lack of transverse fibres and weak parenchyma matrix cause its proneness to split.

### 2.2.3 Bamboo's limitations as a construction material

Although bamboo is a strong and highly renewable natural material, there are limitations in the use of bamboo in the construction industry which makes it less desirable for practitioners than structural timber. These limitations include: i) lack of a reliable design standard which limits the engineers to use it as a building material; ii) the variation in bamboo's cross-section makes it difficult to form a reliable connection; iii) proneness to splitting; and iv) low transverse strength.

Engineered bamboo products have mitigated these limitations by reforming the cross-section of the bamboo into a more conventional form, e.g. a rectangle. Engineered bamboo products have lessened bamboo's impediments in its use as a structural element, most notably cross-sectional variation and inefficiency to create a solid connection.

## **2.3 Engineered Bamboo**

Bamboo is a sustainable, biodegradable and abundant resource, and is primarily used in the form of composite products such as bamboo scrimber, ply bamboo, oriented strand board and, most importantly, laminated bamboo lumber (Abdul Khalil et al., 2012; Yu et al., 2015; Wang et al., 2017).

Laminated bamboo lumber and bamboo scrimber are the two most known engineered bamboo products which are widely accessible and used for the flooring and the surface applications. However, these applications do not employ the true structural capacity of bamboo. Thus, in recent years more researchers have been interested to investigate the structural performance of the engineered bamboo products and promote its applications in the construction industry (Sharma et al., 2015a; Li et al., 2018; Gong et al., 2016; Paudel, 2008).

### **2.3.1 Bamboo scrimber**

The bamboo scrimber, also known as bamboo bundle veneer or parallel strand bamboo, is produced by splitting and crushing bamboo culm, coating the bundles in resin and then compressing (hot or cold) to the desired density and thickness (Figure 2.4). Researchers have developed several methods of processing and producing bamboo scrimber (Nugroho and Ando, 2001; Nugroho and Ando, 2000; Lee et al., 1998). Bamboo scrimber has a higher rate of raw material usage compared to other bamboo-based composite products due to its unique manufacturing process (Yu et al., 2015; Sharma et al., 2014). It also possesses higher density and higher mechanical properties which can potentially make it an ideal sustainable structural material (Zhong et al., 2017; Gong et al., 2016). However, it is less favourite as a building material due to its high density and high residual stress (Wang et al., 2017).



**Figure 2.4:** Bamboo scrimber

### 2.3.2 Laminated Bamboo Lumber

The laminated bamboo lumber appears to be an ideal building material according to many researchers due to its easy and well-established production process and high strength to weight ratio (Sharma et al., 2015a; Mahdavi et al., 2012; Li et al., 2018). The manufacturing process of laminated bamboo lumber is depicted in Figure 2.5. Laminated bamboo lumber is produced by splitting bamboo culm into small strips and planing the edges to form strips with a rectangular cross-section. The strips were then coated in treatments and resin, and finally, laminated horizontally or vertically to produce laminated bamboo boards (Figure 2.6). The process of manufacturing laminated bamboo lumber makes it denser than bamboo itself and most of the softwood timbers (Sharma et al., 2015a).

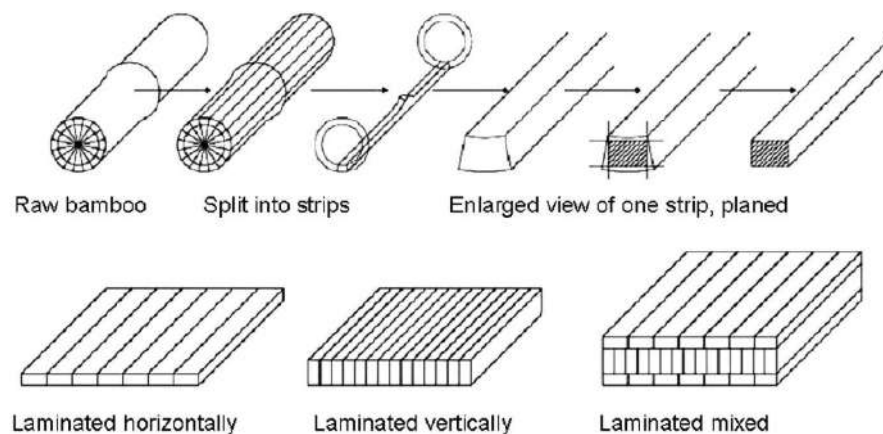


**Figure 2.5:** General production procedures of laminated bamboo board (Rittironk and Elnieri, 2008)



**Figure 2.6:** Laminated bamboo lumber cross-section

### **2.3.3 Mechanical characteristics of laminated bamboo lumber**

Laminated bamboo is considered to be a fibre reinforced composite material by its nature, and the density of the fibres in the laminated bamboo significantly influences its mechanical performance (Penellum et al., 2018). In addition, the treatment process can impact the mechanical properties. Among various methods of treating laminated bamboo lumber, thermal treatment increases the compressive and shear strengths parallel to fibres, while caramelisation decreases the tensile strength parallel to fibres (Sharma et al., 2015b). Bleaching and carbonising are also other methods of treating the bamboo strips before lamination. These treatment methods are usually undertaken by the manufacturer to achieve the desired colour.

With respect to the mechanical properties, laminated bamboo lumber has comparable stiffness but higher strength than some of the most commonly used wood species such as Spruce, Douglas fir and Birch (Rittironk and Elnieri, 2008). Although global research has investigated the structural performance of laminated bamboo for structural applications, manufacturing process, equilibrium moisture content and treatment process can influence the reported properties (Sharma et al., 2015a; Li et al., 2016; He et al., 2015a).

Laminated bamboo under tension behaves similar to wood and bamboo itself; an elastic deformation with the brittle failure (Sharma et al., 2015a). Laminated bamboo which is

made of the middle part the bamboo wall exhibits higher tensile behaviour (Rassiah et al., 2014). Therefore, in the production of the laminated bamboo lumber, mostly the middle parts were used and the outer and inner layers were trimmed.

Li et al. (2013) evaluated the compressive performance of laminated bamboo and reported that the mean and characteristic compressive strength and modulus with respect to the bamboo's height increase. However, this increase is coupled with an increase in strength variation. Laminated bamboo behaves in a tri-linear manner in compression. This behaviour starts with an elastic initiation followed by elastic-plastic deformation, and finally, large plastic deformation. This, unlike under tension, shows higher ductility (He et al., 2015a).

### **2.3.4 Environmental impacts of laminated bamboo lumber**

The timber construction can have economic and environmental benefits to the construction industry as they are predominantly pre-manufactured and brought to site for rapid assembly. This is, not only reduces the cost of the construction and the machinery required on-site but it also reduces the weight of the structure, thus, less material for the foundation. Some might argue that the use of timber can introduce deforestation, however, generally this deforestation is to increase the agriculture lands and not logging timber (Ramage et al., 2017). However, global attention was drawn toward managing the timber resources strategically while planting more tree for the future.

Bamboo is a rapidly renewable material with a growth rate that has no competitor among trees. The maturing time for bamboo culm is 4-5 years and this is considerably faster than tree counterparts such as Sitka Spruce, which is harvested after 35-45 years (Moore, 2011). This fast-growing quality and its ability to be harvested yearly while new bamboo starts to emerge from the ground, make bamboo highly advantageous over wood. Bamboo's yearly yield per forest area is higher than trees so one laminated bamboo frame house with a floor area of 175 m<sup>2</sup> can be constructed using one hectare of bamboo forest (Flander and Rovers, 2009).

Depending on the bamboo product, the production efficiency can be as high as 80% for products like bamboo scrimber and about 30% for laminated bamboo lumber (Lugt, 2008). The biomass can be used in the secondary industries such as producing chopsticks, toothpicks, pencils and charcoal. Bamboo biomass can also be used to generate energy

through bamboo-based biomass gasifier. This process converts bamboo into combustible gas which can be used in the combustion engine or gas turbines (Banik, 2015a).

The environmental life cycle analysis (LCA) of bamboo was carried out by Lugt et al. (2006) and the environmental impact of bamboo was evaluated.

## 2.4 Engineered Timber and Bamboo Composites

Engineered wood composite products have become more prevalent in the structural design and the demand is rising as the industry seeks sustainable and natural materials. Optimised and engineered sections such as cross-laminated timbers and I-beams have changed the course of environmentally friendly construction. The wood composites have mitigated the strength variation and low stiffness limitations of the structural solid timbers.

### 2.4.1 Wood engineered composites

Glue laminated timber or Glulam is one of the well-known timber composites that comprises of layers of solid timbers that are vertically or horizontally laminated. Glulam has enabled architects and engineers to design and construct longer spans and taller buildings.

Cross-laminated timber (CLT) is another wood composite that the solid lumbers are laminated in a 90° degree with respect to the layer below. This provides higher stiffness and rigidity and contributes toward resisting higher loads in the longer spans.

Timber I-beams and I-joists have also been in use for many years and well-embraced by the construction industry as they provide the optimum structural performance using less material (Leichti et al., 1990b).

### 2.4.2 Engineered bamboo composites

The research on bamboo products is primarily focused on the characterisation of bamboo and engineered bamboo products for the structural applications (Trujillo et al., 2017; Sharma et al., 2016; Trujillo and López, 2016; Sharma et al., 2015a; Paudel, 2008). Considering the superior tensile and compressive strengths of the engineered bamboo products, little attention was drawn to combining engineered bamboo and wood to create

a high-performance composite material (Kaboli and Clouston, 2019; Xu et al., 2018; Sinha and Clauson, 2012).

### **2.4.3 Glue laminated bamboo beams**

Glue laminated bamboo beams are reported to have immense mechanical properties with strength-wise considerably stronger than the conventional wood composites beams (Li et al., 2016; Zhang et al., 2014). The dominant characteristic of engineered bamboo glulam beam over the solid and engineered wood products is the flexural and tensile strengths (Sinha et al., 2014). Similar to wood, the mode of failure for these type of beams is also categorised as tensile and brittle failures.

One innovative type of engineered bamboo material, with the trademark of GluBam, developed by Xiao et al. (2008), has shown great performance and potential to be used in the construction. Xiao and his research team have investigated various aspects of GluBam. The applications of this beam are currently limited to a few case studies such as roof trusses (Xiao et al., 2013), short-span bridges (Xiao et al., 2014a) and structural beams for the residential buildings (Xiao et al., 2014b).

### **2.4.4 Bamboo and engineered bamboo as a reinforcement**

Bamboo and engineered bamboo were attempted to be employed as the reinforcement to the concrete members substituting the synthetic materials such as steel and glass fibres (Ferreira et al., 2016; Ikponmwosa et al., 2015; Ghavami, 1995). These studies have all concluded that bamboo reinforced concrete possesses great mechanical properties and can potentially replace the steel to reduce the cost of the housing in the developing countries thereby saving the natural resources and aid the economy of the local industry.

On the other hand, bamboo fibres which are regarded as "natural glass fibre", possess high strength to weight ratio, easy accessibility, low cost and biodegradability which make it stand out in the composite manufacturing (Abdul Khalil et al., 2012; Yang et al., 2010). The reported tensile strength of the bamboo fibres is 500-575 N/mm<sup>2</sup> which is substantially higher than that of structural steel ( $f_t=300$  N/mm<sup>2</sup>) and glass fibres ( $f_t = 124-150$  N/mm<sup>2</sup>) (Abdul Khalil et al., 2012). Thus, this superior strength has encouraged researchers and manufactures to use it as the reinforcement for the composite materials.

### **2.4.5 Engineered bamboo and timber hybrid beams**

Wood is a natural material with numerous environmental and structural advantages, but it also possesses limitations such as long growth cycle and strength variations. In addition, some fast-growing wood species such as spruce can perform weakly in tension and bending. Although Glulam beams have enhanced the strength and stiffness of these materials and minimised the variations in the material properties. An optimum scenario is to employ these low-performance wood species combined with the stronger species in the composite beams.

Engineered bamboo is believed to have high mechanical performance whilst its constituent material, bamboo, is the fastest growing plant on the earth (Sharma et al., 2014). Combining engineered bamboo and low-grade timber not only would result in a hybrid material which suppresses the limitations of both but also enhances the structural performance. This helps boost the economy of those fast-growing wood species. The engineered bamboo and timber composite beam is an emerging field of investigation which currently is limited to the laboratory investigations (Kaboli and Clouston, 2019; Xu et al., 2018; Sinha and Clauson, 2012).

In a recent study by Xu et al. (2018) the flexural performance of the engineered bamboo and spruce hybrid beam was compared with the laminated wood beams. They reported that the horizontal shear failure is one of the frequently occurred modes of failure in the composite beams, indicating that the mid-depth lacks the reinforcement. The reported bending modulus of a six layers laminated beam that bottom two layers and the top layer were laminated bamboos and the mid-layers were spruce, was 6110 N/mm<sup>2</sup>. This bending modulus was lower than the spruce glulam beam ( $MOE_{spruce} = 7770$  N/mm<sup>2</sup>). However, the strength of this composite was 46% higher than that of the spruce laminated. Considering the results of Xu et al. (2018), the performance of the hybrid beams can be improved significantly by addressing the horizontal shear tearing in the wood species. By doing so, the composite beam will perform to its full flexural capacity.

Lee et al. (1997) investigated the suitability of the laminated bamboo to be used as a structural material by combining it with southern pine **Oriented Strand Board (OSB)**. Top and bottom layers of the composite beam were laminated bamboo and core was **OSB**. They concluded that using laminated bamboo as flanges improves the stiffness by a factor of

up to 2 and the bending strength by a factor of 3.4. A similar experiment conducted by [Sinha and Clauson \(2012\)](#) but using Douglas fir instead of OSB in the core region. They reported that the bamboo timber composite beam has an enhanced bending strength when compared to Douglas fir Glulam beams, however, the stiffness was only comparable. The horizontal shear stress was also reported as one of the prime failure reasons.

Researchers have also attempted to reinforce the low-grade wood resources by using engineered bamboo in a composite material ([Kaboli and Clouston, 2019](#); [Chen et al., 2017](#)). Not only this promotes the use of sustainable materials but can lead to international joint collaborations.

[Kaboli and Clouston \(2019\)](#) have introduced laminated veneer bamboo into the tensile layer of the vertically laminated Eastern hemlock Glulam beams. They reported that the composite material illustrated 16% higher bending modulus and 57% higher bending strength compared the unreinforced beams. The composite beam has also shown about 30% better ductile behaviour.

[Chen et al. \(2017\)](#) have investigated the mechanical properties of the composite beams which comprised laminated veneer bamboo and wood veneer made of the poplar tree. Various lay-ups of material were investigated under different loading conditions, i.e. loading perpendicular or parallel to the glue line. They concluded that by placing engineered bamboo at the top and bottom layers, the flexural properties of the composite material increases considerably. However, the laminated bamboo veneer is denser than wood veneer, thus more laminated veneer used in the composite, the higher the weight of the end product will be. Thus, [Chen et al. \(2017\)](#) have reported that to achieve the optimal lay-up with respect to the cost and the performance, top and bottom layers, and mid-depth layer need to be the stronger material, in this case, laminated bamboo veneer.

[Liu et al. \(2016\)](#) have investigated the impact performance of bamboo and poplar laminated composite, and bamboo and bi-directional woven glass fibres composite. [Ashaari et al. \(2016\)](#) have studied the physical and mechanical properties of the compreg laminated bamboo and wood. The compregnation technique is where the laminae were impregnated with resin and hot-pressed to form the laminate. Despite the higher mechanical properties of this product, the density of the composite was high as well.

To date, several studies have investigated different aspects of developing engineered bamboo and timber composite material. Considering all the reviewed studies here, the laminated bamboo and timber composites possess comparable properties, and in many respects better than engineered wood products with the added high renewability advantage. However, the horizontal shear/tearing failure was reported as one of the dominant failure modes in many combinations. This mode of failure may be due to high strength difference between the outer and inner layers, i.e. the flanges and the web. This can cause challenges in the path towards promoting the use of the fast-growing natural resources. A possible solution is to enhance the mid-depth of the beam to prevent this mode of failure while also improving the stiffness of the composite material.

Therefore, this study aimed to develop a composite beam by strengthening the mid-depth by introducing a laminated bamboo web. The concept of this study is elucidated in Section 2.5.1 and the experimental and the analytical evaluations are presented in the following chapters.

### **2.4.6 Engineered bamboo and timber I-beams**

The I-beams are undoubtedly among the top structurally optimised sections which are very efficient in regards to the bending and shear resistance. The flexural stiffness is high due to the concentration of the materials away from the neutral axis, thus provides higher load-bearing capacity (Harte and Baylor, 2011). The flanges carry most of the bending moment while the web takes the shear stress. The I-sections have been in use in the timber industry in the form of I-joists and I-beams for several years.

Prefabricated wood I-joists have contributed immensely in the timber house construction. They are optimised, lightweight and cost-efficient than sawn timbers. Many forms such as multi-webs and different flange-web joints have also been researched by scholars and have been in use for many years (Leichti et al., 1990b; Jahromi et al., 2006).

Although laminated bamboo seems to be an ideal material to be used in the flanges of an I-beam, it is not well recognised in the structural composite production. Research is yet to address several aspects such as finger joint configuration and equilibrium moisture content relevancy to the mechanical properties. In attempts to promote the engineered bamboo products in the construction industry, researchers have been working on developing

engineered bamboo I-joist and I-beams (Aschheim et al., 2010; Tang et al., 2019; Paniagua and Moya, 2014).

Aschheim et al. (2010) have explored the possibility of using the finger-jointed laminated bamboo in the I-joist production. They manufactured two types of engineered bamboo I-joists which are differentiated by the web's material; using bamboo oriented strand boards and three-ply laminated bamboo in the web and finger-jointed laminated bamboo in the flanges. Based on their results, finger joints significantly impacted the mechanical performance of the I-joist and the beams failed predominantly at the joints. Thus, further investigation on developing an efficient finger joint profile is required. The flexural strength of the engineered bamboo I-joist was 36 N/mm<sup>2</sup> and the bending modulus was 14 kN/mm<sup>2</sup>.

Glulam was also used in the fabrication of I-joists. Tang et al. (2019) have investigated the structural performance of Glulam I-joists for the short- and long-spans (2.4m and 7.5m). This composite I-joist exhibited higher mechanical performance than the laminated bamboo and timber I-joists. The finger joints were the fracture initiator and lateral-torsional buckling was also reported, which signifies the importance of the cross-sectional integrity.

Engineered bamboo I-beams can provide sufficient strength and stiffness to be used in the short- to medium- span beams and bridges. Wu (2014) conducted experimental studies to develop I-shaped engineered bamboo beams. Although they reported enhanced mechanical performance for the tested beams, the web and flanges connection can be improved in their manufactured I-beams. They have used steel bolts and brackets to strengthen the connection. This type of connection can cause stress concentrations and impose early failure, and it did.

In summary, engineered bamboo I-shaped beams and joists exhibited higher mechanical strengths and comparable stiffness, however, the variety in the available constituent materials introduced variation in the reported mechanical performance of the final products. The finger joints can provide solid connections to achieve longer and deeper laminated bamboo lumbers, however, due to the fibrous nature of the bamboo, developing a reliable finger joint profile seems a necessity in achieving this. To date, there have been no reported investigations on the development of the laminated bamboo multi-web I-beams.

This study aimed to develop laminated bamboo I beam without any finger joint to evaluate

the performance and the weakness of the proposed beam. Furthermore, laminated bamboo double I-beams have also been targeted to manufacture and evaluate for the first time.

## 2.5 Laminated Bamboo Composite Beams

During this study three laminated bamboo-composite beams were designed and developed.

i) [I-Bone Laminated Bamboo Hybrid Beam \(IBHB\)](#), ii) [Engineered Bamboo I-Beam \(BIB\)](#) and iii) [Engineered Bamboo Double I-Beam \(BDIB\)](#).

### 2.5.1 The concept of I-bone laminated bamboo hybrid beam

The I-bone laminated bamboo hybrid beam is a new concept in the engineered wood products with no similar product reported in the literature. This composite beam consists of an I-shaped laminated bamboo embedded in the glulam beam. The composition of the laminated bamboo and low-grade timber potentially provides higher structural qualities while promoting the better utilisation of these natural resources. The elements of the I-shaped laminated bamboo were joined together using the adhesive in the grooved channel, similar to the wood I-joists. The side timber provides additional structural integrity and stability while improving the horizontal shear resistance which was one of the dominant modes of failure in the engineered bamboo beams.

### 2.5.2 Cross-sections of the composite beams

Figure 2.7 illustrates the proposed cross-sections. These lay-ups have not been investigated through experimental nor analytical studies before. Hence, the findings of this study shed new light on the innovative ways of using engineered bamboo in the construction industry. Due to the cumbersome manufacturing process of these beams in the laboratory environment with the limited equipment, two prototypes of each section were fabricated and tested. The fabrication process recommendations using industrial machinery is also provided in the correlating chapters.

The primary reason to the proposed cross-sections is the fact that an I-beam is highly optimised in regards to material use while providing better structural performance than solid sections. Thus, it is aimed to create a load-bearing I-beam for these sections. On the

other hand, the proposed cross-section have similar dimensions to the experimental studies conducted by [Sinha and Clauson \(2012\)](#) and [Kaboli and Clouston \(2019\)](#). This is to enable the findings of this study compared with the properties reported by these studies.

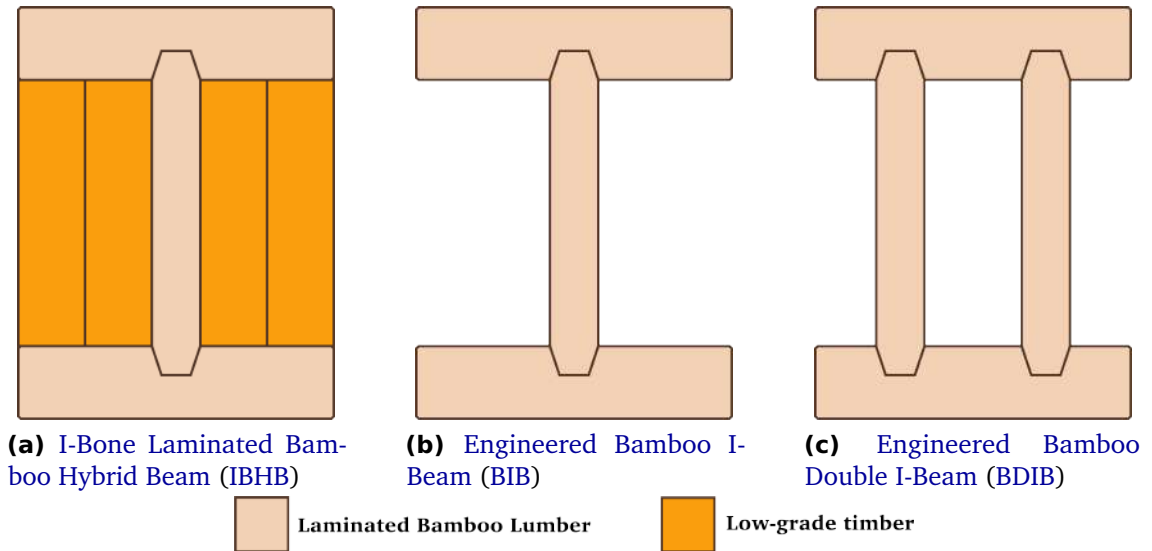


**Figure 2.7:** Laminated bamboo composite beams cross-sections

### 2.5.3 Potential advantages and limitations

[IBHB](#) can potentially have several advantages over the timber or other laminated bamboo composite beams. Employing low-grade timber can develop the value-added market to the underutilised wood species. Combining engineered bamboo and timber reduces the weight of the composite while enhancing the strength and stiffness. The cross-section of [IBHB](#) has better dimensional stability and is compatible with the available joist connectors.

[IBHB](#) has also more resistant to warping and splitting as these commonly occur in the timber members. The side-timbers provide extra resistance to the shear stress while preventing the flanges from buckling. Due to the efficient cross-section, [IBHB](#) can span longer and reduce the weight and size of the conventional Glulam beams.

With respect to the limitations of these beams, the production of the [IBHB](#) requires the side-clamping mechanism and this may impose new costs to the manufacturer. In addition, these beams are not easily customisable for particular joints or shapes. For example, the end of the beams cannot be profiled to fit into the joint. The height of these beams is also another limiting factor in manufacturing them.

In regards to the laminated bamboo double I-beam, thermal and sound insulations can be injected between the webs to increase the efficiency.

Another drawback of these beams is their connection to the columns which may required special design depending on the connection.

Engineered bamboo is a costly material when compared to solid timber and glue laminated beams in the western countries (Rittironk and Elnieri, 2008). However, majority of the cost lies in the transportation from the country of origin, e.g. China. Therefore, engineered bamboo composite beams can be cost-efficient in the regions where bamboo grows locally. In addition, future policies to promote the sustainable construction can lead to decreasing the cost production and shipping of engineered bamboo products.

### 2.5.4 Prospective applications

Due to the high strength to weight ratio of IBHB and BDIB and with further investigations and investment, these materials can rival the existing engineered wood products such as Glulams, laminated veneer lumbers and CLTs. They can be used in the short- to medium-spans as the load-bearing components. The prospective applications comprise structural girders, columns, posts, truss cords in the roof trusses and any other load-bearing structural members.

## 2.6 Summary

This chapter presented an introduction into the bamboo as the fastest-growing plant on the Earth with the reported daily growth rate of a meter. Bamboo fibres are one of the strongest raw materials with the tensile strength higher than structural steel and the glass fibres. The anatomy and fine structure of bamboo evolved in such a way that is efficient and optimised in material usage. Fine structure of bamboo is the driving forces behind the superior strength due to the fibre orientation and node distribution along the bamboo height.

Despite the higher mechanical properties, bamboo has not found his place in modern construction. This is mainly due to the cross-sectional variation along the culm and inefficiency in creating solid connections because of its natural hollow cylindrical shape.

Engineered bamboo products were developed to mitigate these drawbacks by reforming its natural shape to more practical cross-section, i.e a rectangle.

Laminated bamboo lumber is one of the most known engineered bamboo products. Due to its relatively easy production process, cost-effectiveness and high strength to weight ratio, it attracted researchers' and practitioners' attention to be used in the structural applications. However, the lack of a standardised manufacturing procedure and design guideline, make the construction industry reluctant in employing it in their designs. The interest among researchers is growing to evaluate and develop the engineered bamboo products that are structurally capable of competing with conventional engineered wood products.

Laminated bamboo lumber is one of the widely used engineered bamboo products primarily for the surface applications. With global research into the structural performance of this material, its utilisation as a structural element is foreseeable. Laminated bamboo lumber is lightweight with high strength. However, due to the various manufacturing methods, its reported mechanical performance varies among the available products.

With respect to the environmental benefits of using bamboo and engineered bamboo products in the construction industry, studies have shown that rapid renewability of bamboo can be highly advantageous in terms of preserving the over-used timber resources by substituting them with the engineered bamboo products.

The centre of research interests is around evaluation and characterisation of the engineered bamboo products to establish the production and design guidelines. This is while there is a great potential in developing a composite material using the engineered bamboo and timber. Previous studies have attempted to develop such composite materials using different methodologies and combinations. However, a common mode of failure in many of these developed composite materials was the horizontal shear tearing which caused due to strength difference between engineered bamboo and wood. This can be mitigated by reinforcing the mid-depth of the developed beams.

Therefore, this study aimed to develop an [I-Bone Laminated Bamboo Hybrid Beam](#) to tackle the horizontal shear failure issue and enhance the stiffness of the composite material and laminated bamboo double I beam to investigate the potential of employing laminated bamboo in the construction industry.

# MATERIAL PROPERTIES AND TESTING METHODS

## 3.1 Introduction

This chapter aims to investigate the mechanical properties of the [Laminated Bamboo Lumber \(LBL\)](#) that has been used in the fabrication of the composite beams. The flexural, tensile and compressive properties of the commercially available [LBL](#) were determined through a series of Small Clear Specimen testing procedures detailed in BS EN 373 ([BSI, 1957](#)). The stress-strain relationship of the [LBL](#) was examined, and a simplified relationship was proposed to derive mathematical models for the hybrid beams. A new method of measuring the displacement and rotation was developed based on the stereo vision system. This photogrammetry methodology is also briefly elucidated.

Finally, torsion test and shear field test methods as the recommended testing standards to evaluate the shear properties of the timber materials were investigated. A thorough evaluation of the end effect in the torsional testing procedure regarding the minimum required distance to measure the relative rotations from the supports is presented. Further recommendations based on the results of these experiments were proposed to be implemented in the following BS EN 408 revision.

### 3.2 Materials

This study mainly consists of three materials; the laminated bamboo lumber, the timber and the glue. An introduction into mechanical, physical and environmental characteristics of laminated bamboo was included in Chapter 2 (Section 2.3). The general properties of the materials that were used in this study are presented in this section. Additionally, the material selections and the specification for each study and the stages of the experiments are outlined in the correlating chapter.

Commercially available laminated bamboo boards made of carbonised Moso bamboo strips with 600 mm width, 40 mm thickness and 2440 mm length were purchased from Bamboo Import Europe BV distributor. According to the manufacturer, Dynea Prefere 4410, a low formaldehyde adhesive was used for the lamination of the bamboo strips. These boards have been manufactured using the bamboo strips without any butt-joint or any other form of connections. Although, sometimes, laminated bamboo lumber or boards produced using smaller and shorter strips of bamboo which are butt-jointed at a section to form a longer and wider board. These butt-joints are concealed by the smooth and joint-free layers at the top and bottom surfaces. A scoping study on the impact of these butt-joints on the flexural properties of the vertically laminated bamboo hybrid beams is presented in Chapter 6.

Regarding the timber, structurally graded C16 Norway spruce timbers were purchased. The timbers were chemically treated to preserve their moisture content when kept outdoors. The chemicals penetrated about 3mm into the specimen from each surface and removed using a Planer & Thicknesser prior to the fabrication process.

Both materials, i.e. LBL and timber, have been kept in the same environment during the conditioning period, but their equilibrium moisture contents (EMC) were rather different. The timber characterisation standards, e.g. BS EN 373, 384, 408 (BSI, 1957; BSI, 2010; BSI, 2012), determine the mean and characteristic values based on the 12% moisture content (MC), and where a higher or lower MC was measured, correction factors apply. On the other hand, engineered bamboo has been reported to have about 6-7% moisture content at its equilibrium state (Sharma et al., 2015a). Therefore, employing timber standards to characterise the bamboo and engineered bamboo may not be the best practice.

Although the EMC of timber and bamboo is different, the engineered bamboo and timber

experience a similar change when their moisture content change; the engineered bamboo's and Timber's strength increase by decreasing the moisture content from the material saturation point (Dinwoodie, 1975; Wang et al., 2014; Xu et al., 2014). These similarities make it reasonable to use the timber standards for characterisation of the bamboo and the engineered bamboo materials until a bespoke standard is available.

### 3.3 Implemented Stereo Vision System

Methods based on the photogrammetry and stereo vision systems have attracted interest among the researchers as a measurement tool. There is a wide range of applications for these systems of measurement which have been developed and tested for the research and practical purposes (SuttonMichaelJean2009; Valena et al., 2012). In particular, they have been used to acquire 3-D information of the subject where this information cannot be obtained using the conventional methods.

The point and surface deflection (Maas and Hampel, 2006; Valena et al., 2012), rotation and shear deformation (Valena and Carmo, 2019; Gharavi et al., 2018b), crack detection and propagation (Valena et al., 2017) and strain profile (Carmo et al., 2015) can be easily extracted using the 3-D information acquired from the photogrammetry.

#### 3.3.1 Limitations with the conventional methods

The displacement and the rotation are required to quantify the mechanical properties of structural material. They are generally measured using the mechanical measurement systems such as Linear Variable Differential Transformers (LVDT) or inclinometers. These measurement systems are accurate and convenient to use, however, they possess limitations which make them impractical for particular applications. These limitations include unavoidable physical contact, single-point/section recording system and the hardware necessity for each measurement.

The objectives of this study require a measuring system that addresses these limitations while maintaining a high level of accuracy. Thus, a close-range photogrammetry method based on the stereo-vision system was developed and employed throughout this study.

### 3.3.2 What is photogrammetry?

Humans and most animals use a highly sophisticated 3D vision system for their visual perception. Similarly, photogrammetry computes disparity, distance and 3D coordinates of any object by simulating and simplifying this highly sophisticated vision system. Photogrammetry is generally based on the binocular stereo vision system where two cameras simultaneously capture the images of an object from different positions and angles (He et al., 2015b). The cameras have the same specifications and parameters, e.g. focus length, iso setting, and are mounted at a short distance from each other, similar to the human eye.

### 3.3.3 The principle behind the photogrammetry

In reality, the stereo vision system setup is more complex, thus simplifications based on the assumption made for the simplified stereo-vision system are required. The basic principle behind the photogrammetry is illustrated in Figure 3.1. There is some level of distortion in the acquired images regardless of the type of the cameras and the lenses, hence, to mitigate this issue, calibration is required.

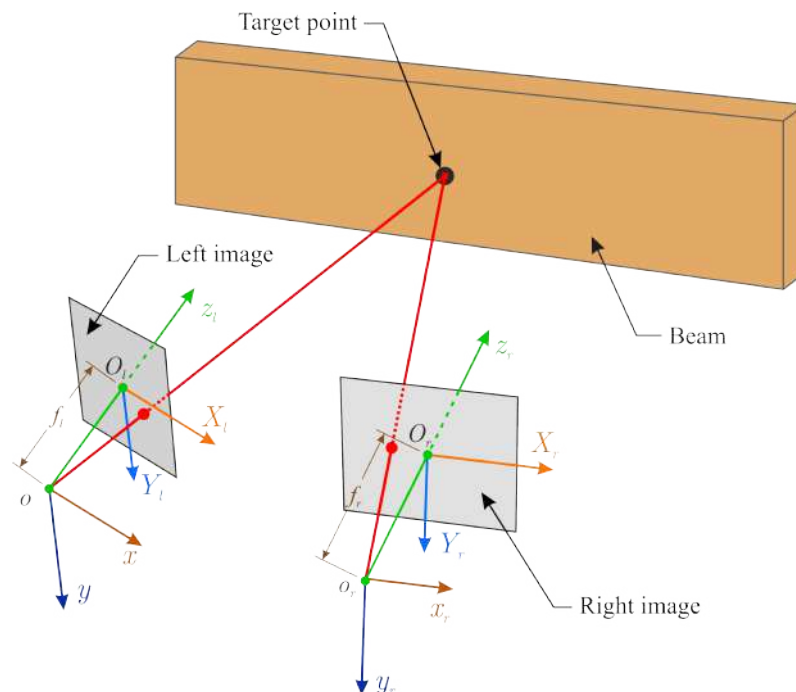


**Figure 3.1:** Binocular stereo vision principle

The 3D coordinates of the target points can be determined using the triangulation and the intersection of the lines. Referencing Figure 3.1, if  $oxyz$  is the camera coordinate systems

(CCS),  $XOY$  is the left and right images coordinate system and  $f$  is the effective focal length. The focal length is the distance between the camera coordinate system (lenses) and the image coordinate system (image sensor within the camera). Parameters that are related to the left and right images are subscripted by  $l$  and  $r$ , respectively. For convenience, the world coordinate system (WCS) is assumed to be the left camera's coordinate system ( $oxyz = o_lx_ly_lz_l$ ).

The spatial positional relationship between the world coordinate system and the right camera coordinate system can be expressed as:

$$\begin{bmatrix} x_r \\ y_r \\ z_r \\ 1 \end{bmatrix} = M \begin{bmatrix} x \\ y \\ z \\ 1 \end{bmatrix} = \begin{bmatrix} r_{11} & r_{12} & r_{13} & t_x \\ r_{21} & r_{22} & r_{23} & t_y \\ r_{31} & r_{32} & r_{33} & t_z \end{bmatrix} \begin{bmatrix} x \\ y \\ z \\ 1 \end{bmatrix} \quad (3.1)$$

where,  $M = [R|T]$ ,  $[R]$  is the rotation matrix and  $[T]$  is the translation transform vector between the world coordinate system ( $oxyz$ ) and the right camera coordinate system ( $o_r x_r y_r z_r$ ):

$$R = \begin{bmatrix} r_{11} & r_{12} & r_{13} \\ r_{21} & r_{22} & r_{23} \\ r_{31} & r_{32} & r_{33} \end{bmatrix}, T = \begin{bmatrix} t_x \\ t_y \\ t_z \end{bmatrix} \quad (3.2)$$

According to the pinhole imaging theory (Wohler, 2013), the following expressions can be made:

$$s_l \begin{bmatrix} X_l \\ Y_l \\ 1 \end{bmatrix} = \begin{bmatrix} f_l & 0 & 0 \\ 0 & f_l & 0 \\ 0 & 0 & 1 \end{bmatrix} \begin{bmatrix} x \\ y \\ z \end{bmatrix}, \quad s_r \begin{bmatrix} X_r \\ Y_r \\ 1 \end{bmatrix} = \begin{bmatrix} f_r & 0 & 0 \\ 0 & f_r & 0 \\ 0 & 0 & 1 \end{bmatrix} \begin{bmatrix} x_r \\ y_r \\ z_r \end{bmatrix} \quad (3.3)$$

For any spatial point in the WCS, the corresponding coordinates in the left and right image can be obtained as follows:

$$\rho \begin{bmatrix} X_r \\ Y_r \\ 1 \end{bmatrix} = \begin{bmatrix} f_r r_{11} & f_r r_{12} & f_r r_{13} & f_r t_x \\ f_r r_{21} & f_r r_{22} & f_r r_{23} & f_r t_y \\ r_{31} & r_{32} & r_{33} & t_z \end{bmatrix} \begin{bmatrix} x \\ y \\ z \\ 1 \end{bmatrix} \quad (3.4)$$

and finally, the 3D coordinate of the object can be obtained as;

$$\begin{cases} x = z \frac{X_l}{f_l} \\ y = z \frac{Y_l}{f_l} \\ z = \frac{f_l(f_r t_x - X_r t_z)}{X_r(r_{31}X_l + r_{32}Y_l + r_{33}f_l) - f_l(r_{11}X_l + r_{12}Y_l + r_{13}f_l)} \\ = \frac{f_l(f_r t_y - Y_r t_z)}{Y_r(r_{31}X_l + r_{32}Y_l + r_{33}f_l) - f_l(r_{21}X_l + r_{22}Y_l + r_{23}f_l)} \end{cases} \quad (3.5)$$

In Equation 3.5, if each camera's focal length ( $f_l$  and  $f_r$ ) and the coordinates of the spatial point in both left and right images are known, the 3D coordinates of the point in WCS can be obtained. The rotation matrix and translation transform vector are determined through the calibration process.

The overall performance of the photogrammetry method strongly depends on the calibration process which determines the photogrammetric parameters such as the relationship between focal lengths, distance to the object and sensor size. The accuracy of the photogrammetry method was examined by [Gharavi \(2015\)](#) and the process was published ([Gharavi et al., 2018b](#)).

### 3.3.4 Calibration process

The camera calibration is a vital procedure in the stereo vision systems. The aim of the calibration is to determine the camera parameters which can be divided into the internal and the external parameters. The internal parameters are the relationship between the camera lens and the image planes and the external parameters described as the position and orientation, i.e. pose, of the cameras relative to the world coordinate system (WCS) and relative to the calibration plate ([SuttonMichaelJean2009](#); [Wohler, 2013](#)). The calibration process starts by acquiring several images of the calibration plate at the different positions and orientations as shown in Figure 3.2.

Each calibration plate is accompanied by an object description file which defines the visual properties of the plate. Usually, the calibration plates are comprised of a finite number of circles with known distances from each other and to the border, as indicated in Figure 3.2. Using acquired images and the description file, the position of the border and the circles can be determined precisely. Using this data, the calibration parameters of the setup, 3D points of the calibration plate and the position and orientation of the cameras relative to each other can be computed.



**Figure 3.2:** Calibration plates

In this study, two types of calibration plates that are identifiable by their size and shape were used. A  $160 \times 245$ mm and a  $100 \times 100$ mm square shape high precision ceramic calibration plates were used which provided a satisfactory accuracy.

### 3.3.5 Photogrammetry setup

As depicted in Figure 3.3, the setup for the employed photogrammetry includes mounting two cameras, referred here as the left and right cameras, at a short distance of each other. This distance can be any distance as long as the target points are visible in both cameras. A remote shutter was used to trigger the cameras at the same time and prevent any accidental movements. Two LED lights lit the dark or unclear surfaces and enabled cameras to take sharper images. In some instances, shoot-through or reflective umbrellas were used to diffuse the sharp lights.

An additional camera was used to capture the applied load from the monitor at the time of measurements. All the cameras triggered simultaneously so the 3-D information of a target point and the applied load were recorded for a particular deflection or rotation.

### 3.3.6 Target points

Two methods/styles of the target points were employed. The first method was through printing the targets (dots) on the adhesive-backed papers and attaching them to the surface of the desired area (Figure 3.4a). The second method was by drawing cross lines using a marker that the intersections of the lines represent the target points (Figure 3.4b). Both of

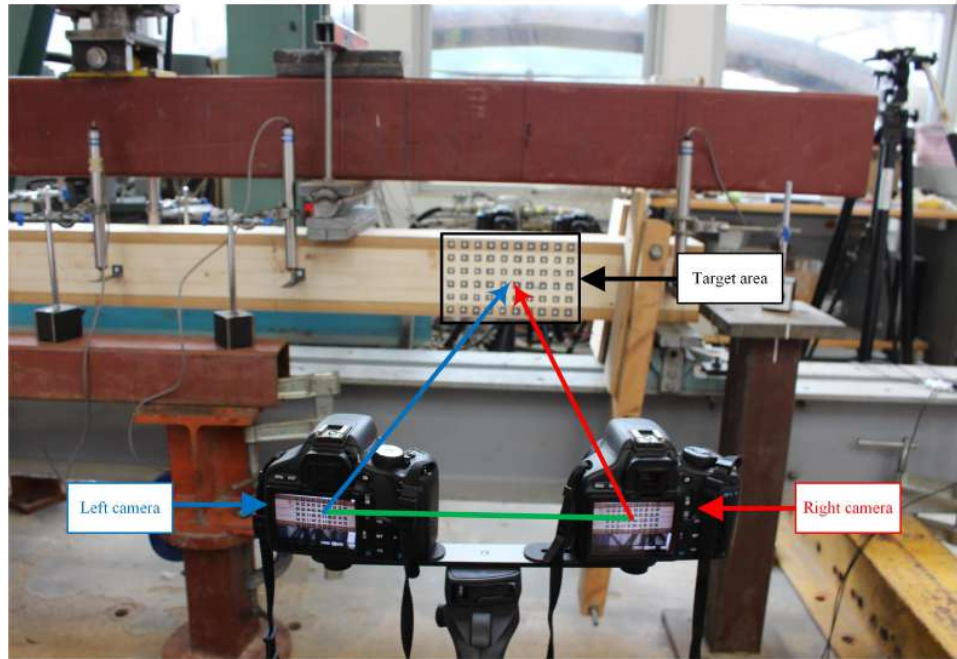
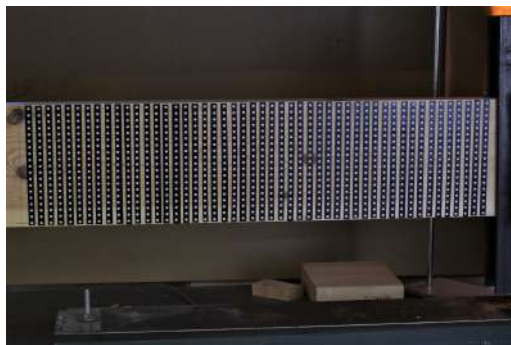
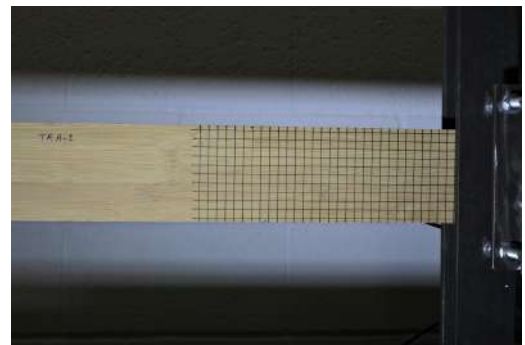


**Figure 3.3:** Stereo vision setup in the Shear Field test



**(a)** Circular target points printed on the paper



**(b)** Cross target points drawn on the surface

**Figure 3.4:** Photogrammetry target points

these methods provided the results with satisfactory accuracy. The stages of extracting the 3D information of each target point were slightly different from each other. Figure 3.5 and Figure 3.6 illustrate the stages of identifying the target points based on each target style.

In the case of the circular targets, once the images were loaded (Figure 3.5a), the process started by selecting the regions of interest based on the greyscale of the target area (Figure 3.5b). This region of interest may cover additional areas within the same greyscale range but must contain all the targeted dots. Pattern recognition filters based on the roundness and size applied to filter-out those additional regions. Then, the centres of the remaining selected regions were appointed as the target point and arranged in a matrix form (Figure

3.5c).

In the case of the cross targets, images were load in the order of capturing (Figure 3.6a), then two edges of the lines at four sides of the cross have been found based on the grayscale difference and the pre-defined threshold range. Next, the mid-point of the edge pairs were calculated and two opposite mid-points formed a line that crosses both points (Figure 3.6b). Finally, the intersection of the two lines was assigned as the target point (Figure 3.5c).

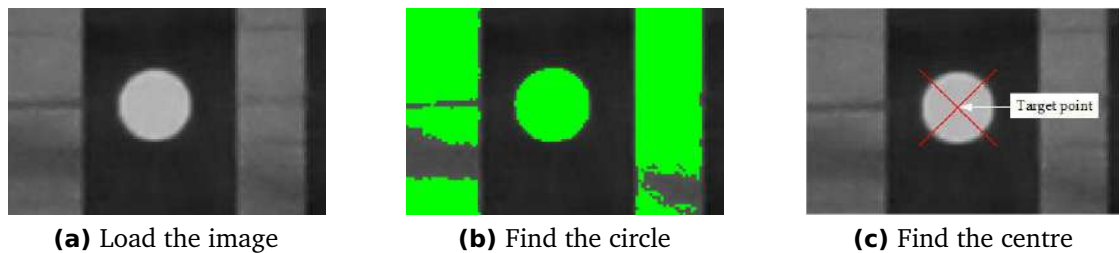


**Figure 3.5:** Extracting the target point based on the dotted target points

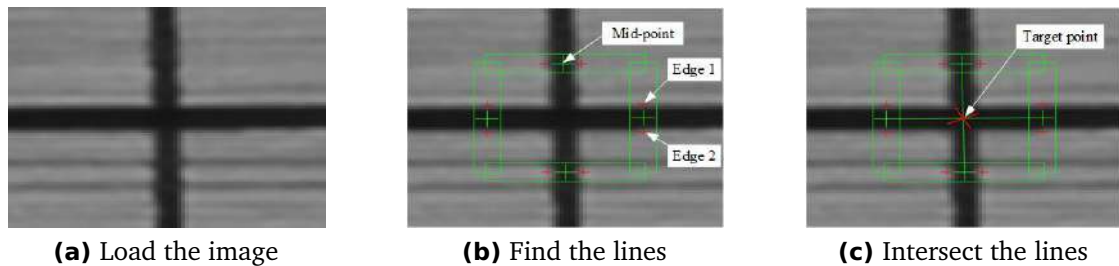


**Figure 3.6:** Extracting the target point based on the crossed target points

### 3.3.7 3-D information acquisition through image processing

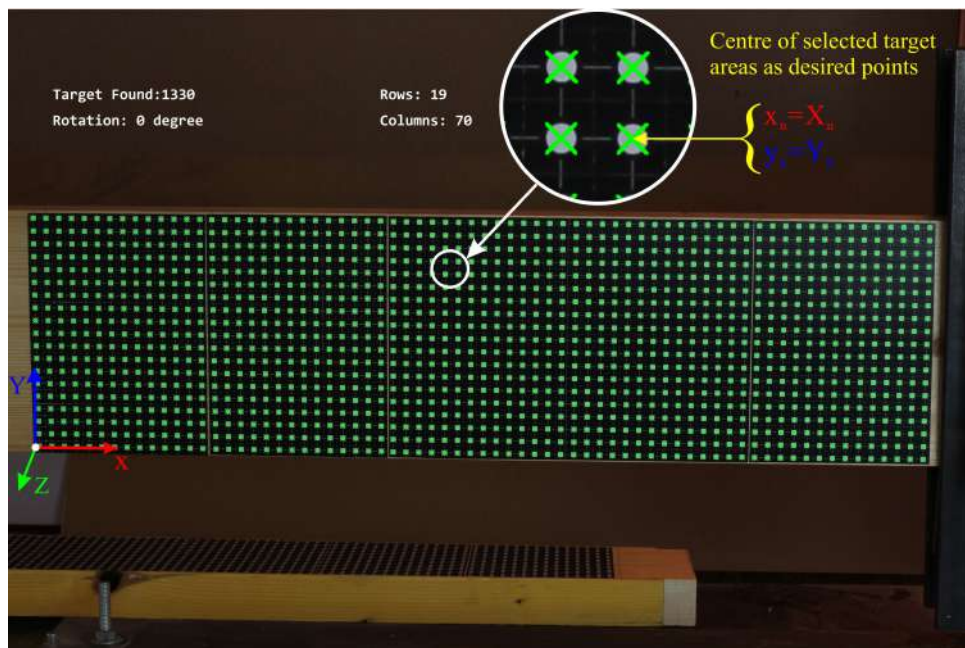
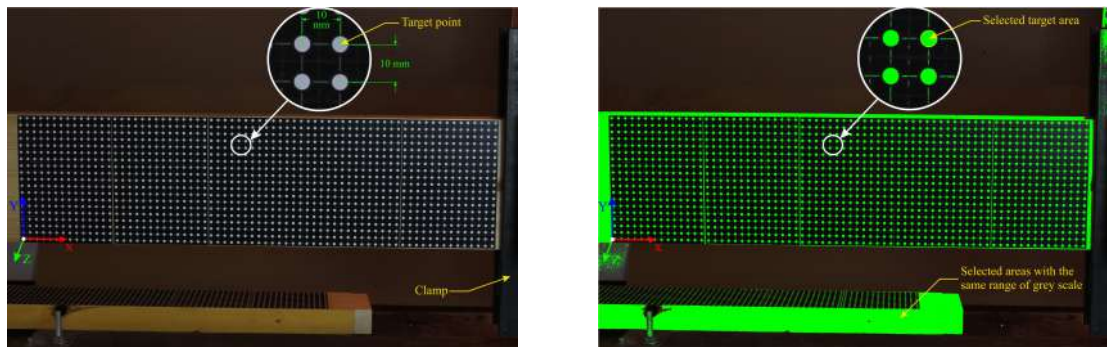
Over-exposed images provide fewer details and consequently, reduces the accuracy of the measurement. Therefore, extra care was taken to obtain sharp and clear images. The matrix of the target points was mapped onto a dark background (Figure 3.7). Each target point was given three degrees of freedom by cutting the glued paper using a sharp knife along each grid lines that lie between the dots. Four Canon EOS 550Ds cameras were selected for this project. The cameras were specified as 18-megapixel digital single-lens reflex cameras and equipped with 50mm Canon EF f/1.8 II fixed focal lenses.

Both left and right images were processed using MvTec Halcon (MvTec Software GmbH, 2012) which is a powerful image processing system. The process of finding the target point

### CHAPTER 3. MATERIAL PROPERTIES AND TESTING METHODS

with different styles has been explained previously in Section 3.3.6. Once all the target points were selected in both left and right images using the selected points the contour of the surface deformation of the beam can be obtained (Figure 3.7c).

The extracted 3D information can be used to determine the deflection and rotations of any section of the beam. This method provides us with the data that conventionally could not be obtained such as surface strain flow and dynamic monitoring capability.



(c) Selected target points after processing

**Figure 3.7:** The photogrammetry's process stages in a torsion test

### 3.4 Static Bending Test

The static bending tests were conducted to evaluate the flexural properties of the laminated bamboo lumber. The tests were carried out using a universal testing machine capable of applying 30kN load, following the specifications detailed in the BS EN 373 (BSI, 1957). The test setup and specifications are illustrated in Figure 3.8.

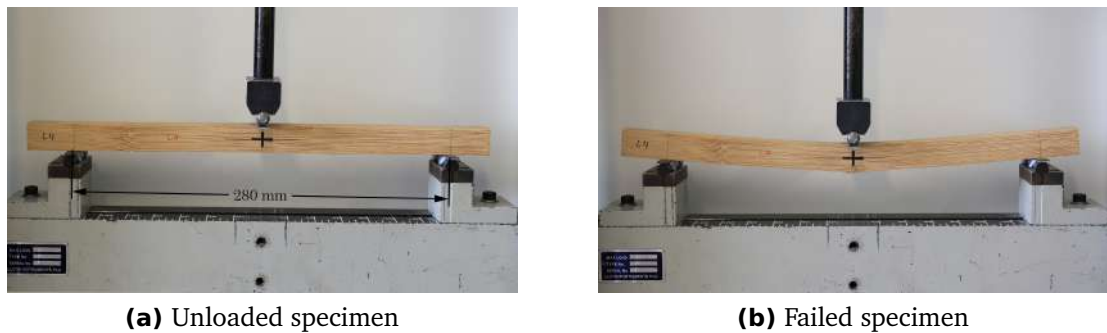


**Figure 3.8:** The static three-Point bending test

#### 3.4.1 Specimen preparation

40 Laminated bamboo specimens were prepared and divided into two groups of 20, based on the bamboo strips' orientation. The cross-sectional dimensions of the specimens were 20×20 mm and the length was 300 mm. The specimens denoted by LBL-FW have the strips flat-wise when the loading applied, i.e. loading is applied perpendicular to the glue-line (Figure 3.9), and for the group represented by LBL-EW, loading is applied parallel to the glue-line (Figure 3.9). In addition, 10 timber specimens were prepared to evaluate the properties of the spruce.

The flexural properties of the laminated bamboo in both orientations were required because in the production of the hybrid beam, both orientations have been used. It is assumed that for both materials the radial and the tangential properties are equal, and only the properties in the longitudinal direction were determined.

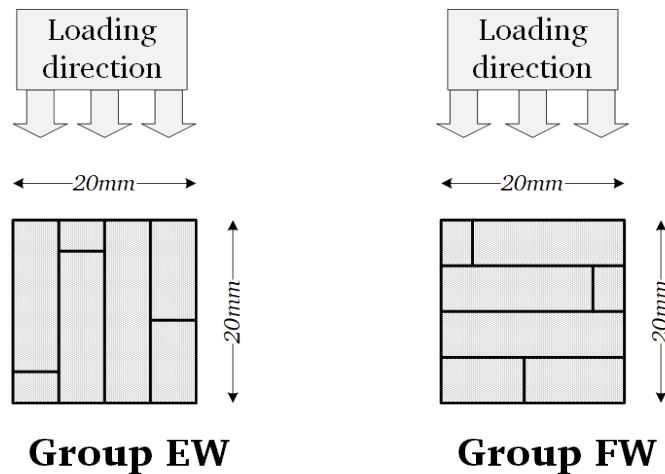


Figure 3.9: Laminated bamboo's strip orientations

### 3.4.2 Testing procedure

The testing span was 280 mm and the loading was applied at the mid-span at a rate of 2.5 mm/min for the laminated bamboo and 2 mm/min for the spruce. Thin steel plates with a width of 8 mm were used between the loading head/supports and the specimens to prevent indentations. The mid-span deflection was measured using the photogrammetry method which is detailed in the previous section (Section 3.3). The photogrammetry method provided accurate measurements while eliminating the physical contact which may influence the flexural properties of the specimen.

### 3.4.3 Results of the static bending test

An example of the load-deflection graphs of the tested materials is shown in Figure 3.10. The results indicate that the laminated bamboo experienced large displacements in which the majority was due to inelastic deformation. The overall behaviour of the specimens initiated with an elastic response, followed by non-linear elasto-plastic deformation and finally a brittle failure. Elastic-plastic deformation was observed where the stiffness of the specimens was decreased markedly. The noise of micro-cracks was audible before the failure at the bottom tensile surface. It is worth noting that cracks initiated at a defect (a knot) in the bottom surface if there was any.

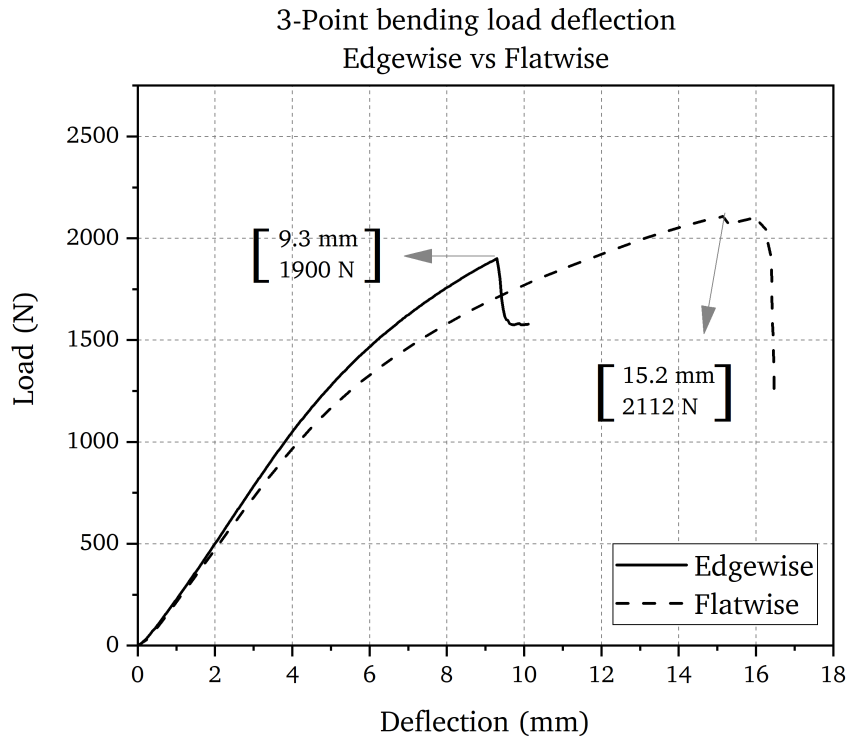


**Figure 3.10:** Example of load-deflection for static bending test

The failures can be categorised as a brittle failure at the tension surface at the mid-span (Figure 3.11a and 3.11b) with the exception of only one horizontal shear failure (Figure 3.11c). No plastic deformation was observed for both orientations.

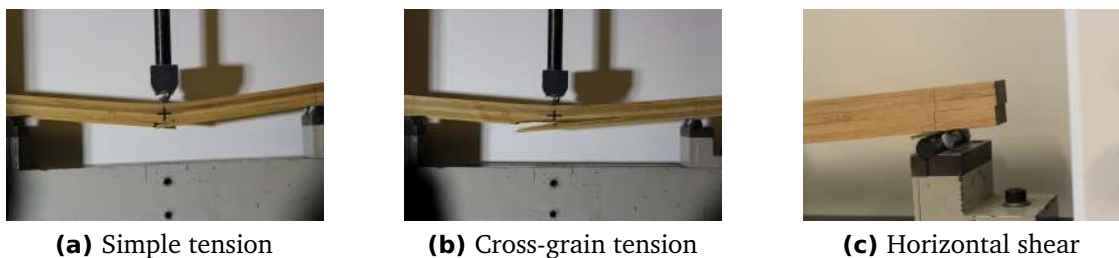


**Figure 3.11:** Failure modes for static bending test

The flexural strength ( $f_b$ ) and Young's modulus ( $E_{L3P}$ ) based on the three-point bending test were calculated using Equations 3.6 and 3.7, respectively.

$$f_b = \frac{3F_{max}L}{2bh^2} \quad (3.6)$$

$$E_{L3P} = \frac{F'L^2}{2\Delta'bh^2} \quad (3.7)$$

### CHAPTER 3. MATERIAL PROPERTIES AND TESTING METHODS

where,  $F_{max}$  is the maximum load,  $L$  is the testing span,  $b$  and  $h$  are the cross-sectional width and depth,  $F'$  and  $\Delta'$  are load and mid-span deflection at the proportionality limit, respectively.

A summary of the results of the static bending is given in Table 3.1 and the detailed results for each specimen are presented in Appendix A. The bending strength of LBL-EW ranged from 73.32 N/mm<sup>2</sup> to 118.98 N/mm<sup>2</sup> and LBL-FW ranged from 72.66 N/mm<sup>2</sup> to 122.27 N/mm<sup>2</sup>. The mean ultimate bending strength of the flatwise specimens ( $f_b = 102.88$  N/mm<sup>2</sup>) was only 4% higher than that of the edgewise ( $f_b = 98.69$  N/mm<sup>2</sup>), while an opposite relationship was concluded by Sharma et al. (2016). Previous studies on the flexural behaviour of LBL have reported a wide range of ultimate bending strengths, ranging from 67.7 N/mm<sup>2</sup> (Lee et al., 1998) to 165.4 N/mm<sup>2</sup> (BANSAL and PRASAD, 2004). The bamboo strip size seems to also affect the overall bending performance of laminated bamboo lumbers (Penellum et al., 2018).

**Table 3.1:** Static three-Point bending test results

Specimen	Density	MC	$F_{max}$	$f_b$	$E_{L3P}$	$E_{LAC}$
	[kg/m <sup>3</sup> ]	[%]	[N]	[N/mm <sup>2</sup> ]	[kN/mm <sup>2</sup> ]	[kN/mm <sup>2</sup> ]
<b>LBL - F</b>	<b>661.66</b>	<b>7.84</b>	<b>1987.62</b>	<b>102.88</b>	<b>8.67</b>	<b>9.03</b>
CoV [%]	8.87	1.61	13.28	13.97	9.10	
<b>LBL - E</b>	<b>655.63</b>	<b>7.8</b>	<b>1943.91</b>	<b>98.69</b>	<b>9.19</b>	<b>9.58</b>
CoV [%]	7.15	0.67%	13.57	13.85%	12.38	
<b>C16</b>	<b>370.58</b>	<b>12.42</b>	<b>952.86</b>	<b>46.85</b>	<b>7.64</b>	<b>7.96</b>
CoV [%]	7.74	1.68%	10.74	10.80%	16.87	

#### 3.4.3.1 Characteristic values

The characteristic value ( $f_{m,k}$ ) of bending strength determined based on 5-percentile of the sample size which is the test value where 5% of values are lower or equal to. The characteristic values in flat-wise and edgewise directions are relatively similar (73.3 and 72.7 N/mm<sup>2</sup>, respectively). This implies that the design strength of laminated bamboo may be independent of the bamboo strips' orientation.

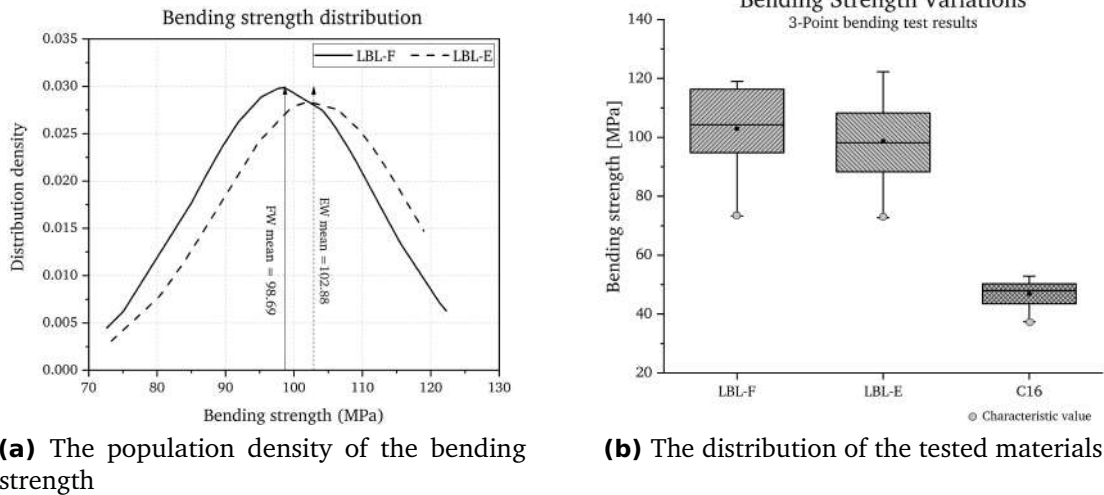


Figure 3.12: The bending strength distribution and variation

### 3.4.3.2 Bending modulus

Regarding Young’s Modulus, LBL-Edgewise ( $E_{EW} = 9.19 \text{ kN/mm}^2$ ) illustrated slightly stiffer behaviour - about 5%, than LBL-F ( $E_{FW} = 8.67 \text{ kN/mm}^2$ ). Sharma et al. (2016) also reported that laminated bamboo loaded edgewise possesses 5-13% higher modulus of elasticity than that of the flat-wise. However, in an earlier study by the same author, i.e. Sharma et al. (2015a), the opposite pattern was reported, where flat-wise illustrated 18% higher Modulus of Elasticity than that of edgewise samples. Li et al. (2018), also concluded that flat-wise loading results in higher bending moduli. In addition, different testing procedures and apparatus’ seem to influence the measured mechanical properties (Sharma et al., 2016). These discrepancies in the reported mechanical properties of the laminated bamboo lumber signify the necessity of a standard manufacturing guideline to achieve a reliable structural material.

### 3.4.4 Impact of the strip orientation on the flexural properties

Figure 3.12 compares the bending strength distribution for both orientations. The overall range is similar, however, LBL-EW skewed to the higher end of the range. The probability densities of both follow a similar pattern. Evidently, laminated bamboo had a higher variation and magnitude in the bending strength in comparison to C16. Figure 3.13 compares the bending modulus distribution densities for both groups of LBL. The LBL-EW showed less variation in the values of Modulus of Elasticity, but the mean and maximum

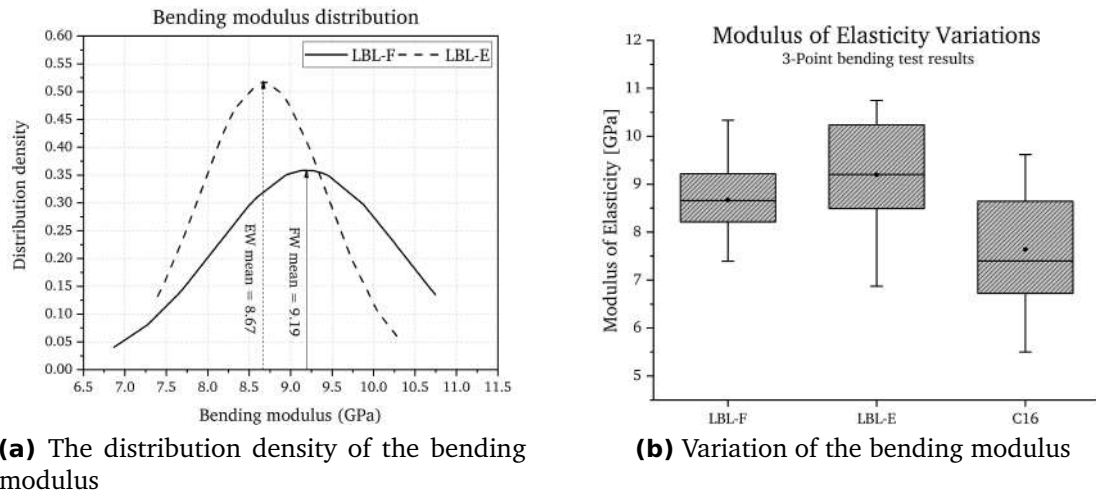


**Figure 3.13:** The bending modulus distribution graphs

bending modulus of LBL-FW is higher. The mean modulus of both orientations is very close to each other and comparable to that of C16. The bamboo strip's orientation seems to influence the bending strength and modulus relationship. The influence can be determined using t-test. The t-test is a statistical method to determine the significant difference between the mean values of two groups. However, the result of a t-test with a 5% confidence level reveals that the bamboo strip's orientations do not have a significant impact on the bending strength and modulus. The p-value for the bending strength was 0.327 and for the bending modulus 0.084. These values fail to reject the null hypothesis which is the equal mean values for both cases, thus the impact is insignificant.

### 3.4.5 Three-point to four-point

The central loading method does not provide a uniform bending moment across a region of the specimen, in addition, the density of the specimen can affect the modulus of elasticity of a wooden specimen when subjected to four-point bending or three-point bending (Brancheriau et al., 2002). The bending modulus resulting from a three-point bending test needed to be converted to a four-point bending equivalent. This is to enable comparison and use of bending moduli for the mathematical evaluations of the hybrid beams. Brancheriau et al. (2002) have proposed a "crossing" formula for this conversion, which takes density and effect of the loading head indentation into account (Equation 3.8).

The converted values are given in Table 3.1, Column  $E_{LAC}$ .

$$E_{LA} = \frac{1.042}{1 - 1.906K \left( E_{L3P} \frac{eh^3}{I^3} - \frac{E_{L3P}h}{G_{TL}l^2} \right)} E_{L3P} \quad (3.8)$$

where:

$$K = 0.515 \left( \frac{h}{e\sqrt{R}E_T} \right)^{2/3} E_T = 795 \left( \frac{\rho}{0.65} \right)^{1.53} \quad (3.9)$$

$$G_{TL} = 976 \left( \frac{\rho}{0.65} \right)^{1.18} \quad (3.10)$$

where  $\rho$  is the density,  $h$  is the cross-sectional depth and  $R$  is the support and loading head radius (if circular). Steel plates with the width of 8 mm have been used for support and loading points, thus  $R = \infty$  is assumed.

### 3.5 Tensile Behaviour Parallel to Fibres

Tensile properties of laminated bamboo lumber were determined using Small Clear Specimen testing procedure, detailed in BS EN 373 (BSI, 1957). The specimens were prepared by selecting strips of laminated bamboo and cut into a recommended profile using a table router in order to enforce the specimen to fail at the intended region (Figure 3.14).

#### 3.5.1 Tensile test specimen preparation

60 laminated bamboo specimens were divided into three groups of 20 based on their conditioning environment and defect condition. The Small Clear Specimen testing procedure requires specimens that are free from any defects, however, this is not obtainable in the case of laminated bamboo. The groups are described in Table 3.2. Group TA describes the specimens that are conditioned for a period of four weeks at the laboratory environment at a temperature of 13-15°C and relative humidity of 75±5, and were mixed in terms of containing knots at the high tensile stress region. TB represents specimens that are conditioned at the recommended environment by BS EN 373 which is 20±1°C temperature and 65%±5 relative humidity for about four weeks. This group contains knots with a size of at least half of the specimen thickness. TC describes the specimens that are like TB conditioned at the controlled environment but did not contain knots at the high-stress region, i.e. middle part.

In addition to the laminated bamboo samples, 10 spruce specimens were prepared and conditioned at a similar environment as of TB and TC. The spruce samples were not cut to

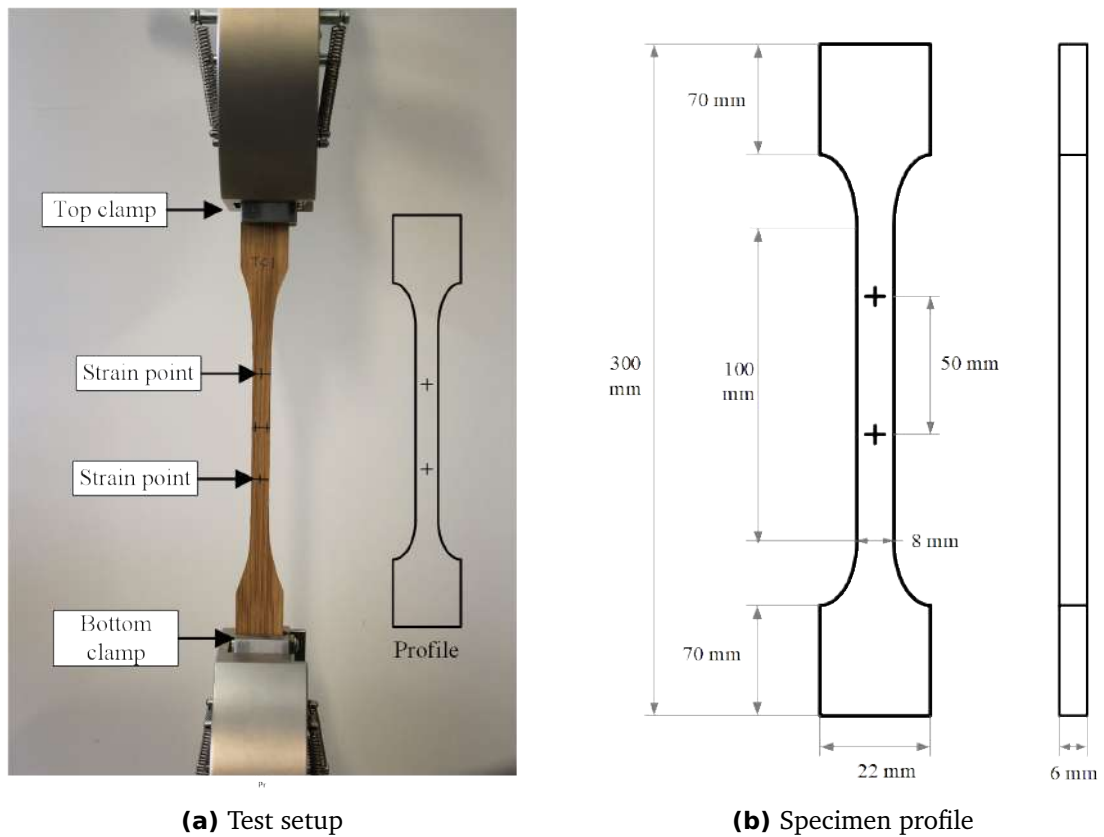


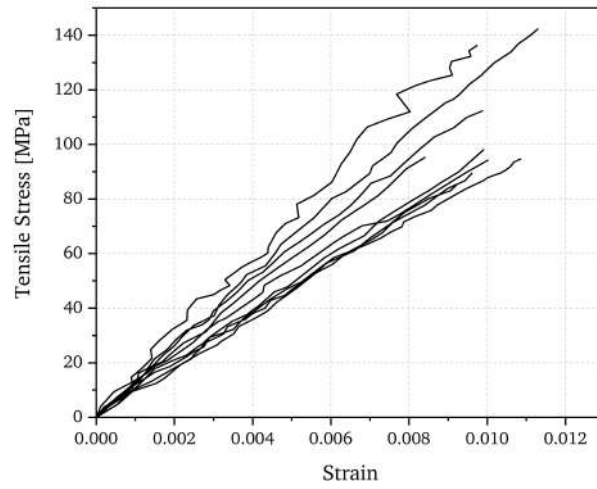
**Figure 3.14:** Small Clear Specimen tensile test

the recommended profile and their dimensions were  $20 \times 6$  mm cross-section and 300 mm length.

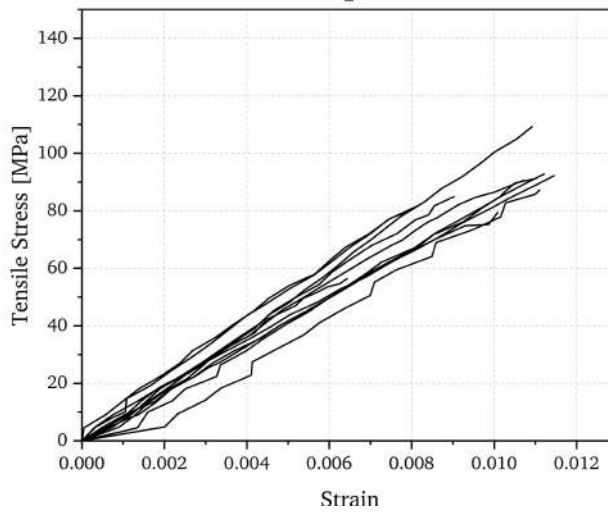
The tensile tests were conducted at the laboratory of Edinburgh Napier University using the same testing machine as one used for the static bending test. The loading was applied at the rate of 1 mm/min for all the tested specimen.

### 3.5.2 Results of the Small Clear Specimen tensile test

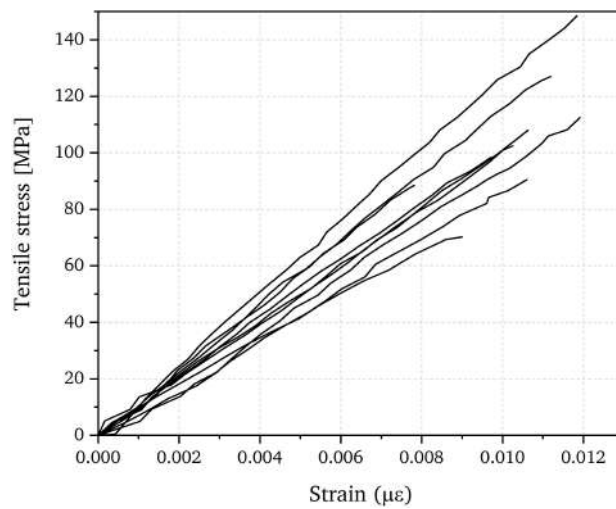
A summary of the tensile test result is presented in Table 3.3 and the stress-strain relationships for the three groups of the laminated bamboo are shown in Figure 3.15. The moisture content of TB and TC which were kept in the conditioning chamber were slightly higher than TA. The tensile strength and modulus of the specimens were calculated using the maximum applied load and the slope of the stress-strain curve at the elastic region, respectively. The following equations given by BS EN 373 (BSI, 1957) were used to calculate



(a) Group TA



(b) Group TB



(c) Group TC

Figure 3.15: Tensile stress-strain relationship

### CHAPTER 3. MATERIAL PROPERTIES AND TESTING METHODS

**Table 3.2:** Specimen descriptions for the tensile test

Specimen	Description
<b>TA</b>	Laminated bamboo specimens that are kept in the laboratory environment with a temperature of 13-15°C and relative humidity of 75% ± 5. They were mixed in terms of containing knot in the middle part.
<b>TB</b>	Laminated bamboo specimens that are kept in the controlled environment of 20°C temperature and 65% ± 5 humidity for about four weeks. This type contains a knot in the middle area.
<b>TC</b>	Laminated bamboo specimens that are kept in the controlled environment of 20°C temperature and 65% ± 5 humidity for about four weeks. This type contains less amount of knot in the middle part.
<b>C16</b>	C16 timber specimens that are kept in the controlled environment of 20°C ± temperature and 65% ± 5 humidity for about four weeks.

the tensile properties.

$$\text{Tensile strength}(f_t) = \frac{F_{max}}{A_{eff}} \quad (3.11)$$

$$\text{Tensile modulus}(E_t) = \frac{F'L}{\Delta'A_{eff}} \quad (3.12)$$

where  $F'$  and  $\Delta'$  are the load and displacement at the proportionality limit.

The bamboo knots appear to have a considerable impact on the tensile properties of the laminated bamboo specimens. Specimens with a knot at the high-stress area resulted in 27.5% lower tensile strength and about 10% lower tensile modulus. The lower tensile properties are due to lower longitudinal fibres in the knots.

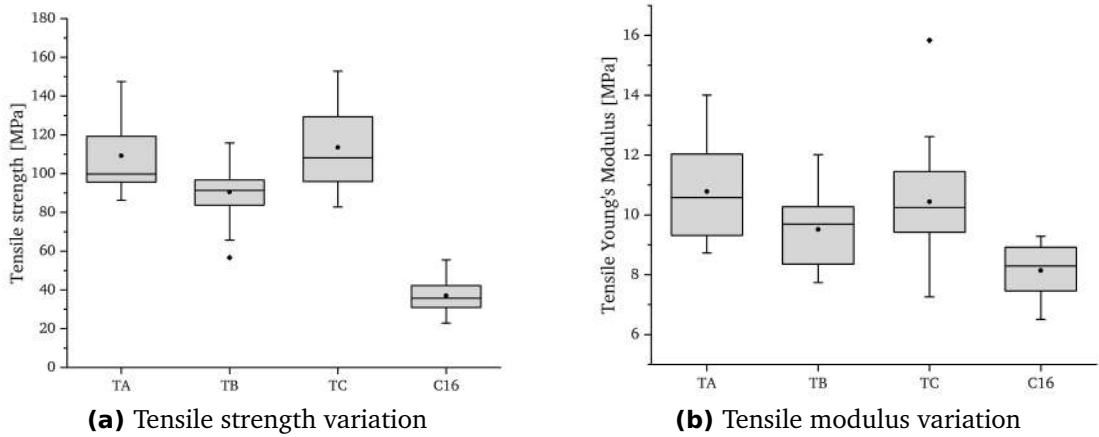


**Figure 3.16:** Tensile strength and modulus comparison and variation

**Table 3.3:** Results of small specimen tensile test

Specimen	$MC$	$A_{eff}$	$F_{max}$	$f_t$	$E_t$
	[%]	[mm <sup>2</sup> ]	[N]	[N/mm <sup>2</sup> ]	[kN/mm <sup>2</sup> ]
<b>TA</b>	<b>7.67</b>	<b>55.97</b>	<b>6163</b>	<b>109.90</b>	<b>10.92</b>
CoV	9.14%	4.78%	21%	20.20%	13.51%
<b>TB</b>	<b>7.96</b>	<b>55.28</b>	<b>5002</b>	<b>90.44</b>	<b>9.51</b>
CoV	7.20%	2.98%	17%	16.42%	12.65%
<b>TC</b>	<b>8.07</b>	<b>55.79</b>	<b>6417</b>	<b>115.23</b>	<b>10.42</b>
CoV	8.58%	2.14%	19%	19.68%	17.88%
<b>C16</b>	<b>13.45</b>	<b>156.42</b>	<b>6188</b>	<b>39.59</b>	<b>8.25</b>
CoV	1.30%	2.18%	27%	26.80%	13.77%

The variations of the tensile strength and modulus for each group are presented in Figure 3.16. These graphs compare the tensile characteristics of laminated bamboo and the Norway spruce wood.

### 3.5.3 Impact of the conditioning environment in the tensile properties

To investigate the impact of the conditioning environment on the tensile properties, t-tests were conducted on the results of the tensile tests - assuming that the null hypothesis ( $H_0$ ) indicates that the mean tensile strength and modulus does not change significantly by

changing the conditioning environment. Thus, the alternative hypothesis ( $H_a$ ) would state the opposite. The mean values for the group TA were compared with the mean values of combined TB and TC. Given the confidence level of  $\alpha = 5\%$ , the results of these experiments showed that the conditioning environment has a significant impact on the tensile modulus ( $p = 0.027 < 0.05$ ) whilst the tensile strength has not been significantly impacted by changing the conditioning environment ( $p = 0.2 > 0.05$ ).

### 3.5.4 Impact of the knots in the tensile properties

As mentioned earlier, the knots imposes the failure in the specimen which can influence the tensile strength of the specimen. With a confidence level of 5%, the results of a t-test on the tensile properties of the group TB and TC revealed that knots significantly affect the tensile strength of the specimen ( $p = 0.0005 < 0.05$ ). However, expectedly, the impact of the knots on the tensile modulus of the specimens was insignificant ( $p = 0.075 > 0.05$ ).

### 3.5.5 Failure mechanism

Despite creating a profile to impose the failure in the middle part, specimens often failed outside of this region. Examples of the failed specimens are illustrated in Figure 3.17. Different types of failure were observed such as bamboo splitting, shear and brittle tension. However, the overall failure mechanism of the laminated bamboo specimens was the brittle failure. Bamboo knots have fibres in the transverse direction and this causes a weak spot in the section which imposes the failure. Based on the failure observations, 65-70% of the failures had an association with a knot in the form of initiation or splitting

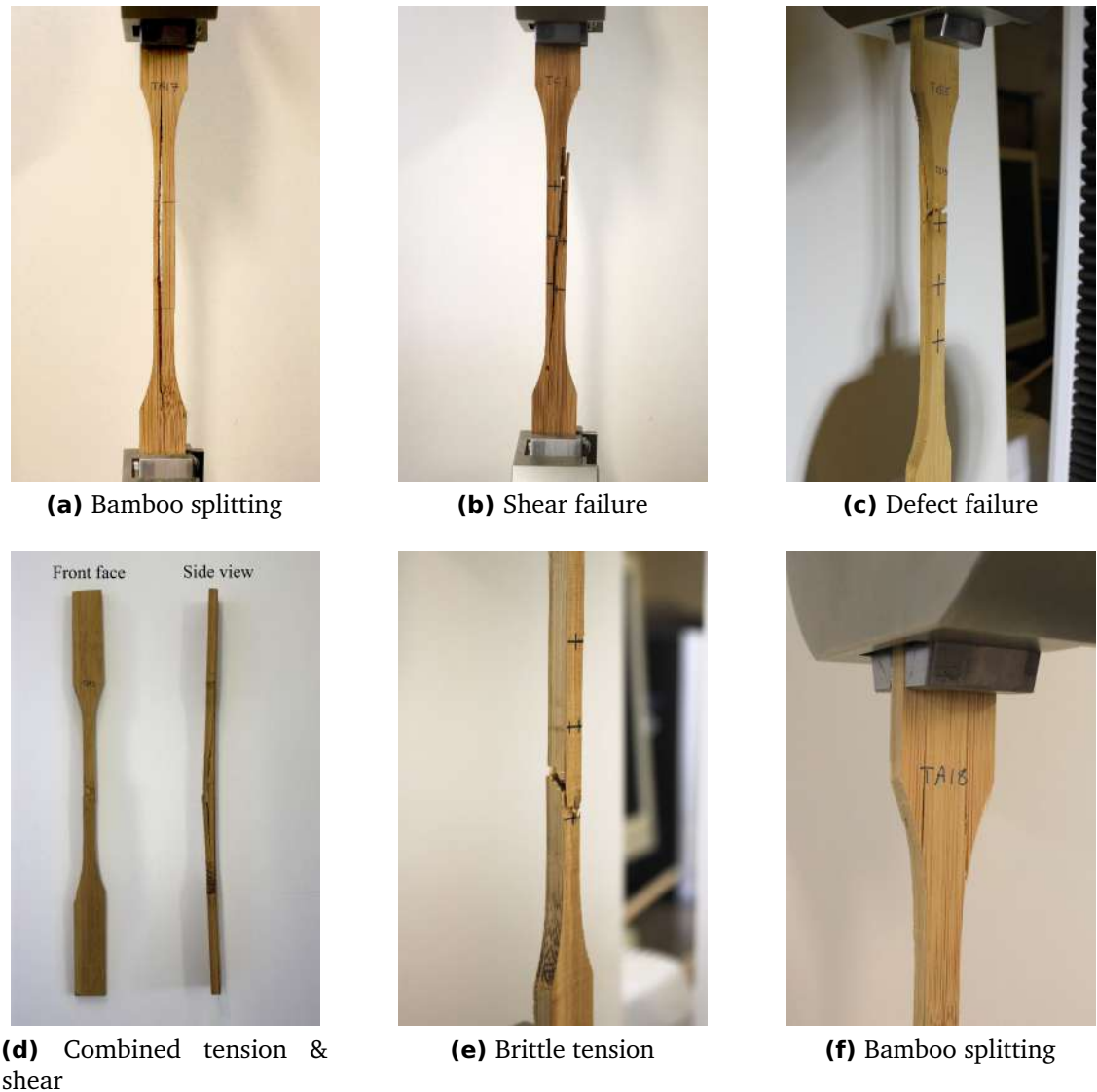


**Figure 3.17:** : Tensile test failure mechanisms

### 3.6 Compression Test Parallel to Fibres

The compression tests were undertaken according to BS EN 373 (BSI, 1957) on both laminated bamboo and spruce specimens. 10 laminated bamboo specimens and five spruce were prepared with the cross-sectional dimensions of 40×40 mm and a length of 120 mm. All testing samples were loaded parallel to their fibres/grain using a compression testing machine at a rate of 0.7 kN/s. The strain and load measurements were carried out using the photogrammetry method. Figure 3.18 illustrates the compression test setup.

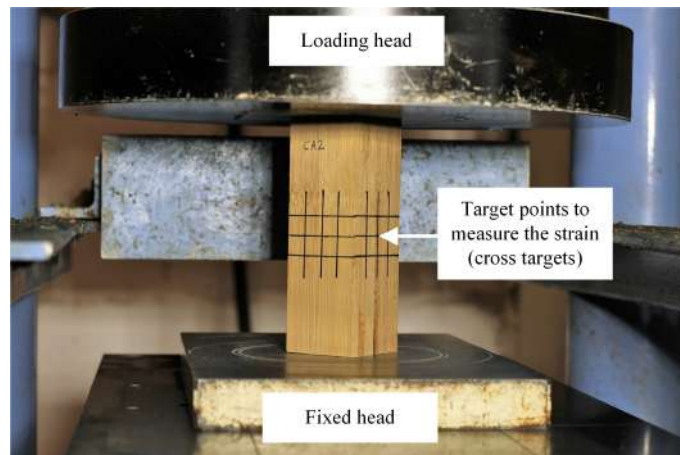


Figure 3.18: Compression test setup parallel to fibres

### 3.6.1 Results of the compression test

Results of the compression test provided in Table 3.4 and an example of a stress-strain graph is illustrated in Figure 3.19. Laminated bamboo under compressive loads undergoes elastic-plastic and plastic deformations. As per BS EN 373 (BSI, 1957), the compressive strength and modulus were determined using the following equations:

$$\text{Compressive strength}(f_c) = \frac{F_{max}}{A_{eff}} \quad (3.13)$$

$$\text{Compressive modulus}(E_c) = \frac{F' L}{\Delta' A_{eff}} \quad (3.14)$$

where  $F'$  and  $\Delta'$  are the load and displacement at the proportionality limit.

Table 3.4: Small clear specimen compression test results

Specimen	$MC$	$A_{eff}$	$F_{max}$	$F'$	$f_{c,ep}$	$E_c$
	[%]	[mm <sup>2</sup> ]	[kN]	[N/mm <sup>2</sup> ]	[N/mm <sup>2</sup> ]	[kN/mm <sup>2</sup> ]
CA	8.62	1672.36	119	44	62.84	10.67
CoV/%	7%		7%	10%	5%	18%
C16	14.54	1636.56	56	24	30.70	8.00
CoV/%	1%		8%	3%	1%	12%

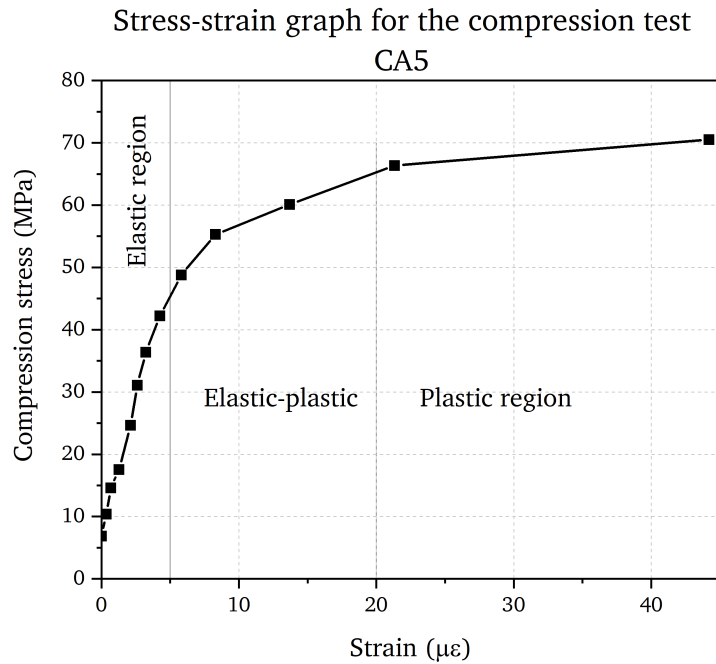


**Figure 3.19:** Stress-strain graph for a compression test

Referencing Figure 3.19, the stress-strain relationship of the laminated bamboo under the compressive loads reveals a highly ductile behaviour. All of the laminated bamboo performed similarly in compression with an elastic initiation, followed by an elastic-plastic and finally, large plastic deformations.

### 3.6.2 Failure mechanism

The laminated bamboo samples demonstrated several types of failure modes including strength failure, splitting and buckling. Strength failure is when the specimen crushes at the top surface and side surfaces bend outward (Figure 3.20a). Shearing failure was also observed in two specimens (Figure 3.20b). The splitting/delamination occurred in some samples which imply insufficient shear strength of glue (Figure 3.20d). Buckling was observed in most of the specimens. The crushing and shear failure were the dominant failure types observed in the spruce samples (Figure 3.20e and 3.20e). Buckling can be reported as the dominant type of failure which was often accompanied by another type of failure such as delamination and bamboo splitting. These observations underline the importance of manufacturing procedures and adhesives used in the lamination process.

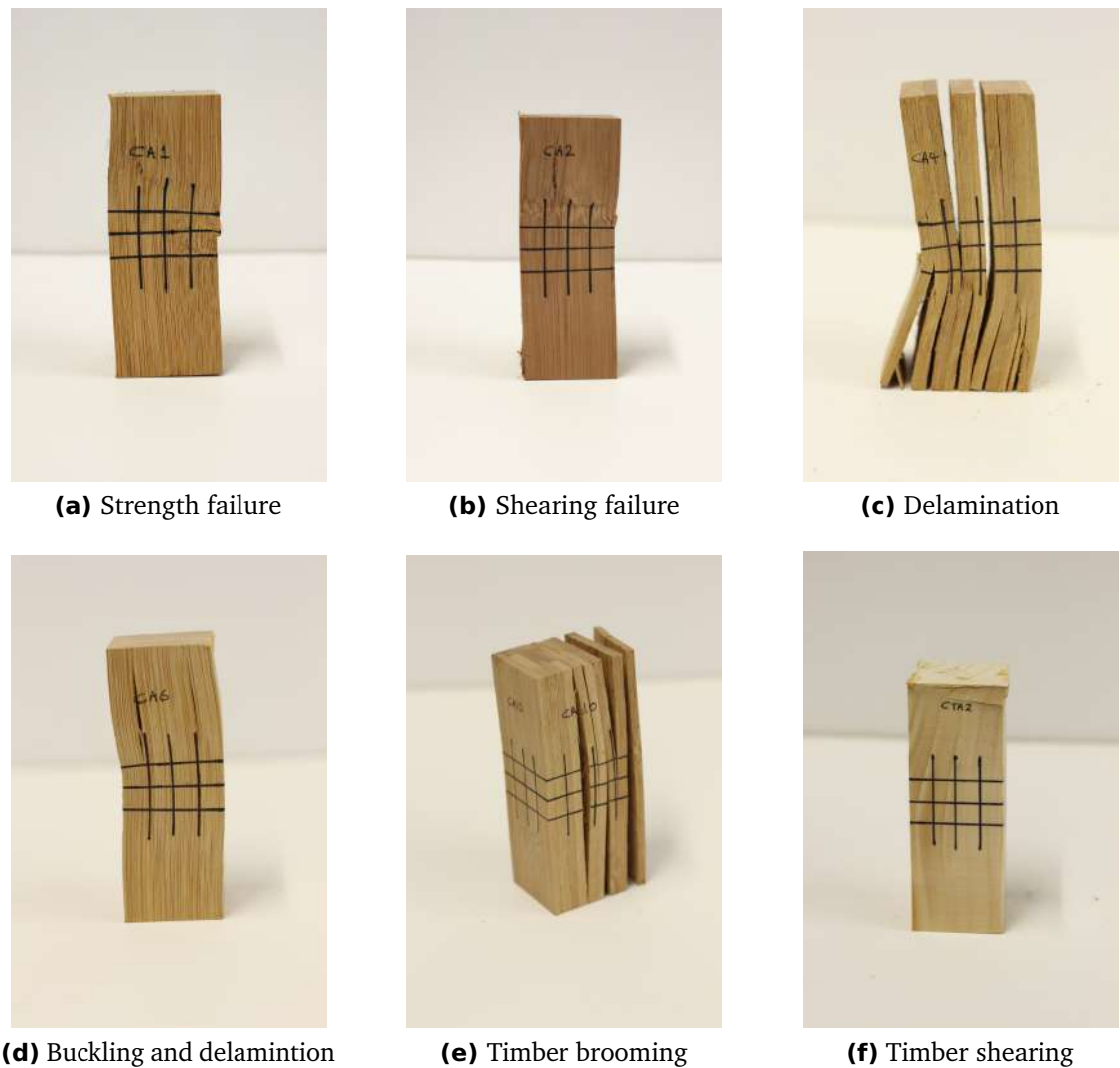


**Figure 3.20:** Compression test failure modes

### 3.7 The Constitutive Model

The stress-strain relationship obtained from the tension and compression tests for the laminated bamboo is shown in Figure 3.21. The laminated bamboo experiences only elastic deformation under tension and tri-linear behaviour under the compression loads. According to the experimental results, the mean values for the compressive yield stress was  $\sigma_{cy} = 50.34 \text{ N/mm}^2$  and yield strain was  $\epsilon_{cy} = 4133 \mu\epsilon$ . For the elastic-plastic state, the mean values were  $\sigma_{ep} = 62.84 \text{ N/mm}^2$  and  $\epsilon_{ep} = 13705 \mu\epsilon$ , and for the ultimate plastic state  $\sigma_{c0} = 70.92 \text{ N/mm}^2$  and  $\epsilon_{c0} = 20873 \mu\epsilon$ . The observed relationship was similar to the previous studies by [Li et al. \(2018\)](#); [Takeuchi et al. \(2016\)](#) and [Li et al. \(2015\)](#).

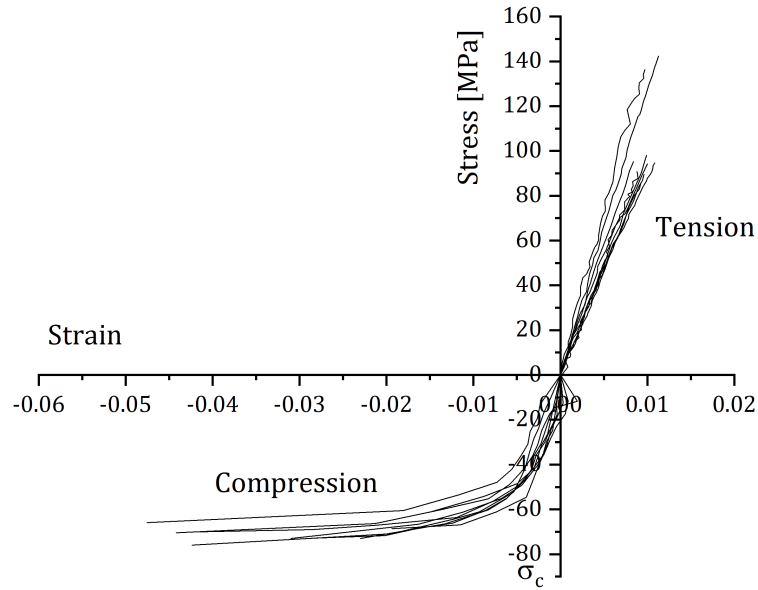


**Figure 3.21:** The stress-strain relationship for the laminated bamboo lumber

### 3.7.1 Proposed stress and strain relationship

A simplified stress-strain relationship based on the results of the tensile and compressive tests, parallel to fibres, can be seen in Figure 3.22. The proposed model was adopted from the model introduced by Buchanan (1990) for wood and the introduction to the laminated bamboo by Li et al. (2016). The difference between the tensile and compressive Young's Modulus was less than 5%, thus an equal value was assumed for both loading situations ( $E$ ). This model will be used to model the laminated bamboo and timber hybrid beams in the following chapters. This relationship can be analytically expressed using the following equations:

$$\sigma = \begin{cases} E\epsilon & \text{for } -\epsilon_{cy} \leq \epsilon \leq \epsilon_{tu} \\ \sigma_{cy} + k_{ep}(\epsilon - \epsilon_{cy}) & \text{for } -\epsilon_{c0} \leq \epsilon \leq -\epsilon_{cy} \\ \sigma_{c0} & \text{for } -\epsilon_{cu} \leq \epsilon \leq -\epsilon_{c0} \end{cases} \quad (3.15)$$

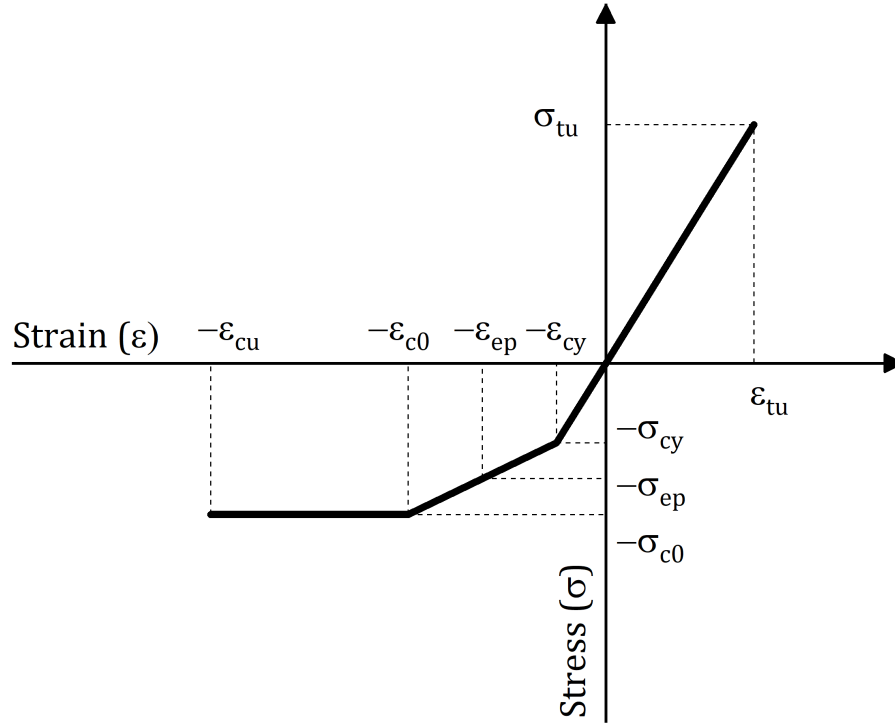


**Figure 3.22:** Proposed stress-strain relationship for the laminated bamboo lumber

Where  $k_{ep}$  is the slope of the elastic-plastic deformation and can be obtained as:

$$k_{ep} = \frac{\sigma_{c0} - \sigma_{cy}}{\epsilon_{c0} - \epsilon_{cy}} E = \frac{\sigma_{ep} - \sigma_{cy}}{\epsilon_{ep} - \epsilon_{cy}} E \quad (3.16)$$

### 3.8 Testing Methods for Determining the Shear Modulus

The shear strength and the shear modulus can sometimes be the limiting factors in designing the timber structures. For instance, relatively deep beams and short span Glulam beams, are prone to fail due to shear loads. Among various methods of measuring the shear modulus of the structural size timber-based materials, the torsion test and the Shear field test method are recommended by the governing testing standards (BS EN 408 (BSI, 2012) and ASTM D198 (ASTM, 2014)).

The torsion test is found to be a more suitable testing method for evaluating the shear properties of the timber beams as it creates the perfectly pure shear states in the specimen. Subsequently, this provides a better representation of the shear behaviour of the material

(Gupta and Siller, 2005a; Gupta et al., 2002a; Davalos et al., 2002; Soltis and Rammer, 1994). The Shear Field test method, on the other hand, determines the shear properties of the material during the four-point bending test which can simulate the beam at the real-life situation when the beam is in service. However, the beam experiences combined stresses, i.e. shear and bending, due to the nature of the bending loads and the beam's deformation.

The shear modulus of the laminated bamboo has not been determined using the torsion test and shear field test method previously, subsequently the suitability of the recommended methods, i.e. torsion test and shear field test method, has not been investigated. To better understand the suitability of the torsion test and shear field test method to evaluate the shear properties of the laminated bamboo and to identifying a proper method to determine the shear modulus of the laminated bamboo, it was aimed to evaluate these testing methods in details. Therefore, the following sections evaluate both of these testing methods and the limitations and advantages of them are discussed. In addition to evaluating these testing methods, the shear modulus of the laminated bamboo was determined using the torsion test. This is because the torsion test provides a better evaluation of the shear properties of the material.

### 3.8.1 Torsion test

The torsion test is regarded as an efficient method of determining the orthotropic shear moduli of a structural sized lumber (Gupta and Siller, 2005b). This section focuses on evaluating the torsion test as a method of determining the shear modulus of the laminated bamboo and timber materials. Throughout this evaluation, it was found that there is a discrepancy in the recommendations of the governing testing standards, i.e. BS EN 408 and ASTM D198. Therefore, to evaluate the shear modulus of the materials, a series of experiments to investigate the effectiveness of the torsion test was carried out.

In general, the shear failures in the wooden specimen can be categorised into three modes, namely: Mode 1) shear failure parallel to the grain (Figures 3.23a and 3.23b), Mode 2) shear failure perpendicular to grain (Figures 3.23c and 3.23d), and Mode 3) rolling shear (Figures 3.23e and 3.23f).

In regards to the torsion test, the failure occurs in the weakest plane which is along either RL or TL plane. Thus, the shear failure seems to occur in Mode 1 (shear failure parallel

to the grain) or Mode 3 (rolling shear) (Gupta et al., 2002b). According to the torsional theory (Boresi and Schmidt, 2003), shear stresses in perpendicular to the grain ( $\tau_{xy}$ ) equals zero, thus, the rolling shear is unlikely to cause the failure in the torsion specimen. On the other hand,  $\tau_{yz}$  and  $\tau_{xz}$  can cause the failure at their maximum points, i.e. middle of the side. Therefore, the torsion test associates with the failure Mode 1, which the failure plans are parallel to the grain.

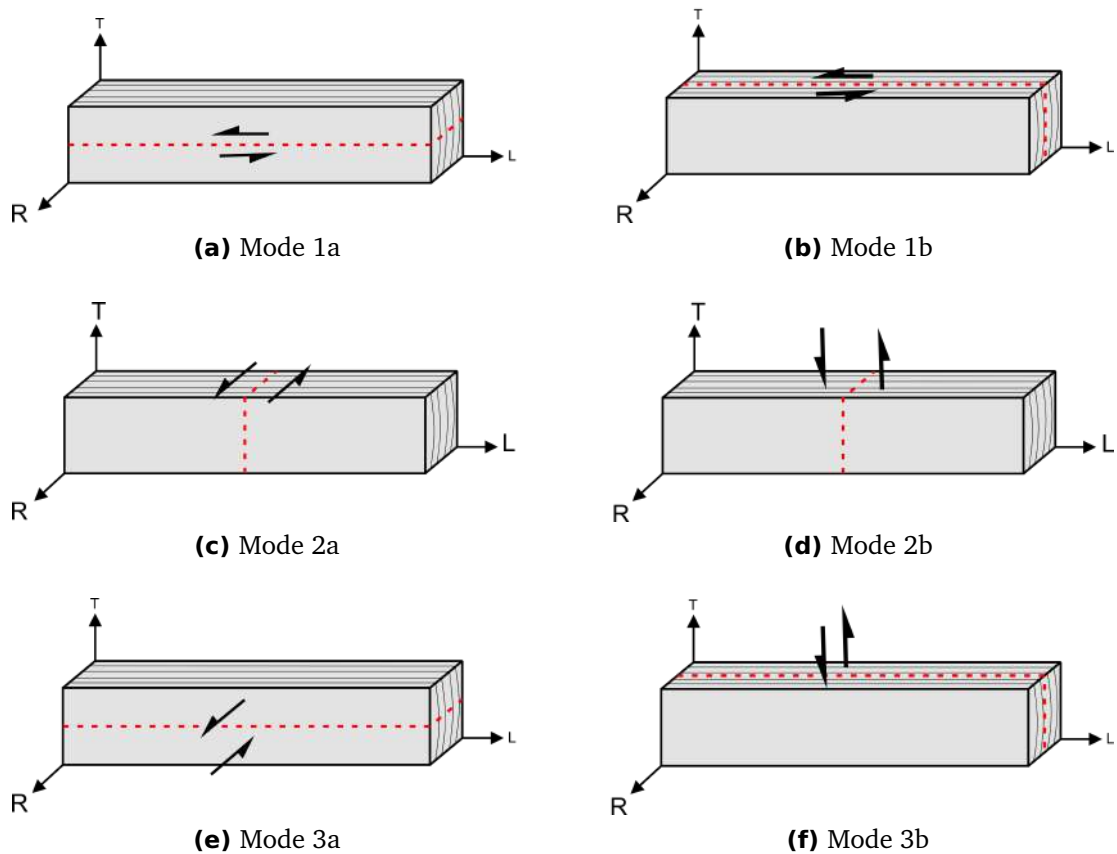


**Figure 3.23:** Failure modes associated with shear stress

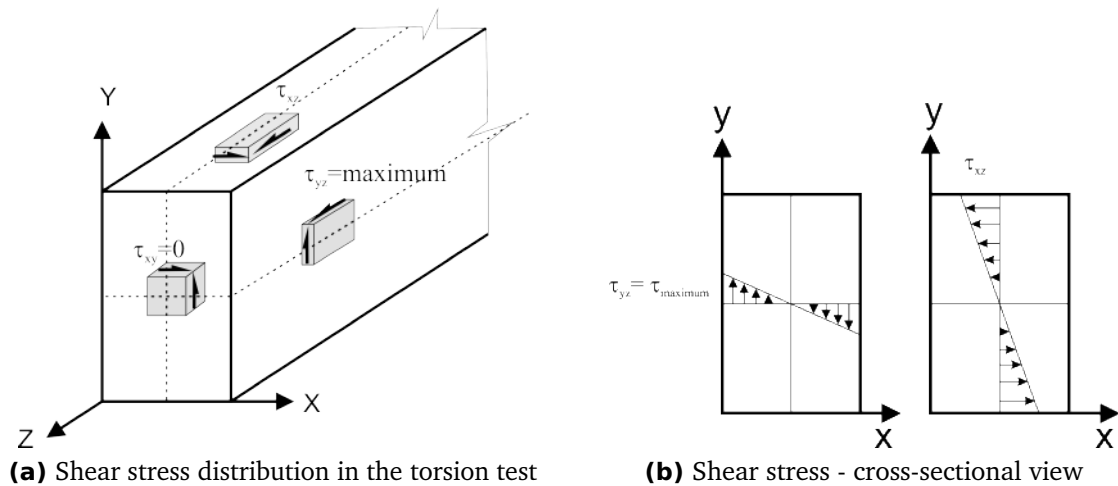


**Figure 3.24:** Shear stress distribution in a torsion specimen

### 3.8.1.1 The identified discrepancy in BS EN 408 and ASTM D198

According to BS EN 408, the rotation of the beam is measured at the distance of two to three times the cross-sectional thickness away from the supports. Whereas, ASTM D198 recommends measuring the rotations at the distance of two times the cross-sectional depth. This discrepancy may not cause considerable measurement error in the beams with the low cross-sectional aspect ratio (cross-section depth over thickness), but it certainly can introduce unnecessary errors in the determination of the shear modulus of the slender beams.

Based on the numerical study by Gupta et al. (2002b), the least distance of two times the cross-sectional depth, plus the grip distance needs to be excluded from either end to obtain a uniform shear stress distribution. Therefore, to provide an appropriate guideline for the industry to measure the shear properties using the torsion test, it is important to understand the shear stress distribution along the beam, especially in regard to the Saint-Venant's end effect and the propagation of this effect from the clamps inwards toward the mid-span.

### 3.8.1.2 Saint-Venant's end effect in torsion test

According to the Saint-Venant's principle, the stress and strain distributions are affected by the local restraints created by clamping the beam at both ends to apply the torque. This effect can be problematic, particularly in terms of the orthotropic or anisotropic materials

(Boresi and Schmidt, 2003; Horgan and Simmonds, 1994). Saint-Venant's principle has based many mechanical tests on measuring deflection and strain profiles. According to this principle, for a mechanical and structural-sized test, a certain distance should be allocated between the measuring section and the supports/loading points. This distance allows the stress and strain in the beam to become uniform and the end effect becomes negligible (Boresi and Schmidt, 2003; Horgan and Simmonds, 1994; Choi and Horgan, 1977).

This phenomenon, also known as end effect, plays an important role, especially in the torsion test, when determining the rotation measuring sections. The distance between the ends and the rotations measuring sections needs to be allocated sufficiently far enough to obtain a uniform shear stress distribution. This is crucial because insufficient distance brings unnecessary errors into the measurement, contrarily, excessive distance creates difficulties and inconveniences for the test setup. In the following section, this distance will be denoted by *end effect decay length* or simply *decay length*.

### 3.8.1.3 The decay length prediction

Studies by Horgan and Simmonds (1994) have shown that for isotropic material, Saint-Venant's end effect can be neglected at approximately a distance of equal to the cross-sectional depth of the beam from the ends. The properties of the isotropic material have equal value in all directions, whereas, the orthotropic and transversely isotropic materials have the longitudinal modulus of elasticity ( $E_L$ ) far greater than its tangential ( $E_T$ ), radial modulus of elasticity ( $E_R$ ) and shear modulus ( $G_{LT}$ ). According to Horgan and Simmonds (1994), there is an exponential relationship between the shear stress ( $\tau$ ) and the decay length; this relationship can be expressed as:

$$\tau \sim C e^{(-kX)} \quad (3.17)$$

$$k \approx \frac{2\pi}{h} \sqrt{\frac{G_{LT}}{E_L}} \quad (3.18)$$

where  $k$  is the decay rate;  $X$  is the location from the support or load;  $C$  is a constant quantity; and,  $h$  is the cross-sectional depth. The characteristic decay length ( $\lambda^*$ ) for an orthotropic or anisotropic material can be determined by:

$$\lambda^* = \frac{\ln(100)}{k} \approx \frac{\ln(100)h}{2\pi} \left( \frac{E_L}{G_{LT}} \right)^{0.5} \quad (3.19)$$

The mean longitudinal modulus of elasticity ( $E_L$ ) for most of the softwood structural timbers ranges from 7 to 16 kN/mm<sup>2</sup> and the mean shear modulus ranges from 0.44 to

1.00 kN/mm<sup>2</sup>. Considering the above equation (3.19), the decay length of the end effect can be estimated between 1.8-3 times the cross-sectional depth ( $h$ ) of the specimen.

### 3.8.1.4 The torsion test detailed in the BS EN 408

The calculated decay length using the analytical solution proposed by [Horgan and Simmonds \(1994\)](#) references the cross-sectional depth as the quantifying measure of the decay length. [Gupta et al. \(2002b\)](#) has also used the cross-sectional depth to quantify this distance. In contrast, the recommendation detailed in BS EN 408 ([BSI, 2012](#)), Clause 11.1.2 for the torsion test considers cross-sectional thickness for this length. According to this standard, the rotations should be measured at a distance of two to three times the cross-sectional thickness from the supports or loads. This distance is perfectly acceptable for the beams with the low cross-sectional aspect ratio, such as a square section.

However, most of the commonly used timber beams in the construction have slender cross-sections with aspect ratios of three to five. Thus, the rotation measuring sections seem too close to the supporting or loading points. This setup can introduce unnecessary error in the rotation measurement due to the end and warping effects (Figure 3.26a). Therefore, a thorough experimental investigation on the end effect for both laminated bamboo and wood species were conducted and presented in the following sections.

### 3.8.1.5 Specimens

Six laminated bamboo and 12 wood specimens were prepared. The specimens had different aspect ratios and different species. The dimensional details of the tested specimens can be found in Table 3.5. Selecting different aspect ratio would provide sufficient evidence to determine the shear modulus changes along the beams with respect to their aspect ratio.

### 3.8.1.6 Experimental procedure

The torsion tests were conducted on the laminated bamboo beams and the timber beams. The test setup is illustrated in Figure 3.25 following the recommendations given by BS EN 408 and ASTM D198. The specimens were mounted edgewise, and torque was applied at one end using a Tinius Olsen Torsion machine capable of applying 1 kN.m at a rate of 4 deg/min while the other end was fixed. Steel clamps were designed and used at both

### CHAPTER 3. MATERIAL PROPERTIES AND TESTING METHODS

**Table 3.5:** Torsion test specimens' details

Specimen	Quantity	Thickness	Depth	Length	MC	Species
TRA	2	40	110	2090	7.1	LBL
TRB	2	40	115	2185	7.1	LBL
TRC	2	40	130	2445	8.0	LBL
AR1.00	2	95	95	1900	12.8	Red Pine
AR2.11	2	45	95	1900	10.4	Red pine
AR3.00	2	75	225	4300	11.2	Spruce
AR3.78	2	45	170	3400	10.4	Spruce
AR4.33	2	45	195	3900	12.0	Red pine
AR4.89	2	45	220	4300	12.5	Spruce

ends of the specimen. The grip distance of these clamps was 70mm and a further 5mm was considered between the specimen's end and the clamp to prevent any undesired stress resultants.

The target areas were arranged symmetrically at both ends (Figure 3.25), and the relative rotation between each symmetrical pair of the vertical lines/sections was obtained through photogrammetry.

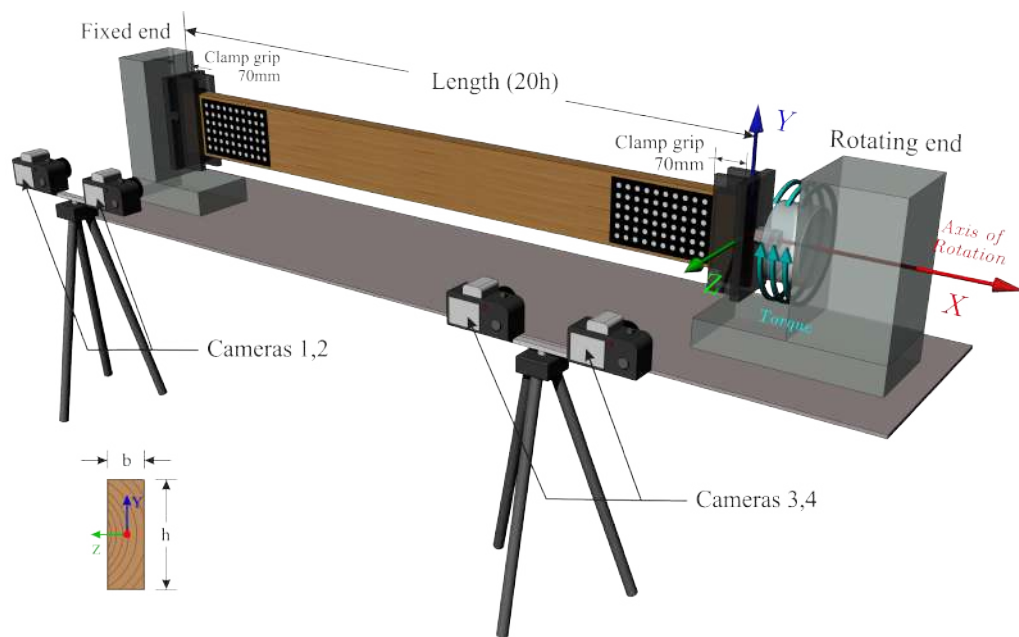
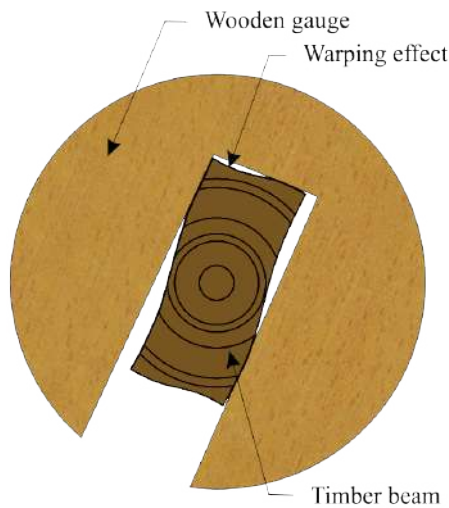


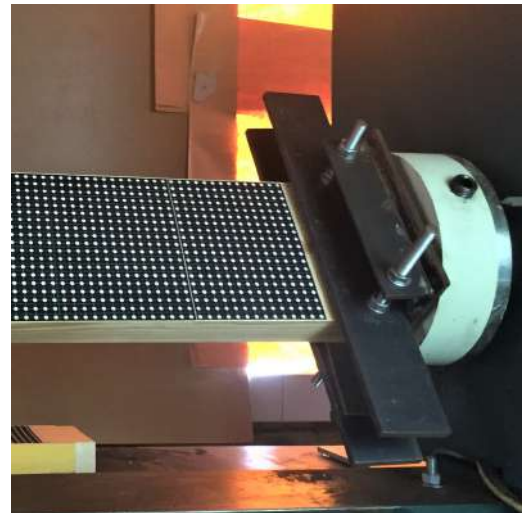
**Figure 3.25:** Torsion test and the photogrammetry setup

3.8.1.7 Rotation measurement system

The photogrammetry method was employed for the rotation measurements instead of the conventional circular wooden gauges (Figure 3.26a). The circular wooden gauges may be suitable for the small scale measurements, but they become inefficient when measuring large rotations at multiple sections. Possible warping effect of the timber beam can influence the measurement using the conventional gauges. On the other hand, the photogrammetry method provided surface depth and disparity that enabled the shear modulus determination at any desired section. The targets for the photogrammetry are shown in Figure 3.26b.



(a) Circular wooden gauge and possible warping effect



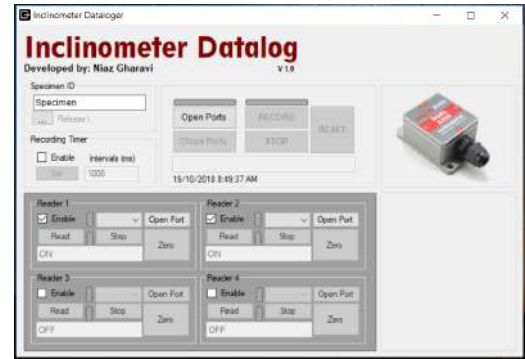
(b) Clamps and the target area

Figure 3.26: Circular gauge and torsion clamping system

For the laminated bamboo lumber specimens, two digital inclinometers were also mounted on the back of the beam to compare the results of the photogrammetry with the readings of the inclinometers (Figure 3.27a). The inclinometers are designed and manufactured by the trade name of RION. These inclinometers are usually used in the automotive and robotics industries for control and measurement systems. To extract the readings of the inclinometers, a C# programme was developed to read and record the data from the multiple inclinometers (Figure 3.27b).



(a) The inclinometer attached on the beam



(b) Developed Inclinometer data-logger

**Figure 3.27:** Inclinometers and developed data-logger

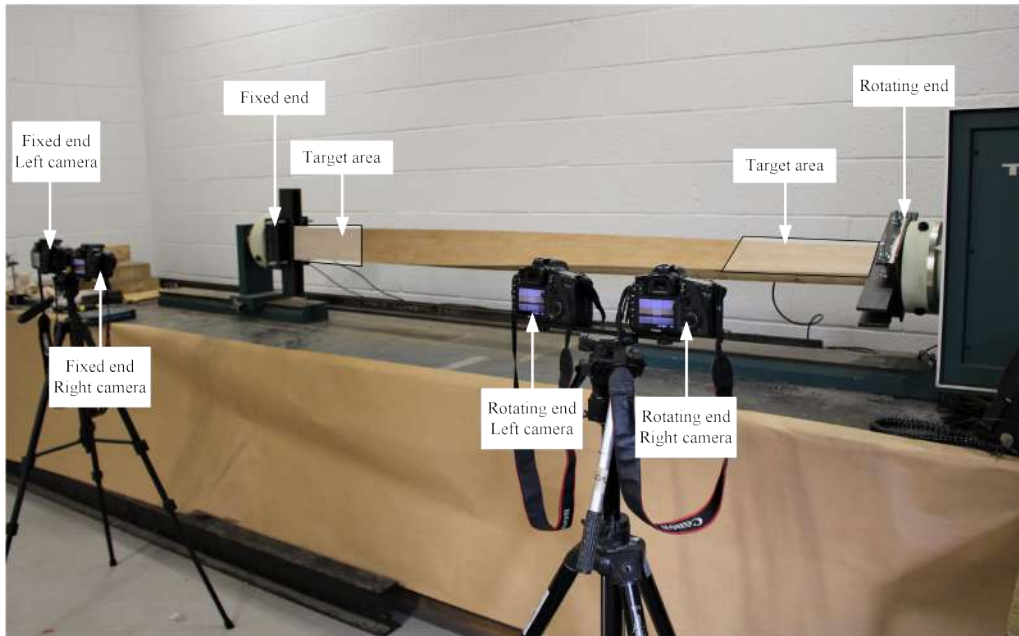


**Figure 3.28:** Photogrammetry setup for the torsion test

### 3.8.1.8 Photogrammetry and inclinometers comparison

Assuming that the measurements of the inclinometers is the true rotation of the beam, the accuracy of the photogrammetry measurement was compared to the readings of the inclinometers. The inclinometers were placed at the distance of 200mm away from the clamp on the opposite side of the photogrammetry target points. Figure 3.29 compares the rotations measured using two systems for TRC1 and TRC2. The comparison was the same for other tested specimen. The error of the photogrammetry measurement was less than 3% of the inclinometer readings.

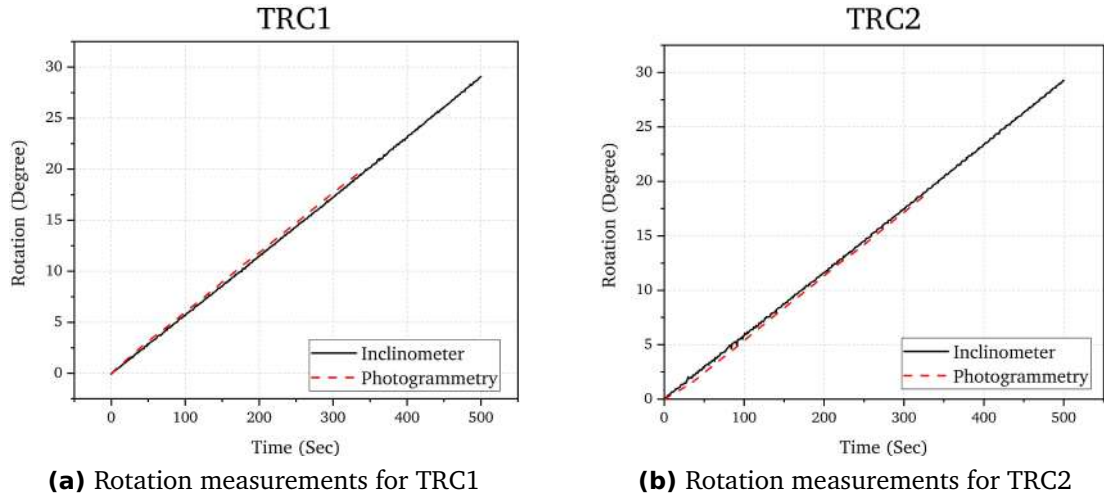


**Figure 3.29:** Rotation measurements comparison between the photogrammetry and the inclinometers

### 3.8.1.9 Analysing process

The images were computed using an image processing software called MvTec HALCON (MVtec Software GmbH, 2012). The 3D coordinates of each target point were extracted using the approach described in Section 3.3. The set of coordinates can profile the surface deformation of the beam. By tracing the coordinates of each vertical lines, the rotation of each section was computed using a linear regression algorithm with a MATLAB programme. Specimens were pre-loaded to  $4^\circ$  rotation to account for systematic and human errors. Then all the subsequent coordinates and forces were referenced to this position.

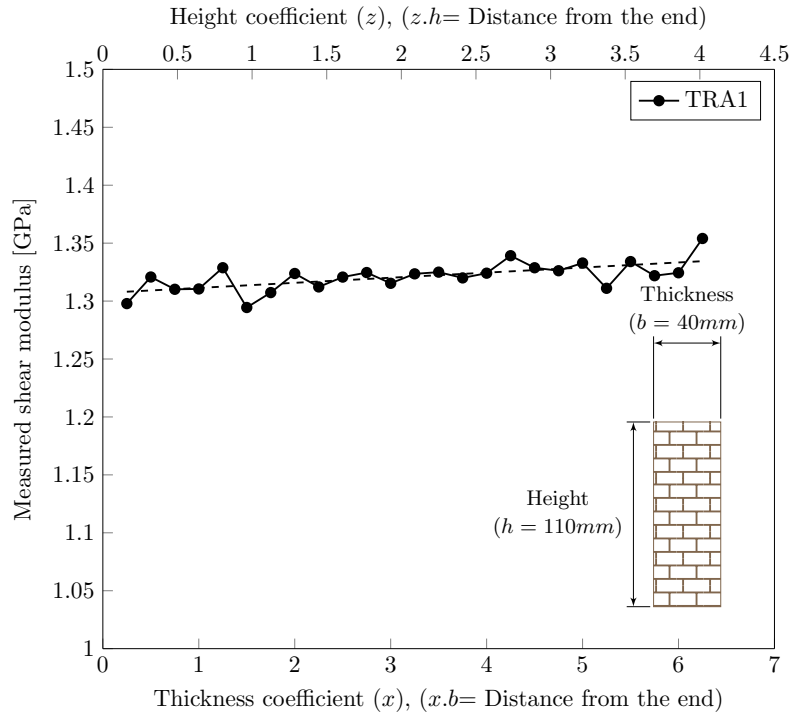
The cameras were triggering simultaneously at the constant intervals to record the torque and the rotation at every section (vertical line). The torque stiffness of each of the vertical sections can be calculated and the corresponding shear modulus can then be determined using the Equation 3.20 based on Saint-Venant's torsion theory;

$$G_{tor} = \frac{k_{tor}}{\eta hb^3} l_1 \quad (3.20)$$

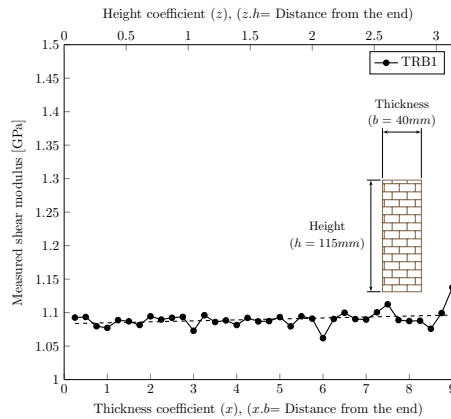
where,  $k_{tor} = \frac{T}{\phi_i}$  is the torque stiffness,  $T$  is applied torque,  $\phi_i$  is relative rotation between each symmetrical pair of vertical sections ( $i$ ),  $G_{tor}$  is the shear modulus and  $l_1$ ,  $\eta$ ,  $h$  and  $b$  are: free testing length, shape factor, cross-sectional depth and thickness of the beam, respectively.

### 3.8.1.10 Results and the proposed decay length

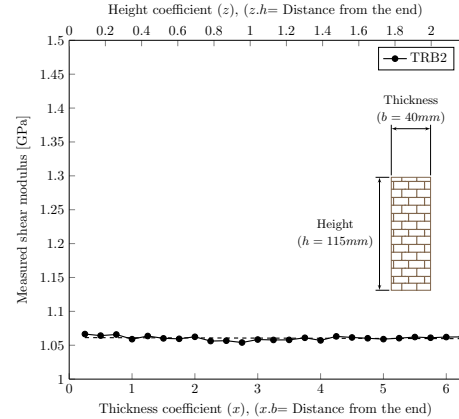
The corresponding shear modulus of each vertical section was calculated from the obtained relative rotations. The calculated shear modulus based on the relative rotation at each vertical section is plotted against the distance of this section from the end, presented in Figure 3.30 for the LBL specimens and Figure 3.31 for wood samples. The 3D coordinates of the target points for TRA1 were unobtainable due to an error in the calibration process.



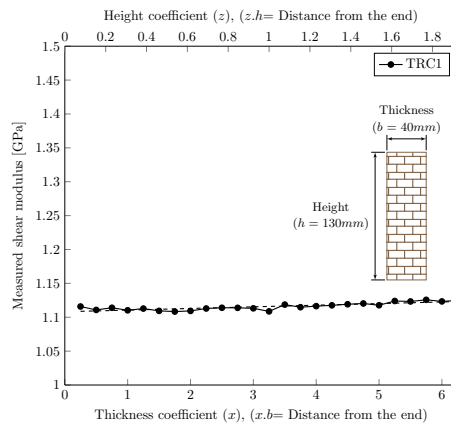
(a) TRA2



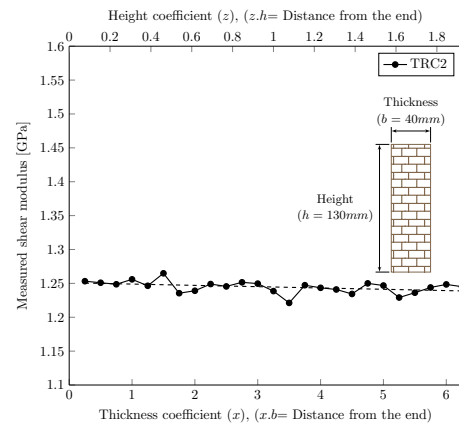
(b) TRB1



(c) TRB2



(d) TRC1



(e) TRC2

Figure 3.30: Laminated bamboo lumber's calculated shear modulus

### CHAPTER 3. MATERIAL PROPERTIES AND TESTING METHODS

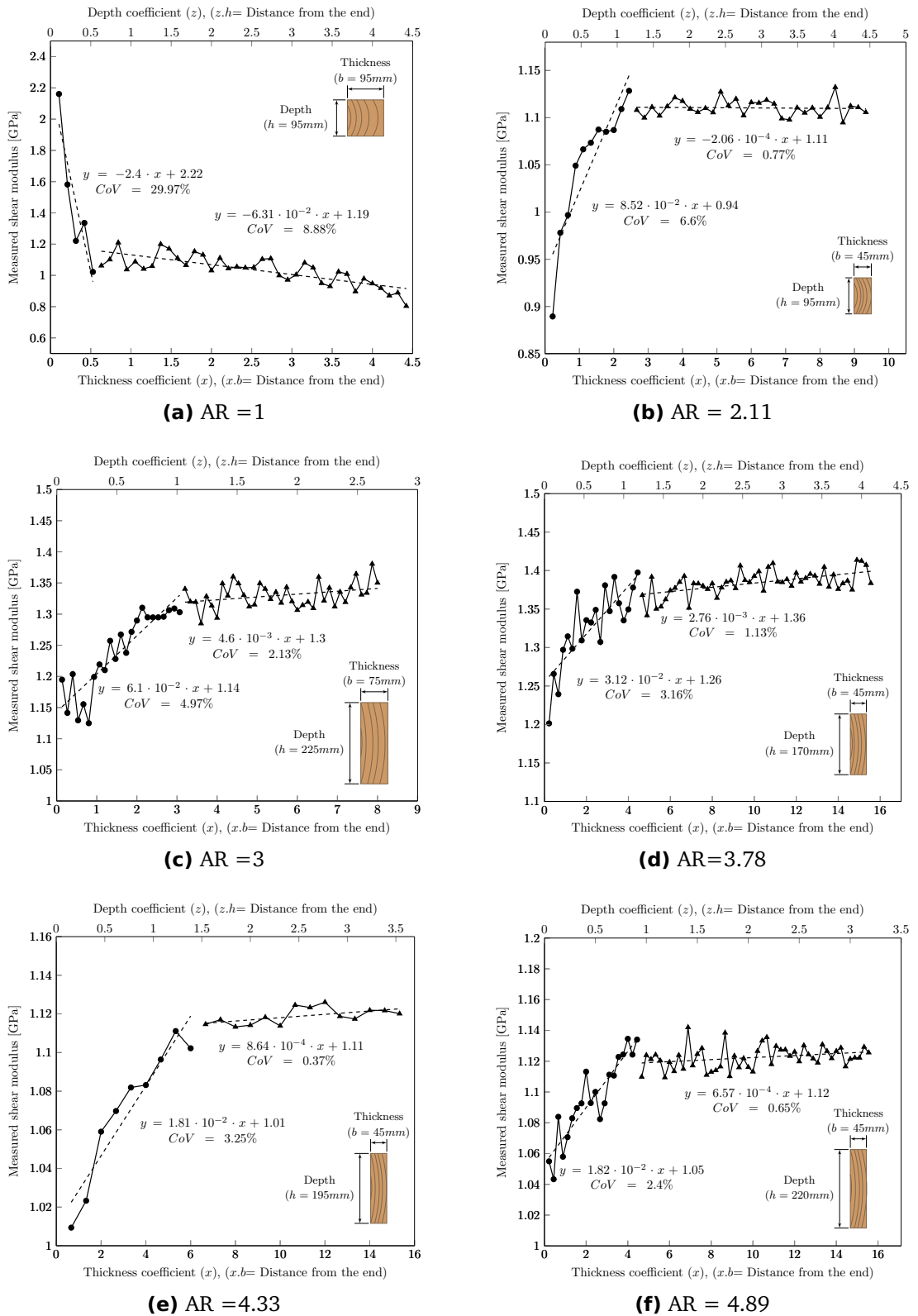


**Figure 3.31:** Measured shear modulus for timber specimens

According to the results of these experiments, there was no significant variation in the

calculated shear modulus of the laminated bamboo with respect to different rotation measuring sections. However, the results of the shear modulus determination for the timber specimens revealed that the shear modulus of the beam varies depending on the rotation measuring sections due to Saint Venant's end effect. The reason for the different shear modulus variation in laminated bamboo and wood is unclear for now and yet to be investigated. On the other hand, the results of these experiments provided shreds of evidence in contrast with the context of BS EN 408.

Based on the Saint-Venant's principle, in order to achieve a uniform shear stress distribution, and subsequently uniform shear modulus, gauge distances should be sufficiently far enough from the ends. The end effect will have an impact on the shear modulus measurement of any section that is not far enough from the end. A simple representation of this impact is in the variation of the determined shear modulus. The variation of the measured shear modulus illustrated in Figure 3.31 evidently shows the decay of the end effect from the ends. The abscissas on the top and bottom are plotted in terms of depth and thickness coefficients. Each Figure was then divided into two segments; segment one has high variation in the shear modulus measurement due to the significant impact of the end effect, whereas segment two experienced low variation, implying considerably low impact.

Since the impact of the end effect is substantially higher in segment one compared to segment two, the length of segment one is considered as the decay length of the end effect. The length of segment one for each specimen with the different aspect ratios have been collected and converted into the corresponding coefficients of depth and thickness using equations equations 3.21 and 3.22.

$$\text{Depth coefficient}(z) = \frac{\text{Length of segment one}}{\text{depth}(h)} \quad (3.21)$$

$$\text{thickness coefficient}(x) = \frac{\text{Length of segment one}}{\text{thichness}(b)} \quad (3.22)$$

It is interesting to note that the specimen with a very low aspect ratio (i.e. AR=1) has relatively higher variation in both segment one and two, compare to those in other specimens (Figure 3.31). This may be because of the fact that the torsional effect of the transverse bending loads travels longer distances in specimens for the low aspect ratio beams.

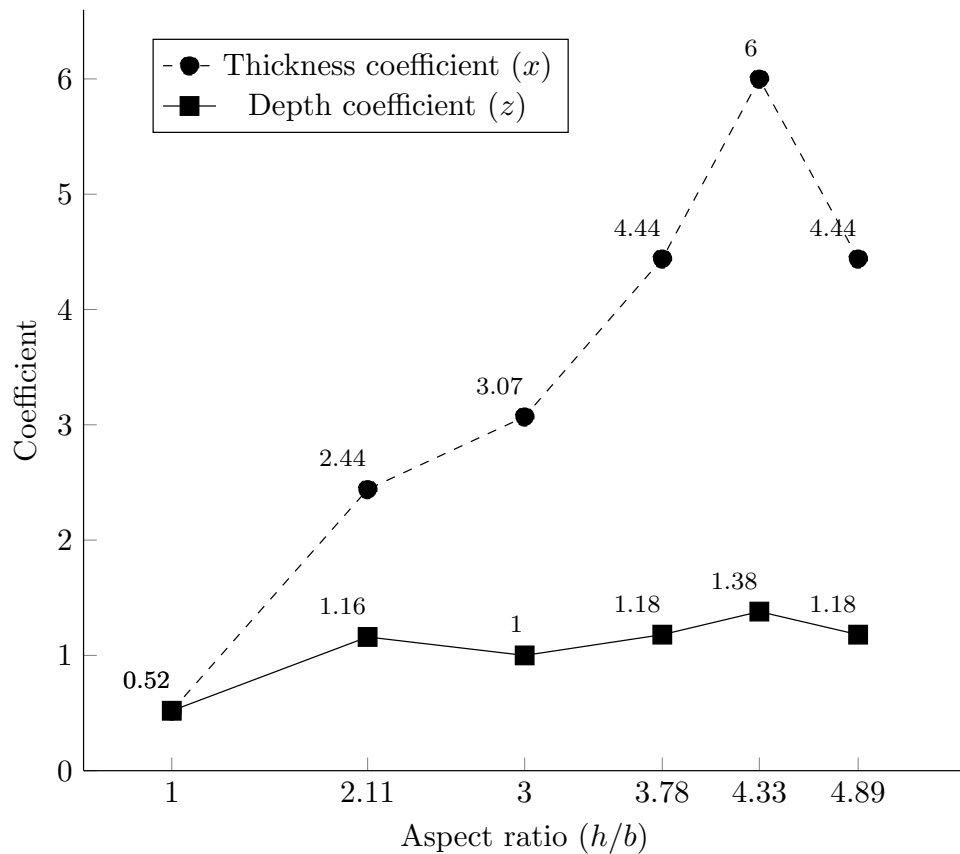


**Figure 3.32:** End effect decay length coefficients of tested aspect ratios

The depth of a specimen is more accepted and agreed as a reference dimension in specifying the end effect decay length, rather than its thickness (Gupta et al., 2002b; Horgan and Simmonds, 1994). It is beneficial for us to compile a comparison using our test results to verify this assumption. The coefficients of both thickness and depth are compared in Figure 3.32. The decay length of the end effect can be estimated using either curves in Figure 3.32 when an aspect ratio is given. However, the coefficient of depth is a more suited parameter when determining the upper bound of the coefficient. Hence, it would be more appropriate to use the depth as the referencing dimension in BS EN 408 (BSI, 2012).

The upper bound of the depth coefficient can be considered as the reference dimension to quantify the end effect decay length. Based on the results of this study, 1.5 to 2 times the cross-sectional depth is the minimum distance required to be excluded from the end when determining the rotation.

The results of this study revealed that the distance recommended by BS EN 408 is clearly not far enough to avoid the impact of the end effect in the shear modulus measurement.

The conclusions drawn from previous numerical and analytical research agree with the results of this experimental study. Gupta et al. (2002b) through a numerical investigation recommended excluding two times the cross-sectional depth, plus the grip distance from either end to obtain a uniform shear stress distribution. Based on the analytical equation proposed by Horgan and Simmonds (1994), the decay length is between 1.8-3 times the cross-sectional depth. The decay lengths suggested by Gupta et al. (2002b) and Horgan and Simmonds (1994) are in a conservative range which is in the safe zone.

### 3.8.1.11 Shear modulus of laminated bamboo lumber

Although the rotation measuring sections have not impacted the measured shear modulus of laminated bamboo, the mean shear modulus between 1.5 to 2 times the cross-sectional depth is considered as the shear modulus of the material. Therefore, the mean shear modulus of laminated bamboo is 1168 N/mm<sup>2</sup>.

### 3.8.2 The Shear Field Test Method

The shear modulus of the structural sized lumber can be determined using the Shear field test method. According to BS EN 408 BSI, 2012, the shear field test method is based on the four-point bending test which creates similar loading situation in reality. However, this method does not provide true shear behaviour of the material due to the nature of the applied load which is combined stress distribution. This method is based on the shear distortion measurement of the beam at the region under the constant shear stress.

Photogrammetry not only enabled accurate measurements of the shear distortion of a beam, but the displacement of a grid of targets (a surface) can also be extracted to investigate the impact of location and size of the constructing square in the shear properties of the beam. This impact was investigated and the results were published in conference and journal papers (Gharavi and Zhang, 2018; Gharavi et al., 2018a).

#### 3.8.2.1 Constructing square

BS EN 408 advise using two metallic arms which act as instruments to measure the diagonal distortion of the constructing square (Figure 3.33a). The diagonals deformation is defined as the shear deformation of the beam. The shear stress distribution over the constructing

square is presented in Figure 3.33b. Determination of the shear modulus  $G_{SF}$  of the beam using the shear field test method was proposed in detail by Brandner et al. (2008). The shear field test method was included in BS EN 408:2010 BSI, 2012 following the recommendations of Brandner et al. (2007) and Brandner et al. (2008).

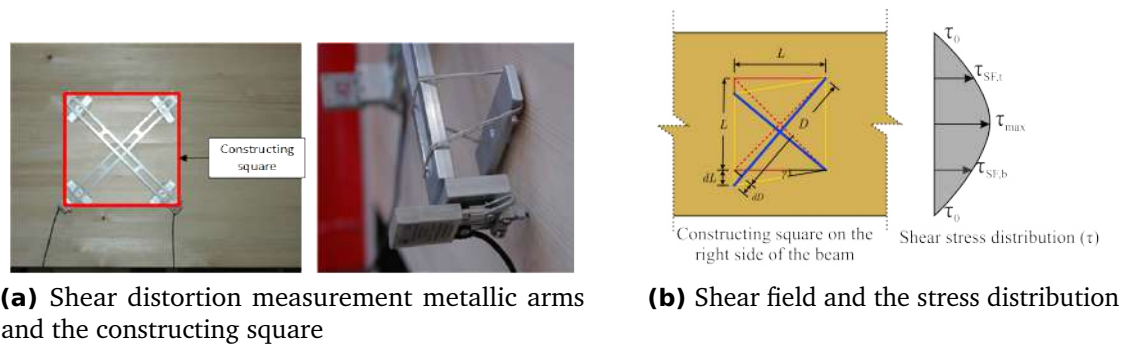


Figure 3.33: The constructing square and the stress distribution

### 3.8.2.2 The concept of the shear field method

According to BS EN 408, the shear distortion of the beam needs to be measured at the middle of the constant shear span by determining the changes in diagonals of the constructing square (Figure 3.34a) when subjected to flexural loading, as illustrated in Figure 3.34b.

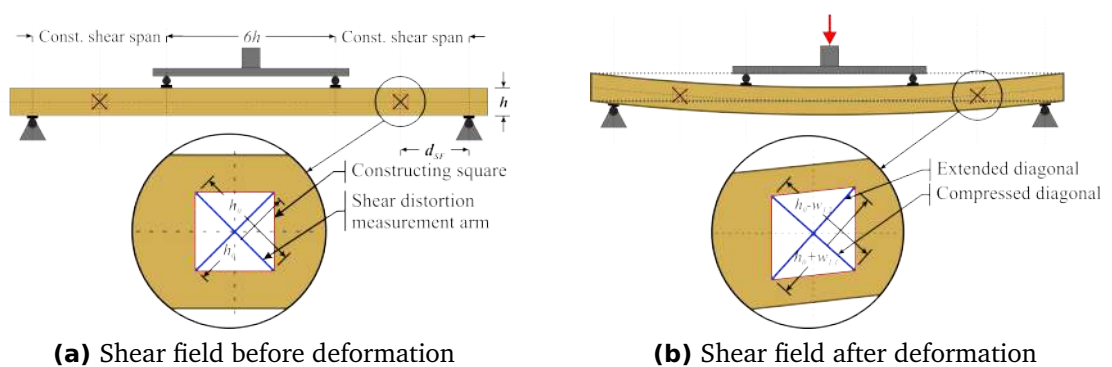


Figure 3.34: The concept of shear deformation in the shear field test method

The shear modulus of the beam can be determined using the Equation 3.23.

$$G_{SF} = \alpha \frac{h_0(V_{s,2} - V_{s,1})}{bh(w_2 - w_1)} \quad (3.23)$$

where,  $\alpha = \frac{3}{2} - \frac{h_0^2}{4h^2}$ ,  $h_0$  is length of the un-deformed square diagonals;  $h$  and  $b$  are the cross-sectional depth and width, respectively;  $w_i$  is the mean deformation of both diagonals of the square at both sides of the beam for the given shear load; and  $V_{s,i}$  is the shear load as  $i$  being the load increment.

Although the square size was considered when assigning the shear correction factor ( $\alpha$ ), the impact of the size has not been experimentally investigated. According to [Brandner et al. \(2008\)](#), shear correction factor ( $\alpha$ ) can be determined using (Equation 3.24).  $\alpha$  is based on the relationship between shear stress distribution over the whole cross-section of the beam and shear stress distribution over the shear field area (Figure 3.33b).

$$\alpha = \frac{\tau_{SF}}{\tau_0} + \frac{3(\tau_{max} - \tau_{SF})}{2\tau_0} \quad (3.24)$$

In terms of the location of the square within the shear constant area, BS EN 408 recommends placing the square in the middle of the span. On the other hand, [Brandner et al. \(2008\)](#) placed the square at the fixed distance of  $d_{SF} = 500mm + L/2$  from the adjacent end.

Six glue-laminated beams were tested according to the guideline given in BS EN 408. Analysis of Variance (ANOVA) was performed on the acquired data to evaluate the impact of size and position of the square in the determination of the shear modulus of the beam.

### **3.8.2.3 Experimental procedure**

The shear field test was conducted following the specifications given in BS EN 408 BSI, [2012](#). Each specimen was supported vertically and transversely. The vertical supports were spanned 16 times the cross-sectional depth ( $h$ ), while the lateral restraints were provided to prevent any out of plane displacement. The loading was applied at a constant rate of 6 mm/min.

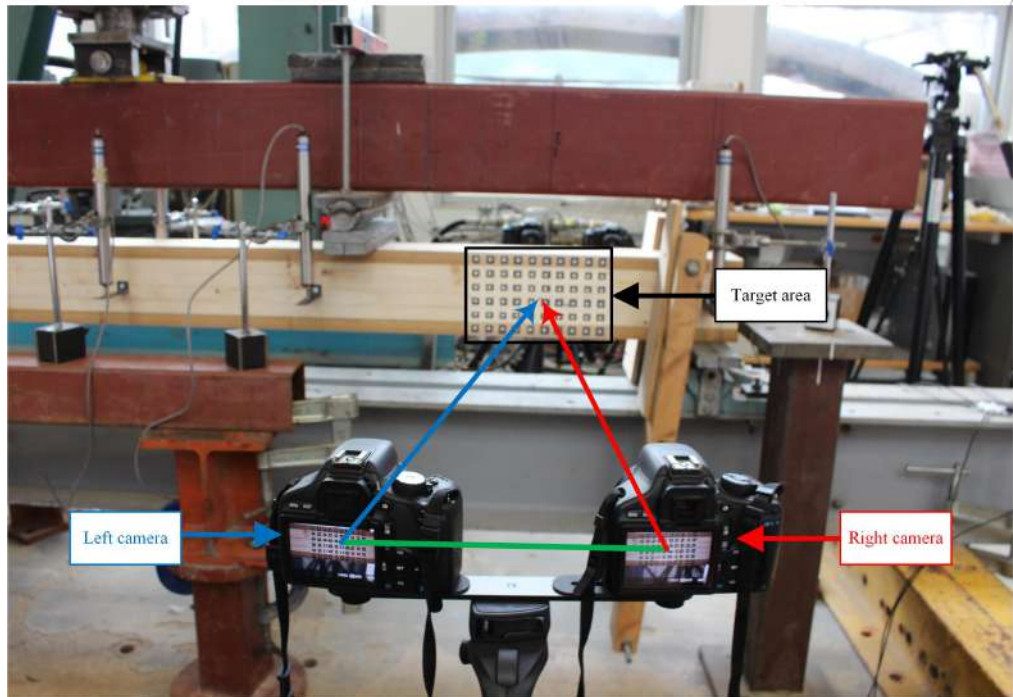


**Figure 3.35:** Photogrammetry setup for the shear field test method

The shear deformation was captured by the developed photogrammetry method using two Canon EOS 70D cameras on one side and two Canon EOS 550D cameras on the other. The cameras captured the images every 5kN load increment simultaneously until the fracture happened. The captured images were processed using MvTec HALCON (MvTec Software GmbH, 2012) to extract the 3D coordinates of each target point in the world coordinate system. Comparing every step with the initial coordinate of any target point reveals the displacement of the point in three dimensions.

The target points were mapped on the sides of the beams in a grid-like layout (Figure 3.36). Each target was spaced 25 mm from adjusting targets and can be considered as a corner of a square. Therefore, several squares with different sizes and positions were considered using these target points. Using each constructing square, the shear modulus of the beam can be determined following Equation 3.23.

Based on the square sizes and positions, four cases were considered for analysis (Figure 3.36a to Figure 3.36d). Cases one, two and three evaluate the impact of the square position using small, medium and large size squares, respectively. Case four evaluates the impact of the square size when the squares were placed at the centre of the constant shear span. The

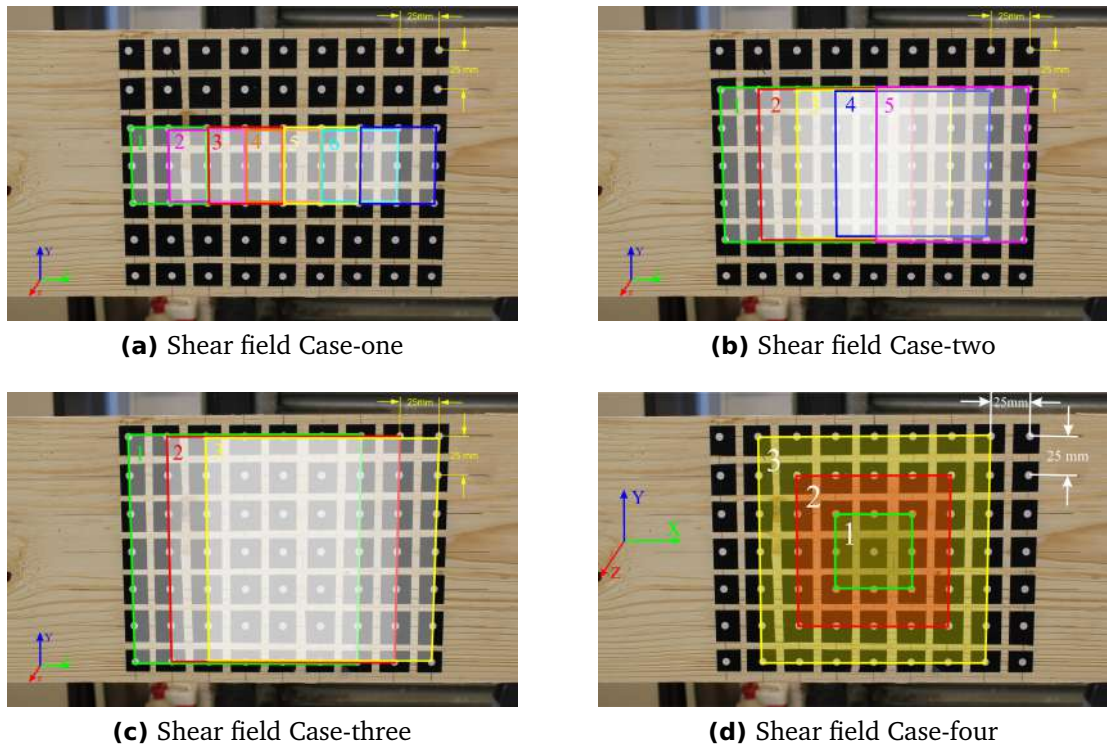


**Figure 3.36:** Four cases of the constructing square's sizes and positions

squares in each model are symmetric to the neutral axis - this is due to the fact that the shear field test method is based on parabolic and symmetric shear stress distribution over the cross-section of the beam (Brandner et al., 2008).

#### 3.8.2.4 Analysis of variance on the shear modulus variation

Analysis of Variance (ANOVA) has been carried out to evaluate the impact of the size and the position of the constructing square in the determination of the shear modulus. The study was based on the position of three types of squares with different dimensions, which can be seen in Figures 3.36a, 3.36b and 3.36c. The calculated shear modulus of the beams for each cases can be found in Tables 3.6-3.8. The ANOVA analysis has indicated that the position of the square is not an affecting factor in the determination of the shear modulus of a beam. This, clearly, confirms the constant shear deformation of a beam within the constant shear stress area in the four-point bending test. Although, in the areas close to the loading or support, the deformation may change due to the end effect.

On the other hand, the impact of the size of the constructing square on the variation of the shear modulus of the beam was analysed in case-four. As can be seen from Figure

### CHAPTER 3. MATERIAL PROPERTIES AND TESTING METHODS

**Table 3.6:** Measured shear modulus\* for small squares (Fig. 3.36a)

Square No.	Beam 1	Beam 2	Beam 3	Beam 4	Beam 5	Beam 6
1	1299.1	1054.2	1214.2	1225.6	1282.9	1117.2
2	1257.2	1012.0	1096.5	1137.0	1533.6	1187.2
3	1269.3	1132.5	1163.9	1306.3	1259.2	1262.1
4	1239.1	1311.5	1082.7	1394.4	1224.8	1226.8
5	1249.3	1284.1	1057.7	1555.6	1171.2	1177.9
6	1269.1	1201.4	1092.3	1423.1	1113.6	1282.9
7	1351.0	1148.2	1173.2	1287.4	1059.5	1172.4
<b>Mean</b>	<b>1282.5</b>	<b>1163.4</b>	<b>1125.8</b>	<b>1332.8</b>	<b>1235.0</b>	<b>1203.8</b>
CoV[%]	2.98	9.55	5.13	10.35	12.45	4.75

\* The measure shear modulus are in N/mm<sup>2</sup> or MPa

**Table 3.7:** Measured shear modulus\* for medium squares (Fig. 3.36b)

Square No.	Beam 1	Beam 2	Beam 3	Beam 4	Beam 5	Beam 6
1	1266.0	1116.7	1148.4	1359.5	1261.2	1136.9
2	1258.2	1122.9	1154.0	1465.7	1296.2	1340.6
3	1276.2	1155.6	1130.3	1478.6	1258.2	1329.0
4	1297.8	1162.0	1135.9	1421.4	1313.7	1365.0
5	1377.0	1277.2	1193.0	1400.6	1176.3	1287.8
<b>Mean</b>	<b>1321.5</b>	<b>1197.0</b>	<b>1170.7</b>	<b>1380.1</b>	<b>1218.7</b>	<b>1212.4</b>
CoV[%]	3.72	5.55	2.14	3.41	4.20	7.04

\* The measure shear modulus are in N/mm<sup>2</sup> or MPa

**Table 3.8:** Measured shear modulus\* for large squares (Fig. 3.36c)

Square No.	Beam 1	Beam 2	Beam 3	Beam 4	Beam 5	Beam 6
1	1412.6	1216.8	1344.5	1604.7	1418.0	1279.2
2	1384.0	1222.9	1375.7	1595.3	1412.9	1775.1
3	1415.3	1235.8	1409.5	1583.7	1536.2	1670.2
<b>Mean</b>	<b>1413.9</b>	<b>1226.3</b>	<b>1377.0</b>	<b>1594.2</b>	<b>1477.1</b>	<b>1474.7</b>
CoV[%]	1.23	0.79	2.36	0.66	4.79	16.59

\* The measure shear modulus are in N/mm<sup>2</sup> or MPa

## CHAPTER 3. MATERIAL PROPERTIES AND TESTING METHODS

**Table 3.9:** Measured shear modulus\* based on the square size (Fig. 3.36d)

Square size	Beam 1	Beam 2	Beam 3	Beam 4	Beam 5	Beam 6
Small square	1239.2	1311.5	1082.7	1394.4	1224.8	1226.8
Medium square	1276.2	1155.6	1130.3	1478.6	1258.2	1329.0
Large square	1384.0	1222.9	1375.7	1595.3	1412.9	1775.0
CoV[%]	5.79	6.36	13.15	6.77	7.73	20.20

\* The measure shear modulus are in N/mm<sup>2</sup> or MPa

3.36a, three squares with different dimensions were considered and using the distortion measurements of each square corresponding shear modulus was determined. The shear modulus of each beam against the square sizes, i.e. Small, Medium and Large, are given in Table 3.9. The null hypothesis for the impact of square size was set to; "*The size of the square will have no impact on the variation of the shear modulus of the tested beam*". The ANOVA factor,  $F(2, 15) = 3.84$ , for the size impact rejects the null hypothesis. This implies that the size of the square will have an impact on the determination of the shear modulus. Based on the results of these experiments, measured shear modulus of the beam increased with the square size in five out of six tested samples. The higher determined shear modulus in large squares may be due to heterogeneous characteristics of wood and non-uniform deformation near the edges. More research needs to be conducted on the significance of the impact of the square size in the determination of the shear modulus for different cross-sections and species.

### 3.9 Summary

The mechanical properties of laminated bamboo lumber were investigated through Small Clear Specimen and structural sized testing processes. A unique measurement system, i.e. photogrammetry, based on the stereo vision principle was developed and employed for the objectives of this study. The photogrammetry technique is a non-destructive, non-contact and multi-points measurements system. Despite the high accuracy and efficiency, this system relies on the programming skills and the calibration process.

The flexural, tensile and compressive properties of the laminated bamboo and Spruce were investigated through a series of Small Clear Specimen experiments. The three-point bending tests revealed that the orientation of the bamboo strips when producing the

### CHAPTER 3. MATERIAL PROPERTIES AND TESTING METHODS

---

laminated bamboo lumber does not have a significant impact on the flexural properties of the laminated bamboo. Laminated bamboo illustrated 120% higher bending strength ( $f_b = 100.78 \text{ N/mm}^2$ ) than C16 ( $f_s = 46.87 \text{ N/mm}^2$ ), and the bending modulus of the laminated bamboo ( $E_b = 9.3 \text{ kN/mm}^2$ ) is 17% higher than that of the spruce specimen ( $E_s = 7.96 \text{ kN/mm}^2$ ).

Tension and compression tests indicated that laminated bamboo possesses superior strength and stiffness compared to wood samples. Laminated bamboo behaviour is elastic in the tension and tri-linear in compression. In compression, laminated bamboo initiated by an elastic deformation is followed by elastic-plastic and finally, plastic deformations. The slope of the stress-strain of the elastic region in both tension and compression is similar, thus Young's Modulus is equal for both loading conditions. The results of t-tests on the impact of the conditioning environment on the tensile properties of the laminated bamboo showed that the conditioning environment significantly impacts the tensile modulus, but does not affect the tensile strength. Additionally, the existence of knots impacts the tensile strength, but not the tensile modulus.

A constituent model based on the experimental results and the reported literature was developed to define the mechanical properties of the laminated bamboo lumber. Based on this model, laminated bamboo has an elastic behaviour in tension and tri-linear in compression.

Regarding the shear properties of the laminated bamboo, the suitability of the torsion test and the shear field test method were investigated. The torsion test and the shear field tests on the structural-sized specimens were conducted based on the recommendations of the governing codes of practices, i.e. BS EN 408 and ASTM D198.

A thorough investigation into the torsion test revealed that BS EN 408, as a testing reference in the UK, might not fully consider the Saint-Venant's end effect. BS EN 408 recommends measuring the beam's rotation at a distance of two to three times the cross-sectional thickness. Whereas, ASTM D198 suggests to measure the rotation at the distance of two times the cross-sectional depth.

Based on the results of a series of torsional tests on the timber samples, a distance of about 1.5 - 2 times the cross-sectional depth is required to be excluded due to end effect from

### **CHAPTER 3. MATERIAL PROPERTIES AND TESTING METHODS**

---

both ends when measuring the rotation of a beam. The end effect decay length needs to be excluded to obtain a uniform shear stress distribution. On the contrary, the shear modulus of the laminated bamboo was observed to be independent from the rotation measuring sections. The mean shear modulus of the laminated bamboo is  $1168 \text{ N/mm}^2$ . The causes for the discrepancy in the shear modulus variation in the wood and laminated bamboo are unclear and yet to be investigated further.

In regard to the shear field test method, results of the experimental study and analysis of variance revealed that the size of the constructing square, where the shear distortion measured, may influence the measured shear modulus. The shear modulus seems to increase by selecting a larger square.

# I-BONE LAMINATED BAMBOO HYBRID BEAM

## 4.1 Introduction

This chapter focuses on the development and evaluation of an [I-Bone Laminated Bamboo Hybrid Beam \(IBHB\)](#). The concept of the I-bone laminated bamboo timber hybrid beam was introduced in the Introduction (Chapter 1) and further detailed in Chapter 2.

The manufacturing process for the industrial production of the [IBHB](#) along with the prospective challenges and limitations are described, including the experimental investigation resulting from a structural-sized four-point bending test. The flexural and shear properties of the beams were determined according to BS EN 408 ([BSI, 2012](#)). Mathematical models considering both linear and non-linear stress distribution of laminated bamboo and timber were developed and compared with the experimental values. The manufacturing process, including component fabrication, gluing and preparing the hybrid beams, and experimental work were conducted in the laboratories of Edinburgh Napier University.



**Figure 4.1:** Manufactured beams for this stage of the experiments

## 4.2 Beams and Fabrication Process

### 4.2.1 Beams

Figure 4.1 illustrates the manufactured beams. The aim of this chapter is to develop and investigate the mechanical properties of [I-Bone Laminated Bamboo Hybrid Beam \(IBHB\)](#) (Figure 4.1a). Additionally, a [Laminated Bamboo Sandwich Beam \(BSB\)](#) (Figure 4.1b) and a [Glue Laminated Beam \(GB\)](#) (Figure 4.1c) were produced and tested for comparison purposes.

In total, four [IBHBs](#) with two different types of adhesive were manufactured, these adhesives are [Phenol Resorcinol Formaldehyde \(PRF\)](#) and [Melamine Formaldehyde \(MF\)](#). This was to determine which adhesive is better suited for a stronger bond between laminated bamboo and wood. While some research revealed that the type of adhesive affects the bond between laminated bamboo and wood ([Sinha and Clauson, 2012](#)), most Glulam manufacturers use the two types of adhesive used in this study.

### 4.2.2 Materials

For the testing, commercially available laminated Moso bamboo was provided by Bamboo Import Europe BV. Laminated bamboo was constructed using bamboo strips with a thickness of 4-5 mm and a width of 22 mm. Bamboo strips do not have any joint in the production of laminated bamboo. The nominal dimensions of the boards were 40 mm thick, 600 mm wide and 2440 mm long.

## CHAPTER 4. I-BONE LAMINATED BAMBOO HYBRID BEAM

For the timber, C16 structurally graded spruce was used, sourced to Norway and locally purchased from St Andrews Timber & Building Supplies Ltd. The dimensions of the timber were 45 mm thick, 170 mm wide and 2400 mm long. Since a collaboration with a manufacturer could not be secured to prepare the samples, the timber was obtained with larger sizes to enable the trimming and reduction of thickness.

Regarding adhesives, Hexion Inc. provided two types of two-component adhesives. These adhesives were: a phenol, resorcinol, formaldehyde resin (*AG-5675Q*) that was mixed with paraformaldehyde hardener (*CASCOSET FM-6310L*) to form a durable and structural bond, and a two-component liquid melamine formaldehyde resin (*Cascomel 4720*) with liquid hardener Wonderbond Hardener (*5025A*).

### 4.2.3 Fabrication process

Figure 4.2 illustrates the three types of beams that were designed and produced for this study; they each have similar cross-sectional dimensions. Four **IBHB** were divided into two groups of two, based on the type of adhesive used for their fabrication. Group 1 uses **Melamine Formaldehyde (MF)**, and group 2 uses **Phenol Resorcinol Formaldehyde (PRF)**. One **BSB** and one **GB** were produced, both using **PRF** glue. Nominal dimensions of each beam are shown in Figure 4.2 and values are given in Table 4.1.

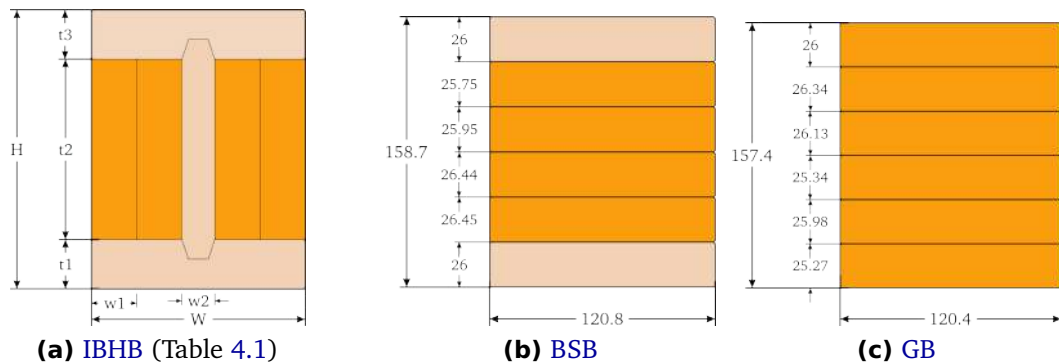


**Figure 4.2:** Schematic cross-sections of the beams

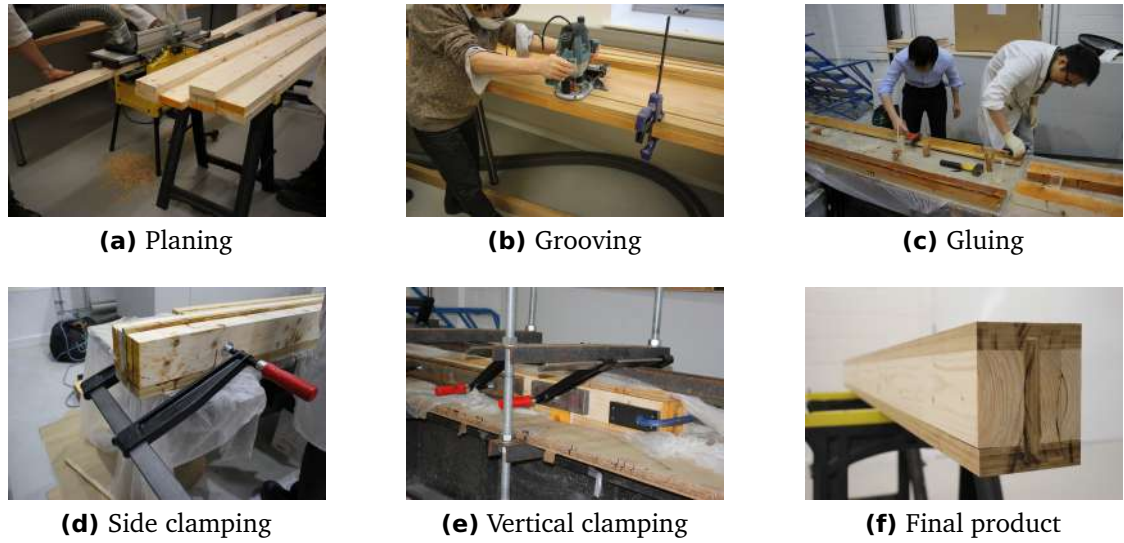


Figure 4.3: Manufacturing procedures

Table 4.1: Nominal dimensions of the manufactured beams

Beam	Length	$a$	$l_1$	Width	Height	$w1^*$	$w2^*$	$t1^*$	$t2^*$	$t3^*$
IBHB1-1	2390	660	990	127.87	164.8	55	20	30	105	30
IBHB1-2	2390	660	990	125.80	164.7	55	20	30	105	30
IBHB2-1	2395	660	990	128.73	164.0	55	20	30	105	30
IBHB2-2	2395	660	990	125.17	164.5	55	20	30	105	30
BSB	2260	662	936	120.84	158.7	-	-	26	-	26
GB	2260	662	936	125.17	164.5	-	-	26	-	26

\* Labels assigned in Figure 4.2 and the values are nominal not actual.

Prior to fabrication, the laminated bamboo and timber were conditioned in a controlled laboratory environment, with a temperature of 14-16°C and humidity of 70-80% for three weeks before processing them. This was to ensure both materials were in equilibrium and prevent any possible warping and expansion.

The manufacturing process for each beam was carried out across two weeks in the same laboratory environment. The process started by cutting the material to the required dimensions within 24 hours of gluing. For IBHB, grooves and chamfers were cut using a hand router. The parts were then glued, assembled and clamped to produce the final product. The manufacturing steps shown in Figure 4.3 can be described as following:

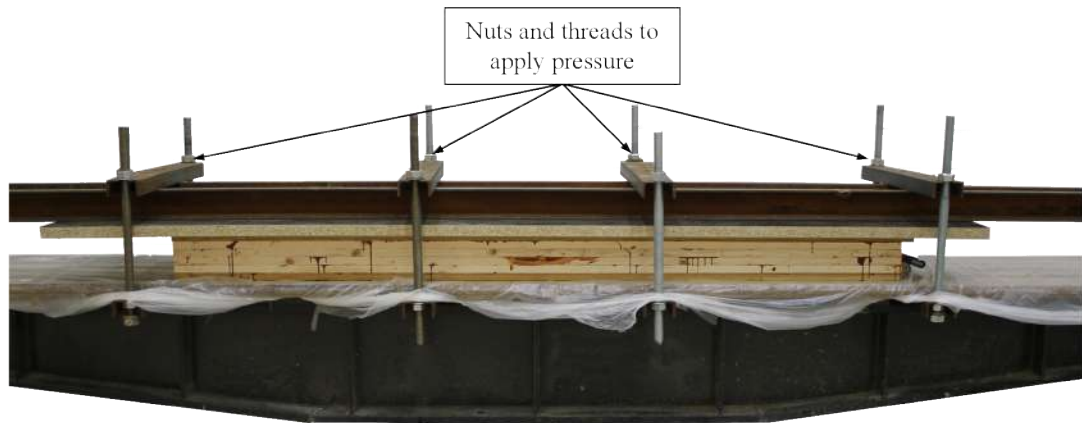


**Figure 4.4:** Vertical clamping system

1. Manufacturing started by cutting laminated bamboo and timber to the required dimensions and reducing the thickness using a thickness planer. The channels and grooving were manually cut by a hand router with a bevel shaped bit at  $75^\circ$ .
2. The side timbers were laminated, and their surfaces trimmed to remove uneven edges and excess glue.
3. Adhesives were mixed to the ratio recommended by the manufacturer. This ratio is 2.5 parts by water resin to one part hardener for PRF and four parts by water resin to one part hardener for MF type adhesive. The mixtures were applied on both adjacent surfaces of each component at a spread rate of  $200\text{-}225\text{ g/m}^2$ .
4. After gluing, transverse pressure was applied using four G-Clamps and vertical pressure of between  $0.8\text{-}1\text{ N/mm}^2$  was applied using a pressure rig (Figure 4.4). The pressure was applied for a minimum of 8 hours (overnight).
5. Once the pressure was removed from the beams, they rested without tension for another 24 hours. The edges were trimmed, and excess glue removed for finishing.

#### 4.2.4 Manufacturing Challenges

The manufacturing was conducted in separate stages to refine process at each stage. However, producing the beams in a laboratory environment brought additional issues, including:

1. The staff needed to be trained to be able to work the required machinery.
2. Due to the lack of proper equipment and skills, the process of cutting and reducing the thickness were difficult and challenging. The material waste was also higher than expected due to lack of proper machinery.
3. Each component had to be precisely cut to reduce gaps in the final product (Figure 4.5a). To achieve this precision, several groups of undergraduate and masters students were asked to assist in the fabrication of the beams as part of their final year dissertation.
4. The glue had to be applied quickly and uniformly with hand glue spreaders. Mixing and applying glues using industrial machines can distribute the adhesives evenly across the surfaces while minimising the glue waste.
5. The pressure was applied using a clamping system that used nuts and threads as illustrated in Figure 4.4. The applied pressure was approximated by measuring the applied torque on the nuts using a digital torque meter. Torque to the applied pressure conversion can be conducted using Equation 4.1.

$$\text{Force} = \frac{\text{Torque}}{\text{Lever arm length} \times \text{Sin}(\text{bolt connection angle})} \quad (4.1)$$

### 4.2.5 Manufacturing Recommendations

To mitigate the challenges and limitations of manufacturing IBHB, the following recommendations are proposed:

1. The constituent materials need to be conditioned in the same environment to mitigate the warping effect, expansions and swellings.
2. Each component needs to be cut precisely to reduce the gap between them. Computer Numerical Control (CNC) machines would provide accurate and precise cuts.
3. Although two-side gluing was used in these experiments, single-side is also applicable as recommended by Glulam production code of practice BS EN 14080 (BSI, 2013a). For one-sided gluing it is recommended by the glue manufacturer to apply at the rate of 400-450 g/m<sup>2</sup>.

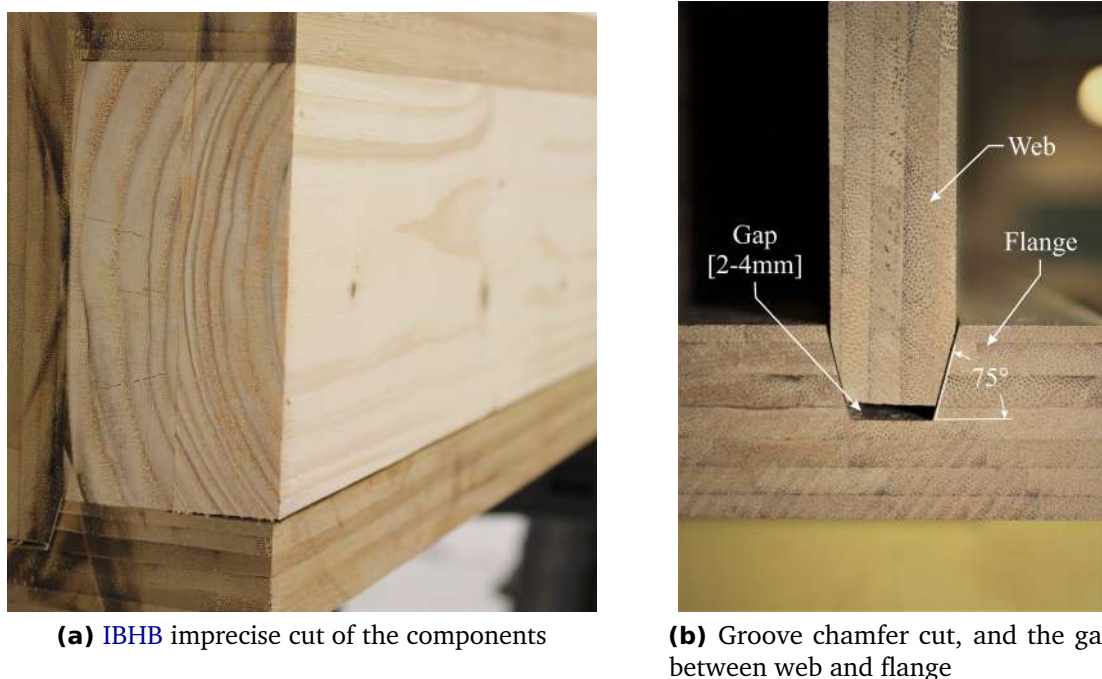


**Figure 4.5:** IBHB foreseeable defect and required groove cut

4. A 2-4mm gap is recommended between the laminated bamboo web and flanges in the channel (Figure 4.5b). This is to ensure the side timbers are in full contact with the flanges without resulting in undesired stresses in flanges.
5. The groove and channel were cut at 75° to ensure full contact and form a rigid connection between web and flanges. The rigidity of the formed joint in the web and flanges connecting point determines the efficiency of the fastening system as the tapered and groove connection performed up to 92% stiffer against the plane connection, i.e. without tapered groove (Leichti et al., 1990a). Based on the multiple trial in this study, the groove angle can be different, but it is best to keep it less than 90° and higher than 60°.

After trimming, the beams were prepared for testing and the final products can be seen in Figure 4.6. Despite a few fabrication problems, the overall joint and connection of components were deemed satisfactory.



(a) I-Bone Laminated Bamboo Hybrid Beam

(b) Laminated Bamboo Sandwich Beam

**Figure 4.6:** Final products

### 4.3 Experimental Evaluations

#### 4.3.1 Beam preparation for testing

After the fabrication of the beams, excess glue and uneven edges were removed using a thickness planer. Beams were then conditioned for four weeks before being tested. The dimensions of the beam were measured and target points for photogrammetry were attached.

#### 4.3.2 Four-Point bending test

The beams were tested in a four-point bending test according to the specifications outlined in BS EN 408 (BSI, 2012). The test arrangements depicted in Figure 4.7 and test setup is shown in Figure 4.8. The loading span was 15 times the cross-sectional height and loading points were six times the height ( $l_1$ ) apart from each other. Steel plates, 80 mm wide, were inserted to minimise the indentation.

Loading was applied at a constant rate of 6 mm/min until failure at about 8-11 minutes. The beams were simply supported, and lateral restraints were placed to prevent out of plane displacement.

#### 4.3.3 Measurement apparatus

Six Displacement Transducers (LVDTs) were used to record the ultimate deflection and curvature of the beams. The LVDTs were placed at mid-span and at a distance 2.5 times the

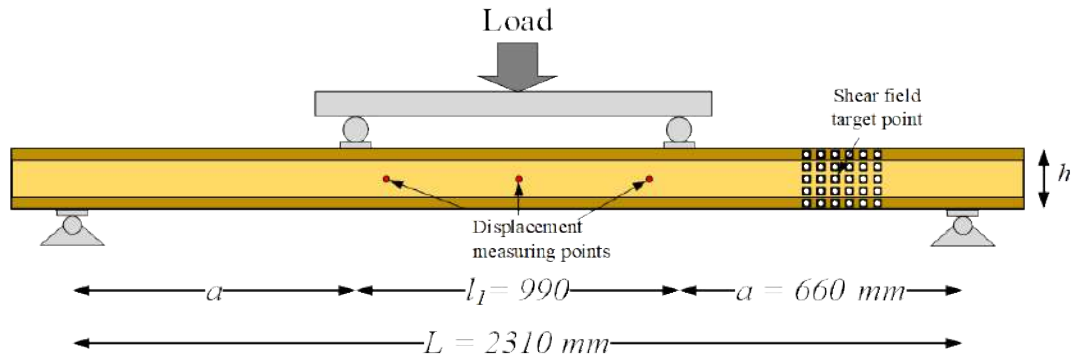


**Figure 4.7:** Four-point bending test configurations

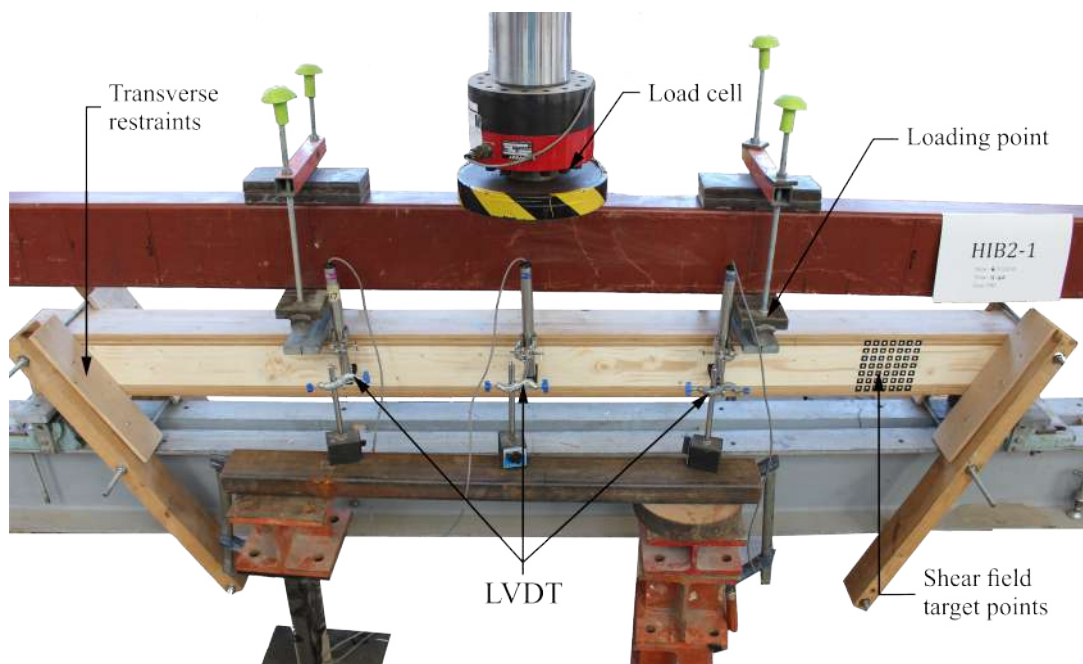


**Figure 4.8:** Four-Point bending test setup

height on either side of mid-span, on both sides as BS EN 408 recommends. The reading of the deflection was undertaken from the start of the test until beam failure.

#### 4.4 Thermal and Moisture Expansions

The temperature change can lead to the dimensional change in wood and wood-based products. A dry wood expands by increasing the temperature, and shrinks if the temperature is reduced. However, for the wood with a moisture content greater than 4%, this effect is rather different. Two reactions occur when a moist wood heated; the wood starts to expand due to thermal expansion phenomenon and then the water within the fibres

starts to evaporate which make the wood shrink. The shrinkage effect of the moisture loss is far greater than thermal expansion, thus, the moist wood shrinks in total when heated (WoodHandbook2010). The specific gravity of the wood material is proportionate to the linear thermal expansion coefficient in the radial and tangential directions (Weatherwax and Stamm, 1956).

Change in the moisture content seems to have a negligible effect on the thermal expansion coefficient according to Goli et al. (2019). However, the change in the moisture content of wood induces dimensional change which is greater than that of thermally-induced expansion. Wood Handbook (WoodHandbook2010) suggests that the dimensional change due to moisture variation within the range of 4% to 14% can be estimated using the following equation:

$$\Delta D = D_l [C_T (M_2 - M_1)] \quad (4.2)$$

where  $\Delta D$  is the dimensional change,  $D_l$  is the length before the change,  $C_T$  is the dimensional change coefficient in the tangential direction,  $M_1$  and  $M_2$  are the moisture content before and after the change.

### 4.4.1 How bamboo behaves due to moisture and thermal changes?

The physical characteristics including thermal expansion, shrinkage and swelling data of bamboo and engineered bamboo products are scarce in the literature. Bamboo and wood are hygroscopic, means they tend to absorb moisture from the surrounding air. Bamboo's moisture-related dimensional changes are much higher than that of thermal expansion. Moreover, the transverse (radial and tangential) expansions are also much higher (1-5 times of the magnitude) than longitudinal changes (Huang et al., 2017; Long et al., 2010). Unlike wood, bamboo's shrinkage in the radial direction is reported to be greater or equal to its tangential direction. This is due to lack of radial fibres in the bamboo's wall (Liese and Köhl, 2015). Regardless of this difference, it can be assumed that bamboo and wood behaves similarly to moisture and thermal changes. However, the magnitude of their dimensional change varies.

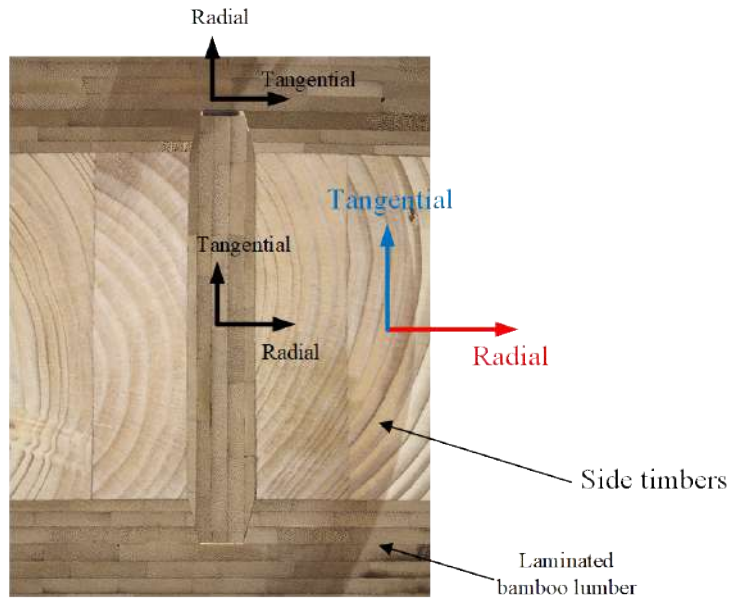


**Figure 4.9:** IBHB's principal directions with respect to grain direction

#### 4.4.2 The moisture and temperature change in the IBHB

In the case of IBHB, tangential expansion is important since it can induce internal stresses to the flanges if side timbers and LBL web expand in the tangential direction. Figure 4.9 shows the principal directions of the constituent materials of IBHB. The side timbers and laminated bamboo web are oriented in the same directions hence compromise each other when temperature and moisture change. Equation 4.2 can represent the dimensional change for both timber and bamboo. Giving a similar moisture change and initial length ( $D_1$ ), the dimensional change coefficient (shrinkage coefficient) determines the rate of changes between side timbers and LBL web.

The shrinkage coefficient of Norway spruce in the tangential direction is 4.81% (Hansson et al., 2017) which is lower than most of the reported shrinkage coefficients (6%-12%) by Wood handbook (WoodHandbook2010). This is because C16 Norway spruce has a low density which leads to low dimensional changes. On the other hand, the tangential shrinkage coefficient of bamboo widely ranges from 4.87% to 7.769% (Yu et al., 2008).

According to the shrinkage coefficients of the timber and bamboo, the dimensional change of laminated bamboo web is slightly higher than side timbers. This means that in the case of expansion there will be no undesired stresses induced from side timber to the flanges. Contrary, there will be small pressure applied to the flanges by side timber when the beam

shrinks. However, the magnitude of this stress is small since the shrinkage coefficients of both materials are similar.

## **4.5 Failure Mechanism**

The failure mechanism of the beams can be categorised into two modes: mode 1 assigned to the scenario that the beam fails within elastic deformation. This failure comprises the fracture due to shear, delamination or tensile. On the contrary, Mode 2 refers to the situation that the beam undergoes elastic-plastic deformation due to compression yield.

### **4.5.1 Glulam beam failure**

As depicted in Figure 4.10, the Glulam beams failed at the tensile surface and propagated to the adjacent layers, followed by delamination across the glue-line. A defect, e.g. a knot, initiated the failure at the mid-span. The failure observation and load-deflection graph of the Glulam beam revealed a brittle failure with no sign of elastic-plastic deformation whereas Glulam beams generally undergo elastic-plastic deformation. This form of failure can be due to insufficient clamping pressure or excess natural defects.



**Figure 4.10:** Glulam Beams' failure

### **4.5.2 Laminated bamboo sandwich beam failure**

Similar to GB, BSB failed in the elastic range with no sign of elastic-plastic deformation. However, BSB fractured rather differently than Glulam beams. The failure can be categorised as a horizontal shear failure, where the beam fails in the mid-depth without reaching



**Figure 4.11:** Bamboo sandwich beam failure

its full flexural capacity. This mode of failure implies the weakness is in the shear region of the cross-section. This weakness can be due to a strength difference between the bamboo and timber material (C16), which causes the timber to fail before the bamboo layers. Another possibility may be due to the insufficient shear strength of the adhesive, or again, insufficient clamping pressure (Figure 4.11).

#### **4.5.3 I-bone laminated bamboo hybrid beam failure**

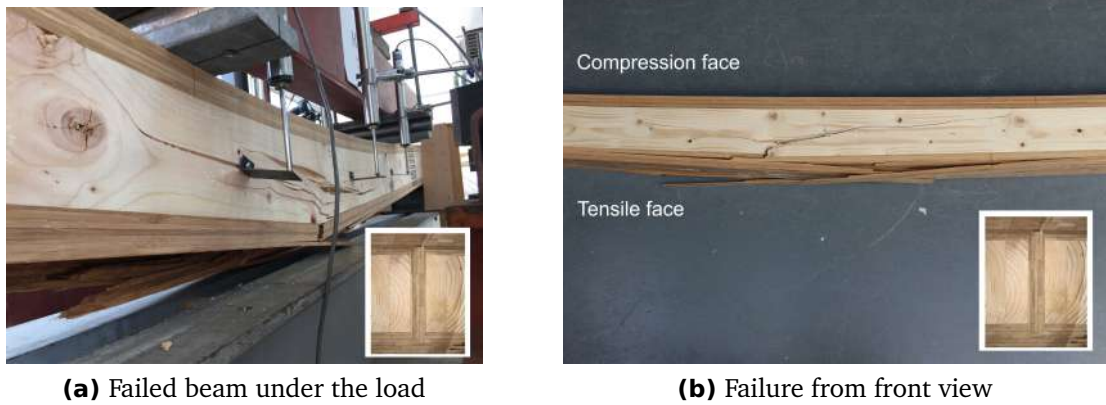
In contrast to the control samples, **IBHB** exhibited a considerably stronger performance with elastic-plastic deformation which indicates compressive yield. Failure observations (Figure 4.12) and the load-deflection graph of **IBHB** show an elastic start with higher bending moduli than the other two, **GB** and **BSB**, followed by elastic-plastic deformation, and finally a brittle failure. This mode of failure is more favourable in timber-based composite beams which indicate ductile behaviour.

Figure 4.13 shows that failure initiated at the tensile surface and immediately propagated to the adjacent layer. Sounds of micro-cracks were audible before fracture, however, they were not as frequent as in the timber Glulam beam. No compression failure was observed.

Based on the results of this study, MF resin performed considerably better than **PRF** in



Figure 4.12: IBHB failed under flexural load



(a) Failed beam under the load

(b) Failure from front view

Figure 4.13: I-bone laminated bamboo hybrid beam failure (Glue: MF)

bonding laminated bamboo and timber. IBHB-PRF illustrated shear failure which implies insufficient bonding strength between adjacent lamina (Figure 4.14). This weakness in IBHB-PRF substantially impacted the flexural properties of the hybrid beam. Laminated bamboo lamina at the tensile surface was undamaged and delamination only occurred at the connection between the bottom flange and the web.

Research conducted by Sinha and Clauson (2012) also concluded that the type of adhesive is an affecting factor on the flexural strength of a bamboo hybrid material. They reported that isocyanate-based resin performs better compared to PRF. In line with Sinha and Clauson (2012)'s findings, the results of these experiments revealed that PRF might not be a suitable resin in bonding bamboo-based products with wood.

The surface pH value, wettability and buffering capacity are reported as the influencing factors in the gluability of the bamboo and engineered bamboo products (Chaowana,



(a) Failed beam under the load



(b) Delamination of the beam at the flange connection

**Figure 4.14:** I-bone laminated bamboo hybrid beam failure (Glue: PRF)

2013). Therefore, further research is required to identify the significance of this impact and the reasons for this incompatibility.

## 4.6 Results of the Experimental Evaluations

### 4.6.1 Flexural properties

The beams were categorised as long beams with a loading span equal to or longer than 15 times their cross-sectional depth. The failure mechanisms were described in the previous section. Load-deflection curves of GB, BSB and IBHB are shown in Figure 4.15 and details are given in Table 4.2. Density measurements were undertaken after each test on a small sample of the specimen.

It is apparent that MF resins create a better bond between laminated bamboo and wood than PRF resins. IBHB-MF experiences elastic-plastic deformation as well as elastic displacement whereas IBHB-PRF failed at the end of the elastic region. On the other hand, both resins illustrated a similar stiffness and proportionality limit which can be seen in the constitutive behaviour of both materials, depicted in Figure 4.15. MF resin provides IBHB with full flexural capacity. Comparing the ultimate load-bearing capacity seems invalid for these cases, as a mode of failure for IBHB-PRF and IBHB-MF is different. The properties of IBHB-MF will be the reference property for IBHB in the following sections. Figure 4.16 compares the load-deflection graphs of beams tested in this stage of experiments. This graph reveals that introducing a web into the BSB not only increases the maximum load-bearing capacity

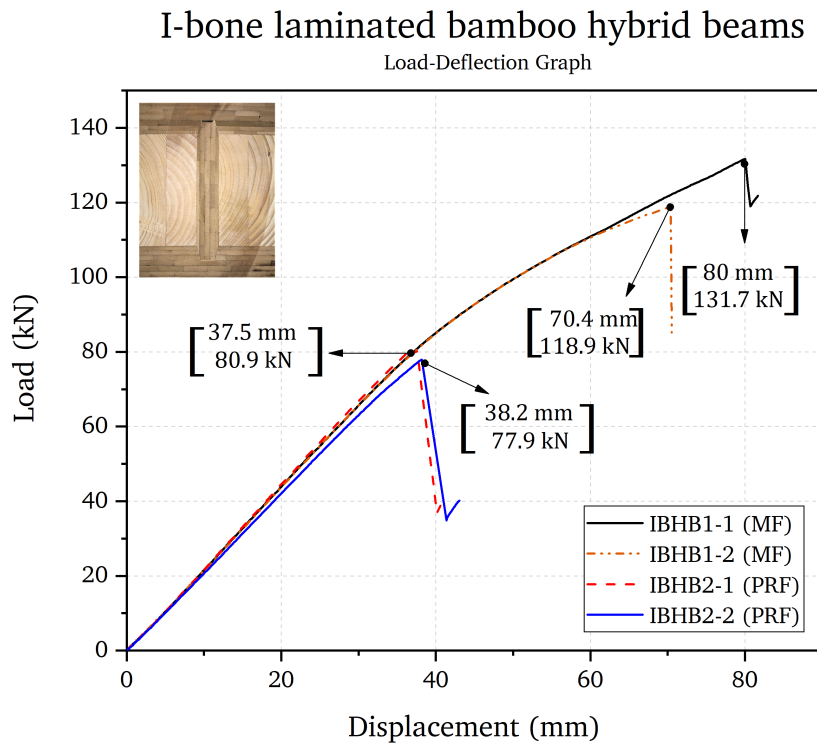


**Figure 4.15:** IBHB beams’ load-deflection graph

**Table 4.2:** The four-point bending test outcomes

Beam	Glue	Failure mode*	Density	$F_{max}$	$W_{max}$	$M_{max}$
			[kg/m <sup>2</sup> ]	[kN]	[mm]	[N.mm]
HIB1-1	MF	2	538.6	131.68	80.06	43.45
HIB1-2	MF	2	540.1	118.93	70.39	39.25
HIB2-1	PRF	1	537.8	80.93	37.53	26.71
HIB2-2	PRF	1	538.2	77.92	38.19	25.71
HB	PRF	1	470.0	76.54	41.75	25.34
GL	PRF	2	429.2	39.04	28.22	12.92

\* Failure mode scenarios are described in Section 4.5

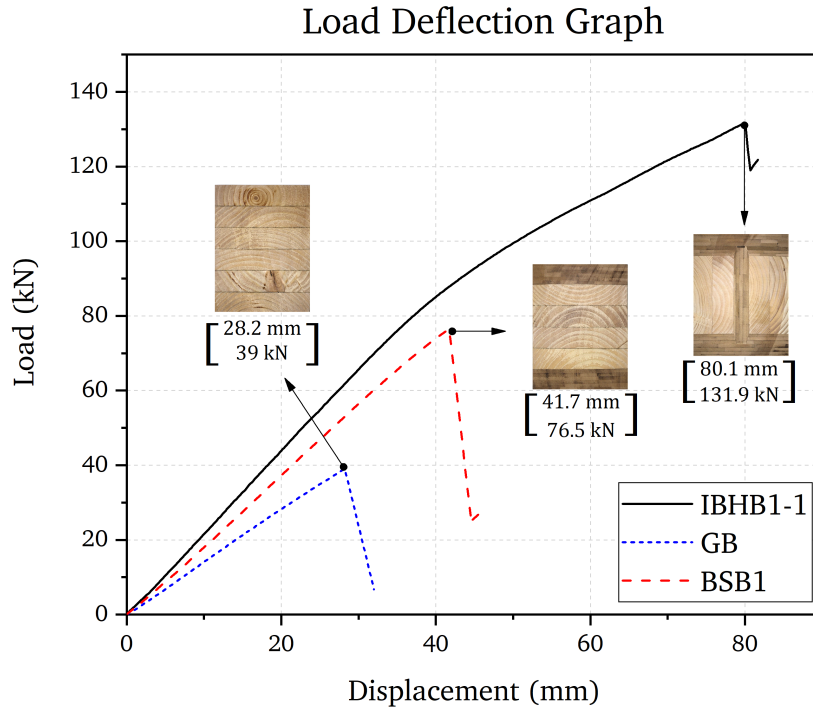


**Figure 4.16:** Load-deflection comparison between the tested beams

but also enhances the stiffness. **IBHB** was 72% stronger in terms of load-bearing capacity compare to **BSB**. The laminated bamboo web enhances the load-bearing capacity by improving the cross-sectional rigidity and stability. Compared to the Glulam beam, **BSB** had 96% higher load-bearing capacity and **IBHB** had up to 237% higher. In an attempt to quantify the mechanical properties, strength and stiffness were determined as they are two primary material attributes that describe the load and deflection resistance, respectively. The **Modulus of Elasticity (MOE)** was determined from the relationship between load and curvature based on the Euler-Bernoulli beam theory at the elastic range which is situated between 10-40% of the maximum applied load. The **Modulus of Rupture (MOR)** was determined based on the ultimate flexural stress at the extreme tensile fibre.

**MOR** and **MOE** of the tested beams were calculated based on the assumptions of the Euler-Bernoulli beam theory using equations 4.3 and 4.4, respectively.

$$MOR = \frac{3F_{max}a}{bh^2} \quad (4.3)$$

$$MOE = \frac{al^2_1(F_2 - F_1)}{16I(w_2 - w_1)} \quad (4.4)$$

where,  $a$  is the distance between loading point and the nearest support,  $l$  is the span of

**Table 4.3:** Flexural properties based on the four-point bending test

Beam	Glue	Specific Gravity (SG)	$F_{max}$	MOE	MOR	MOR/SG
			[kN]	[kN/mm <sup>2</sup> ]	[N/mm <sup>2</sup> ]	
<b>IBHB1-1</b>	<b>MF</b>	0.539	131.68	13.04	75.05	139
<b>IBHB1-2</b>	<b>MF</b>	0.540	118.93	13.51	69.03	128
<b>IBHB2-1</b>	<b>PRF</b>	0.538	80.93	13.36	46.28	86
<b>IBHB2-2</b>	<b>PRF</b>	0.538	77.92	13.88	45.55	85
<b>BSB</b>	<b>PRF</b>	0.470	76.54	8.26	49.93	106
<b>GB</b>	<b>PRF</b>	0.429	39.04	6.6	25.98	61

the beam,  $I$  is the moment of inertia,  $F_{max}$  is the maximum load,  $w$  is displacement, and  $b$  and  $h$  are cross-sectional width and height, respectively.

The flexural properties of the tested beam are presented in Table 4.3. The results of **IBHB** show a potential increase in the bending strength of 189% and 50% compared to the Glulam and **BSB** control samples, respectively.

**MOE** of the **IBHB** was also enhanced because of the introduction of laminated bamboo web. **MOE** of **IBHB** is doubled compared to **GB** and 60% higher than **BSB**. Based on the results of this test, introducing an **LBL** web into the hybrid beam enhances both bending strength and stiffness. This enhancement is more obvious and significant in terms of bending strength considering the fact that laminated bamboo has higher tensile and compressive strengths.

#### 4.6.2 Ductility

Ductility describes the ability of the material to deform easily after its yielding point, without fracture. The ductility can be defined as the ratio of the curvatures at the maximum loading point ( $\kappa_m$ ) to the curvature at the proportional limit ( $\kappa_p$ ), i.e. where beam yields in the compressive zone (Plevris and Triantafillou, 1992). Ductility and curvature ( $\kappa$ ) can be calculated using the Euler-Bernoulli beam theory as follows:

$$Ductility = \frac{\kappa_m}{\kappa_p} \quad (4.5)$$

The curvature of a beam in a four-point bending test can be determined using triangulation of deflection measurement points (Figure 4.17). According to BS EN 408, the deflection

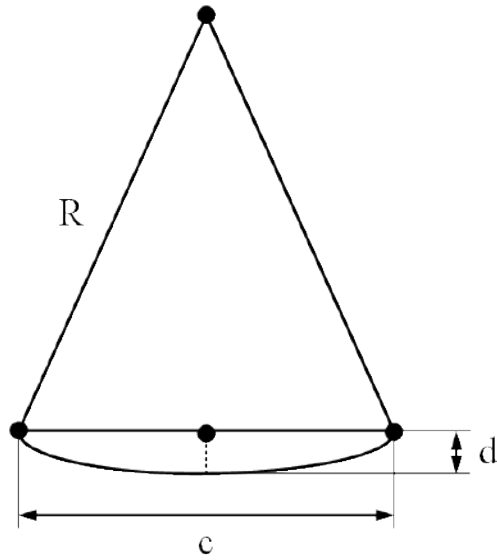


**Figure 4.17:** Triangulation principle to calculate the curvature

**Table 4.4:** Ductility and stiffness of the tested beams

Beam	Glue	Ductility	Flexural Rigidity
IBHB1-1	MF	2.29	420.88
IBHB1-2	MF	1.92	412.93
IBHB2-1	PRF	1.09	417.41
IBHB2-2	PRF	1.09	409.62
BSB	PRF	1	231.80
GB	PRF	1	266.19

measurement was carried out in three points on each side of the beam. These points were located at 2.5 times the cross-sectional depth apart. Assuming that Figure 4.17 represents the deformed beam and three points are the three deflection measuring points we have:

$$R = \frac{c^2 + 4d^2}{8d} \quad (4.6)$$

$$\kappa = \frac{1}{R} = \frac{8d}{c^2 + 4d^2} \quad (4.7)$$

where  $R$  is the radius of the curved beam,  $c$  is the distance between left and right deflection measuring points and  $d$  it the local displacement of the beam.

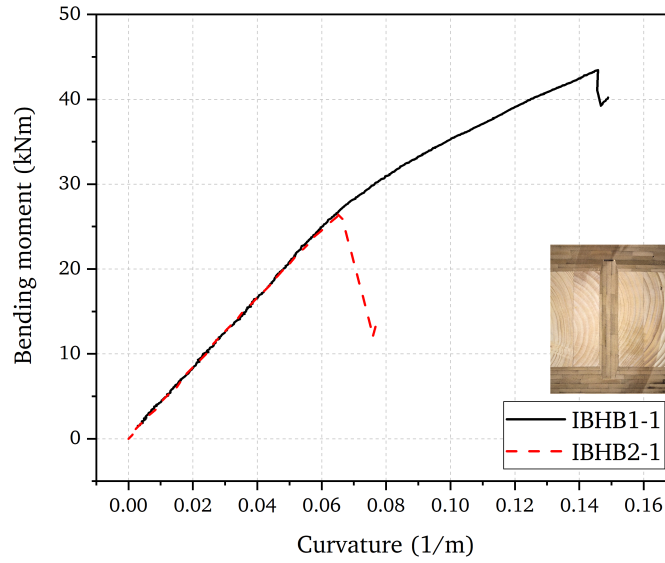


**Figure 4.18:** Moment-curvature relationship

### 4.6.3 Flexural rigidity

The flexural rigidity ( $EI$ ), also known as stiffness, of a beam in bending, can be determined using the bending moment and curvature relationship presented in Equation 4.10. Assuming  $w$  is the vertical displacement,  $M$  is bending moment and  $\kappa$  is the curvature, the following equations can be derived:

$$M = EI \frac{d^2w}{dx^2} \quad (4.8)$$

$$\kappa = \frac{d^2w}{dx^2} \quad (4.9)$$

$$EI = \frac{M}{\kappa} \quad (4.10)$$

Figure 4.18 illustrates the moment-curvature relationship for IBHB made with MF and PRF resins. Based on this relationship, the stiffness of the hybrid beams were determined and presented in Figure 4.19. The beam's stiffness decreases when the compression yield occurs in the beams and this is clearly visible in the flexural stiffness to the bending moment diagrams. The mean stiffness of the elastic deformation in the moment-curvature relationship is considered to be the beam's flexural rigidity and the values are presented in Table 4.4.

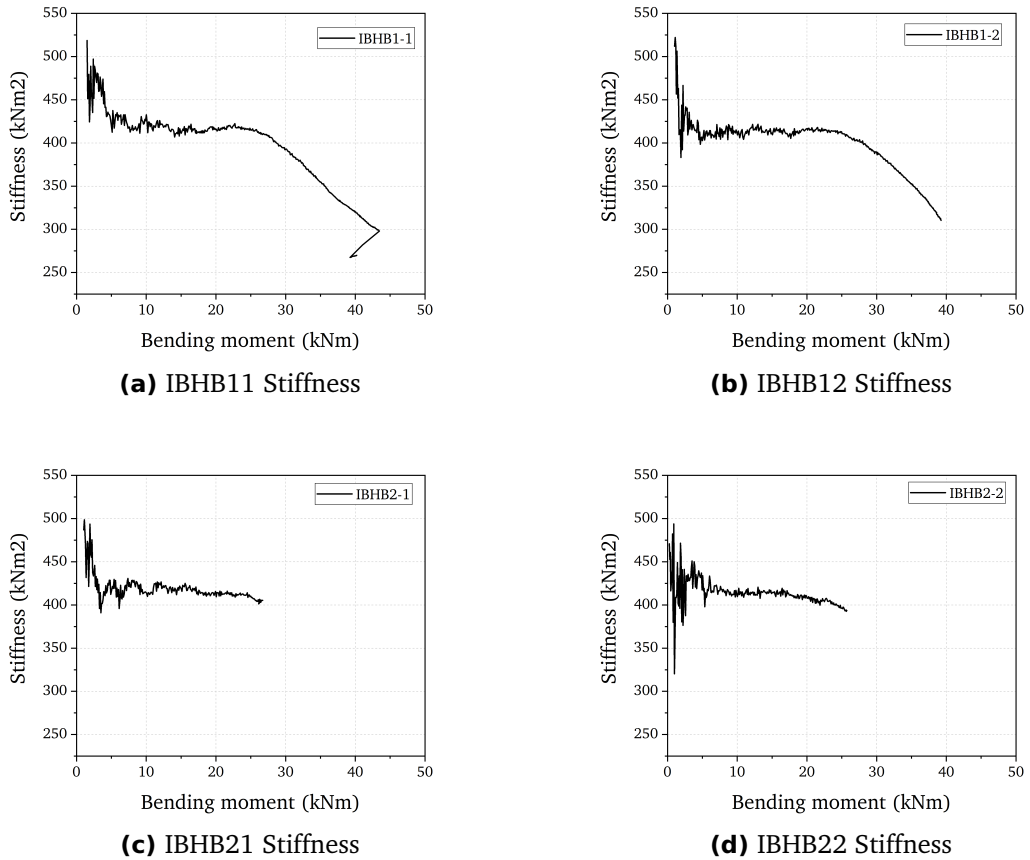


**Figure 4.19:** Flexural rigidity variation against the applied bending moment of IBHBs

## 4.7 Shear Properties of IBHB

### 4.7.1 Shear stress calculations

The shear stress of the IBHB can be calculated using the following equation:

$$\tau = \frac{V}{Ib} \int ydA \quad (4.11)$$

If  $Q = \int ydA$  is the first moment of area, then:

$$\tau = \frac{VQ}{Ib} \quad (4.12)$$

where  $V$  is the transverse shear force,  $Q$  is the first moment of area, i.e. the section above the area of interest,  $I$  is the moment of inertia and  $b$  is the width of the section.

For a rectangular cross-section, the shear stress of a beam is determined using the following equation.

$$\tau = \frac{V}{2I} \left( \frac{h^2}{4} - y^2 \right) \quad (4.13)$$

where  $h$  is the depth of the section and  $y$  is the distance from the neutral axis.

Maximum shear stress can usually be assigned as the shear strength of the beam and occurs in the natural axis for a prismatic beam with symmetric loading conditions. This maximum value is obtained as follows:

$$Q = \frac{bh^2}{8} \quad (4.14)$$

$$y = 0 \rightarrow I = \frac{bh^3}{12} \quad (4.15)$$

Substituting these values give the following equation:

$$\tau_{max} = \frac{3V}{2A} \quad (4.16)$$

In a four-point bending test, loading is applied using two loading points. Due to the symmetry in applying loads, shear force at the constant shear area can simply be determined as half of the maximum applied load, giving:

$$\tau_{max} = \frac{3F_{max}}{4A} \quad (4.17)$$

Whilst the beams did not fail due to shear, the shear strength of the beam is determined and shown in Table 4.5.

#### **4.7.2 Determining shear modulus using the Shear Field test method**

Another parameter that can be determined using a four-point bending test is the Shear Modulus ( $G$ ) of the beam. Shear modulus of a beam can be calculated by measuring the shear distortion of the beam at the region under constant shear stress. Test arrangements and specifications are detailed in BS EN 408 (BSI, 2012). BS EN 408 followed the recommendations of Brandner et al. (2008) when revising its 2010 edition. The method introduced a way of determining shear modulus which better reflects a beam in service.

##### **4.7.2.1 Shear distortion measurements**

As described in Chapter 3 section 3.8.2, BS EN 408 advised using two metallic arms which act as instruments to measure the changes of a constructing square's diagonals.

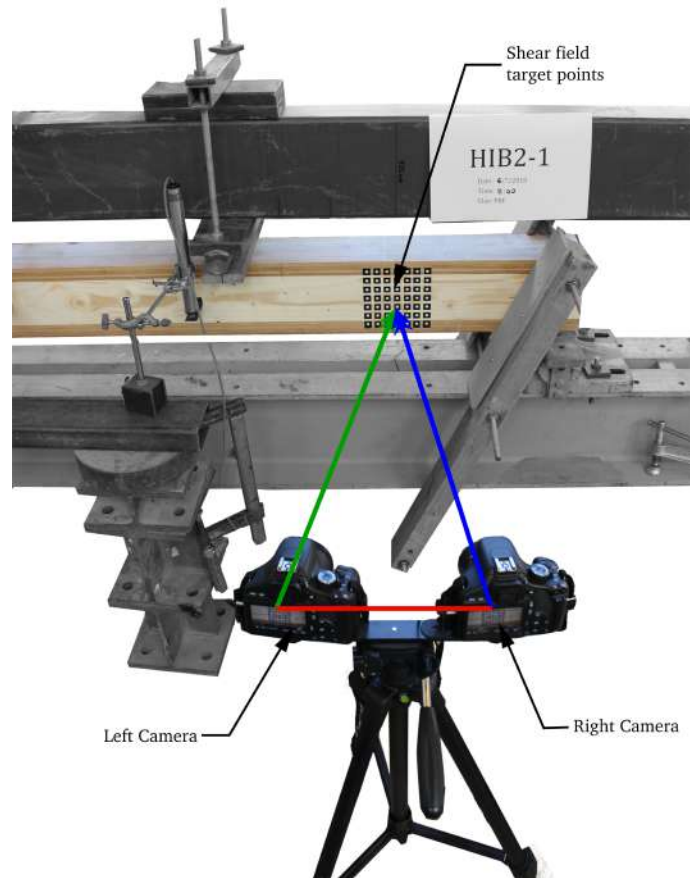


**Figure 4.20:** Stereo vision setup in the four-point bending test

The deformations of these diagonals are defined as the shear deformation of the beam. While this method of measurement has a number of attractive features, such as ease of use and less required technical knowledge, there are certain drawbacks associated with its use. These include unavoidable physical contact, single-point measurements and setup difficulties.

On the other hand, this study extensively uses the photogrammetry method for various measurements and Figure 4.20 shows the setup for this experiment. The fundamentals of this method of measurement are outlined in Chapter 3 Section 3.3, and a summary of the image processing stages are presented in the following section.

#### 4.7.2.2 Photogrammetry procedure

During the four-point bending test, images of the target area and load screen were captured at 5kN intervals. This provides sufficient readings to determine the shear distortion of the

**Table 4.5:** Shear properties of the tested beams

Beam	Glue	$F_{max}$	$\tau$	<b>G</b>
		[kN]	[N/mm <sup>2</sup> ]	[kN/mm <sup>2</sup> ]
<b>IBHB1-1</b>	MF	131.68	4.69	2.34
<b>IBHB1-2</b>	MF	118.93	4.31	2.39
<b>IBHB2-1</b>	PRF	80.93	2.88	2.32
<b>IBHB2-2</b>	PRF	77.92	2.84	2.85
<b>BSB</b>	PRF	76.54	2.99	-
<b>GB</b>	PRF	39.04	1.53	-

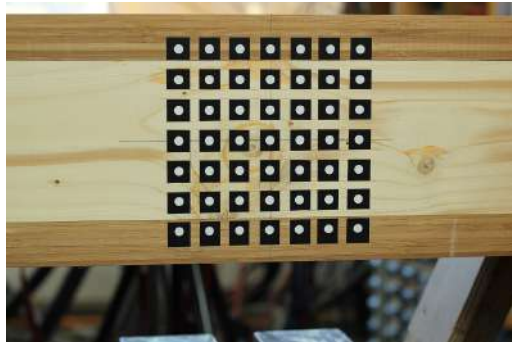
beam. The image processing began by preparing both left and right images (Figure 4.21a) and then regions of interest, selected using a threshold algorithm based on the greyscale (Figure 4.21b). Following this, the target points were selected using filters based on the size of each circle and roundness of the identified regions (Figures 4.21c and 4.21d). Finally, using a recursive algorithm and intersection concept, 3D coordinates of each target point were determined (Figure 4.21e). Using 3D coordinates of each target point every 5kN, the displacement of each target can be determined and thus the shear distortion of the constructing square. Shear modulus of the beam is determined using only one constructing square (four target points). Nonetheless, to evaluate the impact of location and size of the constructing square, 49 target points (7 × 7) were mapped at 15mm horizontal and vertical spacing (Figure 4.21e).

#### 4.7.2.3 Shear modulus determination

The shear modulus of a beam can be determined using Equation 4.18 as recommended by BS EN 408 (BSI, 2012). The calculated values from this experiment are presented in Table 4.5.

$$G_{tor,s} = \alpha \frac{h_0(V_{s,2} - V_{s,1})}{bh(w_2 - w_1)} \quad (4.18)$$

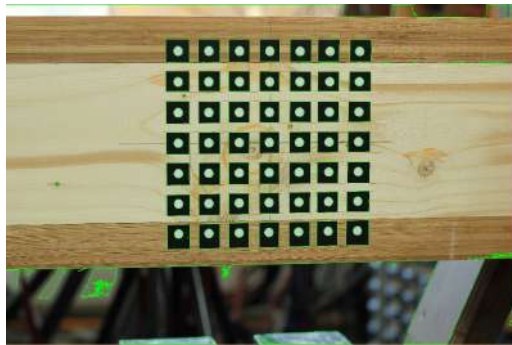
where  $\alpha = \frac{3}{2} - \frac{h_0^2}{4h^2}$ ,  $h_0$  is length of the square diagonals before deformation,  $h$  and  $b$  are the cross-sectional depth and width, respectively,  $w_i$  is the mean deformation of both diagonals of the square at both sides of the beam for a given shear load, and  $V_{s,i}$  is the shear force with  $i$  being the load increment.



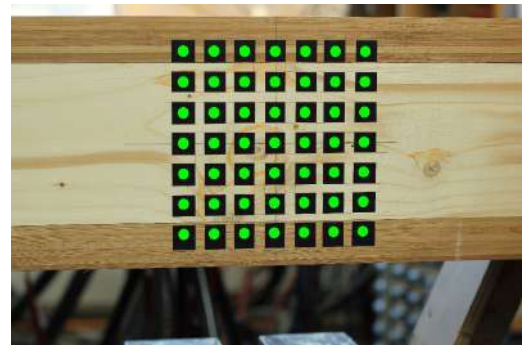
(a) Loading images



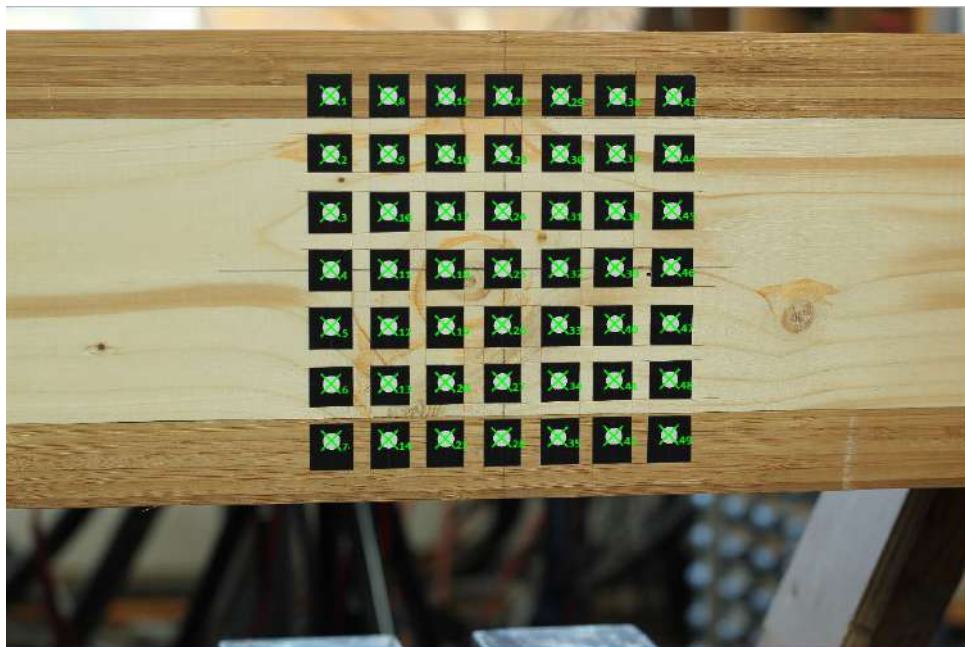
(b) Identify the desired regions based on the greyscale



(c) Select the outline of the region



(d) Select the target point based on the circle size and roundness



(e) Apply a recursive algorithm to determine the target points

**Figure 4.21:** Image processing procedure to determine the 3D coordinates of target points

## 4.8 Analytical Approach for Modelling HIB

The ultimate state and limit state of IBHB were approximated using mathematical models using transformed sections and beam theory. The ultimate bending moment of the IBHB was also modelled considering linear and non-linear behaviour of the material.

Limit state is categorised into two groups; **Ultimate Limit State (ULS)** and **Serviceability Limit State (SLS)**. ULS associates with stability and integrity of the structure when designing and constructing, hence it is controlled by stress and load. On the other hand, SLS associates with suitability and durability of the structure during its lifespan, regarding living condition. SLS is controlled by several criteria, e.g. deflection, cracks, vibration, etc. Considering the recommendation for the deflection limit in SLS, given by BS EN 1995-1-1 (BSI, 2006),  $\delta_{serv} = l/250$  is deemed to be the allowable deflection.

### 4.8.1 Mid-Span deflection

For the four-point bending test, the beams were simply supported and loaded symmetrically with equal forces. Based on beam theory, assuming that the beam behaves in a linear elastic manner, maximum deflection occurs in the mid-span. Maximum deflection can be determined using equation 4.19.

$$\delta_{max} = \frac{Pal^2}{48EI_H} \times [3 - 4(\frac{a}{l})^2] \quad (4.19)$$

where  $P$  is the total applied load on the beam,  $a$  is the distance between loading point and the nearest support,  $l$  is the span of the beam and  $EI_H$  is the flexural stiffness of the hybrid beam.

Both limit states are usually correlated with the linear behaviour of the material. Since laminated bamboo and timber are both within the elastic range when determining the limit state values, the superposition method can be employed to obtain the stiffness ( $EI$ ) of the hybrid beam. Laminated bamboo is divided into flanges and web as the orientation of bamboo strips in flanges are flat-wise and edgewise in the web.

$$EI_H = E_B^f I_B^f + E_B^w I_B^w + E_T I_T \quad (4.20)$$

Laminated bamboo is subscripted by  $B$  and timber by  $T$ . The superscripts  $f$  and  $w$  represent the flanges and the web of the hybrid beam, respectively.

**Table 4.6:** Constituent material properties

Material	Flexural		Tension		Compression	
	MOR	MOE	$f_t$	$E_t$	$f_c$	$E_c$
	[N/mm <sup>2</sup> ]	[kN/mm <sup>2</sup> ]	[N/mm <sup>2</sup> ]	[kN/mm <sup>2</sup> ]	[N/mm <sup>2</sup> ]	[kN/mm <sup>2</sup> ]
LBL-F	102.88	9.03	113.49	10.42	70.92	10.67
LBL-E	98.69	9.58	113.49	10.42	70.92	10.67
C16	46.85	7.96	39.59	8.16	34.42	8

The material properties of both materials were determined in Chapter 3 using a Small Clear Specimen testing procedure, and a summary of these results can be found in Table 4.6. In general, the measurement of material properties based on Small Clear Specimen testing is in an ideal condition where the influence of knots and defects is minimised. The experimental and theoretical mid-span deflections for IBHBs within the elastic range are shown in Figure 4.22. The theoretical values confirm the experimental results and the relative errors are less than 5%. This implies that Equation 4.19 provides a close approximation of deflection, particularly within the serviceability limit.

#### 4.8.2 Prediction of the flexural bearing capacity

The ultimate states and strength analysis can be carried out using the stress-strain relationship obtained from Small Clear Specimen testing results, Chapter 3. To calculate and analyse the proportional and ultimate state of the beams, linear and non-linear analysis were carried out based on the following material behavioural assumptions.

For the laminated bamboo, the proposed uniaxial stress-strain relationship follows a tri-linear behaviour, as shown in Figure 4.23. Under tension, laminated bamboo exhibited elastic behaviour with brittle failure at ultimate tensile strength ( $\sigma_{t,B}$ ), corresponding to the ultimate strain ( $\epsilon_{t,B}$ ). Conversely, in compression, a bilinear behaviour is observed with elastic deformation until the compression yield point ( $\sigma_c$ ) at the corresponding strain ( $\epsilon_c$ ), followed by plastic behaviour. Wood material (C16) is idealised here as an elastic material with an ultimate tensile state of ( $\sigma_{t,w}$  and  $\epsilon_{t,w}$ ), and compression state of ( $\sigma_{c,w}$  and  $\epsilon_{c,w}$ ). Young's modulus of LBL is denoted by  $E_B$  and timber is  $E_T$ .

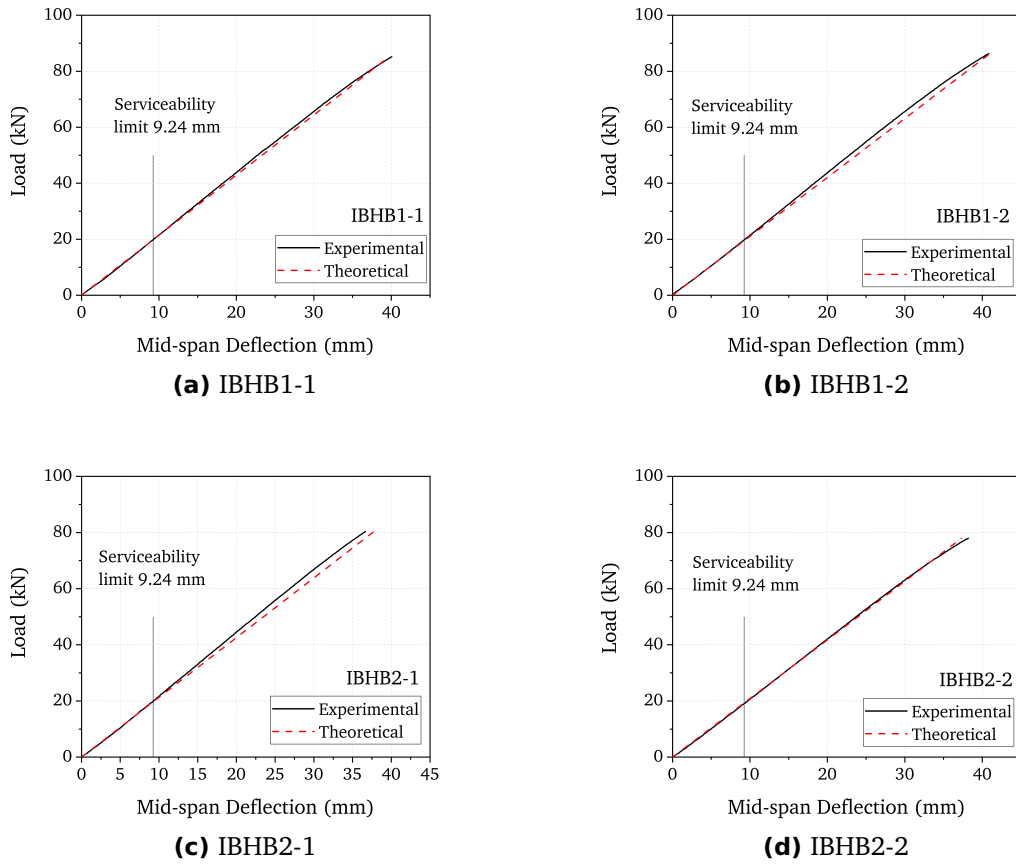


Figure 4.22: Experimental and theoretical mid-span deflections of IBHBs (elastic range)

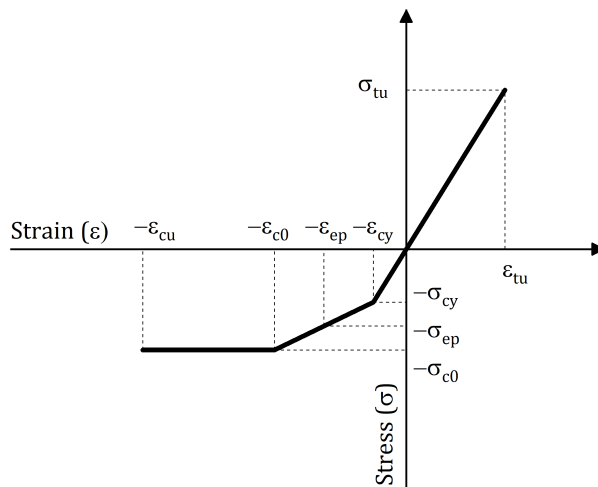


Figure 4.23: Proposed laminated bamboo stress-strain relationship

#### 4.8.2.1 Linear analysis

For linear behaviour, it was assumed that both constituent materials perform linearly with a constant Young's modulus in the tension and compression regions. This assumption is valid based on the results of the Small Clear Specimen test on the laminated bamboo. Using the transformed section, the hybrid beam transformed into a laminated bamboo I-beam based on Young's modulus ratio of laminated bamboo to timber ( $n = E_B/E_T$ ). The assumptions of the Euler-Bernoulli beam theory apply here; plane sections remain plane in the constant moment region after the deformation and the adhesive provides sufficient surface bond and capable of transmitting the stress between the adjacent laminae. Based on this theory, the strain and curvature relationship can be expressed by the following:

$$\epsilon = -y \frac{d\theta}{dx} = -\kappa y \quad (4.21)$$

where  $\kappa$  is the curvature and  $y$  is the distance between the neutral axis and the strain point.

Since the loading and the geometry of the beam is symmetric it is reasonable to assume that the neutral axis lies at the centre of the cross-section with respect to height. Although, this might not be a valid assumption when the beam undergoes elastic-plastic deformation or is perfectly plastic. According to the superposition principle, the ultimate normal bending capacity of the IBHB can be obtained by:

$$M_u = M_B + M_T \quad (4.22)$$

$$M_u = \int_{A_B} \kappa E_B y^2 dA + \int_{A_T} \kappa E_T y^2 dA \quad (4.23)$$

$$M_u = (\kappa EI)_B + (\kappa EI)_T \quad (4.24)$$

$$\kappa_B = \frac{\epsilon_B^t}{c} \quad \kappa_T = \frac{\epsilon_T^t}{(h - 2t)/2} \quad (4.25)$$

where  $M_u$  is the ultimate bending capacity of the hybrid beam, subscripts  $B$  and  $T$  represent laminated bamboo and timber, and  $\epsilon_B^t$  and  $\epsilon_T^t$  are the tensile strain of laminated bamboo and timber at the yielding point, respectively.  $I$  is the second moment of area, and  $c$  is the distance from extreme tensile fibres to the neutral axis.

The IBHB-MF experienced elastic-plastic deformation before failure due to tension, thus the bending moment shown in Table 4.3 can be compared with the theoretical calculation obtained from Equation 4.24. Table 4.7 compares the experimental measurements with the theoretical values; the calculated ultimate bending moments are in the conservative range

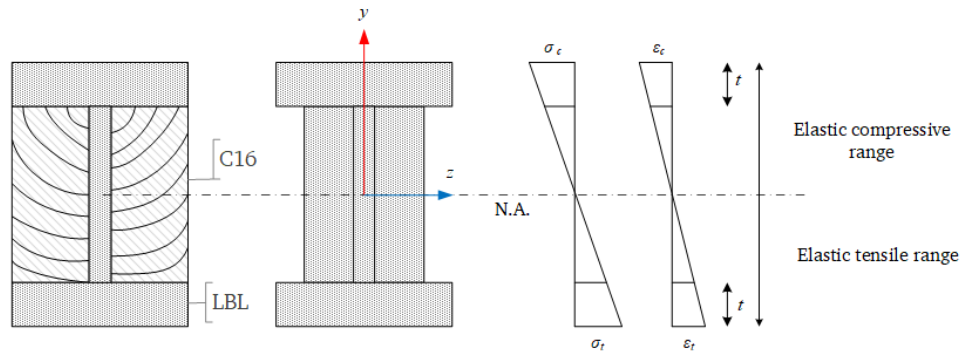


**Figure 4.24:** Transformed section and corresponding linear stress distribution

of the measurement. This inconsistency may be due to elastic-plastic deformation of the beam where the beam yields in the compressive range, causing a reduction in load-bearing capacity of the hybrid beam. Therefore, a correction factor ( $\gamma_p = 0.85$ ) is introduced to account for the plasticity of the hybrid beam.

$$M_u = \gamma_p \left[ \frac{\epsilon_B^t}{c} \times E_B I_B + \frac{2\epsilon_T^t}{(h - 2t)} \times E_T I_T \right] \quad (4.26)$$

**Table 4.7:** Comparison between experimental and theoretical flexural bearing capacities.

Beam	$M_B$ kN.m	$M_T$ kN.m	$M_{u,cal}$ kN.m	$M_{exp}$ kN.m	Error	$M_{u,corr}$ kN.m	Error
IBHB1-1	43.188	7.70	50.89	43.45	17%	43.25	-0.5%
IBHB1-2	43.222	7.04	50.26	39.25	28%	42.72	8.8%

#### 4.8.2.2 Non-linear analysis

Bamboo and engineered bamboo are similar to wood regarding their brittle nature due to the tension induced configurations, thus non-linear analysis based on the plasticity of the material is not recommended for analysis and design (Porteous and Kermani, 2013). Furthermore, BS EN 408 (BSI, 2012) and ASTM D198 (ASTM, 2014) use linear elastic behaviour of the structural-size beam to calculate the mechanical properties.

However, to add another dimension to this study, the ultimate flexural bearing capacity based on the non-linear behaviour of the hybrid beam is also determined and compared to

## CHAPTER 4. I-BONE LAMINATED BAMBOO HYBRID BEAM

experimental results. The transformed section method is used, thus a laminated bamboo I-beam with the web width of  $b_w = \frac{b_f - b_b}{n} + b_b$  is considered for the analysis. Referencing Figure 4.25, the ultimate bending moment of the hybrid beam can be determined by the equilibrium of forces and stress distribution in the section, thus:

$$M_u = \int_{-c}^{(a+b)} \sigma(y) b_i y_i dy \quad (4.27)$$

Looking into stress distribution and equivalent acting forces, we have:

$$M_u = \sum_{i=1}^n F_i \times y_i \quad (4.28)$$

To simplify the calculation process, It is assumed that  $a = t$ , therefore we have:

$$\begin{aligned} M_u &= \sigma_{cy} \times b_f \times a \times \left(b + \frac{a}{2}\right) \\ &+ \frac{1}{2} \times (\sigma_{c,ep} - \sigma_{cy}) \times b_f \times a \times \left(b + \frac{2a}{3}\right) \\ &+ \frac{1}{2} \times \sigma_{cy} \times b_w \times b \left(\frac{2b}{3}\right) \\ &+ \frac{1}{2} \times \sigma_{t2} \times b_w \times (c - a) \frac{2(c - a)}{3} \\ &+ \sigma_{t2} \times b_f \times a \times \left(c - \frac{t}{2}\right) \\ &+ \frac{1}{2} \times (\sigma_t - \sigma_{t2}) \times b_f \times a \times \left(c - \frac{a}{3}\right) \end{aligned} \quad (4.29)$$

Referencing Figure 4.25, using strain distribution geometry we have:

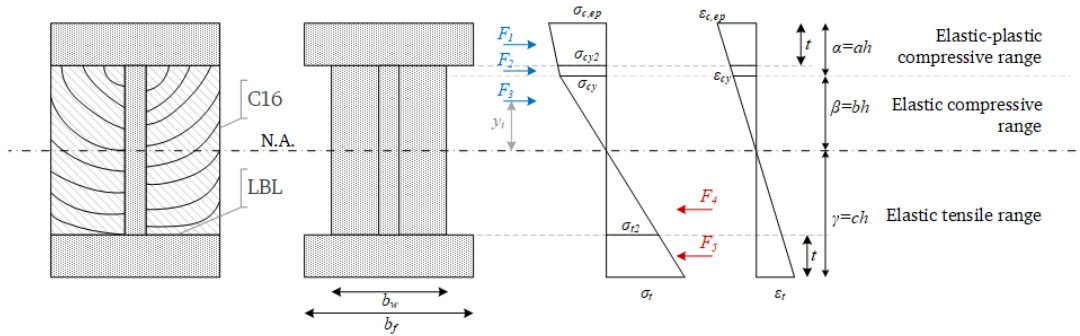


**Figure 4.25:** Transformed section and corresponding non-linear stress distribution

$$\frac{bh}{\epsilon_{cy}} = \frac{h}{\epsilon_t + \epsilon_{c,ep}} \rightarrow b = \frac{\epsilon_{cy}}{\epsilon_t + \epsilon_{c,ep}} \quad (4.30)$$

$$\frac{ah}{\epsilon_{c,ep} - \epsilon_{cy}} = \frac{h}{\epsilon_t + \epsilon_{c,ep}} \rightarrow a = \frac{\epsilon_{c,ep} - \epsilon_{cy}}{\epsilon_t + \epsilon_{c,ep}} \quad (4.31)$$

$$\frac{ch}{\epsilon_t} = \frac{h}{\epsilon_t + \epsilon_{c,ep}} \rightarrow c = \frac{\epsilon_t}{\epsilon_t + \epsilon_{c,ep}} \quad (4.32)$$

In terms of failure progression of the IBHB, four possible modes of failure can be defined in this study, as follows:

- 1: Both laminated bamboo and timber remain linear elastic and beam fails in extreme tensile fibre at bottom flange (laminated bamboo) due to tension.
- 2: Both laminated bamboo and timber remain linear elastic and beam fails in web (timber layer) due to tension.
- 3: Top layer of laminated bamboo yields in compression and followed by fracture in tensile layer.
- 4: Laminated bamboo and wood yield in compression and subsequently the beam fails in tension.

Irrespective of each mode, a beam fails in the tension due to the fracture in LBL or timber. Therefore, ultimate flexural capacity is the minimum of the bending moments calculated based on the following two scenarios; a) tensile fracture in wood, b) tensile fracture in LBL. The former may happen due to excessive defects in the wood, substantial strength difference between wood and LBL or failure in the glue-line. However, if the production follows the recommendations in BS EN 14080 (BSI, 2013a), and the adhesive meets the requirements of BS EN 301 (BSI, 2013b) and BS EN 302-2 (BSI, 2013c), this mode is unlikely to occur. The ultimate bending moment calculated for scenario (a) is denoted by  $M_a$ .

Scenario (b), on the other hand, is most likely to occur and is a more favourable mode of failure for a load-bearing structural element, due to elastic-plastic deformation. Using Equation 4.29, and assuming that the tensile strength of the web (both the side timbers and the middle LBL) is equal to the LBL tensile strength due to the section transformation ( $\sigma_{t2}$ ) the bending moment due to this mode of failure can be predicted. The ultimate bending moment calculated is denoted by  $M_b$ . Considering these two modes of failure, the ultimate

flexural bearing capacity of the IBHB can be predicted as:

$$\begin{aligned}
 M_u &= \sigma_{cy} \times b_f \times \alpha h \times \left(\beta h + \frac{\alpha h}{2}\right) \\
 &+ \frac{1}{2} \times (\sigma_{c,ep} - \sigma_{cy}) \times b_f \times \alpha h \times \left(\beta h + \frac{2\alpha h}{3}\right) \\
 &+ \frac{1}{2} \times \sigma_{cy} \times b_w \times \beta h \left(\frac{2\beta h}{3}\right) \\
 &+ \frac{1}{2} \times \sigma_{t2} \times b_w \times (\gamma h - \alpha h) \frac{2(\gamma h - \alpha h)}{3} \\
 &+ \sigma_{t2} \times b_f \times \alpha h \times \left(\gamma h - \frac{\alpha h}{2}\right) \\
 &+ \frac{1}{2} \times (\sigma_t - \sigma_{t2}) \times b_f \times \alpha h \times \left(\gamma h - \frac{\alpha h}{3}\right)
 \end{aligned} \tag{4.33}$$

where,

$$\sigma_{t2} = \left(\frac{\gamma - \alpha}{\gamma}\right) \sigma_t \tag{4.34}$$

And by re-arranging we have:

$$\begin{aligned}
 M_u &= \sigma_{cy} b_f h^2 \left(\frac{\alpha\beta}{2} + \frac{\alpha^2}{6} + k_1 \frac{\beta^2}{3}\right) \\
 &+ \sigma_{c,ep} b_f h^2 \left(\frac{\alpha\beta}{2} + \frac{\alpha^2}{3}\right) \\
 &+ \sigma_t b_f h^2 \left(k_1 \frac{(\gamma - \alpha)^3}{6\gamma} + \frac{\alpha^3}{3\gamma} + 2\alpha^2 + \alpha\gamma\right)
 \end{aligned} \tag{4.35}$$

Where  $E_B^E$  is Young's Modulus of laminated bamboo in edge-wise orientation,  $E_B^F$  is in flat-wise orientation, and  $k_1 = \frac{b_w}{b_f}$ .

Table 4.8 compares the experimental results with the theoretical results of the non-linear analysis for ultimate flexural bearing capacity of IBHBs. The predicted results are in good agreement with the experimental results. It must be noted that the yield ( $\epsilon_{cy}$ ) and elastic-plastic ( $\epsilon_{c,ep}$ ) strain measurement of the laminated bamboo are based on the strain measurement in the compression test using linear regression.

**Table 4.8:** Non-linear flexural capacity results.

Beam	$M_{exp}$	$\sigma_{cy}$	$\sigma_{c,ep}$	$\sigma_t$	$M_{u,cal}$	Error
	kN.m	N/mm <sup>2</sup>	N/mm <sup>2</sup>	N/mm <sup>2</sup>	kN.m	
IBHB1-1	43.45	50.34	59.43	103.42	44.01	1%
IBHB1-2	39.25	50.34	59.43	103.42	42.65	9%

## **4.9 Comparison with other Experimental Studies**

The flexural properties of **IBHB** and **BSB** were measured and predicted in the previous sections. A comparison of these results with other experimental studies is presented in Table 4.9. Although many aspects are required to be considered when comparing the structural components including the shear and bearing capacity, the scope of this investigation is to evaluate the flexural properties of the tested beams. Considering the environmental advantages of producing the laminated bamboo compared to the Glulam and LVL, **IBHB** shows high added value to the construction industry as well as to the bamboo forestry if a commercially viable production process is used to harvest and utilise it.

Based on the results of this experiment, it is evident that **IBHB** exhibits a promising flexural strength ( $72 \text{ N/mm}^2$ ) compared to GL32 ( $35 \text{ N/mm}^2$ , characteristic value) and glue-laminated timbers ( $28.6 - 62.6 \text{ N/mm}^2$ ). **IBHB**'s bending strength is also comparable to that of the laminated veneer lumber (LVL). The strength to weight ratio, on the other hand, is important to reduce the weight of a structure while enhancing the performance. The strength to weight ratio of **IBHB** ( $\text{MOR}/\text{SG} = 133 \text{ N/mm}^2$ ) is the highest among the listed materials. This indicates that **IBHB** seems to have great potential to be used as a structural element.

**IBHB** has a comparable Modulus of Elasticity in comparison to all the materials listed except LVL. To enhance the stiffness of the **IBHB**, methods of pre-stressing the engineered beams using compressed wood (Anshari et al., 2012) or reinforcing it using synthetic materials are recommended (Vahedian et al., 2019; Guan et al., 2005; Borri et al., 2005).

Many of the listed experimental studies have not determined the shear modulus of the beams. Because the process of measuring the shear distortion requires special tools thus it has been avoided. The shear modulus of **IBHB**, **BSB** and GL32 are presented in Table 4.9.

The results of this study showed the enhanced structural performance of the **IBHB** in comparison with control samples and some of conventional engineered wood products. However, **IBHB** possesses limitation which required to be addressed in order to be widely accepted in the construction industry. For example, creating curved beams, sloped beams and free-shape beams can be difficult from the manufacturing point of view. On the other hand, there is a potential to pre-stress **IBHB** which is feasible due to high tensile strength

#### **CHAPTER 4. I-BONE LAMINATED BAMBOO HYBRID BEAM**

---

of laminated bamboo. Creating ducts and holes in [IBHB](#) requires additional reinforcements which can be investigated in future studies.

**Table 4.9:** Comparison of the mean flexural properties for IBHB and other wood-based products

	MOE		MOR		G	MOR/SG	Reference
	Specific Gravity (SG)	[kN/mm <sup>2</sup> ]	[N/mm <sup>2</sup> ]	[kN/mm <sup>2</sup> ]			
I-Bone Laminated Bamboo Hybrid Beam (IBHB)	0.54	13.28	72.04	2.4	133.4	Current study	
Laminated Bamboo Sandwich Beam (BSB)	0.47	11.68	49.93	2.1	106.2	Current study	
Laminated Bamboo Lumber (LBL)	-	9.48	87.74	-	-	Li et al. (2018)	
Laminated Bamboo Lumber (LBL)		12.18	89.2	-	-	Sinha et al. (2014)	
Glue Laminated Beam (GL32)	0.44	13.5	38	0.65	86.4	BSI (2013a)	
Laminated veneer Douglas fir	0.52-0.62	9-13.7	38-63.9		73-103	Kretschmann et al. (1993)	
Glue laminated Douglas-fir	0.51	13.9	47.2	-	92.5	Marx and Moody (1981)	
Glue laminated Spruce	0.45	13.36	49.6	-	110.2	De Lorenzis et al. (2004)	
Glue laminated Beech	0.65-0.71	12.3-15.5	43.3-63.7	-	66-90	Frese and Blaß (2006)	
Glue laminated timber	0.4-0.6	9-14.5	28.6-62.6	-	71-104	Cai and Ross (2010)	
Laminated veneer lumber	0.4-0.7	9-19.2	33.8-86.2		84-123	Cai and Ross (2010)	

### 4.10 Summary

This chapter focused on investigating the production procedure and the flexural behaviour of the **I-Bone Laminated Bamboo Hybrid Beam (IBHB)**. Despite the limitations regarding the size and length of the specimen, the results of the conducted experiments indicated a promising potential of **IBHB** to be used as a structural element. The mechanical properties of **IBHB** are higher or comparable to that of engineered wood products with the advantages of utilising the low-grade timber species as load-bearing component and the fast-growth cycle of bamboo.

**IBHB** can be produced efficiently using the computer-controlled machinery which provides accurate cuts and minimises the waste. Additionally, the biomass produced can be used as a fuel in the production of other wood-based materials such as Oriented Strands Boards and chipboards. Nonetheless, a solid connection between flanges and the web ensures the rigidity of the cross-section and minimises the weak spots along the beam. The side timbers are recommended to be a low-grade solid timber or wood products. The side timbers contribute towards the cross-sectional integrity and the horizontal shear resistance of the hybrid beam.

The failure of the **IBHB** is categorised as a tensile brittle failure initiated at the extreme tensile fibres of the beam. However, there is a possibility of failure in the wood or the connection between the flanges and the web. The type of adhesive seems to be an affecting factor in predicting the failure type. The results of this study, in line with the previous experiments in the literature, concluded that the **Phenol Resorcinol Formaldehyde (PRF)** type adhesive may not be a suitable resin for laminated bamboo and wood connection.

Regarding the mechanical properties, the **IBHB** illustrated great flexural properties with a bending strength of 69-75 N/mm<sup>2</sup> and bending modulus of 13-13.5 kN/mm<sup>2</sup>. These values are higher than most of the wood-composite products and are comparable to those of hardwood Glulam beams. The shear strength and modulus of this beam were also shown to substantially increase compared to the control samples. Furthermore, the analytical models based on linear and non-linear behaviours of the laminated bamboo lumber are presented. These models are in good agreement with the experimental results when considering plasticity and non-linear behaviour. Nonetheless, assuming a linear behaviour also resulted in the good prediction of the serviceability and ultimate limit states.

#### **CHAPTER 4. I-BONE LAMINATED BAMBOO HYBRID BEAM**

---

Additional research is needed on size and length variations, along with investigating the compatibility of the different adhesive types on the laminated bamboo and timber connection. Considering that laminated bamboo has less mechanical and physical variation compared to solid timber, it is likely that innovative structural materials such as **IBHB** will be in high demand.

The **IBHB** comprises an innovative layout combination providing enhanced mechanical properties for the structural engineers and attractive appearance for the architects. It has received great interests from the industry to commercialise it. Therefore, a patent application is submitted to the governing body in the UK.

# LAMINATED BAMBOO I-BEAM AND DOUBLE I-BEAM

## 5.1 Introduction

This chapter presents the fabrication process, experimental investigation and mathematical modelling of laminated bamboo I-beam and double I-beam. The four-point bending tests were conducted to investigate the flexural behaviour of the beams. Analytical models were derived to approximate the ultimate limit states. The failure mechanism was also discussed and recommendations for the production of these materials were included.

I-beams are well-known sections in structural design due to its optimised use of the material and high moment of inertia which result in higher flexural bearing capacity. Generally, engineered bamboo products have higher density when compared to most of softwood products (Xiao, 2016; Sharma et al., 2015a). Thus, in an attempt to reduce the weight and optimise the cross-section of the glulam beams, [Engineered Bamboo I-Beam \(BIB\)](#) (Figure 5.1a) and [Engineered Bamboo Double I-Beam \(BDIB\)](#) (Figure 5.1b) were manufactured. This stage of the experiments is a pilot study on the development of a laminated bamboo I beams and double I beam. Hence, the focus was only on the flexural behaviour of this material.

A thorough search of the relevant literature yielded that no attempts have been made to produce an engineered bamboo double I-beam. Whilst engineered bamboo I-joist and

## CHAPTER 5. LAMINATED BAMBOO I-BEAM AND DOUBLE I-BEAM

I-beams using various manufacturing methodologies have been investigated (Chen et al., 2015; Wu, 2014; Aschheim et al., 2010).

The results of this study have provided insights into the importance of the side timbers in the I-Bone Laminated Bamboo Hybrid Beam (IBHB), which was presented in Chapter 4. This importance is identified in terms of the enhancement of the structural integrity and the cross-sectional stability while improving the shear resistance of the beam.

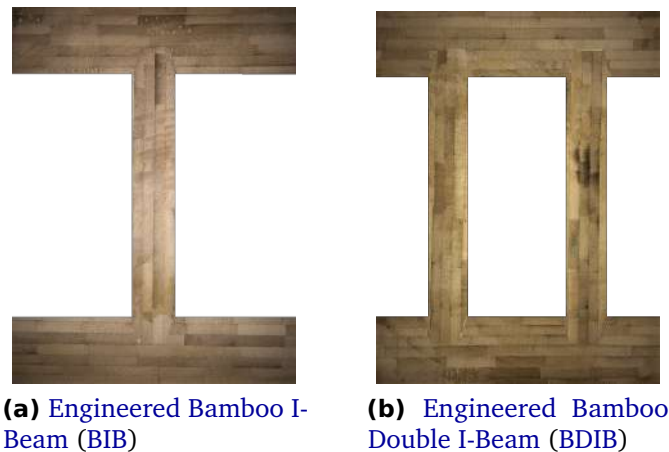


**Figure 5.1:** Laminated bamboo I-beam and double I-beam

## 5.2 Fabrication Process

The manufacturing process followed the steps for that of IBHB described in Chapter 4. The web's thickness, the flanges' thickness and height were similar to that of IBHB. The groove chamfer was also created with 75° angle and 13 mm depth. The glue was applied at either side of the joining surfaces at the rate of 200-235 g/m<sup>2</sup> per surface.

Due to the variety in the material properties of the laminated bamboo and the fabrication processes, care must be taken when comparing the composite materials from various studies.

### 5.2.1 Material

Laminated bamboo with no joint and bamboo strips of 4-5 mm thick and 22 mm wide was used for both BIB and BDIB. Mechanical properties of employed laminated bamboo were determined using small specimen testing procedure and presented in Chapter 3. The mean

## CHAPTER 5. LAMINATED BAMBOO I-BEAM AND DOUBLE I-BEAM

modulus of elasticity and bending strength of laminated bamboo when the bamboo strips oriented flat-wise were  $8.67 \text{ kN/mm}^2$  and  $102.88 \text{ N/mm}^2$  and when oriented edge-wise were  $9.19 \text{ kN/mm}^2$  and  $98.69 \text{ N/mm}^2$ , respectively.

Regarding the adhesive, a two-component type adhesive composed of liquid [Melamine Formaldehyde \(MF\)](#) resin (*Cascomel 4720*) and liquid hardener Wonderbond Hardener (*5025A*) was used for both types of beams. The mix ratio followed the recommendation of the glue manufacturer, which is four parts by the water of resin to one part of hardener.

### 5.2.2 Dimensions of the I-beams

Figure 5.2 illustrates the nominal dimensions of both [BIB](#) and [BDIB](#). One laminated bamboo I-beam and two double I-beams were manufactured. All beams were 2.4m long with the bamboo strips oriented flat-wise for the flanges and the edgewise for the web.

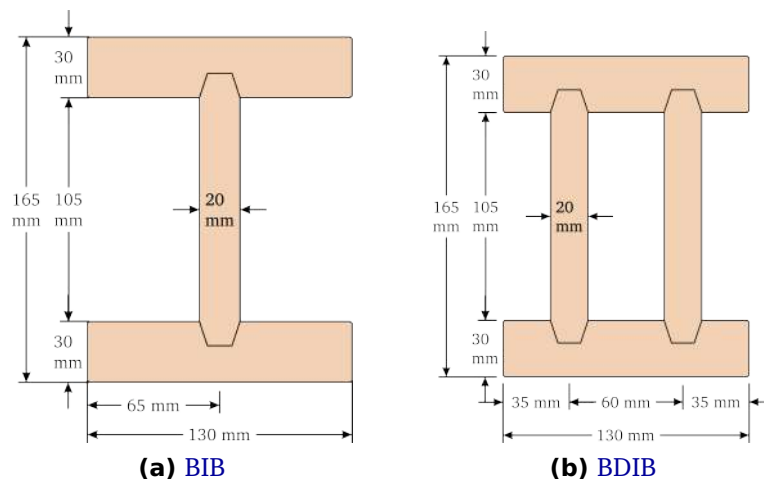


Figure 5.2: BIB and BDIB's nominal dimensions

### 5.2.3 Manufacturing challenges

The production of these composite beams in a laboratory environment encountered challenges due to the lack of expertise and limited equipment. In addition to the limitations mentioned in Chapter 4, the following problems were identified while producing the laminated bamboo I-beams.

One of the bamboo's weaknesses is its proneness to splitting due to longitudinal orientations of the fibres as the main load-bearing component. The lack of transverse reinforcement in

## CHAPTER 5. LAMINATED BAMBOO I-BEAM AND DOUBLE I-BEAM

---

bamboo contributes to the splitting of the material during the fabrication of the laminated bamboo I-beams, as indicated in Figure 5.3a. This introduces serious damages to the flanges which can trigger early failure. This type of failure was observed during the four-point bending test (which will be elucidated in Section 5.4), where it was identified that excess clamping pressure and inaccurate tapering of the web were responsible for the splitting and failure.

This problem can be mitigated by identifying the proper amount of clamping pressure which is sufficient enough to create a strong bond while considering the transverse shear resistance of laminated bamboo which causes splitting. In addition, CNC machines can be used to cut the components accurately, leaving no undesired clamping stress in the flanges. Inaccurate chamfer and groove cuts can also result in twisted or crooked fabrication as illustrated in Figure 5.3b.

Due to the inaccuracy in the groove and chamfers cut in one of the BDIBs, 100 g/m<sup>2</sup> extra glue was added to fill the gaps. Although the addition of extra glue can increase the bonding condition, however the excess glue that spills can be difficult to remove after fabrication. Therefore, the proper amount of glue and accurate cuts can be used to minimise glue spillage (Figure 5.3c). Channel in the flanges and chamfer the edges of the web is also necessary (Figure 5.3d).

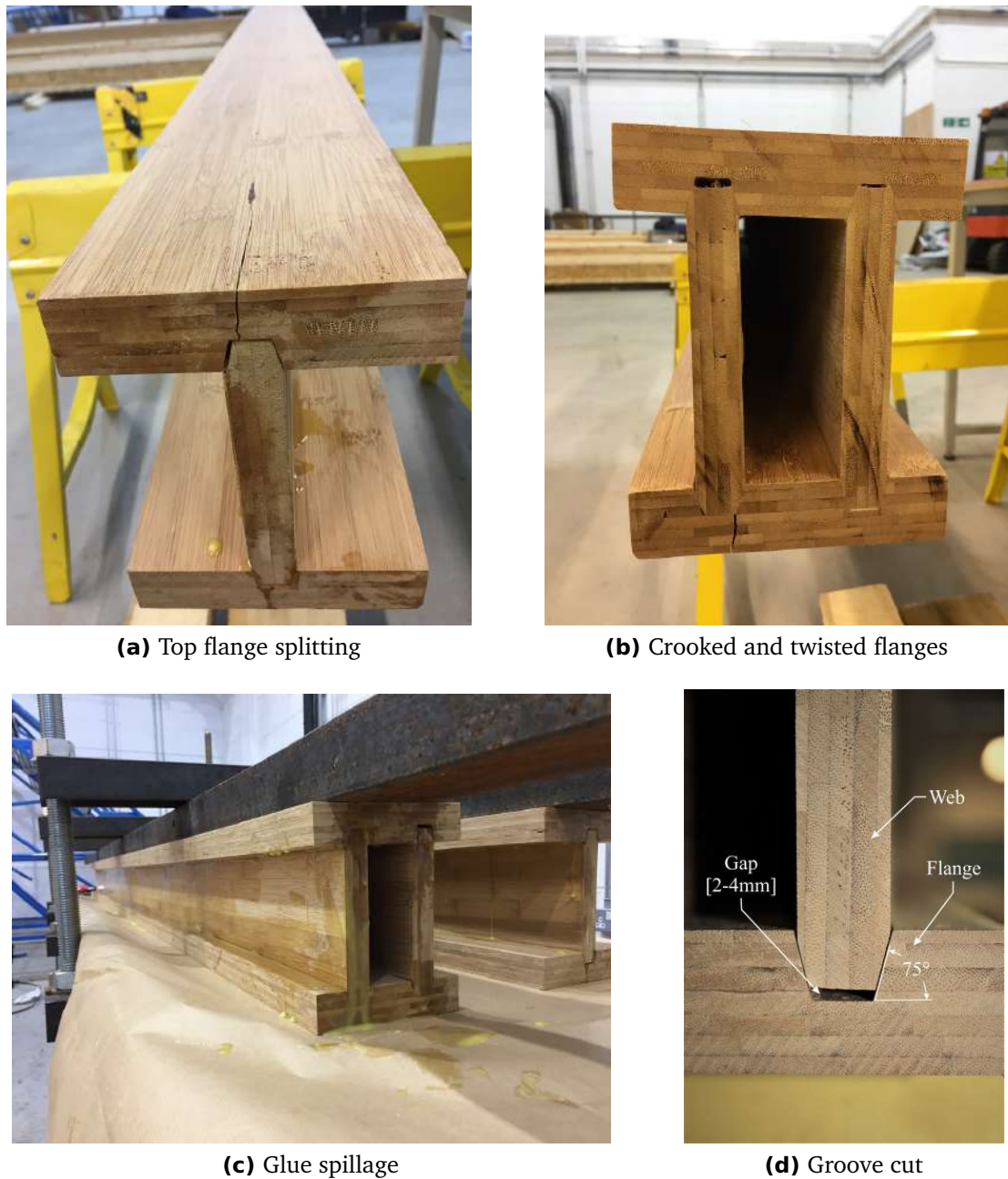


**Figure 5.3:** Laminated bamboo I-beams fabrication limitations and challenges

#### 5.2.4 Final products

Final products can be seen in Figure 5.4. The fabricated beams were clamped for a minimum of six hours and rested unstressed for a week in the laboratory environment. Excess glue was removed, and uneven edges were trimmed. The connections were considered satisfactory upon visual inspection.



(a) Engineered Bamboo I-Beam (BIB)



(b) Engineered Bamboo Double I-Beam (BDIB)

Figure 5.4: Laminated bamboo I-beams final products

## 5.3 Experimental Procedures for BIB and BDIB

### 5.3.1 Measurements

#### 5.3.1.1 Specimen's density

The density of the beams was measured using small samples which were obtained from the fractured beam at the closest section to the fracture. BIB fractured at the web along the entire beam, this makes impossible to sample from the whole cross-section. Thus, samples from the top and bottom parts of a pre-defined section, that its volume was measured prior to the test, were cut and used for the density measurement.

The density of the beam is defined as the ratio of the mass ( $m$ ) to the volume ( $V$ ) of a section (Equation 5.1). The determined densities are presented in Table 5.1. The values of density were converted into Specific Gravity (SG) based on the density of water at 4°C (1000 kg/m<sup>3</sup>)

$$\rho = \frac{m}{V} \quad (5.1)$$

Looking into density measurements, IBHB possesses lower density while providing higher load-bearing capacity. The density of the BIB and BDIB were similar to the density measurement of the Small Clear Specimen of the laminated bamboo determined in Chapter 3.

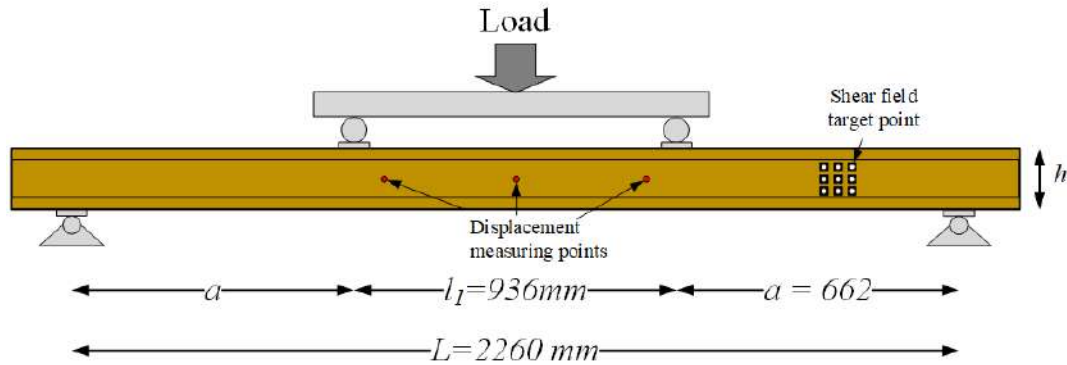


**Figure 5.5:** The four-point bending test configuration

### 5.3.1.2 Moisture content

Moisture Content (MC) of the beams was calculated using the oven-dry method detailed in BS EN 13183-1 (BSI, 2002). The samples that were used to measure the density were used to determine the moisture content of the beams.

### 5.3.2 The four-Point bending test

BIB and BDIBs were tested under four-point bending test. The test followed the recommendation presented in BS EN 408 (BSI, 2012). Figure 5.5 shows the test setup and specifications. The beams span was 2260 mm, slightly lower than the recommended span.

The mid-span deflection and the beam's curvature were recorded using six 100 mm LVDTs which were placed at both sides of the timber. Loading was applied at a constant rate of 6 mm/min until failure. Lateral restraints were placed to prevent out-of-plane displacements.

Table 5.1 presents the measurements for this stage of the experiments and compared with the measurements of IBHB. BIB showed 62% lower load-bearing capacity and 72% lower maximum deflection compared to IBHB. Although the mode of failure and load-bearing behaviour affect the ultimate readings, these values imply the significant contribution of the side timbers. Reinforcing the mid-depth not only enhances the shear resistance but increases the load-bearing capacity as well.

Expectedly, BDIB performed significantly better in term of load-bearing than BIB. BDIB showed only 8-14% lower loading capacity compare to IBHB. The BDIB did not fail due to shear in tests where shear resistance is provided by an additional web. The additional web

## CHAPTER 5. LAMINATED BAMBOO I-BEAM AND DOUBLE I-BEAM

**Table 5.1:** The four-Point bending test measurements data

Beams	Glue	Length [mm]	MC [%]	Density [kg/m <sup>3</sup> ]	$\Delta_{max}$ [mm]	$F_{max}$ [kN]	$M_{max}$ [kN.m]	
	BIB	MF	2260	8.62	659	46.47	81.09	26.8
	BDIB1	MF	2260	9.08	662.5	75.80	118.02	39.1
	BDIB2	MF	2260	9.11	661.2	72.76	114.35	37.9
	IBHB	MF	2310	-	538.6	80.06	131.68	43.5

MF: Melamine Formaldehyde resin, MC: Moisture Content

seems sufficient to undertake the shear stress, contribute to the cross-sectional stability and prevent lateral-torsional buckling.

### 5.4 Failure Observations

The failure observation of both beams revealed interesting insights into the flexural behaviour of the composite beams. The following sections describe the pattern in details, including the different modes of failure observed from shear and tensile failure. The compression yields were also determined from load-deflection graphs.

#### 5.4.1 Laminated bamboo I-beam

The failure of BIB can be categorised as a horizontal shear failure at the web. While this mode of failure is highly expected, it is primarily associated with lack of shear resisting elements in the mid-section area where the shear stress is at highest. As depicted in Figure 5.6, the failure of BIB occurred at the web in a region near the tensile flange. Another possible explanation for this type of failure is the structural instability in withstanding longitudinal forces by twisting the flanges and creating a weak point that initiate a crack.

Compression flange was also split due to the crack initiated during the manufacturing process which made a weak section on the flange (Figure 5.6a). Bamboo and subsequently laminated bamboo is highly prone to splitting due to minimum resistance in the transverse direction. The emphasis was therefore placed on identifying an appropriate depth of the grooving.



(a) Laminated bamboo splitting



(b) Horizontal shear failure

Figure 5.6: BIB failure observations

#### 5.4.2 Laminated bamboo double I-beam

In regards to BDIB, two types of failure were observed: i) A favourable tensile failure where extreme tensile fibres failed due to tension, and ii) horizontal shear failure. These failures can be seen in Figures 5.7 and 5.8. A compressive yield and a brittle tensile failure are concluded from the load-deflection graph. Expectedly, the fracture was initiated at the mid-span, at the extreme tensile fibre, before propagating into the web.

The observations indicated a tendency of I-beams to fracture at the bamboo knots (Figure



Figure 5.7: BDIB1 failure observations



(a) Tensile fracture

(b) Horizontal shear failure

Figure 5.8: BDIB2 failure observations

5.8b). Knots might induce an additional weakness in the beam, however, due to the distribution of knots across and along the beam, the impact will be mitigated and the beam can be considered as a homogeneous material.

In addition to the fracture, micro-exploding of bamboo strips were observed. This is because of the separation of fibres and parenchyma matrix which causes a micro-explosion at the time of fracture. This phenomenon is similar to exploding pattern of reinforced concrete.

## 5.5 I-Beams in Flexure

BIB and BDIBs performed considerably well in terms of load-bearing and elastic-plastic behaviour. Failure modes revealed that BIB may not be able to withstand the horizontal

shear stresses, thus reinforcements would be required. While **BDIB** showed higher shear resistance, however, signs of the horizontal shear failure have been observed.

### 5.5.1 Load deflection analysis

Figure 5.9 illustrates typical load-deflection graphs for laminated bamboo I-beams. The flexural behaviour of the beams indicates that all of them started with an elastic deformation until beams began to yield at the compression region, making them undergo elastic-plastic deformation. Brittle failure was identified as the mode of failure for all of the beams.

Evaluating the load-deflection graphs revealed that **BIB** has lower bending moduli and **IBHB** has the highest value (Figure 5.10). Furthermore, **IBHB** showed 62% higher load-bearing capacity than **BIB**. Since **BIB** failed due to horizontal shear, it can be concluded that the side timbers have a big contribution toward load-bearing capacity as well as the material properties.

**BDIB** performed considerably better when compared to **BIB**. The results of the load-deflection show that **BDIB** experiences similar deflection to **IBHB**. Although **BDIB** shows similar characteristics to **IBHB**, creating a solid connection within an I-beam section that is made of natural material can be a challenging task.

### 5.5.2 Flexural properties

The flexural properties of the beams can be determined using the beam theory. The **Modulus of Rupture (MOR)** was determined using the maximum bending moment using Equation 5.2. The **Modulus of Elasticity (MOE)** was determined using the slope of the load-deflection graph at the elastic region and between 10% and 40% of the maximum applied load using Equation 5.3. Table 5.2 shows the results of the four-point bending test.

$$MOR = \frac{MY}{I} = \frac{F_{max}ah}{4I} \quad (5.2)$$

$$MOE = \frac{al_1^2(F_2 - F_1)}{16I(w_2 - w_1)} \quad (5.3)$$

The second moment of area for I beams is:

$$I = \frac{(bh^3 - (b - b_w)(h - 2t)^3)}{12} \quad (5.4)$$

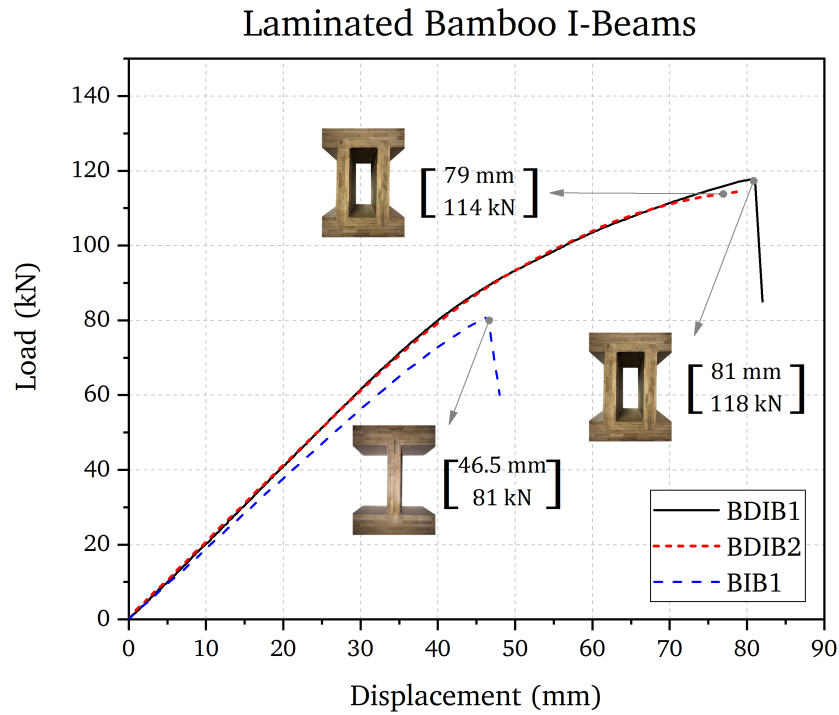


**Figure 5.9:** The load-deflection graph of the laminated bamboo I-beams

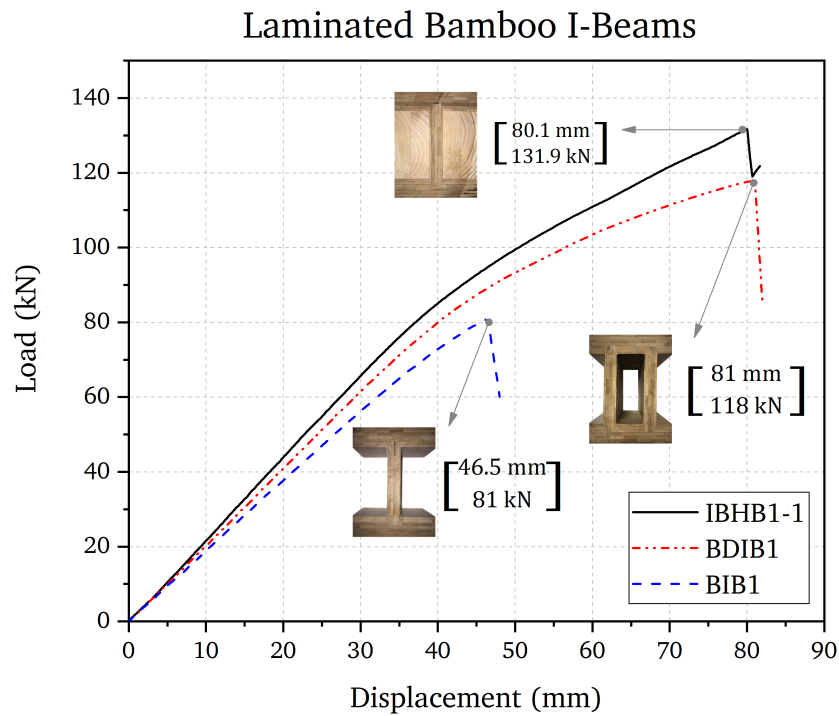


**Figure 5.10:** Comparison of the load-deflection of the tested beams with IBHB

## CHAPTER 5. LAMINATED BAMBOO I-BEAM AND DOUBLE I-BEAM

**Table 5.2:** The four-Point bending test results of the I-beams

Beam	Glue	SG*	MOE [kN/mm <sup>2</sup> ]	MOR [N/mm <sup>2</sup> ]	$\tau^{**}$ [N/mm <sup>2</sup> ]	MOE/SG	MOR/SG
BIB	MF	0.66	9.98	109.60	13.33	15.1	166.3
BDIB1	MF	0.66	11.99	155.15	9.21	17.6	232.8
BDIB2	MF	0.66	10.68	150.33	9.78	17.9	227.8
IBHB1-1	MF	0.54	13.04	75.05	4.69	24.2	139.3

\*Specific Gravity; \*\* Shear stress

where,  $a$  is the distance between the loading point and the adjacent support,  $b$  and  $h$  are the cross-sectional width and depth,  $b_w$  is the width of the web and  $t$  is the thickness of the flanges.

### 5.5.3 Ductility

Similar to IBHB, the ductility of I beams is described as the ratio of the maximum and the yield curvatures (Equation 5.5).

$$\text{Ductility} = \frac{\kappa_m}{\kappa_p} \quad (5.5)$$

As mentioned in the previous chapter, the curvature of a beam in the four-point bending test can be determined using the triangulation of the deflection measurement points.

$$R = \frac{c^2 + 4d^2}{8d} \quad \rightarrow \quad \kappa = \frac{1}{R} = \frac{8d}{c^2 + 4d^2} \quad (5.6)$$

Table 5.3 contains the calculated ductility for BIB and BDIB. It is noticeable that by introducing the side timbers in the IBHB, the material behaves in a more ductile manner. A similar pattern is reported by Kaboli and Clouston (2019). The results indicate that IBHB and BDIB have a similar ductility and 72% higher than BIB. This signifies the importance of the side timbers in enhancing the ductility and integrity of the beam.

### 5.5.4 Flexural rigidity

The flexural rigidity (EI) of a beam in the bending was determined using the bending moment and curvature relationship presented in Figures 5.11a, 5.11c and 5.11e.

$$M = EI \frac{d^2 w}{dx^2} \quad (5.7)$$

---

**CHAPTER 5. LAMINATED BAMBOO I-BEAM AND DOUBLE I-BEAM**

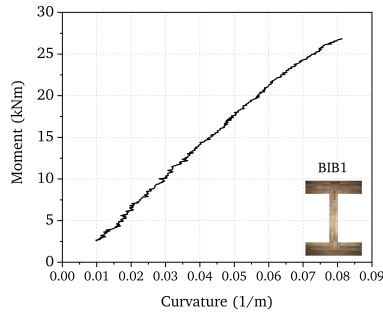
---

**Table 5.3:** Ductility and stiffness of the beams

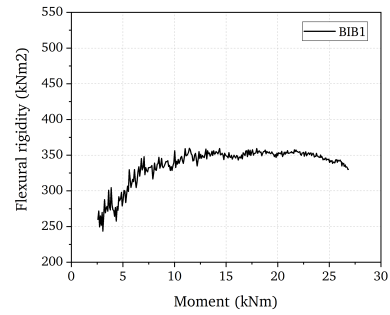
Beam	Ductility	% of BIB	Flexural rigidity	% of BIB
BIB	1.33	0%	351.62	0%
BDIB1	2.20	65%	443.28	26%
BDIB2	2.27	71%	437.09	24%
IBHB1-1	2.29	72%	417.27	19%

$$EI = \frac{\Delta M}{\Delta \kappa} \quad (5.8)$$

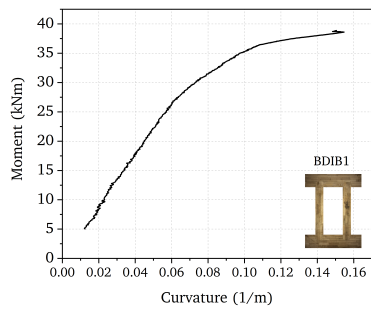
where,  $M$  is the bending moment and  $\kappa$  is the bending curvature.



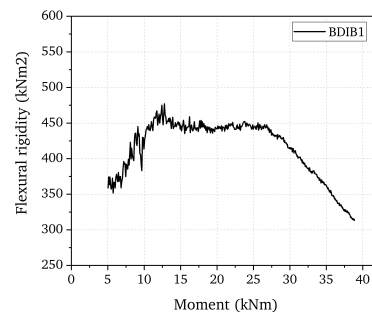
(a) BIB Moment-curvature



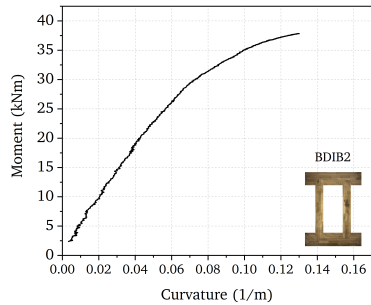
(b) BIB Stiffness



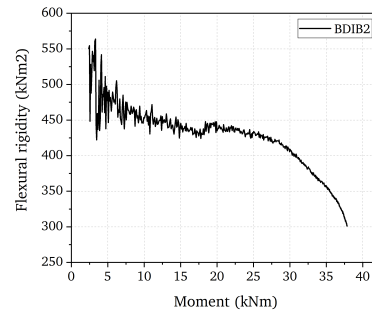
(c) BDIB1 Moment-curvature



(d) BDIB1 Stiffness



(e) BDIB2 Moment-curvature



(f) BDIB2 Stiffness

Figure 5.11: Flexural rigidity of the tested beams

Figure 5.11 compares the stiffness of the tested beams. **BDIB** shows higher stiffness than **BIB** and **IBHB**. Ductility and stiffness of the tested beams are compared in Table 5.3. **IBHB** and **BDIB** illustrated a similar ductility among these beams with about 70% higher ductility compared to **BIB**. With respect to the stiffness, **BDIB** exhibited higher flexural rigidity compared to the other two beams, i.e. **BIB** and **IBHB**, with 25% higher than **BIB** and 6% higher than **IBHB**.

### 5.5.5 Importance of side timbers in IBHB

The four-point bending test underlined the importance of side timbers in the I-bone laminated bamboo hybrid beam. Side timbers mainly contribute toward horizontal shear resistance of the hybrid beam in addition to increasing the contact surface between flanges and the middle web.

BIB failed purely in shear near the tensile flange. Side timbers also contribute to cross-sectional stability and integrity of the beam by preventing unwanted out-of-plane stresses and distortions, e.g. torsion. Additionally, these timbers oriented transversely to enhance the stiffness of the beam, although this can have a negative effect by introducing undesirable stress to the flanges upon changes in the moisture content or humidity.

On the contrary, BIB resulted in higher bending strength ( $MOR = 109.6 \text{ N/mm}^2$ ) than that of IBHB ( $MOR = 75 \text{ N/mm}^2$ ) despite a lower maximum applied load. This is due to the optimised geometry of BIB which consequently results in a lower second moment of area.

### 5.5.6 $\hat{A}$

## 5.6 Shear Stress Calculations

In regard to the I-beams, calculating the shear strength does not provide the true shear properties of the material, as the beams have not failed due to the shear stress. Nonetheless, the shear strengths of the beams were calculated at the failure point in the following steps.

The shear stress of a beam when subjected to flexural loads is:

$$\tau = \frac{V_y}{I_{zz}b} \int y \, dA \quad (5.9)$$

If  $Q = \int y \, dA$  is the first moment of area we have:

$$\tau = \frac{V_y Q_z}{I_{zz}b} \quad (5.10)$$

where  $V$  is the transverse shear force,  $Q$  is the first moment of area, i.e. section above the area of interest,  $I$  is the moment of inertia and  $b$  is the width of the section.

According to the beam theory, the shear stress due to bending is maximum at the centroidal axis for a prismatic beam with the symmetric loading conditions. Hence, the first moment

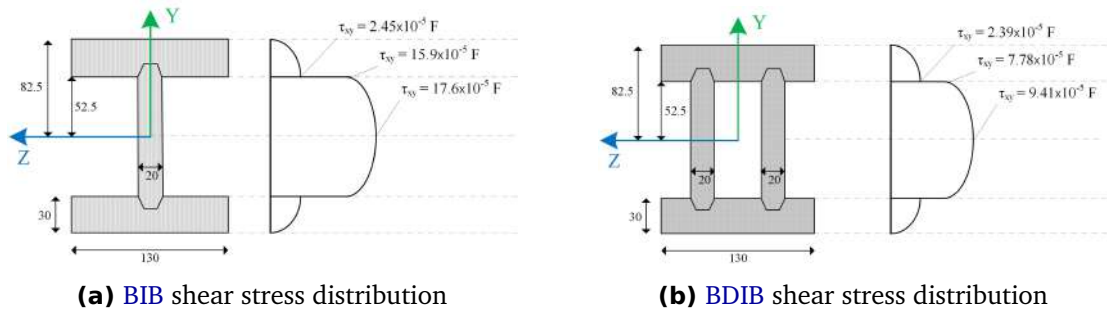


Figure 5.12: Shear stress distribution for BIB and BDIB

of the area can be determined using:

$$Q_z = \frac{bt(h-t) + b_w(h/2-t)^2 - y^2}{2} \quad (5.11)$$

$y=0$  yields the maximum:

$$Q_{max} = \frac{bt(h-t)}{2} + \frac{b_w(h-2t)}{8} \quad (5.12)$$

Figure 5.2 provides dimensions of BIB and BDIB.

$b$ is the width of the flanges	$b = 130$ mm
$h$ is the height of the beam	$h = 165$ mm
$t$ is the thickness of the flanges	$t = 30$ mm
$b_w$ is the width of the web	$b_w = 20$ mm for BIB
	$b_w = 40$ mm for BDIB

Substituting these values in Equations 5.10 and 5.12 would yield:

$$Q_{BIB} = 290812.5 - 10y^2 \quad Q_{BDIB} = 318375 - 20y^2 \quad (5.13)$$

This yield:

$$\tau_{max} = \frac{F_{max} Q_z}{2b_w I_{yy}} \quad (5.14)$$

Equation 5.14 describes the shear distribution of the beams across the cross-section. The maximum shear stress occurs where  $Q$  is maximum ( $y = 0$ ). In addition, the flanges and web joining points are the critical points as well. Due to a sudden change in the shear resisting breadth, shear stress sharply increases when moving from flanges to the web. Figure 5.12 illustrates the shear distribution of BIB and BDIB.

## 5.7 Deflection Prediction of the Beams

### 5.7.1 Flexural deflection

The deflection of a beam can be simply approximated using Euler-Bernoulli beam theory based on the linear behaviour of the material and assuming that plane sections remain plane during the loading using Equation 5.15. However, shear stress induces shear distortion during the loading and this makes planes to warp and distort, resulting in an additional deflection.

$$\Delta_f = \frac{Pal^2}{48EI} \times \left[ 3 - 4\frac{a^2}{l} \right] \quad (5.15)$$

### 5.7.2 Shear deflection

The shear distortion created due to the shear stress is generally considered to have secondary effects thus often neglected from the calculations. The total deflection of a beam comprises of flexural deflection ( $\Delta_f$ ) and shear deflection ( $\Delta_s$ ) and can be determined as follows:

$$\Delta_t = \Delta_f + \Delta_s \quad (5.16)$$

Let the shear stress at the neutral axis denoted by  $\tau_{NA}$  the shear strain at the neutral axis denoted by  $\gamma_{NA}$  and the shear modulus of the material is G:

$$\tau_{NA} = \gamma_{NA}G \quad \rightarrow \quad \gamma_{NA} = \frac{\tau_{NA}}{G} \quad (5.17)$$

The additional deflection arising due to the shear deflection can be determined using the triangulation:

$$\frac{\delta v_s}{\delta x} = \gamma_{NA} \quad \rightarrow \quad \frac{\delta v_s}{\delta x} = \frac{\tau_{NA}}{G} \quad (5.18)$$

In Section 5.6, the shear stress of the beams have been developed. For a simply supported beam with two concentrated loads we have:

$$Q_{max} = 263250 + 1378.175b_w \quad (5.19)$$

$$\tau_{NA} = \frac{F(263250 + 1378.175b_w)}{2b_wI} \quad (5.20)$$

By substitution, we have:

$$\frac{\delta v_s}{\delta x} = \frac{F(263250 + 1378.175b_w)}{2b_wIG} \quad (5.21)$$

Then:

$$v_s = \frac{F(263250 + 1378.175b_w)x}{2b_wIG} + A \quad (5.22)$$

Using boundary conditions, at  $x = 0$  the deflection is zero, thus  $A = 0$ . And at the mid-span where the deflection is maximum, we have:

$$\Delta_t = \frac{Fal^2}{48EI} \times \left[3 - 4\frac{a^2}{l}\right] + \frac{F(263250 + 1378.175b_w)}{2b_wIG} \times \frac{l}{2} \quad (5.23)$$

where  $F$  is the applied load,  $a$  is the distance between loading point and the nearest support,  $l$  is the beam's span,  $I$  is the second moment of area,  $b_w$  is the width of the web,  $E$  is the modulus of elasticity of the flanges and  $G$  is the shear modulus of the web.

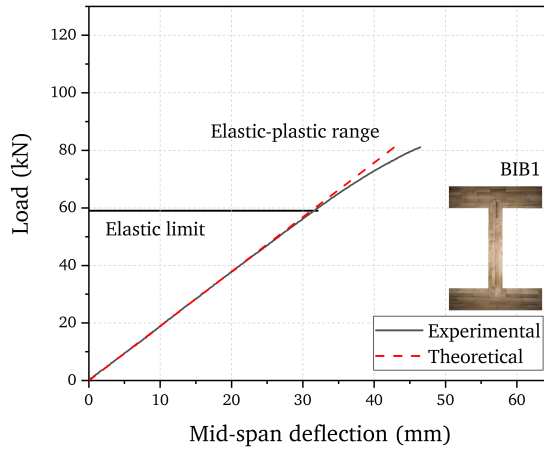
Based on the material properties of laminated bamboo determined in Chapter 3, the theoretical deflection was determined and compared to that of the experimental values. Figure 5.13 compares the calculated deflection with the measured values in the elastic range. The results showed good agreement in the elastic range.

## 5.8 Ultimate Bending Moment Capacity Prediction

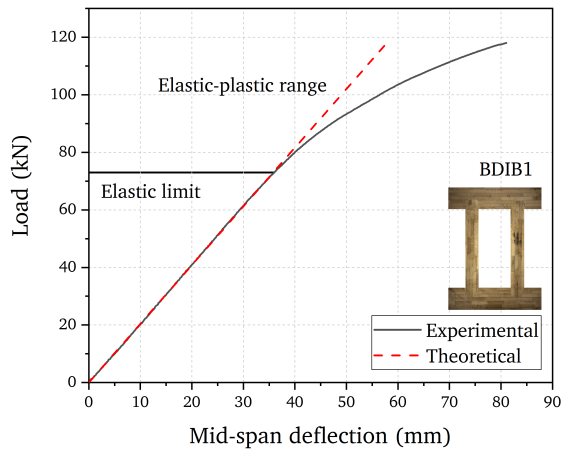
Ultimate bending moment of BIB and BDIB can be predicted based on the proposed stress-strain relationship of laminated bamboo lumber described in Chapter 3 and the following assumptions:

1. Laminated bamboo is an orthotropic material with two orthogonal planes of symmetry.
2. A solid bond between the flanges and the web was assumed as no delamination was observed during the experiments.
3. The rupture was assumed to occur in the far extreme fibre of the tension surface.
4. In term of BIB, since the web failed due to horizontal shear, thus, it is assumed that the flanges will be considered as the flexural load-bearing elements.
5. The Young's modulus for compression and tension has an equal value.

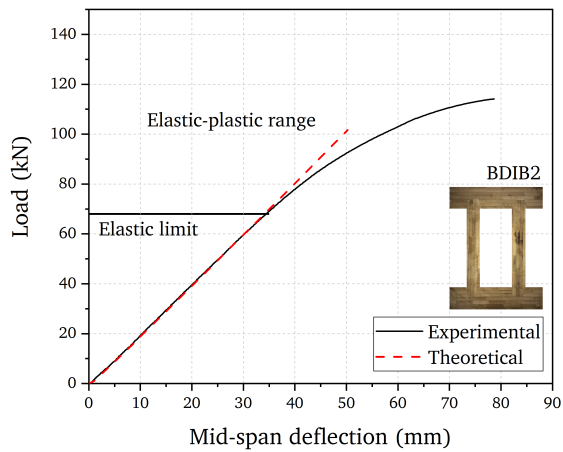
Two cases were considered depending on the strain values in the cross-section:



(a) BIB1



(b) BDIB1



(c) BDIB2

Figure 5.13: Experimental and theoretical load-deflection comparison

**Case 1:** when the stress distribution across the cross-section is linear and the maximum strain in the tension surface is lower than the yield strain in the compression ( $\epsilon_{ult} \leq \epsilon_{cy}$ ). This means that the beams were in the linear and elastic region.

**Case 2:** when the tensile stress is higher than the compression yield point ( $\epsilon_{cy} < \epsilon_{ult} < \epsilon_{cu}$ ). This means that the beam is in the elastic-plastic region.

### 5.8.1 Moment capacity of BIB

The bending moment of BIB is determined using the beam theory. Referencing Figure 5.14 as the stress distribution over the cross-section of BIB, we have:

$$F_t = F_c \quad (5.24)$$

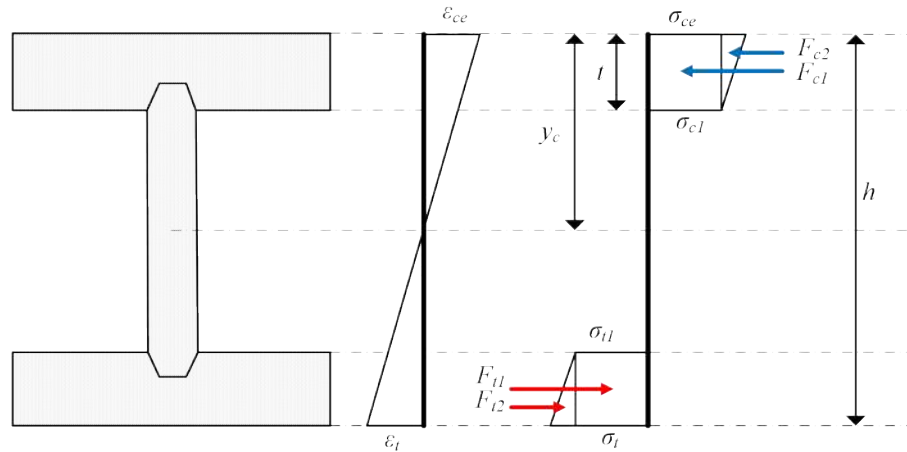


Figure 5.14: BIB stress distribution

For the compression region we have:

$$\sigma_{c1} = \left(1 - \frac{t}{y_c}\right) \sigma_{ce} \quad (5.25)$$

$$F_c = F_{C1} + F_{C2} \quad (5.26)$$

$$F_{c1} = bt\sigma_{c1} = \left(1 - \frac{t}{y_c}\right) bt\sigma_{ce} \quad (5.27)$$

$$F_{c2} = \frac{bt(\sigma_{ce} - \sigma_{c1})}{2} = \frac{bt^2}{2y_c} \times \sigma_{ce} \quad (5.28)$$

$$F_c = \left(1 - \frac{t}{y_c}\right) bt\sigma_{ce} + \frac{bt^2}{2y_c} \sigma_{ce} = \left(1 - \frac{t}{2y_c}\right) bt\sigma_{ce} \quad (5.29)$$

And for the tension region:

$$\sigma_{t1} = \left(1 - \frac{t}{h - y_c}\right) \sigma_t \quad (5.30)$$

$$F_t = F_{t1} + F_{t2} \quad (5.31)$$

$$F_{t1} = bt\sigma_{t1} = \left(1 - \frac{t}{h - y_c}\right) bt\sigma_t \quad (5.32)$$

$$F_{t2} = \frac{bt(\sigma_t - \sigma_{t1})}{2} = \frac{bt^2}{2(h - y_c)} \sigma_t \quad (5.33)$$

$$F_t = F_{t1} + F_{t2} = \left(1 - \frac{t}{2(h - y_c)}\right) bt\sigma_t \quad (5.34)$$

From the proposed stress-strain relationship and for an elastic analysis we have:

$$\epsilon_{ce} = \frac{y_c \epsilon_t}{h - y_c} \quad (5.35)$$

$$\sigma_{ce} = E_t \epsilon_{ce} \quad (5.36)$$

$$\sigma_t = E_t \epsilon_t \quad (5.37)$$

The location of the neutral axis ( $y_c$ ) can be determined using Equation 5.35 and Equation 5.36.

$$\left(1 - \frac{t}{2y_c}\right) bt\sigma_{ce} - \left(1 - \frac{t}{2(h - y_c)}\right) bt\sigma_t = 0 \quad (5.38)$$

$$\left(1 - \frac{t}{2y_c}\right) btE_t \times \frac{y_c \epsilon_t}{h - y_c} - \left(1 - \frac{t}{2(h - y_c)}\right) btE_t \epsilon_t = 0 \quad (5.39)$$

Once the location of the neutral axis is determined, the ultimate bending moment of BIB can be obtained using the bending moment equilibrium.

$$M = F_c \times d_c + F_t \times d_t \quad (5.40)$$

$$M = \left(1 - \frac{t}{y_c}\right) btE_t \times \frac{y_c \epsilon_t}{h - y_c} \times \left(y_c - \frac{t}{2}\right) + \frac{bt^2}{2y_c} \times \frac{y_c \epsilon_t E_t}{h - y_c} \times \left(y_c - \frac{t}{3}\right) + \left(1 - \frac{t}{h - y_c}\right) btE_t \epsilon_t \times \left(h - y_c - \frac{t}{2}\right) + \frac{bt^2}{2(h - y_c)} E_t \epsilon_t \times \left(h - y_c - \frac{t}{3}\right) \quad (5.41)$$

By simplifying:

$$M = E_t \epsilon_t bt \left( \frac{y_c - t}{h - y_c} \times \left(y_c - \frac{t}{2}\right) + \frac{t}{2(h - y_c)} \times \left(y_c - \frac{t}{3}\right) + \left(1 - \frac{t}{h - y_c}\right) \times \left(h - y_c - \frac{t}{2}\right) + \frac{t}{2(h - y_c)} \times \left(h - y_c - \frac{t}{3}\right) \right) \quad (5.42)$$

$$M = E_t \epsilon_t bt \left( \frac{2y_c^2 - 3ty_c + t^2}{2(h - y_c)} + \frac{3ty_c - t^2}{6(h - y_c)} + \frac{2(h - y_c)^2 - 3t(h - y_c) + t^2}{2(h - y_c)} + \frac{3t(h - y_c) - t^2}{2(h - y_c)} \right) \quad (5.43)$$

Table 5.4: BIB bending moment prediction

Beam	h	b	$E_t$	$\epsilon_{ce}$	$\epsilon_t$	$y_c$	$M_{exp}$	$M_{th}$	Error
	[mm]	[mm]	[N/mm <sup>2</sup> ]			[mm]	[N.m]	[N.m]	
BIB	169	130.43	9030	9.9E-03	8.8E-03	89.7	26.84	46.81	74.41%

Further simplification yields:

$$M_{BIB} = \frac{E_t \epsilon_t b t}{6(h - y_c)} (6y_c^2 - 6ty_c + 6(h - y_c)^2 + 2t^2) \quad (5.44)$$

Equation 5.44 yields the theoretical bending moment based on the linear behaviour of the material. The calculated bending moment and the measured experimental values are compared in Table 5.4. The calculated bending moment predicts the beam due to the flexural failure, however, in this case BIB failed due to the shear stress.

### 5.8.2 Bending moment capacity of BDIB

For BDIB, the flexural loading carried by the flanges and the web, and in both cases, i.e. linear and nonlinear behaviour, were considered for this analysis.

#### 5.8.2.1 Linear analysis

Referencing Figure 5.15 as the linear stress distribution over the BDIB's cross-section, it is assumed that the tensile strain is less than or equal to the compression yield strain. This provides us with an elastic deformation and a constant modulus of elasticity. Following the equilibrium of forces, we have:

$$F_{cf} + F_{cw} = F_{tf} + F_{tw} \quad (5.45)$$

The subscript  $c$  represents the compression region,  $t$  represents the tensile region,  $f$  refers to the flanges and  $w$  refers to the web.

$$F_{cf} = 1/2(\sigma_{ce} + \sigma_{c1})b_f t = \frac{2y_c - t}{2y_c} b t \sigma_{ce} \quad (5.46)$$

$$F_{cw} = 1/2\sigma_{c1}b_w(y_c - t) = \frac{(y_c - t)^2}{2y_c} b_w \sigma_{ce} \quad (5.47)$$

Where:  $\sigma_{c1} = (1 - t/y_c)\sigma_{ce}$

$$F_{tf} = 1/2(\sigma_t + \sigma_{t1})b_f t = (2(h - y_c) - t)/(2(h - y_c))b t \sigma_t \quad (5.48)$$

$$F_{tw} = 1/2\sigma_{t1}b_w(h - y_c - t) = (h - y_c - t)^2/2(h - y_c)b_w \sigma_t \quad (5.49)$$

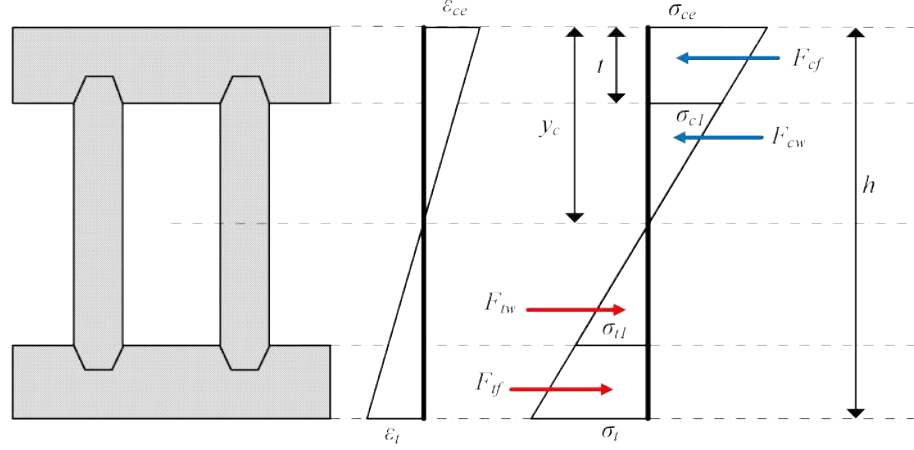


**Figure 5.15:** BDIB linear stress distribution

Where:  $\sigma_{t1} = (1 - t/(h - y_c))\sigma_t$  By substituting Equations 5.46 to 5.49 in Equation 5.45 we can determine the location of the neutral axis (NA) using the following equation:

$$\frac{2y_c - t}{2y_c}bt\sigma_{ce} + \frac{(y_c - t)^2}{2y_c}b_w\sigma_{ce} - \frac{2(h - y_c) - t}{2(h - y_c)}bt\sigma_t - \frac{(h - y_c - t)^2}{2(h - y_c)}b_w\sigma_t = 0 \quad (5.50)$$

Once NA is determined, the bending moment can be predicted as following:

$$M_{BDIB} = \sum F_i d_i$$

$$M_{BDIB} = F_{cf}d_{cf} + F_{cw}d_{cw} + F_{tf}d_{tf} + F_{tw}d_{tw} \quad (5.51)$$

For a trapezoid shape of the stress distribution at the compression zone, the centroid lies at

$$d_i = \frac{3y_c - t}{6y_c - 3t} t \text{ from the top edge and for the tension region } d_i = \frac{3(h - y_c) - t}{6(h - y_c) - 3t} t$$

$$M_{BDIB} = \frac{2y_c - t}{2y_c}bt\sigma_{ce} \times \left( y_c - \frac{3y_c - t}{6y_c - 3t}t \right) + \frac{(y_c - t)^2}{2y_c}b_w\sigma_{ce} \times \frac{2(y_c - t)}{3} +$$

$$\frac{2(h - y_c) - t}{2(h - y_c)}bt\sigma_t \times \left( h - y_c - \frac{3(h - y_c) - t}{6(h - y_c) - 3t} \right) +$$

$$\frac{(h - y_c - t)^2}{2(h - y_c)}b_w\sigma_t \times \frac{2(h - y_c - t)}{3} \quad (5.52)$$

From the on relationship we have:  $\epsilon_{ce} = \frac{y_c \epsilon_t}{h - y_c}$  and therefore  $\sigma_{ce} = E_t \frac{y_c \epsilon_t}{h - y_c}$ .

$$M_{BDIB} = \frac{2y_c - t}{2y_c}btE_t^f \frac{y_c \epsilon_t}{h - y_c} \times \left( y_c - \frac{3y_c - t}{6y_c - 3t}t \right) + \frac{(y_c - t)^2}{2y_c}b_w E_t^w \frac{y_c \epsilon_t}{h - y_c} \times$$

$$\frac{2(y_c - t)}{3} + \frac{2(h - y_c) - t}{2(h - y_c)}btE_t^f \epsilon_t \times \left( h - y_c - \frac{3(h - y_c) - t}{6(h - y_c) - 3t} \right) +$$

$$\frac{(h - y_c - t)^2}{2(h - y_c)}b_w E_t^w \epsilon_t \times \frac{2(h - y_c - t)}{3} \quad (5.53)$$

## CHAPTER 5. LAMINATED BAMBOO I-BEAM AND DOUBLE I-BEAM

**Table 5.5:** BDIB bending moment prediction based on the linear stress-strain relationship

Beam	h	b	$E_f$	$E_w$	$\epsilon_{ce}$	$\epsilon_t$	$M_{exp}^*$	$M_{th}^*$	Error
	[mm]	[mm]	[N/mm <sup>2</sup> ]	[N/mm <sup>2</sup> ]			[N.m]	[N.m]	
BDIB1	168	130.42	9030	9580	9.9E-03	8.8E-03	39.06	41.8	+6.9%
BDIB2	168	130.44	9030	9580	9.9E-03	8.8E-03	37.85	41.8	+10.3%

\* the bending moments at the proportionality limit.

Simplifying the above equation we have:

$$\begin{aligned}
 M_{BDIB} = & E_t^f \epsilon_t b t \frac{2y_c - t}{2(h - y_c)} \times \frac{6y_c^2 - 6ty_c + t^2}{6y_c - 3t} + E_t^w \epsilon_t b_w \frac{(y_c - t)^3}{3(h - y_c)} + \\
 & E_t^f \epsilon_t b t \frac{2(h - y_c) - t}{2(h - y_c)} \times \frac{6(h - y_c)^2 - 6t(h - y_c) + t^2}{6(h - y_c) - 3t} + \\
 & E_t^w \epsilon_t b_w \frac{(h - y_c - t)^3}{3(h - y_c)} \tag{5.54}
 \end{aligned}$$

Equation 5.54 yields the bending moment capacity of the BDIB until the proportionality limit point. The predicted values for the tested beam are presented in Table 5.5. The predicted bending moments have a good agreement with the experimental values.

### 5.8.2.2 Non-linear analysis

For a non-linear analysis of BDIB a bilinear behaviour, as illustrated in Figure 5.16, was assumed for the stress distribution. The first task would be determining the location of the neutral axis and depth of the compression yield. To it, we used the proposed bilinear behaviour proposed in Chapter 3 and by adopting the Bazan-Buchanan law (Malhotra and Bazan, 1980; Buchanan, 1990). For simplicity, it is assumed that the compression yield depth is within the top flange. Based on the strain distribution we can predict the location of  $y_c$  and  $k$ , thus we have:

$$\frac{\epsilon_{ce}}{y_c} = \frac{\epsilon_t}{h - y_c} = \frac{\epsilon_{cy}}{y_c - ky_c} \tag{5.55}$$

$$\begin{aligned}
 F_{c1} &= \frac{1}{2} b k y_c (\sigma_{ce} + \sigma_{cy}) \\
 F_{c2} &= \frac{1}{2} b (t - k y_c) (\sigma_{cy} - \sigma_{c1}) \\
 F_{c3} &= \frac{1}{2} b_w (y_c - t) \sigma_{c1} \tag{5.56}
 \end{aligned}$$

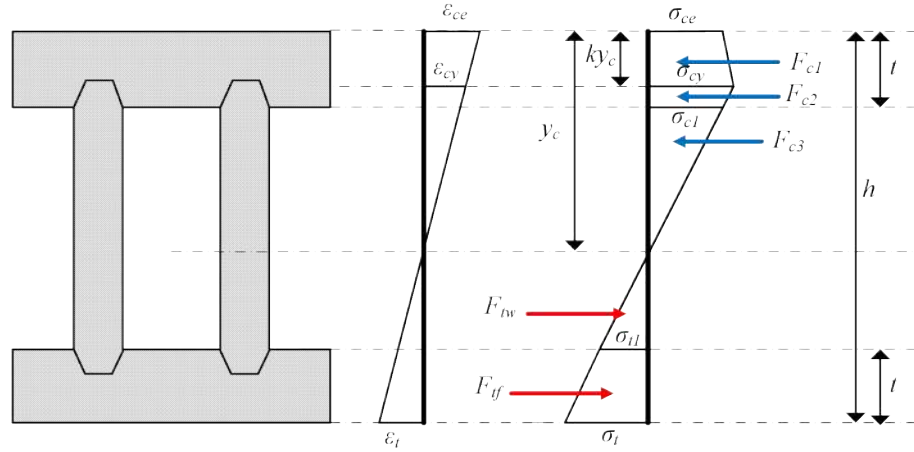


Figure 5.16: BDIB nonlinear stress distribution

From stress distribution we have:

$$\sigma_{cy} = \frac{y_c - ky_c}{h - y_c} \sigma_t \quad (5.57)$$

$$\sigma_{c1} = \frac{y_c - t}{h - y_c} \sigma_t \quad (5.58)$$

And from the Bazan-Buchanan law we have:

$$\sigma_{ce} = \sigma_{cy} - k_{ep}(\epsilon_{ce} - \epsilon_{cy}) \quad (5.59)$$

where  $k_{ep}$  defines as the slop of the elastic-plastic zone in the stress-strain relationship of the laminated bamboo and expressed as:

$$k_{ep} = \frac{\sigma_{ce} - \sigma_{cy}}{\epsilon_{ce,u} - \epsilon_{cy}} \quad (5.60)$$

And for the tension region we have:

$$F_{t1} = \frac{1}{2} \sigma_{t1} b_w (h - y_c - t)$$

$$F_{t2} = \frac{1}{2} b t (\sigma_t + \sigma_{t1})$$

Following a similar procedure as of linear analysis, the equilibrium of compression, the tension loads and the bending moment across the cross-section, we can determine the bending moment of BDIB considering the non-linear behaviour.

$$M = F_{c1} \times d_{c1} + F_{c2} \times d_{c2} + F_{c3} \times d_{c3} + F_{t1} \times d_{t1} + F_{t2} \times d_{t2} \quad (5.61)$$

$$\begin{aligned}
 M_{BDIB} = & \frac{1}{2}bk y_c(\sigma_{ce} + \sigma_{cy}) \times \left( y_c - ky_c + \frac{\sigma_{cy} + 2\sigma_{ce}}{3(\sigma_{cy} + \sigma_{ce})}ky_c \right) + \\
 & \frac{1}{2}b(t - ky_c)(\sigma_{cy} - \sigma_{c1}) \times \left( y_c - ky_c - \frac{\sigma_{cy} + 2\sigma_{c1}}{3(\sigma_{cy} + \sigma_{c1})}(t - ky_c) \right) + \\
 & \frac{1}{2}b_w(y_c - t)\sigma_{c1} \times \frac{2}{3}(y_c - t) + \frac{1}{2}\sigma_{t1}b_w(h - y_c - t) \times \frac{2}{3}(h - y_c - t) + \\
 & \frac{1}{2}bt(\sigma_t + \sigma_{t1}) \times \left( h - y_c - \frac{3(h - y_c) - t}{6(h - y_c) - 3t} \right)
 \end{aligned} \tag{5.62}$$

Simplifying the above equation we have:

$$\begin{aligned}
 M_{BDIB} = & \frac{1}{2}bt(\sigma_{ce} + \sigma_{cy}) \times \left( y_c - t + \frac{\sigma_{cy} + 2\sigma_{ce}}{3(\sigma_{cy} + \sigma_{ce})}t \right) + \frac{1}{2}b(ky_c - t)(\sigma_{cy} - \sigma_{c1}) \times \\
 & \left( y_c - ky_c + \frac{\sigma_{cy} + 2\sigma_{c1}}{3(\sigma_{cy} + \sigma_{c1})}(ky_c - t) \right) + \frac{1}{2}b_w(y_c - ky_c)\sigma_{c1} \times \frac{2}{3}(y_c - ky_c) + \\
 & \frac{1}{2}\sigma_{t1}b_w(h - y_c - t) \times \frac{2}{3}(h - y_c - t) + \frac{1}{2}bt(\sigma_t + \sigma_{t1}) \times \\
 & \left( h - y_c - \frac{3(h - y_c) - t}{6(h - y_c) - 3t} \right)
 \end{aligned} \tag{5.63}$$

Equation 5.63 predicts the ultimate bending moment in the laminated bamboo double I-beam. The associated values of Young's modulus ( $E_t$ ), tensile strain ( $\epsilon_t$ ), compressive yield strain ( $\epsilon_{cy}$ ) were obtained from the Small Clear Specimen tests. The stress values ( $\sigma_t, \sigma_{cy}$  and  $\sigma_{ce}$ ) were determined using the measured strains and Equations 5.57 - 5.59. These values are presented in Table 5.6.

**Table 5.6:** BDIB nonlinear stress-strain relationship prediction

Beam	$\epsilon_{cy}$	$\epsilon_{ce}$	$\frac{\sigma_{cy}}{[N/mm^2]}$	$\frac{\sigma_{c1}}{[N/mm^2]}$	$k_{ep}$	$\frac{\sigma_{ce}}{[N/mm^2]}$	$\frac{\sigma_t}{[N/mm^2]}$	$\frac{\sigma_{t1}}{[N/mm^2]}$
BDIB1	5.62E-3	9.95E-3	66.05	77.54	1986	57.45	103.42	64.08
BDIB2	5.62E-3	9.95E-3	66.68	78.29	2177	57.26	104.42	64.70

The analytical prediction of the ultimate bending moment for the tested beams for this stage was derived and the predictions are compared with the experimental values in Table 5.7. Based on the predicted values, this model can approximate the ultimate bending capacity of BDIB with a good agreement to the experimental values with only 2-5% error.

**Table 5.7:** BDIB bending moment prediction for non-linear analysis

Beam	$M_{exp}$	$M_{th}$	Error
	[N.m]	[N.m]	%
BDIB1	39.06	39.80	+2%
BDIB2	37.85	39.80	+5%

## 5.9 Discussion and Summary

This chapter presented the fabrication process and the evaluation of the [Engineered Bamboo I-Beam \(BIB\)](#) and [Engineered Bamboo Double I-Beam \(BDIB\)](#). Furthermore, comparisons were drawn on the flexural properties of these beams and the I-bone laminated bamboo hybrid beam ([IBHB](#)).

The fabrication process of [BIB](#) and [BDIB](#) was similar to that of [IBHB](#) with regards to the dimension of the flanges and the web(s). As the [MF](#) type resin provided a better bond, thus, it was used for this stage. In addition to the challenges in the fabrication of [IBHB](#), it was noticed that due to the nature of bamboo, the laminated bamboo might split along its fibres. Therefore, accurate cuts are required in order to prevent splitting.

The four-point bending test as detailed in the BS EN 408 was conducted on each beam. The mid-span deflection and the curvature of the beams were measured using six LVDTs. The beams were loaded at the rate of 6 mm/min until fracture. Samples from the fractured beams were obtained for the density and the moisture measurements.

The [BIB](#) failed due to the horizontal shear stress exceeding the horizontal shear strength limit and the failure occurred at the web near the bottom flange. This is because of shifting the neutral axis downward toward the tension zone when the compression flange starts to yield. This downward shifting caused the excess shear stress near the bottom flange, hence failure occurred.

On the other hand, [BDIB](#) illustrated both the tensile failure and horizontal shear failure. This behaviour indicates that the beam possesses sufficient cross-sectional integrity and strength and the laminated bamboo performed to its full flexural capacity. Shear failure was also observed and this may be due to the lateral-torsional buckling created by twisted

and crooked cross-section, thus making the force distribution uneven on each web.

The load-deflection graph of the tested beams revealed that the I-beam composites performed in a similar pattern as of **IBHB**. This pattern initiated with an elastic deformation until the ultimate tensile strain at the bottom surface is less than or equal to the compressive yield strain of laminated bamboo. At this point, the laminated bamboo in the compression region started to yield from its extreme far fibres. This introduced an elastic-plastic deformation which is defined as non-linear behaviour in the stress-strain relationship. The failure of the beams occurs without the pure plasticity which categorises it as a brittle failure.

The **BDIB** showed about 70% more ductile behaviour than **BIB**, whilst **IBHB** also showed 72% higher ductility than **BIB**. The flexural rigidity was determined as the slope of the moment-curvature graph. **BDIB** outperformed both **IBHB** and **BIB** by 6% and 25%, respectively. This higher stiffness is the result of the optimised cross-section of the **BDIB**.

The **IBHB** showed 62% higher load-bearing capacity and 72% higher ultimate deflection compared to the **BIB** as the direct influence of the side timbers. Moreover, **IBHB** showed 12-15% higher load-bearing capacity and comparable maximum deflection to **BDIB**.

Despite the lower maximum failure load, the **BDIB** showed higher bending strength (**MOR**) than **IBHB**. This is due to the difference in the second moment of area which is lower in the **BDIB** thus **MOR** was higher. The results of this study revealed that **IBHB** possesses 31% and 9% higher **MOE** compared to **BIB** and **BDIB**, respectively. This is due to the introduction of the side timbers, which enhance the flexural rigidity while contributing to the shear resistance of the beam.

Based on the measurements of the material density, **IBHB** expectedly has a lower density than the other two composites. The density of **IBHB** was 538.6 kg/m<sup>3</sup> which makes this material efficient in regard to the modulus of elasticity to density ratio. In contrast, the **BDIB** due to the optimised cross-section had a higher ratio of **MOR** to density among the tested beams.

The shear stress in the beam at the failure point was determined. The shear stress calculation revealed that **BIB** experienced higher shear stresses due to the lower moment of area, which induces the web to fracture due to the horizontal shear stress. The compression yield of the laminated bamboo can also be identified as an impacting factor in this mode of

failure.

The experimental results, the analytical models to approximate the ultimate deflection and the bending moment were derived based on linear and non-linear behaviour of the laminated bamboo. The proposed bi-linear material properties of wood by Bazan-Buchanan was adopted for laminated bamboo when developing the non-linear stress distribution over the cross-section of the **BDIB**. The predicted values for both linear and non-linear analysis were in the good agreement of the experimental results.

Whilst **BIB** and **BDIB** exhibited improved flexural performance, these beams can have disadvantages compared to engineered wood products. For example, web stiffening required to prevent bearing failure and torsional resistance. Therefore, the size limitation needs to be applied.

In addition, notching and cutting holes are not permitted for these beams as they can considerably reduce the rigidity and performance of these beams. Lower fire resistance, cross-sectional stability and vibrational problems can be named as other disadvantages of I-beams compared to solid section engineered wood products.

# BUTT-JOINTED LBL IN A HYBRID BEAM

## 6.1 Introduction

Laminated Bamboo Lumber (LBL) are, sometimes, produced using shorter and smaller strips of bamboo which butt-jointed at a section to form a longer and wider lumber or board (Figure 6.1). This is to reduce production costs and design requirements. These butt-joints are concealed by the smooth and joint-free layers for the surface applications, e.g. kitchen worktops.

Generally, laminated bamboo lumber with butt-joints cannot be used for structural purposes, simply because they carry no moment at the butt joint. However, as the butt-joints are not in the same section in every bamboo strip layer (Figure 6.1), these type of laminated bamboos may be used as a component of the hybrid/composite materials. The butt-joints reduce the flexural rigidity of the laminated beam and considered as gaps (Jaeger and Bakht, 1990). However, in the case of a hybrid beam, butt-joints will perform like micro-butt-joints and allow LBL to transfer the bending moment to some extent.

This chapter presents the investigation of the impact of the butt-joints on the flexural properties of the hybrid beams made of the timber and LBL. The mechanical properties of the Vertically Laminated Hybrid Beam (VLHB) were examined and compared with the Glulam control samples. The experiments' results then compared with the theoretical

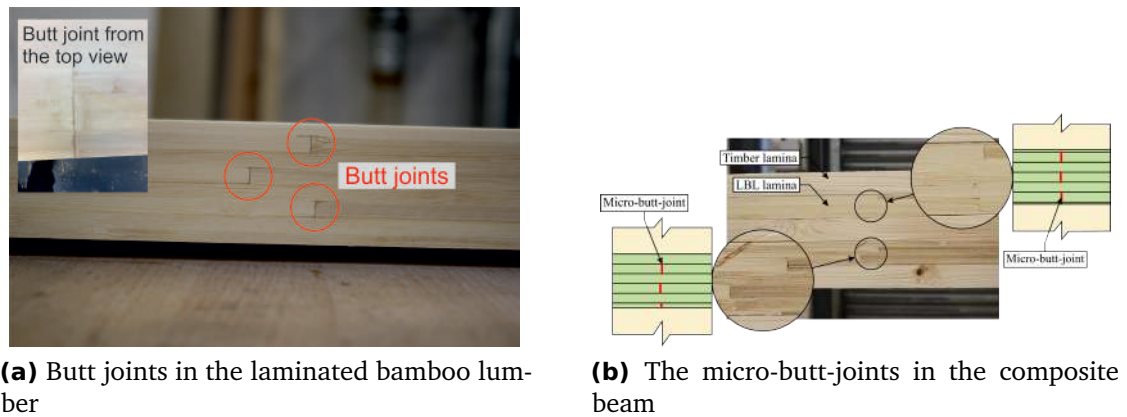


**Figure 6.1:** Butt-joint in the laminated bamboo lumber and the composite beam

models. Furthermore, the three-point bending tests were conducted using beams without any butt-joints, to compare the hybrid beams with and without butt-joints.

## 6.2 Butt-Joint in the Four-Point Bending Test

### 6.2.1 Specimens

Three VLHB and three Glulam beams were produced. The nominal dimensions of the beam are shown in Figure 6.2. The laminated bamboo lumber was made of Moso bamboo strips which were originated from China with the thickness of 5 mm and the width of 21 mm. The laminated bamboo was 3 meter long and the butt-joints were located at a meter away from either end. The timber was Norway spruce and structurally graded as C24.

The manufactured beams were 142.5 mm wide and 178 mm deep. The length of the beams was 3 meters and the span of the loading was 2850 mm. Two butt-joints were a meter apart from each other as shown in Figure 6.2.

### 6.2.2 Experimental procedure

The four-point bending test conducted according to BS EN 408 (BSI, 2012). The specimens were loaded parallel to their glue line, this is to ensure that each lamina experiences a similar stress distribution across the depth. 80 mm wide bearing steel plates were used for both VLHB and Glulam control samples between the loading head and the specimen to minimise indentation. Test arrangement is illustrated in Figure 6.3. The loading was applied at a rate of 6 mm/min and the deflection of the beam was measured using six

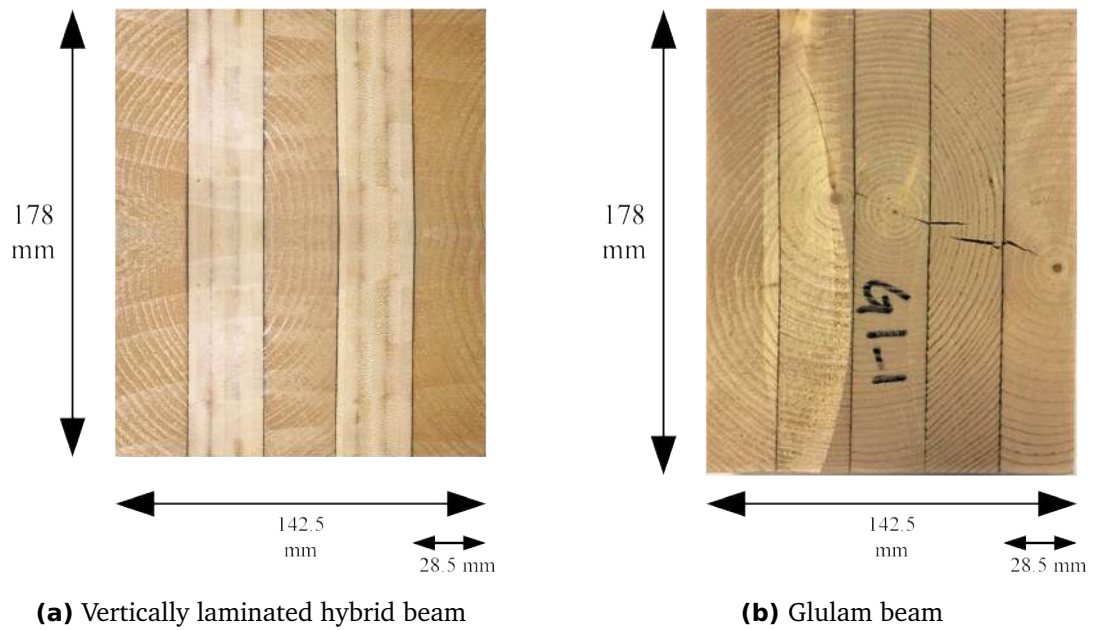


Figure 6.2: VLHB and GL nominal dimensions

LVDTs at three points at each side of the beam as specified by BS EN 408 (Figure 6.3). The measurements of the bending test are presented in Table 6.1.

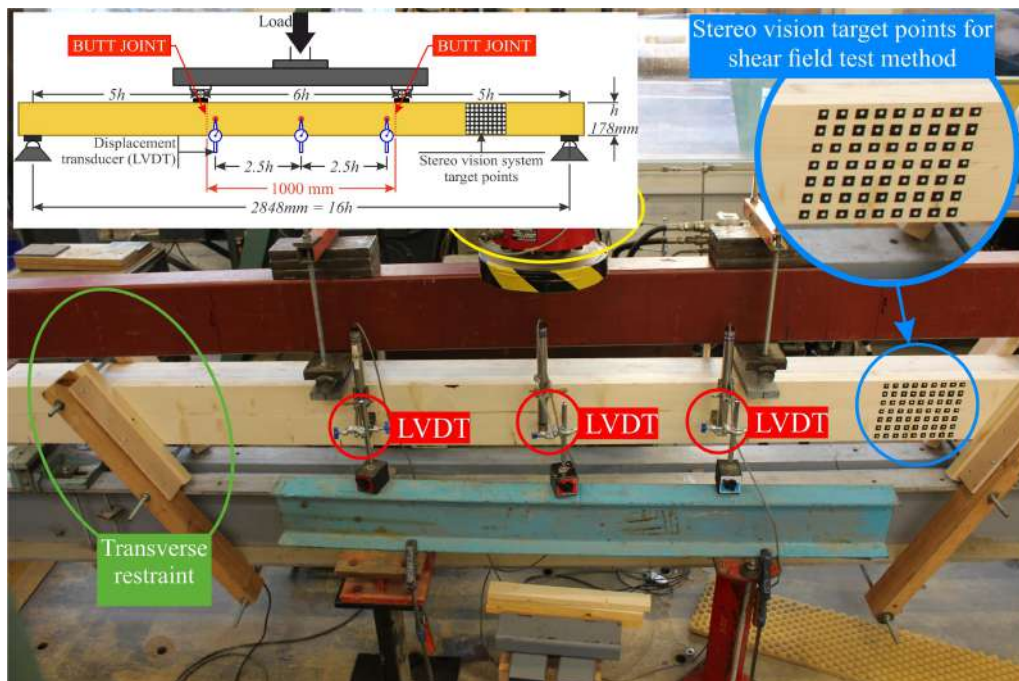


Figure 6.3: Four-point bending test setup

**Table 6.1:** Four-point bending test readings

Specimen	Width	Depth	Length	$M_{max}$	$F_{max}$	$W_{max}$
	[mm]	[mm]	[mm]	[kN.m]	[kN]	[mm]
VLHB1	142.3	178.1	2850	34.21	76.88	48.5
VLHB2	142.4	177.9	2850	33.93	76.25	55.3
VLHB3	141.8	178.0	2850	36.45	81.91	50.6
GL1	142.3	177.7	2850	28.14	63.25	42.9
GL2	142.3	178.0	2850	27.22	61.17	39.1
GL3	142.1	177.9	2850	34.01	76.42	48.2

### 6.2.3 Results of the four-point bending test

Modulus of Elasticity (MOE) and Modulus of Rupture (MOR) are two commonly used quantities in the characterisation of the structural materials. The measured flexural properties and the shear modulus of the tested beams can be found in Table 6.2. The results of this study revealed that the VLHBs exhibited 16% higher bending strength compare to the Glulam control samples despite the weakness in the butt-joint section (46.1 N/mm<sup>2</sup> opposed to 39.7 N/mm<sup>2</sup>, respectively). On the other hand, lower MOE for VLHB (12.97 kN/mm<sup>2</sup>) than control samples (13.9 kN/mm<sup>2</sup>) was observed. In regards to the shear modulus, VLHB showed 14% higher shear modulus.

### 6.2.4 Deformation behaviour of the tested beams

Figure 6.4 compares the typical load and deflection relationship for the VLHB. As can be seen, the flexural behaviour of the hybrid beams with the butt-joint is very similar to the Glulam beam. This behaviour initiated with linear elastic deformations with slight elastic-plastic before a brittle failure. The load at the rupture for the VLHB was higher but not significantly. Figure 6.5 shows the typical load-deflection graph for the VLHBs. The maximum values are shown on the graph.

### 6.2.5 Failure analysis

The mode of failure was similar for all the VLHBs. The fracture started at the butt-joint in the tension surface and followed by the fracture in the outer timber laminae. No

**Table 6.2:** Four-point bending test results

Specimen	Density	MOE	MOR	G
	[kg/m <sup>3</sup> ]	[kN/mm <sup>2</sup> ]	[N/mm <sup>2</sup> ]	[N/mm <sup>2</sup> ]
VLHB1	521.2	12.94	45.48	1479
VLHB2	520.3	11.14	45.15	1258
VLHB3	534.7	14.84	48.67	1329
<b>Mean</b>	<b>525.4</b>	<b>12.97</b>	<b>46.43</b>	<b>1355</b>
cov	1.2 %	14.3 %	4.2 %	8.3 %
GL1	438.3	12.65	37.58	1276
GL2	449.1	14.82	36.21	1156
GL3	492.3	14.22	45.36	1130
<b>Mean</b>	<b>459.9</b>	<b>13.90</b>	<b>37.72</b>	<b>1187</b>
cov	5.1 %	8.1 %	12.4 %	6.6 %

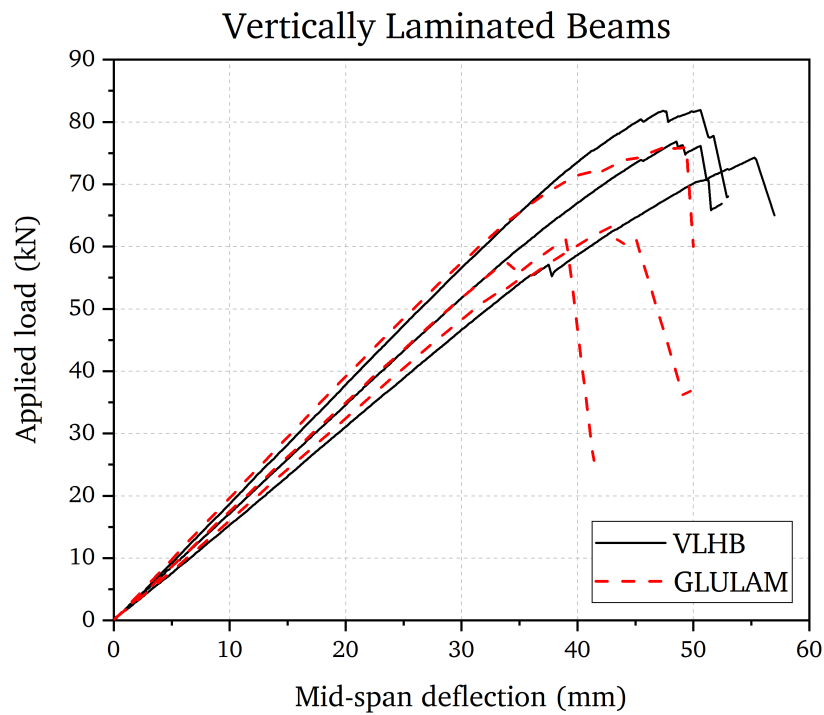


**Figure 6.4:** Load-deflection of the tested beams in four-point bending test

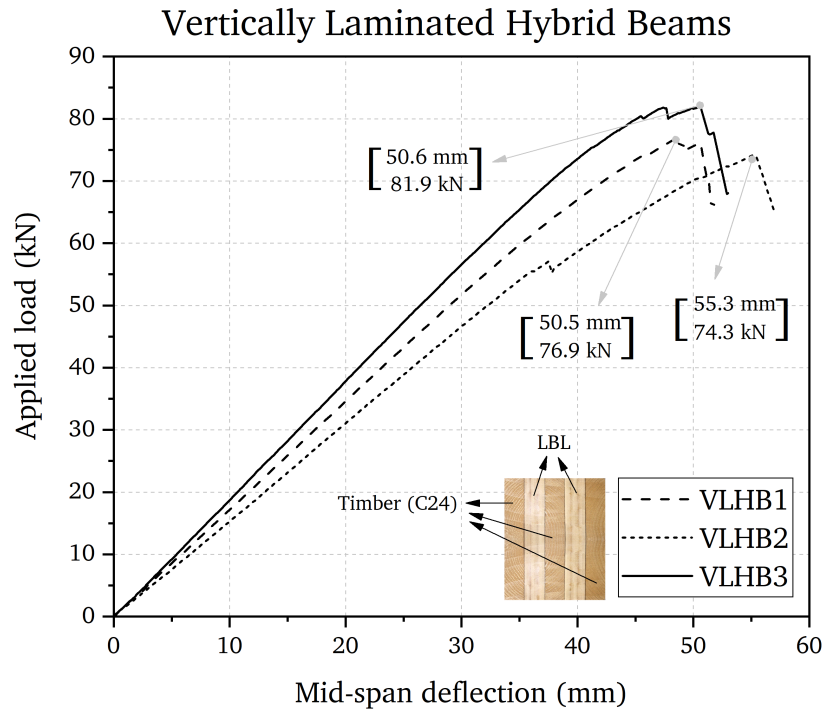


Figure 6.5: VLHB load-deflection graph

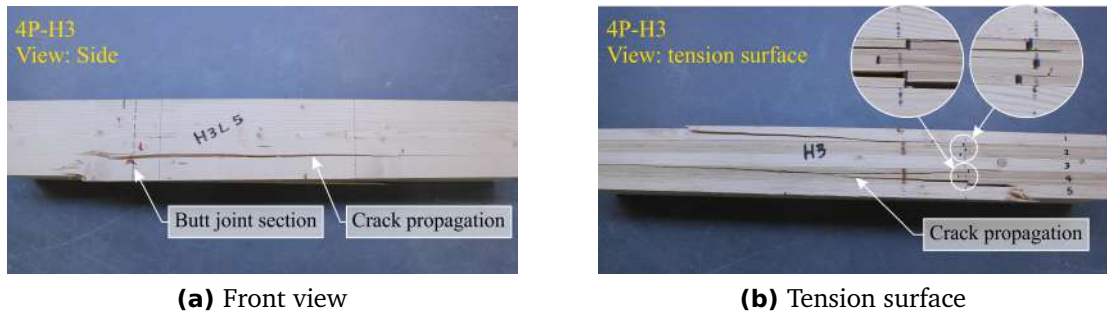


Figure 6.6: VHB3 failure observations

compression failure nor delamination was observed. The micro-cracking sounds were audible before the failure. The failure images of VLHB3 can be seen in Figure 6.6. This signifies the weakness induced by the butt-joints, thus using butt-jointed laminated bamboo for the structural application is not advised.

The Glulam samples experienced a similar failure pattern; a brittle failure at the tension surface, but delamination was also observed (Figure 6.7).



**Figure 6.7:** Glulam beam failure observations

### 6.3 Three-Point Bending Test Without Butt-Joints

The three-point bending test was conducted using the specimens which were cut from either end of the full-size specimen. Each of these specimens was then cut in half with respect to their depth. Six specimens were prepared with the dimensions of 142.5 mm width, 88 mm depth and a meter long. The loading span was 880 mm long as illustrated in Figure 6.8.

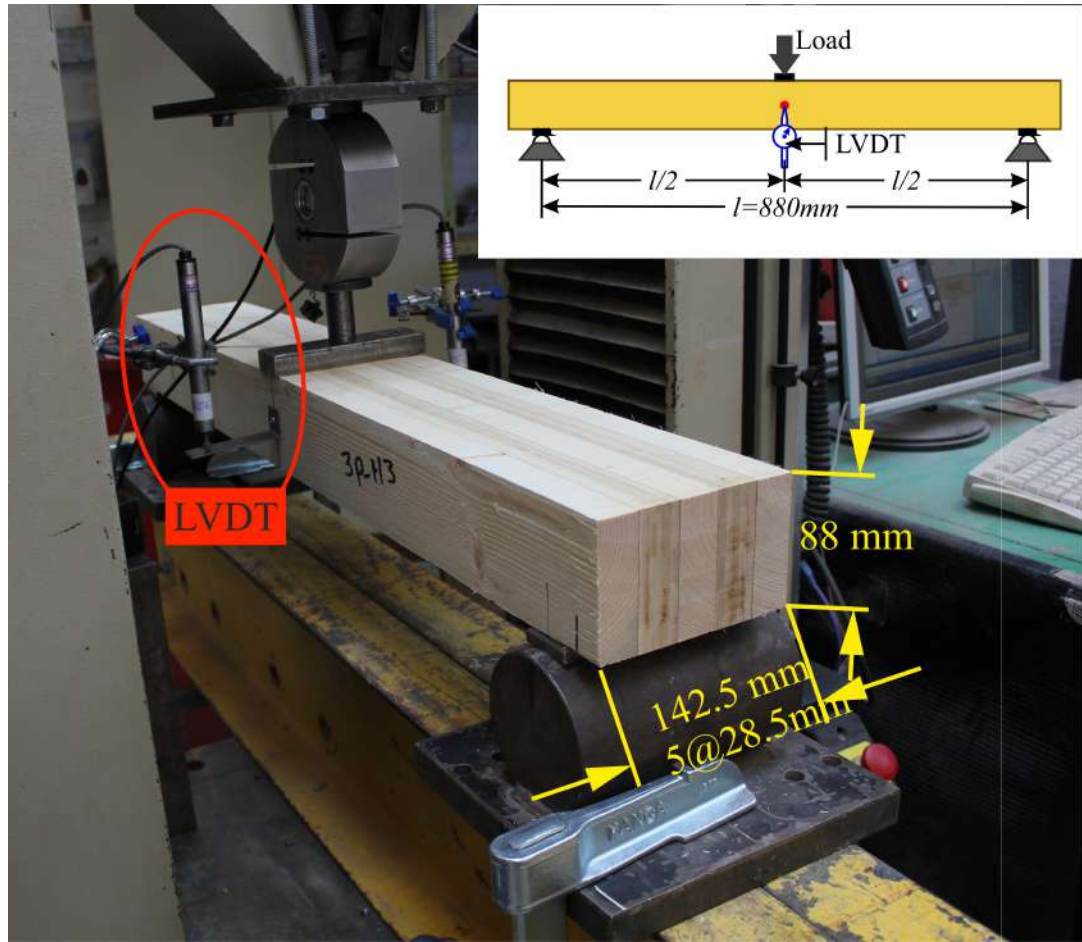


Figure 6.8: Three-point bending test for BTHB

Modulus of Elasticity and Rupture of the specimens, in three-point bending test, were calculated using Equations 6.1 and 6.2, respectively.

$$MOE = \frac{F'l^3}{4\Delta'bh^3} \quad (6.1)$$

$$MOR = \frac{3F_{max}l}{2bh^2} \quad (6.2)$$

where  $F'$  is the load at proportional limit and  $\Delta'$  is the deflection at mid length at limit of proportionality.

### 6.3.1 Results of the three-point bending test

The MOE and MOR determined using the three-point bending test can be found in Table 6.3. Based on these results, VLHB without butt-joints performed significantly better in term of bending strength compared to the glulam control samples. The measured MOR for

**Table 6.3:** Comparison of 4-Point bending test (with butt-joint) and 3-Point bending test (without butt-joint).

Specimen	4-Point bending		3-Point bending	
	MOE/kN/mm <sup>2</sup>	MOR/N/mm <sup>2</sup>	MOE/kN/mm <sup>2</sup>	MOR/N/mm <sup>2</sup>
VHB1	12.94	45.48	8.13	73.45
VHB2	11.14	43.97	7.37	67.45
VHB3	14.84	48.67	8.92	76.91
<b>Mean</b>	<b>12.97</b>	<b>46.04</b>	<b>8.14</b>	<b>72.60</b>

the VLHB without butt-joint was 72.60 N/mm<sup>2</sup> compare to 46.04 N/mm<sup>2</sup> of VLHB with butt-joint and 39.72 N/mm<sup>2</sup> of the Glulam control samples.

The modulus of elasticity in three-point and four-point bending tests cannot be compared directly as in the three-point bending test the shear effect and the indentation of the loading head were neglected. These deficiencies make the determined values underestimated (Brancheriau et al., 2002). The four-point bending test, on the other hand, gives a better estimation of the flexural modulus due to measuring the displacement in the shear-free span. The measured MOE for VLHB in the three-point bending test (MOE<sub>3P</sub>=8.14 kN/mm<sup>2</sup>) is well below the measured values in the four-point bending test with butt-joint (MOE<sub>4p</sub>=12.97 kN/mm<sup>2</sup>) as well as control glulam samples (MOE<sub>4p</sub>=13.9 kN/mm<sup>2</sup>). Since the calculation of the bending modulus is independent of the maximum applied load and only relies on the slope of the elastic region of the deformation, it can be concluded that the butt-joint does not impact the bending modulus.

### 6.3.2 Failure Mechanism of the VLHB in three-point bending

The failure of the specimen without butt-joints was rather different from the four-point bending test results. The outer timber laminae failed first and this followed by the middle timber lamina failure (Figure 6.10a). Finally, the laminated bamboo failed after all the timber laminae fractured (Figure 6.10b). Looking into the load-deflection graphs, the VLHB without butt-joint showed signs of the plastic behaviour, although this can be due to failure of each bamboo strips individually.

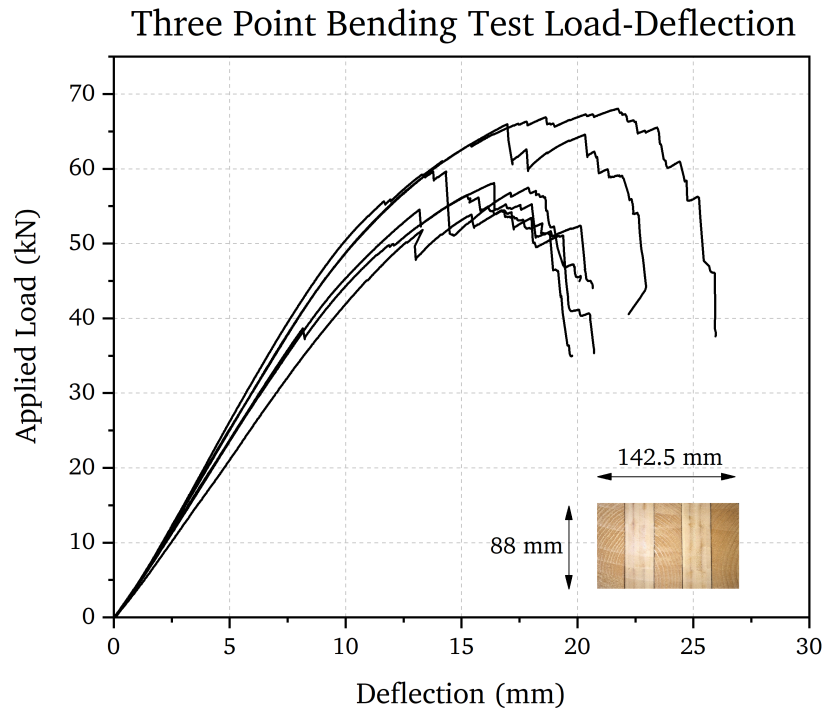


**Figure 6.9:** Three-point bending test load-deflection graph

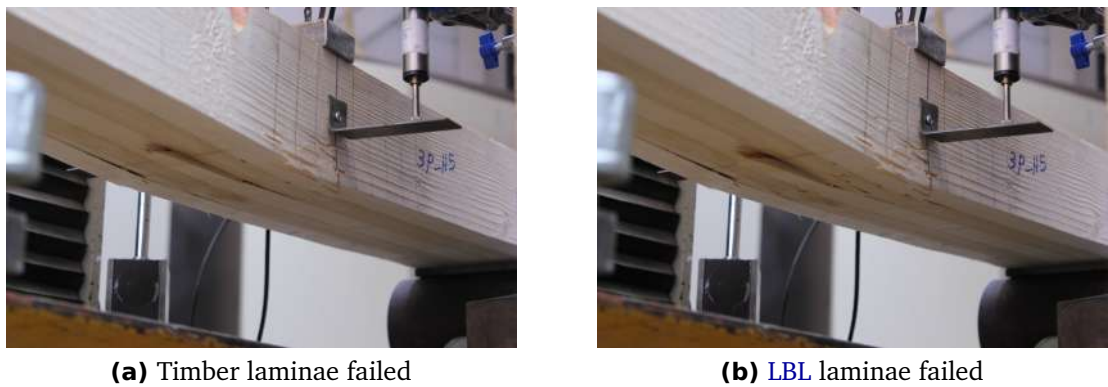


**Figure 6.10:** Three-point bending failure observations

## 6.4 Analytical Study

### 6.4.1 Prediction of the damaged length

The butt joint referred in this study is considered as a weak cross-section of the laminated bamboo lamina. The butt-jointed laminated beams are often used in the construction of glue-laminated bridges or pre-stressed laminated timber bridges (Ekholm et al., 2013; Dansoh et al., 2003). To investigate the effect of the butt-joint in the flexural properties of the VLHB, an analytical model which is developed by Jaeger and Bakht (1990) was adopted. For simplicity of the modelling, it is assumed that the cross-section is fully butt-jointed and the faces of the joints are not in contact at this section. Based on this assumption, the laminated bamboo lamina carries no moment at the butt-joint. Therefore, the effective second moment of area ( $I$ ) in this section reduces to only the second moment of area of the timber laminae. As moving away from the joint, the horizontal shear stresses which act on the vertical faces that are glued to the adjacent laminae develop flexural moment as illustrated in Figure 6.11.

The horizontal equilibrium is valid for any part of the cross-section. Thus, the horizontal shear forces at both sides of each LBL lamina equals the developed moment at the section (Equation 6.3). The horizontal equilibrium is valid for any part of the cross section. Thus,

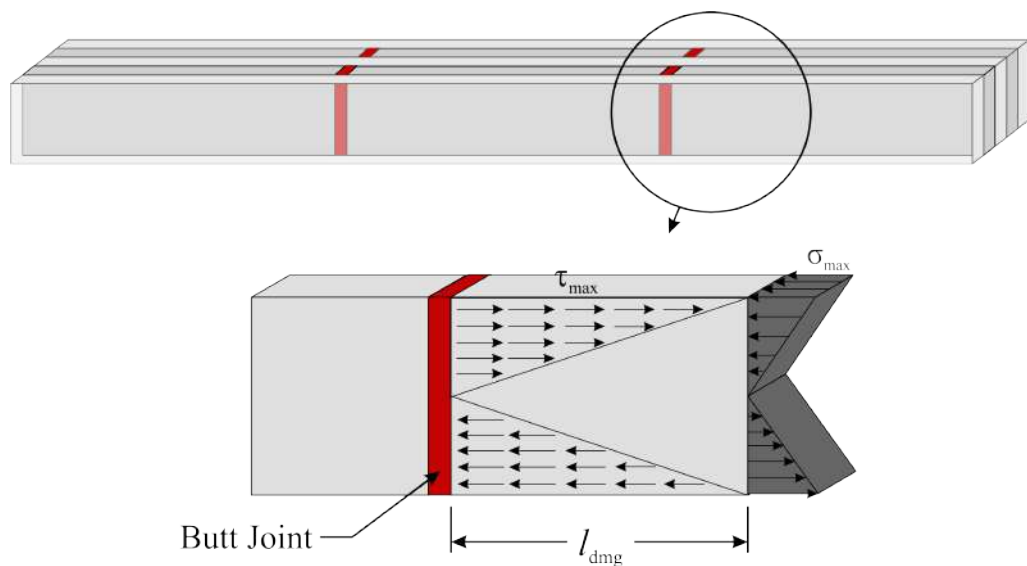


**Figure 6.11:** Developed shear and flexural stresses in the damaged length

the horizontal shear forces at the both sides of each LBL lamina equals the developed

moment at the section (Equation 6.3).

$$\sigma_{dev}bh = 2\tau_{dev}xh \quad (6.3)$$

where  $\sigma_{dev}$  and  $\tau_{dev}$  are, respectively, the developed bending and shear stresses at any section spaced  $x$  from the butt-joint,  $b$  and  $h$  are the thickness and height of the LBL lamina, respectively.

According to the Equation 6.3, the effect of the butt joint is negligible when the maximum bending moment of the beam equals the maximum shear stress (Figure 6.11). The distance which the effect of the butt-joint disappears is called here as the damaged distance and denoted by  $l_{dmg}$ . Substituting  $l_{dmg}$  with  $x$  in Equation 6.3 gives the damaged distance as the impact of the butt-joint (Equation 6.4).

$$l_{dmg} = \frac{\sigma_{max}b}{2\tau_{max}} \quad (6.4)$$

In regards to the shear stress, the bond between two adjacent laminae is the only source of the shear stress. The type of adhesive which is used in this experiment is **Phenol Resorcinol Formaldehyde (PRF)**, therefore, the maximum shear strength of PRF is taken from the literature (Sinha et al., 2014). Using the beam theory, the maximum flexural stress in the laminated beam can be determined using Equation 6.5.

$$\sigma_{max} = \frac{PaE_b\bar{y}}{E_cI_c} \quad (6.5)$$

where  $P$  and  $a$  are the maximum applied load and the distance of the loading point to the nearest support, respectively.  $E_b$  is the modulus of elasticity of the laminated bamboo,  $E_c$  and  $I_c$  are the modulus of elasticity and moment of inertia of the hybrid beam, respectively.

Based on the Equation 6.4, the laminated bamboo lumber laminae develop flexural rigidity to their maximum at the distance of  $l_{dmg}$  from the butt-joints. The effective moment of inertia of the hybrid beam considered only the timber laminae (3I) at the location of the butt-joint and increases linearly to its full value (5I) at the distance of the damaged length from the butt-joint.

Figure 6.12 illustrates the distribution of the effective moment of inertia along the hybrid beam. The calculated damaged length based on the maximum shear and flexural stress of the LBL laminae is given in Table 6.4.

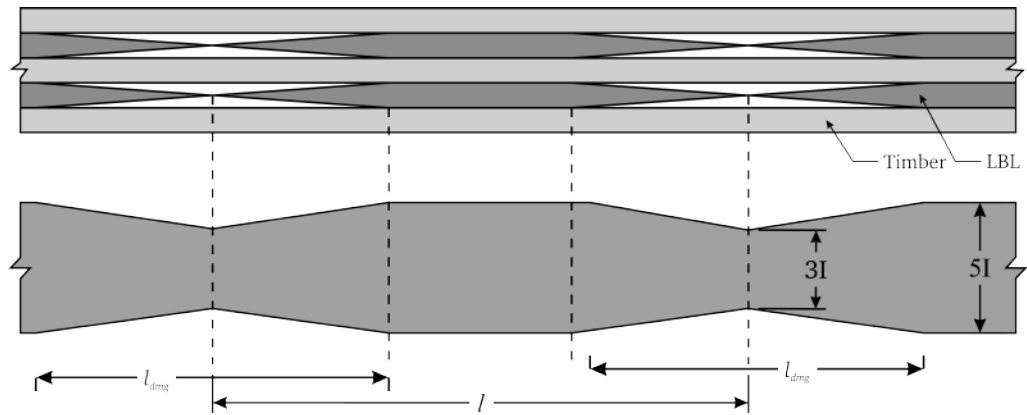


Figure 6.12: Effective moment of inertia along the hybrid beam

Table 6.4: Calculated damaged length of the hybrid beams

Beam	$\sigma_{max}$ [N/mm <sup>2</sup> ]	$\tau_{max}$ [N/mm <sup>2</sup> ]	$l_{dmg}$ [mm]
VLHB1	34.45	9.87	248
VLHB2	38.69	9.87	279
VLHB3	32.13	9.87	230

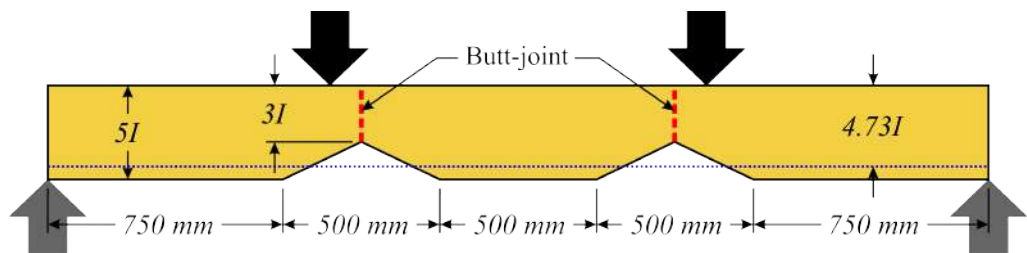


Figure 6.13: Simplified beam for deflection analysis

#### 6.4.2 Deflection at the butt joint

Figure 6.13 shows the schematic illustration of the beam for the deflection analysis. Referencing Table 6.4, it is assumed that the damaged length is  $l_{dmg} = 250\text{mm}$  and the second moment of area develops linearly from the location of the butt-joint away. However, for simplicity, the beam is assumed to have a constant moment of inertia throughout the length of the beam. According to the recommendations of Jaeger and Bakht (1990), this constant moment of inertia can be assumed as following (Equation 6.6).

$$I_e = kNI \quad (6.6)$$

$$k = \frac{1}{2N} \left\{ \lambda \cdot \ln\left(\frac{N}{N-1}\right) + \frac{0.5 - \lambda}{N} \right\}^{-1} \quad (6.7)$$

## CHAPTER 6. BUTT-JOINTED LBL IN A HYBRID BEAM

where  $k$  is the reduction factor,  $N$  is the total number of laminae,  $\lambda = \frac{l_{dmg}}{l}$  and  $l$  is the longitudinal distance between two butt-joints.

Jaeger and Bakht, 1990 studied the reduction factor ( $k$ ) in different cases and proposed a simplified equation for the reduction factor. The simplified equation states that for  $\lambda$  between 0 and 1, reduction factor can be determined as:

$$k = \frac{N - \lambda}{N} \quad (6.8)$$

The simplified beam is also prismatic and simply supported with two loading points. The deflection of the beam in the mid-span was calculated using the Euler-Bernoulli beam theory (Equation 6.9).

$$\delta_x = \frac{Pa(3Lx - 3x^2 - a^2)}{12E_c I_e} \quad a < x < \frac{L}{2} \quad (6.9)$$

where  $P$  is the total applied load,  $E_c$  is the bending modulus of the hybrid beam,  $L$  is the beam span,  $a$  is the distance between loading point to the adjacent support and  $x$  is the distance of the deflection measuring point to adjacent support.

$\lambda = 1$  was assumed to obtain more conservative predictions of the deflection of the beam. The experimental validate the findings of the calculated values with a great agreement.

Figure 6.14 compares the measured deflection with the calculated values. The result of this analysis implies that the impact of butt-joints in the hybrid beam is considerable and cannot be ignored in the calculations. This impact is more obvious in the reduced flexural rigidity and strength, despite the fact that butt-jointed lamina is rigidly constrained with adjacent laminae.

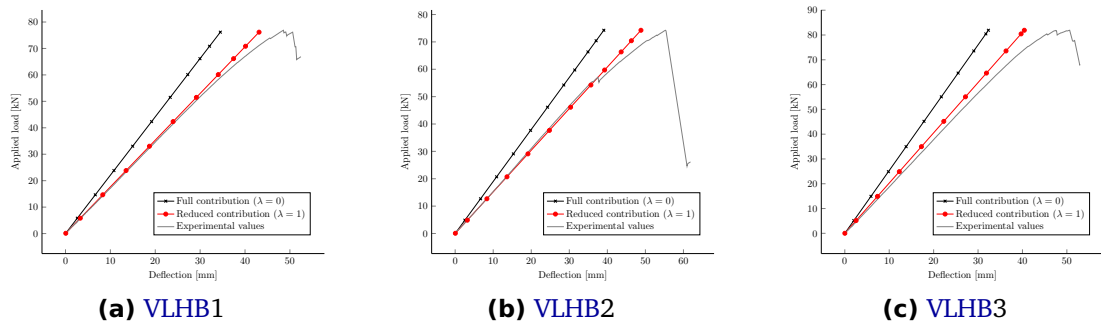


**Figure 6.14:** Experimental and calculated beam deflection

## **6.5 Summary**

This chapter investigated the impact of the butt-jointed laminated bamboo lumber on the basic mechanical properties of the **Vertically Laminated Hybrid Beam (VLHB)**. Laminated bamboo lumbers are often manufactured with concealed butt-joints to obtain longer and wider boards. This butt-joints can be problematic if not identified and examined.

Therefore, a series of experiments was conducted to evaluate this impact and aimed to determine the affected mechanical properties. Three **VLHB** which contain butt-joints and three Glulam control samples were manufactured and tested in the laboratory of Edinburgh Napier University. In addition, six specimens without butt-joints were prepared by cutting from both ends of the full-sized **VLHB** and tested in the three-point bending test.

The results of these experiments revealed that the butt-joint can potentially reduce the bending strength of the vertically laminated hybrid beam by about 60%. However, when compared to the glulam control samples, **VLHB** performed comparably with respect to the mechanical properties. The bending strength of **VLHB** with butt-joint was 16% higher than the control samples but its bending modulus was 12% lower. The load-deflection of both beams, i.e. **VLHB** with butt-joint and Glulam control samples, were similar. Therefore, introducing butt-jointed laminated bamboo to a vertically laminated hybrid beam does not improve the mechanical properties of the beam despite the great strength of the laminated bamboo without butt-joint.

The butt-joint has also weakened the section and induced the failure. The beams started to fracture at the location of the butt-joints and propagated to the adjacent timber laminae. However, in the **VLHB** without butt-joint, timber laminae were first to fracture and then the laminated bamboo.

The bending modulus of the beam has not been affected by the butt-joint as it was determined using the elastic region of the deformation. The load-deflection graph also showed that **VLHB** with butt-joint failed right after the elastic region.

An analytical model to predict the damaged length introduced by the butt-joints was developed based on the model proposed by **Jaeger and Bakht (1990)**. Based on this model, the deflection of the butt-jointed beam was calculated and validated using the experimental

## **CHAPTER 6. BUTT-JOINTED LBL IN A HYBRID BEAM**

---

values. The predicted value was in a good agreement when an appropriate correction factor was applied.

## CONCLUSIONS & RECOMMENDATIONS

Bamboo's fast growth rate and high strength to weight ratio make it an appealing alternative to the conventional building materials. However, the lack of in-depth research and low performance in the transverse direction prevented it from being widely accepted in the construction industry. On-going research on the characterisation of bamboo and engineered bamboo products has progressed substantially in the late decade. This study has focused on the development of pioneering engineered bamboo products by employing them to their full capacity in composite forms. Only a limited number of works have attempted to combine the engineered bamboo with wood to create a high-performance composite material. Thus, this study aimed to develop an I-beam laminated bamboo and timber hybrid beam by combining an optimised I-shaped laminated bamboo with timber. In addition, laminated bamboo I-beam and double I-beam were developed and evaluated.

### 7.1 Summary of the Studies

The experimental study based on prototyping the conceptual cross-sections, including the fabrication and the testing, was conducted in the laboratory of Edinburgh Napier University. The study has targeted the flexural and shear performance of the constructed beams and develop mathematical models to approximate the design quantities.

The flexural, tensile and compressive properties of the laminated bamboo and Spruce were investigated through a series of Small Clear Specimen experiments. The three-point bending tests revealed that the orientation of the bamboo strips when producing the

## CHAPTER 7. CONCLUSIONS & RECOMMENDATIONS

---

laminated bamboo lumber does not have a significant impact on the flexural properties of the laminated bamboo. Laminated bamboo's behaviour is perfectly elastic in the tension and tri-linear in the compression. Under the compressive loads, laminated bamboo initiated by elastic deformation, followed by an elastic-plastic, and finally, large plastic deformation. The slope of the stress-strain of the elastic region in both tension and compression was similar, hence, Young's Modulus was equal for both loading conditions. A constituent model based on the experimental results and the reported properties in the literature was developed to define the mechanical properties of the laminated bamboo lumber.

In summary, laminated bamboo showed high mechanical performance particularly in terms of strength. The mean tensile strength of laminated bamboo was measured at 107.33 N/mm<sup>2</sup> which is significantly higher than most of the structural timbers. It was also noticed that the equilibrium moisture content (EMC) of laminated bamboo, when kept in the recommended standard conditioning environment, was in the range of 7-9%. This EMC is below the EMC of timber (11-13%) and this influences the tensile moduli of the laminated bamboo.

Regarding the shear properties of the laminated bamboo, the suitability of the torsion test and the shear field test method were investigated. The torsion test and the shear field tests on the structural-sized specimens were conducted based on the recommendations of the governing codes of practices, i.e. BS EN 408 and ASTM D198. A thorough investigation into the torsion test revealed that BS EN 408, as a testing reference in the UK, might not fully consider the Saint-Venant's end effect decay length. The end effect decay length needs to be excluded from both ends of the specimen when measuring the beam's rotation to obtain a uniform shear stress distribution. BS EN 408 recommend measuring the beam's rotation at a distance of two to three times the cross-sectional thickness. Whereas, ASTM D198 suggest to measure the rotation at the distance of two times the cross-sectional depth. This discrepancy can introduce measurement errors, subsequently results in the error in the determined shear modulus.

Based on the results of a series of torsional tests on the laminated bamboo and timber samples, a distance of about 1.5 - 2 times the cross-sectional depth is required to be excluded due to end effect from both ends when measuring the rotation of a beam. The shear modulus of the laminated bamboo was observed to be regardless of the rotation

## CHAPTER 7. CONCLUSIONS & RECOMMENDATIONS

---

measuring sections. The mean shear modulus of the laminated bamboo was  $1168 \text{ N/mm}^2$ . The causes for the discrepancy in the shear modulus variation in the wood and laminated bamboo are unclear and yet to be investigated further.

A measurement system based on the photogrammetry and stereo vision systems was developed for the requirements of this study. The photogrammetry technique is a non-destructive, non-contact and multi-points measurements system which provides capabilities of measuring the deformation and disparity during the small- or large scale testing with high accuracy. This methodology tackled several limitations of the conventional methods such as single-point measurements and physical contact. A precise calibration process was undertaken to enhance the accuracy of the measurements.

**I-Bone Laminated Bamboo Hybrid Beam (IBHB)** was developed and tested according to the governing standards. The results of **IBHB** were compared to the laminated bamboo sandwich beam and Glulam control sample. **IBHB** showed considerably higher strength and ductility compare to the control samples. The failure of the **IBHB** was categorised as the tensile brittle failure initiated at the extreme tensile fibres of the beam. However, there is a possibility of failure in the wood or the connection between the flanges and the web. Type of the adhesive is an affecting factor in predicting the location of the failure.

Regarding mechanical properties, **IBHB** exhibited considerable flexural properties with bending strength of  $69\text{-}75 \text{ N/mm}^2$  and bending moduli of  $13\text{-}13.5 \text{ kN/mm}^2$ . These values are at the high end of the wood-composite products properties range and comparable to those of hardwood Glulam beams. Shear strength and modulus of this beam were also showed a substantial increase compare the control samples. The I-bone laminated bamboo hybrid beam comprises an innovative lay-up combination providing enhanced mechanical properties for the structural engineers and attractive appearance for the architects.

The fabrication process of **Engineered Bamboo I-Beam (BIB)** and **Engineered Bamboo Double I-Beam (BDIB)** was similar to that of **IBHB**, as well as the dimension of the flanges and the web(s). The **Melamine Formaldehyde (MF)** type resin provided a better bond when compared to **Phenol Resorcinol Formaldehyde (PRF)** resin. It was noticed that due to the nature of fibres orientations in bamboo, the laminated bamboo exhibited a tendency to split along its fibres. Therefore, accurate cuts are required in order to prevent splitting.

The **BIB** failed due to excess in the horizontal shear stress and the failure occurred at the web near the bottom flange. This signifies the importance of the side timbers in the **IBHB** which contribute to the horizontal shear resistance and cross-sectional stability. The **BDIB** showed about 70% higher ductile behaviour than **BIB** but very similar to the ductile behaviour of **IBHB**.

The **IBHB** showed 62% higher load-bearing capacity and 72% higher ultimate deflection compared to the **BIB** as the direct influence of the side timbers. Moreover, **IBHB** showed 12-15% higher load-bearing capacity and comparable maximum deflection to **BDIB**.

And finally, the impact of butt-jointed laminated bamboo lumber in the vertically laminated composite beam was evaluated through experimental work and the impacted length was determined using a model proposed by [Jaeger and Bakht \(1990\)](#).

### 7.2 Academic Impact of this Research

The followings can be listed as the major contributions of this research:

- This ground-breaking study pioneers a new research area at the structural element level by focusing on the engineering applications of timber and engineered bamboo composite in construction.
- Several composite prototype beams have been developed and evaluated. The outcome of this research provided evidences that these prototypes are structurally enhanced and in-line with promoting the sustainable construction. This study has also provided a new concept and innovative approach for the following-up researcher to adopt when developing new engineered bamboo composite for construction.
- A tailor-made, non-contact and non-destructive method to measure the surface movements of the samples in mechanical property tests was developed and implemented in this study. This multi-point/region measurements system based on the photogrammetry technique which provides capabilities of measuring the deformation and disparity during the small- or large- scale testing with high accuracy.
- During this study, there was an opportunity to review the current testing standard for timber materials, i.e. BS EN 408. The discrepancies and limitations of this testing

standard were studied and identified and as the results of our publications, the current testing standard is under review.

- A C# programme was developed to record the data from inclinometers. This programme can be used to extract multiple readings from inclinometers and record in a readable format.

### 7.3 Recommendations for Further Study

The results of this experimental study provided insights into the strong potential of the laminated bamboo lumber to be used in the construction industry. The followings are the listed further investigations that can strengthen the finding of this study:

- As the next step toward the commercialisation of the proposed conceptual designs, further investigations to fine-tune the production procedure and impact of the manufacturing process on the mechanical performance is recommended. In line with this fine-tuning, a further investigation into the moisture and thermal expansions of different species can provide additional information for the ideal compatibility.
- This study confirmed the finding of [Sinha and Clauson \(2012\)](#) regarding the incompatibility of laminated bamboo and wood when Phenol Resorcinol Formaldehyde type adhesive was used. Further investigations into the impact of the different resins on the inter-laminae shear strength of the adjacent layers are required.
- Research with an industrial partner can be beneficial to pace the investigations. Furthermore, more species of bamboo and timber with different strength grades can be manufactured and evaluated. Glulam manufacturer can fabricate longer and deeper beams, which have not been feasible during this study due to the limitations in the laboratory equipment.
- The cost of manufacturing these materials is an important factor to make them widely available in the western market. Thus, a cost analysis in regards to manufacturing and shipping these materials is recommended.
- As this study focused on the mechanical performance of the developed materials, an investigation into the sustainability at the regions where bamboo is locally available and also western countries can benefit the finding of this study.

## REFERENCES

- Abdul Khalil, H. P S, I. U H Bhat, M. Jawaid, A. Zaidon, D. Hermawan and Y. S. Hadi (2012). “Bamboo fibre reinforced biocomposites: A review”. In: *Materials and Design* 42, pp. 353–368. ISSN: 02641275. DOI: 10.1016/j.matdes.2012.06.015 (cit. on pp. 16, 21).
- Amada, Shigeyasu, Yoshinobu Ichikawa, Tamotsu Munekata, Yukito Nagase and Hiroyuki Shimizu (1997). “Fiber texture and mechanical graded structure of bamboo”. In: *Composites Part B: Engineering* 28.1-2, pp. 13–20. ISSN: 13598368. DOI: 10.1016/S1359-8368(96)00020-0 (cit. on pp. 14, 15).
- Anshari, B., Z. W. Guan, A. Kitamori, K. Jung and K. Komatsu (2012). “Structural behaviour of glued laminated timber beams pre-stressed by compressed wood”. In: *Construction and Building Materials* 29, pp. 24–32. ISSN: 09500618. DOI: 10.1016/j.conbuildmat.2011.10.002 (cit. on p. 114).
- Aschheim, Mark, Luisa María Gil-Martín and Enrique Hernández-Montes (2010). “Engineered Bamboo I-Joists”. In: *Journal of Structural Engineering* 136.12, pp. 1619–1624. ISSN: 0733-9445. DOI: 10.1061/(ASCE)ST.1943-541X.0000235 (cit. on pp. 25, 120).
- Ashaari, Zaidon, Seng Hua Lee and Muhamad Rapie Zahali (2016). “Performance of compreg laminated bamboo/wood hybrid using phenolic-resin-treated strips as core layer”. In: *European Journal of Wood and Wood Products* 74.4, pp. 621–624. ISSN: 1436736X. DOI: 10.1007/s00107-016-1027-0 (cit. on pp. 5, 23).
- ASTM (2014). *D198-09, Standard Test Methods of Static Tests of Lumber in Structural Sizes*, pp. 1–27. DOI: 10.1520/D0198-09 (cit. on pp. 57, 110).
- Banik, Ratan Lal (2015a). “Harvesting Techniques”. In: *Bamboo: The Plant and its Uses*. 1st ed. Springer International Publishing, pp. 193–226 (cit. on pp. 12, 20).

- Banik, Ratan Lal (2015b). “Morphology and Growth”. In: *Bamboo: The Plant and its Uses*. Ed. by Walter Liese and Michael Köhl. Springer International Publishing, pp. 43–89. ISBN: 978-3-319-14133-6. DOI: 10.1007/978-3-319-14133-6\_3 (cit. on p. 12).
- BANSAL, A. K. and T. R. N. PRASAD (2004). “Manufacturing laminates from sympodial bamboos —an Indian experience”. In: *Journal of Bamboo and Rattan* 3.1, pp. 13–22 (cit. on p. 43).
- Benton, Andrew (2015). “Priority Species of Bamboo”. In: *Bamboo: The Plant and its Uses*. Ed. by Walter Liese and Michael Köhl. Springer International Publishing, pp. 31–41. ISBN: 978-3-319-14133-6. DOI: 10.1007/978-3-319-14133-6\_2 (cit. on p. 11).
- Boresi, Arthur P. and Richard J. Schmidt (2003). *Advanced Mechanics of Materials*. 6th ed. New York, USA: John Wiley and sons. Chap. 6, pp. 200–262. ISBN: 978-0471438816 (cit. on pp. 59, 61).
- Borri, Antonio, Marco Corradi and Andrea Grazini (2005). “A method for flexural reinforcement of old wood beams with CFRP materials”. In: *Composites Part B: Engineering* 36.2, pp. 143–153. ISSN: 13598368. DOI: 10.1016/j.compositesb.2004.04.013 (cit. on p. 114).
- Brancheriau, L., Henri Bailleres and D. Guitard (2002). “Comparison between modulus of elasticity values calculated using 3 and 4 point bending tests on wooden samples”. In: *Wood Science and Technology* 36.5, pp. 367–383. ISSN: 00437719. DOI: 10.1007/s00226-002-0147-3 (cit. on pp. 45, 157).
- Brandner, R, E Gehri, T Bogensperger and G Schickhofer (2007). “Determination of modulus of shear and elasticity of glued laminated timber and related examinations”. In: *CIB-W18*. Bled, Slovenia, pp. 40–12–2 (cit. on p. 73).
- Brandner, Reinhard, Bernd Freytag and Gerhard Schickhofer (2008). “Determination of shear modulus by means of standardized four-point bending tests”. In: *Cib W18*. August. St. Andrews, Canada, pp. 41–21–1 (cit. on pp. 73, 74, 76, 102).
- BSI (1957). *BS 373:1957, Methods of testing small clear specimens of timber*. Tech. rep. London, UK: British Standard Institution, pp. 1–32 (cit. on pp. 30, 31, 40, 46, 47, 52, 53).
- BSI (2002). *BS EN 13183-1:2002, Moisture content of a piece of sawn timber. Determination by oven dry method*. Tech. rep. London, UK: British Standard Institution (cit. on p. 125).
- BSI (2006). *BS EN 1995-1-1: Design of timber structures. General. Common rules and rules for buildings*. Tech. rep. London, UK: British Standard Institution (cit. on p. 106).

- BSI (2010). *BS EN 384:2010, Structural timber — Determination of characteristic values of mechanical properties and density*. Tech. rep. London, UK: British Standard Institution (cit. on p. 31).
- BSI (2012). *BS EN 408:2010+A1:2012: Timber structures - Structural timber and glued laminated timber - Determination of some physical and mechanical properties*. Tech. rep. London, UK: British Standard Institution (cit. on pp. 31, 57, 62, 71, 72, 73, 74, 81, 88, 102, 104, 110, 125, 150).
- BSI (2013a). *BS EN 14080:2013, Timber structures — Glued laminated timber — Requirements*. Tech. rep. London, UK: British Standard Institution (cit. on pp. 86, 112, 116).
- BSI (2013b). *BS EN 301:2013, Adhesives , phenolic and aminoplastic , for load- bearing timber structures — Classification and performance requirements*. Tech. rep. London, UK: British Standard Institution (cit. on p. 112).
- BSI (2013c). *BS EN 302-2:2013, Adhesives for load-bearing timber structures — Test methods Part 2 : Determination of resistance to delamination*. Tech. rep. London, UK: British Standard Institution (cit. on p. 112).
- Buchanan, A H (1990). “Bending strength of lumber”. In: *Journal of Structural Engineering*, Vol.116, N.5, pp. 1213–1229. ISSN: 0733-9445. DOI: ISSN0733-9445/90/0005-1213 (cit. on pp. 56, 143).
- Cai, Zhiyong and Robert J. Ross (2010). “Mechanical Properties of Wood-Based Composite Materials”. In: *Wood Handbook - Wood as an engineering material*. Chap. 12, pp. 12–1—-12–12 (cit. on p. 116).
- Carmo, R. N.F., J. Valença, D. Silva and D. Dias-Da-Costa (2015). “Assessing steel strains on reinforced concrete members from surface cracking patterns”. In: *Construction and Building Materials* 98, pp. 265–275. ISSN: 09500618. DOI: 10.1016/j.conbuildmat.2015.08.079 (cit. on p. 32).
- Chaowana, Pannipa (2013). “Bamboo: An Alternative Raw Material for Wood and Wood-Based Composites”. In: *Journal of Materials Science Research* 2.2, pp. 90–102. ISSN: 1927-0585. DOI: 10.5539/jmsr.v2n2p90 (cit. on p. 94).
- Chen, Fuming, Jianchao Deng, Xingjun Li, Ge Wang, Lee M Smith and Sheldon Q Shi (2017). “Effect of laminated structure design on the mechanical properties of bamboo-wood hybrid laminated veneer lumber”. In: *European Journal of Wood and Wood Products* 75.3, pp. 439–448. ISSN: 1436-736X. DOI: 10.1007/s00107-016-1080-8 (cit. on p. 23).

- Chen, Guo, Hai-tao Tao Li, Tao Zhou, Cheng-long Long Li, Yu-qi Qi Song and Rui Xu (2015). “Experimental evaluation on mechanical performance of OSB webbed parallel strand bamboo I-joist with holes in the web”. In: *Construction and Building Materials* 101, pp. 91–98. ISSN: 09500618. DOI: 10.1016/j.conbuildmat.2015.10.041 (cit. on p. 120).
- Choi, I and C. O. Horgan (Sept. 1977). “Saint-Venant’s Principle and End Effects in Anisotropic Elasticity”. In: *Journal of Applied Mechanics* 44.3, pp. 424–430. ISSN: 0021-8936 (cit. on p. 61).
- Clark, L G, X Londoño and E Ruiz-Sanchez (2015). “Bamboo Taxonomy and Habitat”. In: *Bamboo: The Plant and its Uses*. Ed. by Walter Liese and Michael Köhl. 1st ed. Springer International Publishing, pp. 1–30. ISBN: 978-3-319-14133-6. DOI: 10.1007/978-3-319-14133-6\_1 (cit. on pp. 11, 12).
- Committee on Climate Change (2018). *Reducing UK emissions: 2018 Progress Report to Parliament*. Tech. rep. (cit. on p. 1).
- Dansoh, Anim Boanyo, Akio Koizumi and Takuro Hirai (2003). “Compressive and tensile properties of a butt-jointed lamination model”. In: *Journal of Wood Science* 49.5, pp. 405–410. ISSN: 14350211. DOI: 10.1007/s10086-002-0508-4 (cit. on p. 159).
- Davalos, J. F., P. Qiao, J. Wang, H. a. Salim and J. Schlussel (2002). “Shear Moduli of Structural Composites from Torsion Tests”. In: *Journal of Composite Materials* 36.10, pp. 1151–1173. ISSN: 0021-9983. DOI: 10.1177/0021998302036010486 (cit. on p. 58).
- De Lorenzis, Laura, Vincenza Scialpi and Antonio La Tegola (2004). “Analytical And Experimental Study On Bonded-In FRP Bars In Glulam Timber”. In: *Advanced Polymer Composites for Structural Applications in Construction: ACIC 2004*. Vol. 36. 4. Elsevier, pp. 308–315. ISBN: 9781845690649. DOI: 10.1016/B978-1-85573-736-5.50034-0 (cit. on p. 116).
- Dinwoodie, J. M. (1975). “Timber-a review of the structure-mechanical property relationship”. In: *Journal of Microscopy* 104.1, pp. 3–32. ISSN: 00222720. DOI: 10.1111/j.1365-2818.1975.tb04002.x (cit. on p. 32).
- Ekholm, K, R Crocetti and R Kliger (2013). “Stress-Laminated Timber Decks Subjected to Eccentric Loads in the Ultimate Limit State”. In: *Journal of Bridge Engineering* 18.5, pp. 409–416. ISSN: 1084-0702. DOI: 10.1061/(ASCE)BE.1943-5592.0000375 (cit. on p. 159).

- European Commission (2012). *Roadmap 2050 A practical guide to a prosperous low-carbon Europe. Technical analysis*. Tech. rep. Luxembourg: pp. 1–9. DOI: 10.2833/10759. arXiv: ISBN978-92-79-21798-2 (cit. on p. 1).
- Ferreira, Gisleiva C.S., Antonio L. Beraldo, Armando Lopes Moreno Jr. and Augusto Ottoni Bueno Da Silva (2016). “Flexural and shear behaviour of concrete beams reinforced with bamboo”. In: *International Journal of Sustainable Materials and Structural Systems* 2.3/4, p. 335. ISSN: 2043-8621. DOI: 10.1504/ijsmss.2016.078732 (cit. on p. 21).
- Flander, Katleen D. and Ronald Rovers (2009). “One laminated bamboo-frame house per hectare per year”. In: *Construction and Building Materials* 23.1, pp. 210–218. ISSN: 09500618. DOI: 10.1016/j.conbuildmat.2008.01.004 (cit. on p. 19).
- Frese, M. and H. J. Blaß (2006). “Characteristic bending strength of beech glulam”. In: *Materials and Structures* 40.1, pp. 3–13. ISSN: 13595997. DOI: 10.1617/s11527-006-9117-9 (cit. on p. 116).
- Gharavi, N, M Maccallum, A Maciver, A Mohamed and H Zhang (2018a). “Shear Field Size Effect on Determining the Shear Modulus of Glulam beam”. In: *Research & Development in Material Science* 5.3, pp. 1–3. DOI: 10.31031/RDMS.2018.03.000575 (cit. on p. 72).
- Gharavi, Niaz (2015). “Evaluation of Shear Constant for Timber Beam Using a Photogrammetric Approach”. Master’s dissertation. Edinburgh Napier University (cit. on p. 35).
- Gharavi, Niaz and Hexin Zhang (2018). “Study on the Impact of Size and Position of the Shear Field in Determining the Shear Modulus of Glulam Beam Using Photogrammetry Approach”. In: *International Journal of Civil, Environmental, Structural, Construction and Architectural Engineering*. Vol. 12. Rome, Italy: World Academy of Science, Engineering and Technology, pp. 161–166. ISBN: 1307-6892. DOI: 10.5281/zenodo.1315953 (cit. on p. 72).
- Gharavi, Niaz, Hexin Zhang, Yanjun Xie and Tau He (2018b). “End effect on determining shear modulus of timber beams in torsion tests”. In: *Construction and Building Materials* 164, pp. 442–450. DOI: 10.1016/j.conbuildmat.2017.12.191 (cit. on pp. 32, 35).
- Ghavami, K (1995). “Ultimate load behaviour of bamboo-reinforced lightweight concrete beams”. In: *Cement and Concrete Composites* 17.4, pp. 281–288. ISSN: 09589465. DOI: 10.1016/0958-9465(95)00018-8 (cit. on p. 21).
- Goli, Giacomo, Francesca Becherini, Maria Concetta Di Tuccio, Adriana Bernardi and Marco Fioravanti (2019). “Thermal expansion of wood at different equilibrium moisture

- contents". In: *Journal of Wood Science* 65.1. ISSN: 14350211. DOI: 10.1186/s10086-019-1781-9 (cit. on p. 90).
- Gong, Yingchun, Chaoqun Zhang, Rongjun Zhao, Xinting Xing and Haiqing Ren (2016). "Experimental study on tensile and compressive strength of bamboo scrimber". In: *BioResources* 11.3, pp. 7334–7344. ISSN: 19302126. DOI: 10.15376/biores.11.3.7334-7344 (cit. on p. 16).
- Guan, Z. W., P. D. Rodd and D. J. Pope (2005). "Study of glulam beams pre-stressed with pultruded GRP". In: *Computers and Structures*. Vol. 83. 28-30 SPEC. ISS. Pp. 2476–2487. DOI: 10.1016/j.compstruc.2005.03.021 (cit. on p. 114).
- Gupta, Rakesh, Leanne R. Heck and Thomas H. Miller (July 2002a). "Experimental Evaluation of the Torsion Test for Determining Shear Strength of Structural Lumber". In: *Journal of Testing and Evaluation* 30.4, pp. 283–290. ISSN: 00903973. DOI: 10.1520/JTE12318J (cit. on p. 58).
- Gupta, Rakesh, Leanne R. Heck and Thomas H. Miller (2002b). "Finite-Element Analysis of the Stress Distribution in a Torsion Test of Full-Size, Structural Lumber". In: *Journal of Testing and Evaluation* 30.4, pp. 291–302. ISSN: 00903973. DOI: 10.1520/JTE12319J (cit. on pp. 59, 60, 62, 71, 72).
- Gupta, Rakesh and Tobias Siller (2005a). "Shear strength of structural composite lumber using torsion tests". In: *Journal of Testing and Evaluation* 33.2, pp. 110–117. ISSN: 00903973 (cit. on p. 58).
- Gupta, Rakesh and Tobias Siller (2005b). "Stress distribution in structural composite lumber under torsion". In: *Journal of Testing and Evaluation* 55.2, pp. 51–56. ISSN: 00903973 (cit. on p. 58).
- Hansson, Lars, José Couceiro and Bengt Arne Fjellner (2017). "Estimation of shrinkage coefficients in radial and tangential directions from CT images". In: *Wood Material Science and Engineering* 12.4, pp. 251–256. ISSN: 17480280. DOI: 10.1080/17480272.2016.1249405 (cit. on p. 91).
- Harte, A M and G Baylor (2011). "Structural evaluation of castellated timber I-joists". In: *Engineering Structures* 33.12, pp. 3748–3754. ISSN: 01410296. DOI: 10.1016/j.engstruct.2011.08.011 (cit. on p. 24).
- He, Minjuan, Zheng Li, Yongliang Sun and Renle Ma (2015a). "Experimental investigations on mechanical properties and column buckling behavior of structural bamboo". In:

- Structural Design of Tall and Special Buildings* 24.7, pp. 491–503. ISSN: 15417808. DOI: 10.1002/ta1.1176 (cit. on pp. 18, 19).
- He, Tao, Jiu Yin Chen, Xiang Hu and Xian Wang (2015b). “A Study of 3d Coordinate Measuring Based on Binocular Stereo Vision”. In: *Applied Mechanics and Materials* 740, pp. 531–534. ISSN: 1662-7482. DOI: 10.4028/www.scientific.net/AMM.740.531 (cit. on p. 33).
- Horgan, C. O. and J. G. Simmonds (1994). “Saint-Venant end effects in composite structures”. In: *Composites Engineering* 4.3, pp. 279–286. ISSN: 09619526. DOI: 10.1016/0961-9526(94)90078-7 (cit. on pp. 61, 62, 71, 72).
- Huang, Puxi, Wen-Shao Chang, Martin P. Ansell, Chris Rhys Bowen, John Y. M. Chew and Vana Adamaki (2017). “Thermal and hygroscopic expansion characteristics of bamboo”. In: *Proceedings of the Institution of Civil Engineers - Structures and Buildings* 171.6, pp. 463–471. ISSN: 0965-0911. DOI: 10.1680/jstbu.16.00046 (cit. on p. 90).
- Ikponmwosa, Efe, Christopher Fapohunda, Olamiposi Kolajo and Otu Eyo (2015). “Structural behaviour of bamboo-reinforced foamed concrete slab containing polyvinyl wastes (PW) as partial replacement of fine aggregate”. In: *Journal of King Saud University - Engineering Sciences*. ISSN: 10183639. DOI: 10.1016/j.jksues.2015.06.005 (cit. on p. 21).
- Jaeger, Leslie G. and Baidar Bakht (1990). “Effect of butt joints on the flexural stiffness of laminated timber bridges”. In: *Canadian Journal of Civil Engineering* 17.5, pp. 859–864. DOI: 10.1139/190-096 (cit. on pp. 149, 159, 161, 162, 163, 168).
- Jahromi, A. B., B. Zhang, A. Harte, B. Walford, K. Bayne and J. Turner (2006). “Investigating the structural performance of multi-webs I-Beams”. In: *Journal of the Institute of Wood Science* 17.3, pp. 148–158. ISSN: 00203203. DOI: 10.1179/wsc.2006.17.3.148 (cit. on p. 24).
- Kaboli, Hamid and Peggi L Clouston (2019). “Eastern Hemlock in Bamboo-Reinforced Glulam”. In: *Journal of Materials in Civil Engineering* 31.1, pp. 1–10. DOI: 10.1061/(ASCE)MT.1943-5533.0002550. (cit. on pp. 5, 21, 22, 23, 27, 131).
- Kaminski, Sebastian, Andrew Lawrence and David Trujillo (2016). “Structural use of bamboo Part 1: Introduction to bamboo”. In: *TheStructuralEngineer* 94.8, pp. 40–43 (cit. on p. 15).
- Kretschmann, D.E., R.C. Moody, R.F. Pellerin, B.A. Bendtsen, J.M. Cahill, R.H. McAlister and D.W. Sharp (1993). “Effect of various proportions of juvenile wood on laminated

- vener lumber”. In: *Washington: US Department of Agriculture, Forest Service, Forest Products Laboratory* 521, p. 31 (cit. on p. 116).
- Lakkad, S. C. and J. M. Patel (1981). “Mechanical properties of bamboo, a natural composite”. In: *Fibre Science and Technology* 14.4, pp. 319–322. ISSN: 00150568. DOI: 10.1016/0015-0568(81)90023-3 (cit. on p. 15).
- Lee, a W C, X Bai and a P Bangi (1997). “Flexural properties of bamboo-reinforced southern pine OSB beams”. In: *Forest Products Journal* 47.6, pp. 74–78. ISSN: 0015-7473 (cit. on pp. 5, 22).
- Lee, Andy W. C., Xuesong Bai and Audimar P Bangi (1998). “Selected Properties of Laboratory-Made Laminated-Bamboo Lumber”. In: *Holzforschung* 52.2, pp. 207–210. ISSN: 0018-3830. DOI: 10.1515/hfsg.1998.52.2.207 (cit. on pp. 16, 43).
- Leichti, Robert J., Robert H. Falk and Theodore L. Laufenberg (1990a). “PREFABRICATED WOOD COMPOSITE I-BEAMS: A LITERATURE REVIEW”. In: *Wood and Fiber Science* 22.1, pp. 62–79. ISSN: 19457111 (cit. on p. 87).
- Leichti, Robert J., Robert H. Falk and Theodore L. Laufenberg (1990b). “Prefabricated Wood Composite I-Beams: A Literature Review”. In: *Wood and Fiber Science* 22.1, pp. 62–79 (cit. on pp. 20, 24).
- Li, Hai Tao, Andrew John Deeks, Qi Sheng Zhang and Gang Wu (2016). “Flexural performance of laminated bamboo lumber beams”. In: *BioResources* 11.1, pp. 929–943. ISSN: 19302126. DOI: 10.15376/biores.11.1.929-943 (cit. on pp. 18, 21, 56).
- Li, Hai Tao, Jing Wen Su, Qi Sheng Zhang, Andrew John Deeks and David Hui (2015). “Mechanical performance of laminated bamboo column under axial compression”. In: *Composites Part B: Engineering* 79, pp. 374–382. ISSN: 13598368. DOI: 10.1016/j.compositesb.2015.04.027 (cit. on p. 55).
- Li, Hai Tao, Qi Sheng Zhang, Dong Sheng Huang and Andrew John Deeks (2013). “Compressive performance of laminated bamboo.” In: *Composites Part B: Engineering* 54.1, pp. 319–328. ISSN: 13598368. DOI: 10.1016/j.compositesb.2013.05.035 (cit. on p. 19).
- Li, Haitao, Gang Wu, Qisheng Zhang, Andrew John Deeks and Jingwen Su (2018). “Ultimate bending capacity evaluation of laminated bamboo lumber beams”. In: *Construction and Building Materials* 160, pp. 365–375. ISSN: 09500618. DOI: 10.1016/j.conbuildmat.2017.11.058 (cit. on pp. 16, 17, 44, 55, 116).

- Liese, Walter (1985). *Bamboos - Biology, silvics, properties, utilization*. Eschborn : Deutsche Gesellschaft für Technische Zusammenarbeit, pp. 196–393. ISBN: 3880852731 (cit. on pp. 4, 12).
- Liese, Walter (1987). “Research on bamboo”. In: *Wood Science and Technology* 21.3, pp. 189–209. ISSN: 00437719. DOI: 10.1007/BF00351391 (cit. on pp. 4, 11, 14).
- Liese, Walter and Michael Köhl (2015). *Bamboo: The Plant and Its Uses*. Ed. by Walter Liese and Michael Köhl. 1st ed. Springer International Publishing, p. 356. ISBN: 9783319141329. DOI: 10.1007/978-3-319-14133-6 (cit. on pp. 11, 13, 14, 90).
- Liu, Huanrong, Zehui Jiang, Zhengjun Sun, Yan Yan, Zhiyong Cai and Xiubiao Zhang (2016). “Impact performance of two bamboo-based laminated composites”. In: *European Journal of Wood and Wood Products*. ISSN: 1436-736X. DOI: 10.1007/s00107-016-1118-y (cit. on p. 23).
- Long, Ji-bo, Nian Ping Li, Qian Wang, De-jun Zeng and Lin Su (2010). “Analysis on thermal and moisture stress in bamboo reinforced concrete”. Chinese. In: *Journal of Hunan University: Natural Sciences* 37.12, pp. 1–6 (cit. on p. 90).
- Lugt, P. van der, A. A J F van den Dobbelen and J J A Janssen (2006). “An environmental, economic and practical assessment of bamboo as a building material for supporting structures”. In: *Construction and Building Materials* 20.9, pp. 648–656. ISSN: 09500618. DOI: 10.1016/j.conbuildmat.2005.02.023 (cit. on p. 20).
- Lugt, Pablo Van Der (2008). *Design interventions for stimulating bamboo commercialization*, p. 421. ISBN: 9789051550474 (cit. on p. 19).
- Maas, Hans-Gerd and Uwe Hampel (2006). “Photogrammetric Techniques in Civil Engineering Material Testing and Structure Monitoring”. In: *Photogrammetric Engineering & Remote Sensing* 72.1, pp. 39–45. ISSN: 00991112. DOI: 10.14358/pers.72.1.39 (cit. on p. 32).
- Mahdavi, M., P.L. Clouston and S.R. Arwade (2012). “A Low-Technology Approach toward Fabrication of Laminated Bamboo Lumber”. In: *Construction and Building Materials* 29, pp. 257–262. ISSN: 09500618. DOI: 10.1016/j.conbuildmat.2011.10.046 (cit. on p. 17).
- Malhotra, S K and I M M Bazan (1980). “Ultimate bending strength theory for timber beams.” English. In: *Wood Science* 13.1, pp. 50–63 (cit. on p. 143).

- Marx, Catherine M and Russell C Moody (1981). *Bending Strength of Shallow Glued-Laminated Beams of a Uniform Grade*. Tech. rep. FOREST PRODUCTS LAB MADISON WI (cit. on p. 116).
- Moore, J (2011). *Wood properties and uses of Sitka spruce in Britain*. English. Edinburgh (cit. on p. 19).
- MVTec Software GmbH (2012). *HALCON*. Munich, Germany (cit. on pp. 38, 66, 75).
- Nugroho, Naresworo and Naoto Ando (2000). “Development of structural composite products made from bamboo I: fundamental properties of bamboo zephyr board”. English. In: *Journal of Wood Science* 46.April 1999, pp. 68–74. ISSN: 1435-0211. DOI: 10.1007/BF00779556 (cit. on p. 16).
- Nugroho, Naresworo and Naoto Ando (2001). “Development of structural composite products made from bamboo II: Fundamental properties of laminated bamboo lumber”. In: *Journal of Wood Science* 47.3, pp. 237–242. ISSN: 14350211. DOI: 10.1007/BF01171228 (cit. on p. 16).
- Paniagua, Viviana and Róger Moya (2014). “Flexural Performance of I-Joist Fabricated with Glue-Laminated Bamboo and Gmelina arborea Plywood”. In: *Open Journal of Civil Engineering* 04.03, pp. 209–216. ISSN: 2164-3164. DOI: 10.4236/ojce.2014.43018 (cit. on p. 25).
- Paudel, S. K. (2008). “Engineered bamboo as a building material”. In: *First International Conference on Modern Bamboo Structures*, pp. 33–47. ISBN: 9780415475976 (cit. on pp. 16, 20).
- Penellum, Matthew, Bhavna Sharma, Darshil U. Shah, Robert M. Foster and Michael H. Ramage (Mar. 2018). “Relationship of structure and stiffness in laminated bamboo composites”. In: *Construction and Building Materials* 165, pp. 241–246. ISSN: 09500618. DOI: 10.1016/j.conbuildmat.2017.12.166 (cit. on pp. 18, 43).
- Plevris, Nikolaos and Thanasis C Triantafyllou (1992). “FRP-Reinforced Wood as Structural Material”. In: *Journal of Materials in Civil Engineering* 4.3, pp. 300–317. DOI: 10.1061/(ASCE)0899-1561(1992)4:3(300) (cit. on p. 98).
- Popescu, C.-M M. (2017). “Wood as bio-based building material”. In: *Performance of Bio-based Building Materials*, pp. 21–96. ISBN: 9780081009925. DOI: 10.1016/B978-0-08-100982-6.00002-1 (cit. on p. 2).
- Porteous, Jack and Abdy Kermani (2013). *Structural Timber Design to Eurocode 5*. 2nd ed. Blackwell Publishing. ISBN: 978-0-470-67500-7 (cit. on p. 110).

- Ramage, Michael H. et al. (Feb. 2017). *The wood from the trees: The use of timber in construction*. DOI: 10.1016/j.rser.2016.09.107 (cit. on p. 19).
- Rassiah, Kannan, M. M H Megat Ahmad and Aidy Ali (2014). “Mechanical properties of laminated bamboo strips from Gigantochloa Scortechinii/polyester composites”. In: *Materials and Design* 57, pp. 551–559. ISSN: 18734197. DOI: 10.1016/j.matdes.2013.12.070 (cit. on p. 19).
- Rittironk, S. and M. Elnieri (2008). “Investigating laminated bamboo lumber as an alternate to wood lumber in residential construction in the United States”. In: *First International Conference on Modern Bamboo Structures*, pp. 83–96. ISBN: 9780415475976 (cit. on pp. 17, 18, 28).
- Sharma, Bhavna, Helene Bauer, Gerhard Schickhofer and Michael H Ramage (2016). “Mechanical characterisation of structural laminated bamboo”. In: *Proceedings of the Institution of Civil Engineers - Structures and Buildings* 170.4, pp. 250–264. ISSN: 0965-0911. DOI: 10.1680/jstbu.16.00061 (cit. on pp. 20, 43, 44).
- Sharma, Bhavna, Ana Gatóo, Maximilian Bock and Michael Ramage (2015a). “Engineered bamboo for structural applications”. In: *Construction and Building Materials* 81, pp. 66–73. ISSN: 09500618. DOI: 10.1016/j.conbuildmat.2015.01.077 (cit. on pp. 16, 17, 18, 20, 31, 44, 119).
- Sharma, Bhavna, Ana Gatoo, Maximillian; Bock, Helen Mulligan and Michael Ramage (Apr. 2014). “Engineered bamboo: state of the art”. In: *Proceedings of the Institution of Civil Engineers - Construction Materials* 168.2, pp. 57–67. ISSN: 17476518. DOI: 10.1680/coma.14.00020 (cit. on pp. 16, 22).
- Sharma, Bhavna, Ana Gatóo and Michael H. Ramage (2015b). “Effect of processing methods on the mechanical properties of engineered bamboo”. In: *Construction and Building Materials* 83, pp. 95–101. ISSN: 09500618. DOI: 10.1016/j.conbuildmat.2015.02.048 (cit. on p. 18).
- Sinha, Arijit and Milo Clauson (2012). “Properties of Bamboo–Wood Hybrid Glulam Beams”. In: *Forest Products Journal* 62.7-8, pp. 541–544. ISSN: 0015-7473. DOI: 10.13073/FPJ-D-13-00007.1 (cit. on pp. 5, 21, 22, 23, 27, 82, 94, 169).
- Sinha, Arijit, Daniel Way and Skyler Mlasko (2014). “Structural Performance of Glued Laminated Bamboo Beams”. In: *Journal of Structural Engineering* 140.1, p. 04013021. ISSN: 0733-9445. DOI: 10.1061/(ASCE)ST.1943-541X.0000807 (cit. on pp. 21, 116, 160).

- Soltis, Lawrence A and Douglas R Rammer (1994). “Shear strength of unchecked glued-laminated beams”. In: *Forest Product Journal* 44.1, pp. 51–57 (cit. on p. 58).
- Takeuchi, Caori Patricia, Martin Estrada and Dorian Luis Linero (2016). “The Elastic Modulus and Poisson’s Ratio of Laminated Bamboo *Guadua angustifolia*”. In: *Key Engineering Materials* 668, pp. 126–133. ISSN: 1662-9795. DOI: 10.4028/www.scientific.net/KEM.668.126 (cit. on p. 55).
- Tang, Z., B. Shan, W. G. Li, Q. Peng and Y. Xiao (2019). “Structural behavior of glulam I-joists”. In: *Construction and Building Materials* 224, pp. 292–305. ISSN: 09500618. DOI: 10.1016/j.conbuildmat.2019.07.082 (cit. on p. 25).
- Trujillo, D and L.F. López (2016). “13 – Bamboo material characterisation”. In: *Nonconventional and Vernacular Construction Materials*, pp. 365–392. ISBN: 9780081008713. DOI: 10.1016/B978-0-08-100038-0.00013-5 (cit. on p. 20).
- Trujillo, David Jorge Alexander, Michael Ramage and Wen-Shao Chang (2013). “Lightly modified bamboo for structural applications”. In: *Proceedings of the Institution of Civil Engineers - Construction Materials* 166.4, pp. 238–247. ISSN: 1747-650X. DOI: 10.1680/coma.12.00038 (cit. on p. 11).
- Trujillo, David, Suneina Jangra MEng MRes and Joel Matthew Gibson MEng (2017). “Flexural properties as a basis for bamboo strength grading”. In: *Proceedings of the Institution of Civil Engineers - Structures and Buildings* 170.SB4, pp. 284–294. ISSN: 17517702. DOI: 10.1680/jstbu.16.00084 (cit. on p. 20).
- UN Environment and International Energy Agency (2017). *Towards a zero-emission, efficient, and resilient buildings and construction sector. Global Status Report 2017*. Tech. rep. United Nations Environment Programme (cit. on p. 1).
- Vahedian, Abbas, Rijun Shrestha and Keith Crews (2019). “Experimental and analytical investigation on CFRP strengthened glulam laminated timber beams: Full-scale experiments”. In: *Composites Part B: Engineering* 164, pp. 377–389. ISSN: 13598368. DOI: 10.1016/j.compositesb.2018.12.007 (cit. on p. 114).
- Valença, J., E. N.B.S. Júlio and H. J. Araújo (2012). “Applications of photogrammetry to structural assessment”. In: *Experimental Techniques* 36.5, pp. 71–81. ISSN: 07328818. DOI: 10.1111/j.1747-1567.2011.00731.x (cit. on p. 32).
- Valença, J., I. Puente, E. Júlio, H. González-Jorge and P. Arias-Sánchez (2017). “Assessment of cracks on concrete bridges using image processing supported by laser scanning

- survey”. In: *Construction and Building Materials* 146, pp. 668–678. ISSN: 09500618. DOI: 10.1016/j.conbuildmat.2017.04.096 (cit. on p. 32).
- Valença, Jónatas and Ricardo N.F. Carmo (2019). “Evaluation of the shear transfer mechanisms in reinforced concrete beams using photogrammetry”. In: *Structural Concrete* January, pp. 1–16. ISSN: 17517648. DOI: 10.1002/suco.201800279 (cit. on p. 32).
- Wang, Hankun, Wanju Li, Dan Ren, Zixuan Yu and Yan Yu (2014). “A two-variable model for predicting the effects of moisture content and density on compressive strength parallel to the grain for moso bamboo”. In: *Journal of Wood Science* 60.5, pp. 362–366. ISSN: 14350211. DOI: 10.1007/s10086-014-1419-x (cit. on p. 32).
- Wang, R., Y. Xiao and Z. Li (2017). “Lateral Loading Performance of Lightweight Glulam Shear Walls”. In: *Journal of Structural Engineering (United States)* 143.6, pp. 1–11. ISSN: 07339445. DOI: 10.1061/(ASCE)ST.1943-541X.0001751 (cit. on pp. 5, 11, 16).
- Weatherwax, Richard C. and Alfred J. Stamm (1956). “The Coefficients Thermal Expansion of Wood and Wood Products”. In: 1487, p. 24 (cit. on p. 90).
- Wohler, Christian (2013). *3D computer vision: efficient methods and applications*. 2nd ed. London, UK: Springer, p. 390. ISBN: 9781447141495. DOI: <http://dx.doi.org/10.1007/978-1-4471-4150-1> (cit. on pp. 34, 35).
- Wu, Wenqing (2014). “Experimental Analysis of Bending Resistance of Bamboo Composite I-Shaped Beam”. In: *Journal of Bridge Engineering* 19.4, p. 04013014. ISSN: 1084-0702. DOI: 10.1061/(ASCE)BE.1943-5592.0000557 (cit. on pp. 25, 120).
- Xiao, Y (2016). “Engineered Bamboo”. In: *Nonconventional and Vernacular Construction Materials*. Chap. 15, pp. 433–452. ISBN: 9780081008713. DOI: 10.1016/B978-0-08-100038-0.00015-9 (cit. on p. 119).
- Xiao, Y., G. Chen and L. Feng (2013). “Experimental studies on roof trusses made of glulam”. In: *Materials and Structures* 47.11, pp. 1879–1890. ISSN: 1359-5997. DOI: 10.1617/s11527-013-0157-7 (cit. on p. 21).
- Xiao, Y., L. Li and R. Z. Yang (2014a). “Long-Term Loading Behavior of a Full-Scale Glulam Bridge Model”. In: *Journal of Bridge Engineering* 19.9, p. 04014027. ISSN: 1084-0702. DOI: 10.1061/(ASCE)BE.1943-5592.0000600 (cit. on p. 21).
- Xiao, Y., B. Shan, R. Z. Yang, Z. Li and J. Chen (2014b). “Glue Laminated Bamboo (GluBam) for Structural Applications”. In: *RILEM Bookseries* 9, pp. 589–601. ISSN: 22110844. DOI: 10.1007/978-94-007-7811-5\_54 (cit. on p. 21).

- Xiao, Yan, Bo Shan, Guo Chen, Quan Zhou and Li-yong She (2008). “Development of a new type of Glulam-GluBam”. In: *LI Proceedings of the International Conference on Modern Bamboo Structures*. London: CRC Press. Taylor & Francis, pp. 41–47. ISBN: 978-0-415-47597-6. DOI: doi:10.1201/9780203888926.ch510.1201/9780203888926.ch5 (cit. on p. 21).
- Xu, Qingfeng, Kent Harries, Xiangmin Li, Qiong Liu and Jennifer Gottron (2014). “Mechanical properties of structural bamboo following immersion in water”. In: *Engineering Structures* 81, pp. 230–239. ISSN: 01410296. DOI: 10.1016/j.engstruct.2014.09.044 (cit. on p. 32).
- Xu, Qingfeng, Yubing Leng, Xi Chen, Kent A. Harries, Lingzhu Chen and Zhuolin Wang (2018). “Experimental study on flexural performance of glued-laminated-timber-bamboo beams”. In: *Materials and Structures/Materiaux et Constructions* 51.1, p. 9. ISSN: 13595997. DOI: 10.1617/s11527-017-1135-2 (cit. on pp. 21, 22).
- Yang, Zhe, Hongdan Peng, Weizhi Wang and Tianxi Liu (2010). “Bamboo Fiber Reinforced Polypropylene Composites and Their Mechanical, Thermal, and Morphological Properties”. In: *Journal of Applied Polymer Science* 116.5, pp. 2658–2667. ISSN: 00218995. DOI: 10.1002/app (cit. on p. 21).
- Yiping, Lou, Li Yanxia, Kathleen Buckingham, G Henley and Zhou Guomo (Jan. 2010). *Bamboo and Climate Change Mitigation*. Tech. rep. INBAR, Beijing (cit. on p. 4).
- Yu, H. Q., Z. H. Jiang, C. Y. Hse and T. F. Shupe (2008). “Selected physical and mechanical properties of moso bamboo (*Phyllostachys pubescens*)”. In: *Journal of Tropical Forest Science* 20.4, pp. 258–263. ISSN: 01281283 (cit. on p. 91).
- Yu, Yanglun, Rongxian Zhu, Binglin Wu, Yu’an Hu and Wenji Yu (Nov. 2015). “Fabrication, material properties, and application of bamboo scrimber”. In: *Wood Science and Technology* 49.1, pp. 83–98. ISSN: 00437719. DOI: 10.1007/s00226-014-0683-7 (cit. on p. 16).
- Zhang, Ling Fei et al. (2014). “Experimental Study on Glued Bamboo Beam”. In: *Advanced Materials Research* 919, pp. 123–127. ISSN: 1662-8985. DOI: 10.4028/www.scientific.net/AMR.919-921.123 (cit. on p. 21).
- Zhong, Yong, Guofang Wu, Haiqing Ren and Zehui Jiang (2017). “Bending properties evaluation of newly designed reinforced bamboo scrimber composite beams”. In: *Construction and Building Materials* 143, pp. 61–70. ISSN: 09500618. DOI: 10.1016/j.conbuildmat.2017.03.052 (cit. on p. 16).

APPENDIX **A**

**SMALL CLEAR SPECIMEN TESTING  
DATASET**

**Table A.1:** Static bending test results for laminated bamboo specimen oriented in the B direction

Specimen	Density Before [kg/m <sup>3</sup> ]	Density Dry [kg/m <sup>3</sup> ]	MC [%]	B [mm]	H [mm]	L [mm]	$F_{ut}$ [N]	$f_{ut}$ [MPa]	$F_{prop}$ [N]	$\Delta_{prop}$ [mm]	E [GPa]
B1	625.86	594.57	8.39	20.07	20.08	280	2112.01	109.67	980.90	3.98	8.328
B2	641.27	612.11	6.72	20.03	20.04	280	1815.53	94.78	1201.00	4.98	8.215
B3	645.03	607.33	8.07	20.07	20.06	280	1616.94	84.07	1052.00	4.82	7.395
B4	775.57	736.41	7.98	20.12	20.02	280	2041.62	106.39	1470.00	6.08	8.231
B5	779.05	741.78	7.98	20.28	20.33	280	2038.49	102.09	1504.00	5.41	8.947
B6	588.78	564.79	7.81	20.25	20.26	280	1604.65	81.12	1300.00	5.68	7.466
B7	651.35	622.32	8.43	20.15	19.50	280	2165.88	118.68	1501.00	5.67	9.720
B8	603.12	580.81	6.68	20.02	20.16	280	1662.34	85.82	1103.00	4.44	8.318
B9	734.74	701.45	8.48	20.07	20.32	280	1956.39	99.10	1503.00	5.31	9.218
B10	677.72	647.56	8.61	19.81	19.85	280	2212.38	118.98	1103.00	4.53	8.609
B11	662.98	628.57	9.10	20.16	18.82	280	1987.66	116.95	1203.00	5.53	8.885
B12	650.28	627.57	6.95	20.23	20.04	280	2301.23	118.95	1407.00	5.12	9.267
B13	685.31	651.23	8.28	20.03	20.07	280	1926.2	100.27	1104.00	4.59	8.155
B14	676.34	649.54	7.42	23.47	20.29	280	2304.39	100.17	1001.00	3.12	8.991
B15	663.26	630.01	6.72	20.19	19.98	280	2271.23	118.37	1312.00	4.82	9.270
B16	621.93	591.81	6.83	20.11	20.13	280	1422.24	73.32	1203.00	5.21	7.723
B17	662.78	625.42	8.03	20.11	20.11	280	2207.39	113.96	1253.00	4.70	8.938
B18	644.65	612.56	8.00	20.01	20.11	280	2157.77	112.01	1104.00	3.60	10.336
B19	658.25	629.99	8.01	20.06	20.09	280	2242.63	116.36	1105.00	4.28	8.710
B20	606.57	582.47	7.94	20.12	20.25	280	1573.18	80.12	1000.00	4.27	7.699

**Table A.2:** Static bending test results for laminated bamboo specimen oriented in the L direction

Specimen	Density Before [kg/m <sup>3</sup> ]	Density Dry [kg/m <sup>3</sup> ]	MC [%]	B [mm]	H [mm]	L [mm]	$F_{ut}$ [N]	$f_{ut}$ [MPa]	$F_{prop}$ [N]	$\Delta_{prop}$ [mm]	E [GPa]
L1	685.60	652.85	7.65	20.23	20.24	280	2412.93	122.27	1503	4.80	10.24
L2	652.02	623.35	7.90	20.19	20.34	280	2095.01	105.38	1403	5.08	8.93
L3	773.34	766.75	8.34	20.18	20.15	280	2068.19	106.03	1296	4.01	10.74
L4	601.69	570.23	8.05	20.11	20.25	280	1669.65	85.00	1005	4.31	7.65
L5	607.07	575.38	7.71	20.30	20.32	280	1734.11	86.92	1099	4.59	7.72
L6	538.78	510.14	8.53	20.05	20.57	280	1516.87	75.08	1001	4.58	6.87
L7	593.61	568.38	7.12	20.15	20.29	280	1743.14	88.30	1204	4.64	8.47
L8	624.72	594.72	7.06	20.15	20.23	280	1870.60	95.24	1203	4.27	9.27
L9	740.73	712.57	8.56	20.33	20.17	280	2388.84	121.29	1500	4.62	10.68
L10	605.61	581.36	6.98	20.29	20.32	280	1833.93	91.92	1102	3.89	9.13
L11	566.94	542.74	7.67	20.22	20.32	280	1444.63	72.66	1003	4.46	7.28
L12	680.95	650.62	7.49	20.08	20.20	280	2255.28	115.63	1301	4.22	10.23
L13	602.92	579.38	6.74	20.20	20.17	280	1750.15	89.46	1002	3.86	8.59
L14	770.43	735.24	8.10	20.24	20.14	280	2039.79	104.34	1210	3.90	10.28
L15	685.64	650.21	8.44	20.16	20.03	280	1899.88	98.62	1104	3.95	9.46
L16	627.62	596.33	8.06	20.18	20.18	280	1721.65	88.00	1002	3.91	8.49
L17	666.61	637.03	7.72	20.17	20.29	280	2254.33	114.01	1206	3.98	9.88
L18	754.62	721.65	8.69	20.46	20.34	280	2182.25	108.24	1203	3.74	10.24
L19	634.29	604.00	7.85	20.28	20.25	280	1933.63	97.67	1305	4.74	8.98
L20	808.60	773.53	8.06	20.43	19.99	280	2121.24	109.18	1501	4.70	10.75

**Table A.3:** Static bending test results for C16 timber samples

	Density Before [kg/m <sup>3</sup> ]	Density Dry [kg/m <sup>3</sup> ]	MC [%]	B [mm]	H [mm]	L [mm]	$F_{ut}$ [N]	$f_{ut}$ [MPa]	$F_{prop}$ [N]	$\Delta_{prop}$ [mm]	E [GPa]
S1	333.84	312.34	12.54	20.46	20.32	280	875.05	43.51	552.4	3.21199	5.500
S2	368.49	346.68	12.37	20.53	20.45	280	967.67	47.33	678.3	3.15221	6.724
S3	380.47	358.34	12.29	20.39	20.49	280	1025.02	50.28	733.3	3.23429	7.093
S4	335.82	315.79	12.54	20.40	20.43	280	843.31	41.60	653	2.78436	7.399
S5	407.64	386.72	12.70	20.48	20.42	280	1074.35	52.83	579.6	1.89595	9.618
S6	380.94	359.10	12.48	20.55	20.55	280	990.51	47.93	522.2	1.84451	8.709
S7	337.93	320.72	12.08	20.44	20.51	280	765.04	37.35	536.2	2.49295	6.689
S8	404.28	380.57	12.17	20.30	20.43	280	1033.9	51.28	680.5	2.49684	8.646
S9	385.81	363.56	12.61	20.34	20.43	280	1000.88	49.52	661.4	2.50262	8.365
Mean	370.58	349.31	12.42				952.86	46.85			7.64
STD	28.67	27.55	0.21				102.35	5.06			1.29
CoV [%]	7.74	7.89	1.68				10.74	10.80			16.87

**Table A.4:** Tensile test results for C16 timber samples.

Specimen	MC	Area	$F_{ut,T}$	$f_{ut,T}$	$E_T$	Knot	Failure in knot?	Failure location	Failure
	[%]	[mm <sup>2</sup> ]	[N]	[MPa]	[GPa]				
TS1	13.44	159.87	8877.16	55.53	7.39	M-T	No	Bottom	Crushing at the bottom grip
TS2	13.69	154.69	5344.38	34.55	8.04	N/A	N/A	Top	Failure at the top grip
TS3	13.32	156.33	3582.53	22.92	7.53	N/A	N/A	Top	Failure at the top grip
TS4	13.68	155.24	6787.74	43.72	9.01	B	Y	Bottom	Failure at bottom knot at grip
TS5	13.09	162.27	5149.78	31.74	6.51	N/A	N/A	Top	Failure at the top grip
TS6	13.36	158.87	4798.38	30.20	9.28	N/A	N/A	Top	Failure at the top grip
TS7	13.51	152.58	5647.43	37.01	8.82	N/A	N/A	Top	Failure at the top grip
TS8	13.48	153.22	8558.96	55.86	9.44	N/A	N/A	Top	Failure at the top grip
TS9	13.46	152.29	6197.88	40.70	8.54	N/A	N/A	Top	Failure at the top grip
TS10	13.43	158.88	6932.13	43.63	7.00	N/A	N/A	Bottom	Failure at the bottom grip
Mean	13.45		6187.64	39.59	8.16				
STD	0.17		1652.20	10.61	1.02				
COV	1.30		26.70	26.80	12.45				

**APPENDIX A. SMALL CLEAR SPECIMEN TESTING DATASET**

**Table A.5:** Specimen TA tensile test results.

Specimen	MC	Area	$F_{u,T}$	$f_{u,T}$	$E_T$
	[%]	[ $mm^2$ ]	[ $N$ ]	[ $MPa$ ]	[ $GPa$ ]
TA1	8.21	53.84	7680.45	142.64	12.60
TA2	7.04	56.65	6452.34	113.90	11.27
TA3	7.89	54.62	5221.69	95.59	8.73
TA4	6.61	64.61	7703.37	119.24	14.00
TA5	7.53	55.46	5417.24	97.68	11.34
TA6	6.99	53.32	4601.93	86.30	9.25
TA7	9.85	55.15	5559.96	100.81	9.41
TA8	7.09	56.98	5631.28	98.83	9.90
TA9	8.19	56.05	5033.4	89.81	9.31
TA10	7.88	56.71	8361.62	147.45	12.04
TA11	7.52	52.97	4995.84	94.32	10.50
TA12	7.43	58.47	5417.84	92.66	10.20
TA13	8.43	54.95	8681.75	158.00	11.50
TA14	7.45	56.18	6802.98	121.10	9.60
TA15	8.12	55.60	5498.02	98.88	9.88
TA16	7.33	51.02	4470.39	87.62	12.60
TA17	7.18	56.57	5310.9	93.88	11.43
TA18	7.94	55.96	6974.98	124.64	12.64
TA19	7.46	57.78	8124.68	140.60	9.70
TA20	7.19	56.48	5316.15	94.12	12.53
<b>Mean</b>	<b>7.67</b>		<b>6162.84</b>	<b>109.90</b>	<b>10.92</b>
<b>STD</b>	<b>0.70</b>		<b>1324.34</b>	<b>22.20</b>	<b>1.48</b>
<b>COV</b>	<b>9.14</b>		<b>21.49</b>	<b>20.20</b>	<b>13.51</b>

**APPENDIX A. SMALL CLEAR SPECIMEN TESTING DATASET**

**Table A.6:** Specimen TB tensile test results.

Specimen	MC	Area	$F_{u,T}$	$f_{u,T}$	$E_T$
	[%]	[ $mm^2$ ]	[ $N$ ]	[ $MPa$ ]	[ $GPa$ ]
TB1	7.51	55.68	4423.85	79.45	10.51
TB2	7.53	55.96	5144.96	91.94	8.37
TB3	8.38	56.84	4730.59	83.23	8.27
TB4	8.97	54.49	4764.08	87.43	7.81
TB5	8.72	51.98	4420.24	85.04	9.95
TB6	7.73	53.23	3013.65	56.62	10.90
TB7	7.52	57.21	6627.59	115.85	9.79
TB8	7.73	54.98	4987.31	90.71	9.88
TB9	7.69	55.49	5236.61	94.37	8.34
TB10	7.87	56.14	5207.2	92.75	8.25
TB11	6.45	55.31	4685.87	84.72	9.59
TB12	7.58	54.02	5229.06	96.79	10.87
TB13	8.63	56.86	6368.26	112.01	12.01
TB14	8.36	58.52	4556.86	77.87	8.64
TB15	7.73	54.38	5961.54	109.63	9.98
TB16	8.13	56.30	5438.46	96.61	10.05
TB17	7.83	54.99	6077.05	110.50	11.00
TB18	7.84	53.55	4507.44	84.17	7.74
TB19	8.48	52.75	4933.54	93.52	9.58
TB20	8.50	56.87	3735.78	65.69	8.67
<b>Mean</b>	<b>7.96</b>		<b>5002.50</b>	<b>90.44</b>	<b>9.51</b>
<b>STD</b>	<b>0.57</b>		<b>853.87</b>	<b>14.85</b>	<b>1.20</b>
<b>COV</b>	<b>7.20</b>		<b>17.07</b>	<b>16.42</b>	<b>12.65</b>

**APPENDIX A. SMALL CLEAR SPECIMEN TESTING DATASET**

**Table A.7:** Specimen TC tensile test results.

Specimen	MC	Area	$F_{u,T}$	$f_{u,T}$	$E_T$
	[%]	[ $mm^2$ ]	[ $N$ ]	[ $MPa$ ]	[ $GPa$ ]
TC1	6.95	57.85	7680.45	132.78	8.64
TC2	7.72	53.86	6452.34	119.81	15.84
TC3	8.04	57.86	5221.69	90.25	10.01
TC4	10.26	54.16	7703.37	134.98	9.92
TC5	7.52	57.07	5417.24	100.02	11.45
TC6	8.38	55.61	4601.93	82.75	12.62
TC7	7.17	55.63	5559.96	99.94	9.42
TC8	7.76	55.34	5631.28	101.77	11.63
TC9	8.39	56.10	5033.40	89.72	10.46
TC10	8.72	54.71	8361.62	152.84	8.21
TC11	8.21	55.971	5709.61	102.01	8.61
TC12	8.02	54.64	6495.13	118.86	9.46
TC13	8.39	56.25	6069.3	107.90	9.59
TC14	7.52	55.69	7011.58	125.89	10.60
TC15	8.22	55.98	4915.15	87.80	7.26
TC16	8.21	57.00	6179.04	108.40	10.03
TC17	8.08	53.73	7768.49	144.58	11.17
TC18	7.34	56.90	5233.32	91.98	10.90
TC19	8.20	56.14	7066.36	125.86	10.25
TC20	8.31	55.23	8379.48	151.71	12.41
<b>Mean</b>	<b>8.07</b>		<b>6324.54</b>	<b>113.49</b>	<b>10.42</b>
<b>STD</b>	0.69		1184.23	21.82	1.86
<b>COV</b>	8.58		18.72	19.23	17.88

**APPENDIX A. SMALL CLEAR SPECIMEN TESTING DATASET**

**Table A.8:** Failure modes of the tensile specimen

Specimen	Knot location	Failure location	Knot failure?	Failure
TB1	M	B	N	Tension failure
TB2	M	M	Y	Tension failure at the middle at knot, glue line delamination
TB3	M-B	B	Y	Tension failure at the bottom
TB4	M	M	Y	Tension failure at the middle knot and propagates along the glue line
TB5	M	M	Y	Tension failure at the middle knot
TB6	M	M	Y	Tension failure at the middle knot
TB7	M	T	Y	Tension failure at the top grip at a knot, bamboo splitting.
TB8	M	B	N	Tension failure at the bottom part.
TB9	M	B	N	Tension failure at the bottom part
TB10	M	M	N	Tension failure at the middle knot
TB11	M	M	Y	Tension failure at the middle knot
TB12	M	M	N	Tension failure near the middle knot but knot was not the crack initiator.
TB13	M	B	Y	Tension failure at the bottom grip. A knot near the grip caused the crack and split the bamboo.
TB14	B	B	Y	Tension failure at the middle knot
TB15	M	T	y	Tension failure at the middle knot and delamination
TB16	M	B	Y	Tension failure at the middle knot and delamination
TB17	M	B	Y	Failed at the the bottom grip due to stress concentration and knot.
TB18	M	M	Y	Tension failure at the centre
TB19	M	M	N	Tension failure at the middle part
TB20	M	M	N	Tension failure, no delamination